

# **ACCURACY OF THE CLASSICAL HEIGHT SYSTEM**

**ISMAEL FOROUGHI**

**November 2018**



**TECHNICAL REPORT  
NO. 316**

# **ACCURACY OF THE CLASSICAL HEIGHT SYSTEM**

Ismael Foroughi

Department of Geodesy and Geomatics Engineering  
University of New Brunswick  
P.O. Box 4400  
Fredericton, N.B.  
Canada  
E3B 5A3

November 2018

© Ismael Foroughi, 2018

## **PREFACE**

This technical report is a reproduction of a dissertation submitted in partial fulfillment of the requirements for the degree of Doctor of Philosophy in the Department of Geodesy and Geomatics Engineering, November 2018. The research was co-supervised by Dr. Marcelo Santos and Dr. Petr Vaníček, and partial support was provided by the Natural Sciences and Engineering Research Council of Canada.

As with any copyrighted material, permission to reprint or quote extensively from this report must be received from the author. The citation to this work should appear as follows:

Foroughi, Ismael (2018). *Accuracy of the Classical Height System*. Ph.D. dissertation, Department of Geodesy and Geomatics Engineering Technical Report No. 316, University of New Brunswick, Fredericton, New Brunswick, Canada, 213 pp.

## **Abstract**

Measuring the quality of the classical height system through its self-consistency (congruency) is investigated in this dissertation. Measuring the congruency is done by comparing the geoidal heights determined from a gravimetric geoid model with test geoidal heights derived at GNSS/Leveling points. The components of this measurement are computed as accurately as possible, e.g., the Stokes-Helmert approach is used to determine the geoid model, gravimetric and topographic corrections are applied to the spirit leveling observations to derive rigorous orthometric heights at test points, and finally, the geodetic heights are taken from GNSS observations.

Four articles are included in this dissertation, one is discussing a modification to the Stokes-Helmert approach for using the optimal contribution of the Earth gravitational models and the local data. The second paper applies the methodology presented in the first paper and presents the detail results for a test area. The third paper is a discussion on the accuracy of the classical height system against Molodensky's system and presents a numerical study to show that the classical system can be computed as accurately as Molodensky's. The last paper presents a methodology to find the most probable solution of the downward continuation of surface gravity to the geoid level using the least-squares technique. The uncertainties of the geoidal heights are estimated using least-square downward continuation and a priori variance matrix of the input gravity data. The total estimation of the uncertainties of the geoidal heights confirms that geoid can be determined with sub-centimetre accuracy in the flat areas when, mainly, the effect of topographic mass density is taken into account properly, the most probable solution of

downward continuation is used, and the improved satellite-only global gravitational models are merged with local data optimally.

## **Dedication**

*To my mother and father.*

## Acknowledgement

I would like to take this opportunity to express the deepest appreciation to Dr. Petr Vaníček who kindly accepted me as Ph.D. student and patiently supervised me during this journey. He extended my knowledge horizon and guided me towards proper scientific research. I would also like to extend sincere thanks to Dr. Marcelo Santos who has always reminded me of the importance of my work and motivated me to publish my scientific contributions. I am deeply indebted to Dr. Robert Kingdon for being member of my supervising committee and more importantly for his constant guidance, assistance, and invaluable support in every step of my Ph.D. program and during the weekly roundtable meetings.

I am grateful also to my examining board, Dr. Riccardo Barzaghi and Dr. James Watmough, for taking their time and careful review of my dissertation and also thoughtful suggestions.

I would like to thank Dr. Pavel Novák who invited me to visit his research group (new technologies for the information society, NTIS) at University of West Bohemia, Plzeň. Numerous scientific discussions with him and other members including Dr. Robert Tenzer, Dr. Michal Šprlák, and Dr. Martin Pitoňák gave me a broader view of the Earth gravity field and helped me for completion of my Ph.D. program.

I wish to express my gratitude to Dr. Mehdi Goli for his ideas, thoughtful comments, contributions, and useful discussions through email. His prompt responses and helps are greatly appreciated.

Heartful thanks also go to Mr. Michael Sheng for reading the draft of my contributions, productive comments and suggestions during this program.

I would also like to thank Dr. Juraj Janák and Dr. Jianliang Huang for the very enjoyable discussions during their visit research visits of UNB.

And finally, last but by no means least, I thank my parents, siblings, relatives, and friends for their endless spiritual support, encouragement, and understanding. Special thanks to all my friends in Fredericton who have always been beside me and helped me finish this program while being thousand of miles away from my family.



# Table of Contents

Abstract .....	ii
Table of Contents .....	vii
List of Figures .....	x
List of Tables.....	xiv
1 Chapter 1: Introduction .....	1
1.1 Height systems .....	1
1.1.1 Dynamic height system:.....	4
1.1.2 Classical (orthometric) height system:.....	4
1.1.3 Molodensky’s (normal) height system.....	7
1.1.4 Geodetic height system .....	9
1.2 Geoid .....	12
1.2.1 Data Preparation (Transformation to Helmert space “ <i>Helmertization</i> ”)....	14
1.2.2 Evaluation of the Stokes integral .....	21
1.2.3 Transferring back to real space .....	27
1.3 Rigorous Orthometric heights .....	28
1.4 Congruency of the height system .....	31
1.5 Test data set .....	35
1.6 Importance of articles included .....	38
1.6.1 Articles related to geoid model .....	39
1.6.2 The article dealing with orthometric height .....	41
1.6.3 The article related to the quality of the classical height system.....	41
1.7 References .....	43
2 Chapter 2: Optimal combination of satellite and terrestrial gravity data for regional geoid determination using Stokes-Helmert’s method, the Auvergne test case.....	60

2.1	Abstract .....	61
2.2	Introduction .....	61
2.3	Proposed method .....	66
2.4	Numerical results.....	68
2.5	Concluding remarks .....	74
2.6	Acknowledgments .....	75
2.7	References .....	75
3	Chapter 3: Computation of precise geoid model of Auvergne using current UNB	
	Stokes-Helmert's approach .....	78
3.1	Abstract .....	79
3.2	Introduction .....	80
3.3	Stokes-Helmert method, present state and references.....	82
3.4	Input data sets .....	86
3.5	Interpolation of free-air gravity anomalies on topography .....	91
3.6	Computation of geoid model.....	93
3.6.1	Geoid model under the assumption of standard topographic density .....	94
3.6.2	The effect of lateral topographical density variations on the geoid.....	104
3.7	Testing and comparison.....	105
3.8	Discussion and conclusions.....	109
3.9	Acknowledgement.....	111
3.10	References .....	111
4	Chapter 4: In defense of the classical height system.....	119
4.1	Abstract .....	120
4.2	Introduction .....	122

4.3	Review of the height system theory .....	125
4.4	Numerical results.....	130
4.5	Discussion and conclusions.....	139
4.6	Acknowledgement.....	144
4.7	References .....	145
5	Chapter 5: Sub-Centimetre geoid.....	150
5.1	Abstract .....	151
5.2	Introduction .....	153
5.3	Least Squares Downward Continuation (LS DWC) .....	159
5.3.1	The theory .....	159
5.3.2	Numerical evaluation of LS DWC.....	162
5.4	Estimating the uncertainty in the geoidal heights.....	172
5.4.1	Sources of uncertainties .....	172
5.4.2	Uncertainty in the NZ contribution.....	174
5.4.3	Uncertainty in the reference spheroid .....	179
5.4.4	Uncertainty in the FZ contribution.....	180
5.4.5	Uncertainty in the transformation of the co-geoid back to the real space	181
5.5	Numerical evaluation of the geoidal heights and their uncertainties .....	182
5.6	Comparison with the GNSS/Leveling control points.....	189
5.7	Discussion and conclusions.....	194
5.8	Acknowledgments .....	201
5.9	References .....	201
6	Chapter 6: Conclusions .....	208
6.1	Recommendation for future studies .....	212
6.2	References .....	213

Vita

## List of Figures

Figure 1.1: Geometric definition of orthometric height, dashed-lines show the equipotential surfaces between geoid and the Earth surface.....	7
Figure 1.2: Different heights with respect to reference ellipsoid: $H_0$ : orthometric height, $H_N$ : normal heights, $h$ : geodetic height, $N$ : geoidal height, $\zeta$ : height anomaly. ....	9
Figure 1.3: Conventional Stokes-Helmert scheme for geoid determination.....	14
Figure 1.4: Distribution of the terrestrial gravity data in Auvergne .....	36
Figure 1.5: Topography of Auvergne, dashed-lines show the geoid computation area...37	
Figure 2.1: Three main computational steps of Stokes-Helmert's technique .....	65
Figure 2.2: Proposed method to estimate the optimal contributions of near-zone (NZ) and far-zone (FZ) in Stokes's integration. ....	68
Figure 2.3: Topography of the study area (a); distribution of terrestrial gravity data (b). .....	69
Figure 2.4: Direct topographical effect (a); secondary indirect topographical effect on gravity anomalies (b).....	70
Figure 2.5: Free-air gravity anomaly with red-cross signs showing GNSS/Leveling points (a) and Helmert's gravity anomalies (b).....	70
Figure 2.6: Primary indirect topographical effect on geoidal heights in the Auvergne geoid test area.....	72
Figure 2.7: Variation of STD and range of differences between resulting geoid and GNSS/Leveling. ....	73
Figure 3.1: Distribution of the free-air gravity anomalies .....	87
Figure 3.2: Free-air gravity anomalies directly gridded from the original scattered data based on [Duquenne, 2007] database.....	88

Figure 3.3: Topography of the area covered by terrestrial gravity data with the resolution of 30"×30" based on the ACE2 digital elevation model. ....	90
Figure 3.4: Refined spherical Bouguer gravity anomalies on the Earth surface interpolated to 1'×1' geographical grid. ....	92
Figure 3.5: Free-air gravity anomalies on a regular 1'×1' geographical grid obtained from interpolated refined spherical Bouguer gravity anomalies. ....	93
Figure 3.6: Direct topographical effect (a) and direct atmospheric effect (b) used for transformation of the free-air gravity anomalies to the Helmert space. ....	95
Figure 3.7: Secondary indirect topographic effect used for the transformation of the free-air gravity anomalies to the Helmert space. ....	96
Figure 3.8: Helmert's gravity anomalies on the Earth surface (a) and on the geoid (b). .	97
Figure 3.9: Reference Helmert's gravity anomalies computed using DIR-R5 up to degree/order 160 (a) and residual Helmert's gravity anomalies (b). ....	98
Figure 3.10: Ellipsoidal corrections: correction to gravity disturbance (a) and correction for spherical approximation (b). ....	99
Figure 3.11: Reference Spheroid computed using DIR-R5 model and up to degree/order 160 in Helmert's space (a) and residual co-geoid (b). ....	100
Figure 3.12: Far-zone contribution to residual NZ co-geoid, a.k.a., truncation correction (a) and Hörmander correction (b). ....	101
Figure 3.13: Primary indirect topographical effect (a) and primary indirect atmospheric effect (b). ....	102
Figure 3.14: Geoid model in the Auvergne area assuming the standard density of topographic masses $2670 \text{ kg.m}^{-3}$ . ....	103
Figure 3.15: Effects of lateral topographical density variations in Auvergne area: direct topographical density effect (a) and primary indirect topographical density effect (b). .	105
Figure 3.16: Topography over the Auvergne area and locations of control GNSS/Leveling points. ....	106

Figure 3.17: Map of differences between the gravimetric geoid model that includes the lateral topographical density effect and GNSS/Leveling geoid heights at control points. ....	108
Figure 3.18: Histograms of differences between the gravimetric geoid heights (standard density – left; lateral topographical density variation included – right) and GNSS/Leveling geoid heights at 75 control points. ....	108
Figure 4.1: Variation of topography in Auvergne with red crosses showing the positions of levelling-points. ....	131
Figure 4.2: Digitized map of lateral topographical density variation in Auvergne (kg/m <sup>3</sup> ). ....	132
Figure 4.3: Differences between normal and Helmert’s orthometric heights. ....	133
Figure 4.4: NT-gravity anomalies (a) at the Earth surface, (b) differences between NT-gravity anomalies on the Earth surface and the geoid. ....	136
Figure 4.5: The correction terms to Helmert’s orthometric height to get rigorous orthometric height: (a) non-topographic $\epsilon_{HNT}$ , (b) terrain generated $\epsilon_{HR}$ , (c) lateral topographical density anomaly generated $\epsilon_{H\delta\rho}$ , (c). ....	138
Figure 4.6: The cumulative corrections to Helmert’s orthometric height: (a) non-topographic $\epsilon_{HNT}$ , (b) non-topographic and terrain generated $\epsilon_{HNT} + \epsilon_{HR}$ , (c) non-topographic, terrain generated, and lateral topographical density anomaly generated $\epsilon_{HNT} + \epsilon_{HR} + \epsilon_{H\delta\rho}$ . ....	138
Figure 4.7: Geoid model of Auvergne computed by Stokes-Helmert’s method [Foroughi et al., 2016]. ....	140
Figure 5.1: Topographic mass density variations (a), topographic heights (b), distribution of ground (red) and marine (blue) gravity observations (c). Dashed lines show the geoid computation area. ....	165
Figure 5.2: STD values of the gridded gravity anomalies on the Earth’s surface. Dashed line shows the geoid computation area. ....	167

Figure 5.3: LS DWC solution of the gravity anomalies on the geoid: 2-D plot (a) and 3-D plot (c), estimated STDs: 2-D plot (b) and 3-D plot (d). Dashed lines show the geoid computation area. ....	170
Figure 5.4: STDs of the topographic mass density .....	184
Figure 5.5: NZ (a), FZ (b), reference spheroid (c), PITE (d) and PIDE (e) contributions to the geoidal heights .....	185
Figure 5.6: STDs of NZ (a), FZ (b), reference spheroid (c), PITE (d), and PIDE (e) [cm] .....	187
Figure 5.7: Geoidal heights (a), STDs of the geoidal heights (b) .....	189
Figure 5.8: Differences between the geoidal heights and GNSS/Leveling at the control points. ....	190
Figure 5.9: Histogram of the standardized residuals between the geoidal heights (computed from the model) and the GNSS/Leveling derived geoidal heights. ....	193
Figure 5.10: STDs of the residual Helmert anomalies over the geoid computation area .....	196
Figure 5.11: Modified Stokes's function of the degree 140 and $\psi_0 = 1^\circ$ .....	197
Figure 5.12: Differences between previously computed geoid and the geoid computed in this study .....	199

## List of Tables

Table 1.1: Statistics of comparison of the primary geoid and quasigeoid results with GNSS/Leveling points .....	38
Table 3.1: Statistical values of the observed (scattered) free-air gravity anomalies and normal heights at the 244009 measured points of the data set [Duquenne, 2007].....	88
Table 3.2: Statistics of the 243889 scattered and 1'×1' interpolated refined spherical Bouguer gravity anomalies and free-air gravity anomalies. ....	92
Table 3.3: Statistics of Helmertization terms (mGal). ....	95
Table 3.4: Statistics of Helmert's gravity anomalies on the earth surface and on the geoid (mGal). ....	97
Table 3.5: Statistics of reference Helmert's gravity anomalies and residual Helmert's gravity anomalies (mGal).....	98
Table 3.6: Statistics of ellipsoidal corrections (mGal).....	99
Table 3.7: Statistics of final geoid computation components (m). ....	103
Table 3.8: Statistics of the direct and primary indirect density effects on the geoid and statistics of the geoid model assuming the lateral topographical density variation (m).105	105
Table 3.9: Statistics of differences between the rigorous orthometric and normal heights (mm).....	106
Table 3.10: Statistics of differences between the gravimetric geoid heights and GNSS/Leveling geoidal heights computed at 75 control points (m). ....	107
Table 4.1: The statistics of corrections to Helmert's orthometric height (in mm).....	138
Table 4.2: Statistics of cumulative corrections to Helmert's orthometric height (in mm). .....	138
Table 4.3: Statistics of Rigorous orthometric height of levelling-points. ....	140
Table 4.4: Statistics of the fit of various (partially corrected) orthometric heights with the S-H regional geoid model and GNSS- generated orthometric heights. ....	141



Table 4.5: Statistics of the residuals between computed rigorous orthometric heights and those estimated from local geoid S-H model and the GNSS-determined heights; also, residuals between computed normal heights and those estimated from local quasi-geoid KTH model. ....	142
Table 5.1: Abbreviations used throughout this article .....	152
Table 5.2: Estimated STD values of the gridded gravity anomalies on the Earth surface .....	167
Table 5.3: The a posteriori variance factor values of each extended cell .....	171
Table 5.4: Statistics of the LS DWC solution .....	171
Table 5.5: Statistics of contributions to the computed geoidal heights.....	186
Table 5.6: Statistics of the estimated uncertainties .....	187
Table 5.7: Statistics of the geoidal heights and their uncertainties .....	189
Table 5.8: Statistics of comparison of the computed geoidal heights with the geoidal heights at GNSS/Leveling points.....	194

# 1 Chapter 1: Introduction

## 1.1 Height systems

Latitude, longitude, and height of a point are commonly used to represent the location of a point on or near the Earth surface. The first two, called horizontal coordinates, refer to reference ellipsoid and are known as *geodetic latitude* ( $\varphi$ ) and *longitude* ( $\lambda$ ) [Moritz, 2000]. The third coordinate, i.e. height of a point is usually represented in a height system which consists of a reference surface and definition of height above it. The height of a point is defined as the distance (along a specific path) between the point and a reference surface; e.g., height of the point can be measured as the distance between the point and the ellipsoid of revolution along the line perpendicular to ellipsoid which is called the *geodetic height* ( $h$ ), cf., Figure 1.2. For many practical purposes, the height of a point must refer to mean sea level (MSL) rather the ellipsoid of revolution [Vaniček, 1998] which will be discussed in detail later.

Height systems consist of two components, reference (vertical) surface and definition of the height above this surface. Depending on different reference surfaces and definition of heights, there could be different height systems used in practice which generally are divided into two types: ones that are tied to the Earth gravity field (called physical height systems) and measure heights along the plumbline; and ones which ignore the Earth gravity field (called geometric height systems) and measure the heights along a straight line. The first type is more common in practice [Vaniček, 1998].

The goal of this dissertation is to evaluate the quality of a gravity-based height system. The quality of a height system can be measured through the accuracy, precision, resolution, coverage, usability, etc. of the system components. In this section, different types of height systems are summarized first and then a method of measuring the quality of a height system is proposed.

Spirit (differential) leveling is commonly used in practice to measure the height differences between adjacent points. For each setup, the leveling instrument and vertical rods are aligned with respect to the local gravity vector so the local horizontal surface (i.e., tangent to the local equipotential surface) is the reference surface in this technique. The direction of the gravity vector varies from place to place, so a slightly different vertical alignment is used in each set up [Featherstone and Kuhn, 2006]. If a circuit is measured, i.e., a closed spirit leveling “loop” is performed, the algebraic sum of all height differences (called misclosure) is not theoretically zero unless the Earth gravity field is properly taken into account. Thus:

$$\oint dn = \text{misclosure} \neq 0, \quad (1.1)$$

where  $dn$  is the leveling increment (i.e. the height difference between two executive points) and the symbol  $\oint$  denotes a line integral over circuit. The topographic mass inside the Earth is not regularly distributed so the expected misclosure is not the same along different leveling routes chosen. Apart from mass density irregularities, as the height differences are measured along the gravity, the misclosure would not be zero unless the leveling routs were exactly identical. To avoid this problem, an appropriate modification must be applied to the leveling measurements to, at least theoretically, obtain a zero

misclosure and to reflect a physically meaningful height system. The component of gravity perpendicular to the equipotential surface contains the full magnitude of the gravity vector, equals to [Heiskanen and Moritz, 1967, Ch.4]:

$$\overline{|g|} = g = -\frac{dW}{dn}, \quad (1.2)$$

where  $dW$  is the gravitational potential difference between a leveling increment and  $g$  is the gravity vector at the leveling station. Replacing Eq. (1.1) to compute the gravity potential differences rather than leveling height differences yields:

$$\oint g dn = \oint dW = 0. \quad (1.3)$$

Potential differences can therefore be calculated combining leveling and gravimetric observations and are indeed the basis of the theory of height systems [Heiskanen and Moritz, 1967, Ch. 4]. Leveling without gravimetric corrections results in a physically meaningless height system and is not considered in this dissertation. There are different types of gravity correction to derive the height of points in different height systems which will be discussed later. There are a few gravity-based height systems used in practice for different purposes, for instance, classical (orthometric), normal, and/or dynamic height systems which will be discussed here.

### 1.1.1 Dynamic height system:

The geopotential number of a point ( $C$ ) is defined as the difference between the gravitational potential of the point of interest ( $W_A$ ) and a reference geopotential  $W_0$ , that is usually on the potential at the geoid, and can be computed as:

$$C_A = W_0 - W_A = \int_0^A g dn . \quad (1.4)$$

The geopotential number of a point can be computed by integrating the product of gravity measurements by leveling increment along the leveling path from geoid to the point of interest (right hand side of Eq. (1.4)).

The dynamic height of a point is then defined as:

$$H_A^{dyn}(\Omega) = \frac{C_A}{\gamma'_0} , \quad (1.5)$$

where  $\Omega$  represents the geocentric spherical coordinates ( $\Omega: (\lambda, \varphi)$ ) of  $A$  and  $\gamma'_0$  is the normal gravity computed (usually) at the mid-latitude  $\varphi = 45^\circ$ . The dynamic height system [Helmert, 1884] is a scaling of the geopotential numbers, so the flow of fluids from higher to lower height is guaranteed in this system. The geoid is chosen as the reference surface, but the heights in this system are purely physical and have no geometrical meaning, so they are rarely used.

### 1.1.2 Classical (orthometric) height system:

In the classical height system, the reference surface is the geoid and the heights are defined as the distances along the plumbline between the geoid and a surface points. These are called orthometric heights and defined as:

$$H_A^o(\Omega) = \frac{C_A}{\bar{g}_A}, \quad (1.6)$$

where,  $\bar{g}_A$  is the average value of the gravity along the plumbline:

$$\bar{g}_A = \frac{1}{H_A^o(\Omega)} \int_0^{H_A^o} g dH^A(\Omega). \quad (1.7)$$

The path of integration, i.e., the plumbline in Eq. (1.7), is a line that is always perpendicular to the equipotential surfaces between the geoid and the point on the Earth surface. Due to all variations in the Earth gravity field, the equipotential surfaces are not parallel, so the plumbline can be a curved and twisted line (cf., Figure 1.1). Unlike the dynamic heights, orthometric heights have a geometrical meaning too. The geoid is a level surface at mean sea level with the potential  $W_0$ . The separation between the geoid and geodetic reference ellipsoid is called *geoidal height* (or called geoid-ellipsoid separation) ( $N$ ) and is a commonly used term in geoid determination (cf., Figure 1.2).

The definition of orthometric heights and the geoid are both tied to Earth's potential gravity field and therefore have physical meaning. To determine the geoidal heights, the observable quantities of the Earth's potential field (usually gravity anomalies) must refer to the geoid and therefore, at least theoretically, the density of masses at every point between the geoid and topographical surface must be known. Computing the orthometric heights is also a complicated task, as computing the mean value of gravity along the plumbline from geoid to the Earth surface also needs the knowledge of the mass density distribution inside topography or measurement of gravity along the plumbline, the latter

of which is not practical. Topographic density within the Earth can be approximated by some density hypothesis with sufficient accuracy [Helmert, 1884; Sunkel, 1986; Wirth, 1990; Allister and Featherstone, 2001; Tenzer et al., 2005]. A commonly used density hypothesis [Heiskanen and Moritz, 1967, Ch. 4] which approximates the Earth's topography by a constant density and height is called the Bouguer plate or shell and the resulting height using this hypothesis is called *Helmert orthometric height*. Based on the Poincaré-Pray reduction, the vertical gravity gradient is approximated by the linear free-air gradient and simplifies the topography by a shell or plate with a constant density equal to mean density of the crust ( $2670 \text{ kg/m}^3$ ). The mean gravity along the plumbline (integral mean) in the definition of the Helmert orthometric heights (Eq.(1.6)) is approximated by reduced surface gravity to the mid-point. Further discussion on the realization of the orthometric heights will be given in Sec.1.3 and Ch. 4.

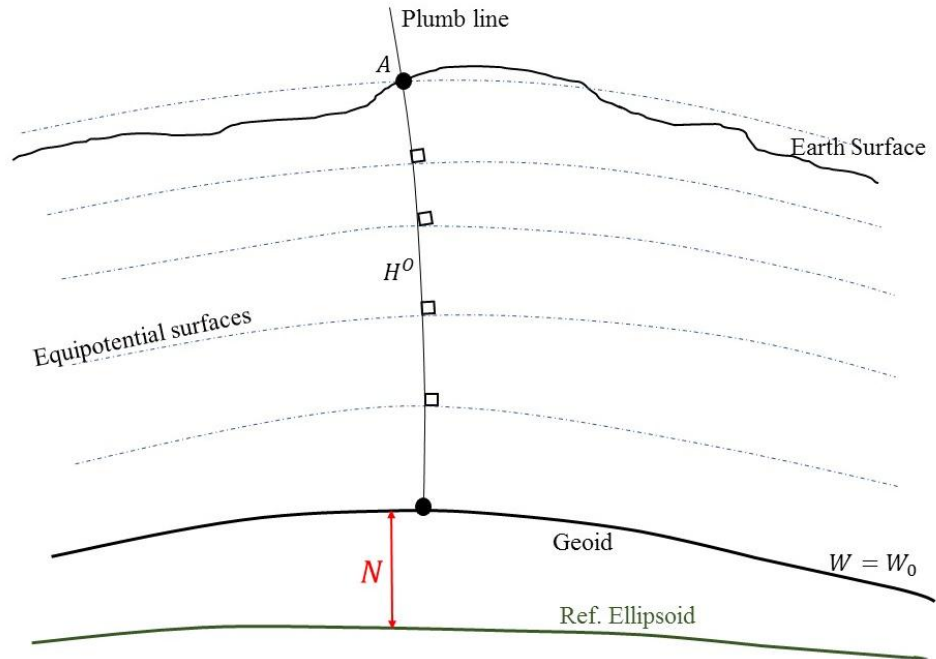


Figure 1.1: Geometric definition of orthometric height, dashed-lines show the equipotential surfaces between geoid and the Earth surface

### 1.1.3 Molodensky's (normal) height system

To overcome the problem of the lack of density knowledge inside the topography, Molodensky et al. [1960] were able to show that the physical surface of the Earth can be determined without using the Earth's inner density. This was accomplished by introducing an approximate gravity field that can be calculated exactly at any point; i.e., the normal gravity field [Heiskanen and Moritz, 1967, Ch. 4]. The normal gravity field is an ellipsoidal approximation of the gravity field that contains the total mass of the Earth and rotates with Earth around its minor axis [Moritz, 2000]. The gravitational potential generated by normal gravity field is denoted by  $U$ . In the formulation proposed by Molodensky et al. [1960], instead of the geoid, gravity anomalies refer to the ground (more



precisely, the *Telluroid*). The telluroid is an auxiliary surface where the normal gravity potential at each point of this surface equals to the actual gravity potential of the corresponding points (the points along the ellipsoidal normal) on the Earth's surface (cf., Figure 1.2).

Assuming the Earth gravity field to be the normal field, that is,  $W = U$ , and  $g = \gamma$  and under the aforementioned assumptions, the Eq. (1.6), i.e., the normal height in the Molodensky height system is defined as follows:

$$H_A^N = \frac{C_A}{\bar{\gamma}_A}, \quad (1.8)$$

where  $\bar{\gamma}$  is the integral mean normal gravity along the normal plumbline computed as:

$$\bar{\gamma}_A = \frac{1}{H_A^N(\Omega)} \int_0^{H_A^N} g dH^N(\Omega). \quad (1.9)$$

In this system, the quasigeoid is used as the datum and heights above this datum are defined as the distances between the reference ellipsoid and the points on the telluroid along the normal plumbline, and are called *normal heights* [Heiskanen and Moritz, 1967, Ch. 4]. The separation between the Earth surface and the Telluroid is called the height anomaly and denoted by  $\zeta$ . The height anomaly, in fact, is the same as the separation between the reference ellipsoid and the quasigeoid (cf., Figure 1.2); i.e., quasigeoidal heights.

### 1.1.4 Geodetic height system

The Earth's surface and its geometric heights can also be depicted by geodetic heights ( $h$ ). Geodetic heights ( $h$ ) are the heights above the reference ellipsoid measured along the ellipsoidal normal. Geodetic heights are usually provided by Global Navigation Satellite System (GNSS) observations. The geodetic height system is purely geometrical and suggested by a few authors for some network control, marine, and air navigation projects, e.g., [Zilkoski, 1993; Steinberg and Papo, 1998; Kumar, 2005] however, this height system is not suggested for projects which involve geophysical applications, terrestrial observations, and fluid flow [Vaníček, 1998].

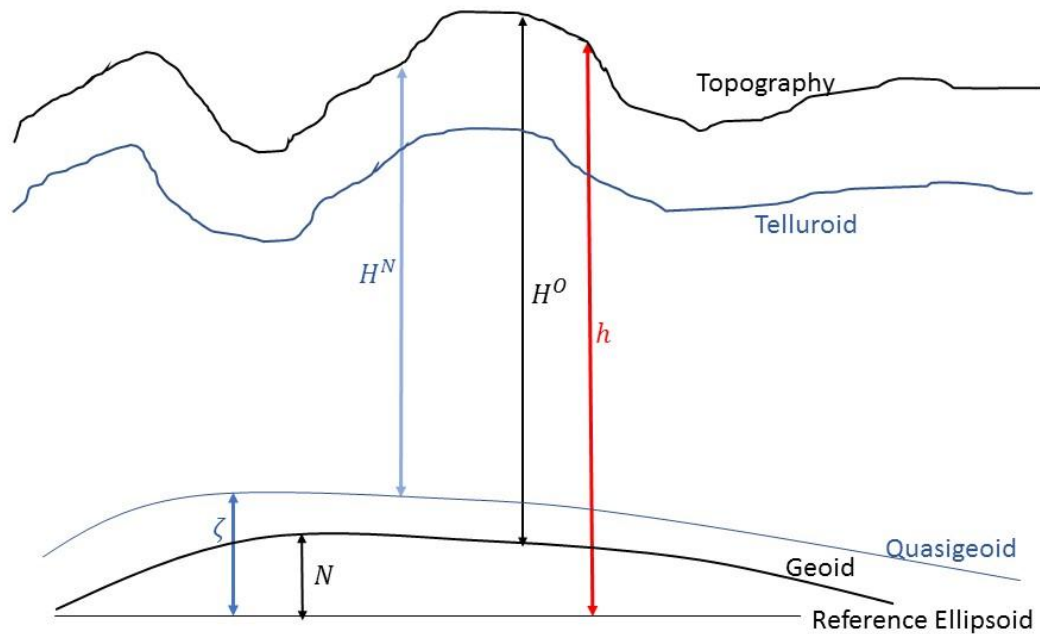


Figure 1.2: Different heights with respect to reference ellipsoid:  $H^O$ : orthometric height,  $H^N$ : normal heights,  $h$ : geodetic height,  $N$ : geoidal height,  $\zeta$ : height anomaly.

The classical and Molodenskij height systems are the two most commonly used height systems for a practical realization of local and national vertical geodetic datums. Due to the problems mentioned above for determining the heights in the classical height system, some countries (most European) decided to define their height system according to Molodensky's definition, [e.g., among others, Lysaker et al., 2006; Krikstaponis et al., 2007; Klees et al., 2008; Yilmiz, 2008; Ågren and Sjöberg, 2014; Li et al., 2015]. However, some other countries, like USA and Canada, define their height system based on the classical definition, [e.g., among others, Vaníček and Martinec, 1994; Kühnreiter, 1998; Bayoud and Sideris, 2003; Tenzer et al., 2003; Saadat et al., 2017].

The computation of the datum in the classical height system (geoid) suffers due to uncertainties in the topographical density distribution but provides the most physically meaningful vertical reference surface. On the contrary, determination of the quasigeoid in the Molodensky height system requires integration over the Earth's surface (Telluroid) which is not a smooth manifold. Furthermore, heights in this system do not have physical meaning. The actual mean gravity along the plumbline between the geoid and the topographic surface is used for the theoretical definition of the orthometric heights in the classical system, whereas the mean normal gravity along the normal plumbline between reference ellipsoid and the Telluroid is calculated explicitly in the definition of the normal heights in the Molodensky system. The problems associated with the classical system, i.e., the density variation of the topography, are being resolved with increasing accuracy as the time passes; however, while the problems that exist in the computation of the quasigeoid will not be resolved by increasing knowledge of the Earth's composition [Vaníček et al., 2012].

There are also some studies intending to compute the differences between geoid and quasigeoid, i.e. differences between normal and orthometric heights. The simplest formula is the classical formulation to compute the separation between geoid and quasigeoid and is not accurate in mountainous areas [Heiskanen and Moritz 1967, Ch. 4]. To derive a more rigorous formula than classical formulation, the terrain correction, topographic density variation, and the effect of geoid generated gravity disturbances were taken into account by Tenzer et al. [2005] and Santos et al. [2006]. Flury and Rummel [2009] also investigated the effect of terrain geometry on the separation of geoid and quasigeoid. Following the derivation of Flury and Rummel [2009], Sjöberg [2010] gave a more exact definition of the geoid to quasigeoid separation which was consistent with the formulation of the fundamental gravimetric equation of physical geodesy. Tenzer et al. [2015] summarized all the expressions for computing the separation between geoid and quasigeoid in spatial and spectral domains and suggested to compute the quasigeoid and then convert to the geoid. The data needed for computing the exact separation between geoid and quasigeoid are the ones needed to compute the geoid, so it does not make sense to compute a non-physical reference surface, i.e., quasigeoid, and then convert it to the geoid.

In this dissertation, measuring the quality of a height system is intended. Geoid and orthometric heights are the components of the classical height system which are discussed in the following sections.

## 1.2 Geoid

After some idealization, the mean surface of the oceans is, so to speak, part of a certain level surface and horizontal everywhere; therefore, it is convenient for heights for practical purposes to be associated with mean sea level (MSL) [Vaniček, 1998]. The MSL everywhere more or less follows a gravity equipotential surface of a constant potential  $W_0$ . The equipotential surfaces of the Earth which approximates the MSL most closely was proposed by C. F. Gauss as the “mathematical figure of the Earth” and called later the *geoid*. Determination of the geoid is a purely physical problem. If the mass density distribution within the Earth were known, gravity potential could be computed at every point and the geoid would simply be the contour connecting all the points with the gravity potential equal to  $W_0$ . The distribution of mass density inside the Earth however is not fully known, but knowing the relation between gravity and gravity potential, and using some gravimetric, geodetic, and topographic information, the geoidal heights can be computed with adequate accuracy. Gravimetric data include local measurements of the Earth gravity field and the global gravity field represented by the spherical harmonics provided by satellite gravity missions. Measurements of the geometry of the Earth, such as, topographical heights or geoidal heights at benchmarks (differences between geodetic and orthometric heights) fits in the geometric source of data sets. Statistical methods may be used to combine these sources of data to determine geoidal heights (e.g., least squares collocation method in Tscherning et al. [1992] and Featherstone and Sproule [2006]; Stokes-Helmert method in Vaniček and Martinec [1994]; least square modification of Stokes method in Sjöberg [2003]). The theory of the Stokes-Helmert’s method developed

at the University of New Brunswick is focused on in this dissertation and is introduced below.

Stokes [1849] introduced the Stokes's integral as an analytical solution for a spherical boundary for the determination of the geoid using gravity measurements. The main requirements of the solution were that gravity values must be available on a sphere and there should not be any masses above this surface. Neither of these assumptions is valid in real space. Gravity anomalies are measured at or above the surface of the Earth and there are topographic masses between the geoid and the Earth surface and atmospheric masses above the Earth surface. To use the Stokes formulation, gravity measurements at or above the Earth surface are used to estimate values on the geoid. This transformation must be done in a space in which the gravity field behaves harmonically, i.e., satisfying the Laplace equation, and the gravity anomalies must be of a solid type [Vaniček et al., 1996]. Helmert [1884] suggested transferring all the gravity measurement to a space where all topographic masses are condensed into a dense layer on or below the geoid to, at least mathematically, avoid the problem of existing masses. Gravity measurements could then be transferred to the Helmert space by removing the effect of this topographic mass condensation to be continued down to the geoid. Poisson [MacMillan, 1930] formulated the Dirichlet boundary value problem and his method was used to get a physically rigorous approach for downward continuation (DWC) of gravity anomalies to geoid level which can be done if gravity anomalies are transferred to a space in which gravity field behaves harmonically. The three formulations of Stokes, Helmert, and Poisson form the theory of the Stokes-Helmert geoid determination approach.

The theory of the Stokes-Helmert approach has been documented in many publications and applied to different regions of the world, [Vaniček and Sjöberg, 1991; Vaniček and Martinec, 1994; Tenzer et al., 2003; Bajracharya, 2003; Huang and Véronneau, 2005; Ellmann and Vaniček, 2007; Janák et al., 2017]. Excluding some minor differences, the conventional scheme of the Stokes-Helmert approach in all abovementioned publications is shown in Figure 1.3.

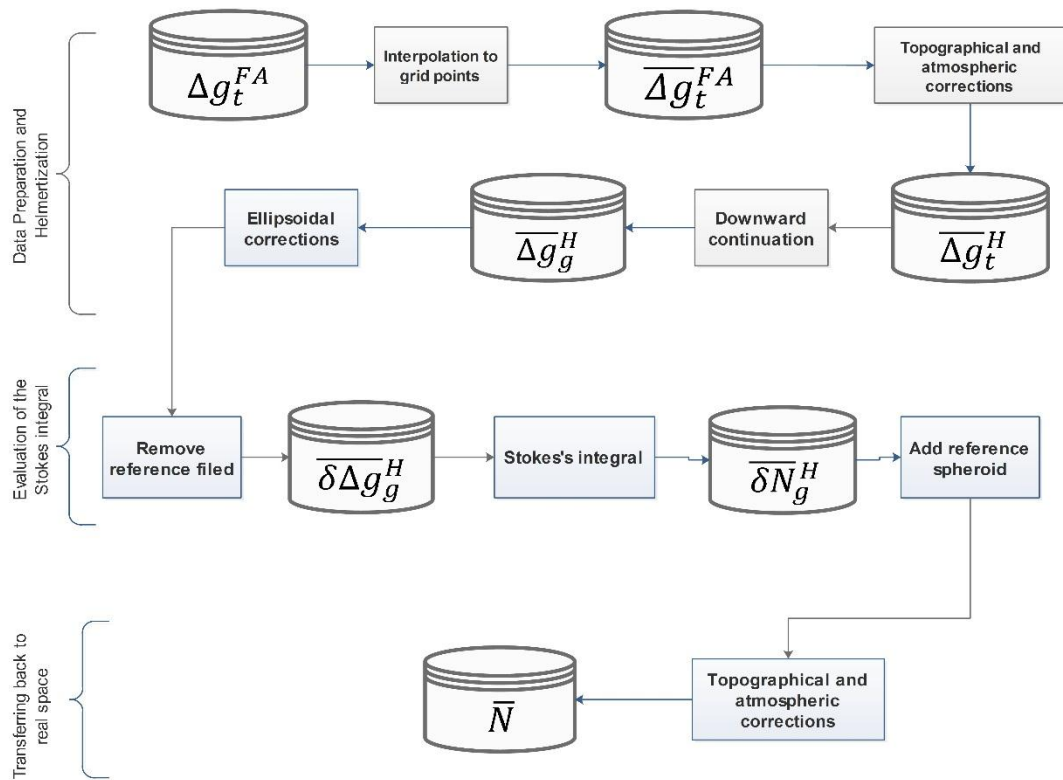


Figure 1.3: Conventional Stokes-Helmert scheme for geoid determination

### 1.2.1 Data Preparation (Transformation to Helmert space “Helmertization”)

In this step the observation data are prepared to be evaluated by the Stokes integral:

- ***Prediction of Free-air gravity anomalies on grid points:***

Free-air gravity anomalies are computed as follows [Vaníček and Krakiwsky, 1986, Ch.6]:

$$\Delta g(r_t, \Omega) = g(r_t, \Omega) - \gamma(H^o - \zeta, \Omega), \quad (1.10)$$

where  $H^o$  is the height of the observation point,  $g(r_t, \Omega)$  is the observed gravity at the point at the surface with a radius  $r_t$  and geocentric coordinates of  $\Omega(\varphi, \lambda)$ ,  $\gamma$  is the normal gravity computed at the Telluroid which is approximated by [cf., Vaníček and Krakiwsky 1986, Ch.21]:

$$\gamma(H^o - \zeta, \Omega) = \gamma_0 - \frac{2g}{R} \times H^o(\Omega), \quad (1.11)$$

and the free-air correction. Conventionally, the input gravity data in the Stokes-Helmert method is mean gravity anomalies at grid points (the cell centres), i.e., the gravity values inside one cell are averaged to get the cell centre value. To predict the gravity anomalies at these points, they should be transferred to a smoother field, e.g., complete spherical Bouguer gravity anomalies (also known as No-Topography or NT anomalies), and then averaged at the grid points with specific resolution. For further details on prediction and averaging the gravity anomalies please see [Kassim, 1980; Vaníček et al., 2004; Janák and Vaníček, 2005; Janák et al., 2017]. The output of this step are mean free-air gravity anomalies ( $\Delta g^{FA}(r_t, \Omega)$ ) on grid points at surface.

- ***Transferring to the Helmert space:***

Helmert's gravity anomalies are computed as follows [Novák, 2000]:



$$\Delta g^H(r_t, \Omega) = \Delta g^{FA}(r_t, \Omega) + \delta A^t(r_t, \Omega) + \delta A^a(r_t, \Omega) + \delta \gamma^t(r_t, \Omega) + \delta \gamma^a(r_t, \Omega) + \varepsilon_{gqg}(r_t, \Omega) + \varepsilon_g(r_t, \Omega). \quad (1.12)$$

In Eq.(1.12),  $\delta A^t(\Omega, r_t)$  is the direct topographical effect (DTE),  $\delta A^a(\Omega, r_t)$  is the direct atmospheric effect (DAE) which are computed as follows:

$$\begin{aligned} \delta A^t(r_t, \Omega) &= \frac{\partial \delta V^t(r_t, \Omega)}{\partial r} = \frac{\partial V^t(r_t, \Omega)}{\partial r} - \frac{\partial V^{ct}(r_t, \Omega)}{\partial r}, \\ \delta A^a(r_t, \Omega) &= \frac{\partial \delta V^a(r_t, \Omega)}{\partial r} = \frac{\partial V^a(r_t, \Omega)}{\partial r} - \frac{\partial V^{ca}(r_t, \Omega)}{\partial r}, \end{aligned} \quad (1.13)$$

where  $\delta V^t(r_t, \Omega)$  is the residual topographical potential defined as a difference between the gravitational potentials of topographical masses ( $V^t(r_t, \Omega)$ ) and of condensed topographical masses ( $V^{ct}(r_t, \Omega)$ ). Correspondingly,  $\delta V^a(r_t, \Omega)$  is the residual atmospheric potential, obtained by subtracting the gravitational potential of the condensed atmospheric masses ( $V^{ca}(r_t, \Omega)$ ) from the potential of the atmospheric masses ( $V^a(r_t, \Omega)$ ).

The  $\delta \gamma^t(r_t, \Omega)$  is the secondary indirect topographical effect (SITE), and  $\delta \gamma^a(r_t, \Omega)$  is the secondary indirect atmospheric effect (SIAE) which are computed as follows:

$$\begin{aligned} \delta \gamma^t(r_t, \Omega) &= \frac{2}{r_g}(V^t(r_t, \Omega) - V^{ct}(r_t, \Omega)) \\ \delta \gamma^a(r_t, \Omega) &= \frac{2}{r_g}(V^a(r_t, \Omega) - V^{ca}(r_t, \Omega)). \end{aligned} \quad (1.14)$$

The secondary indirect atmospheric effect (SIAE) is very small and is not usually computed in the practical determination of the geoidal heights. In the Stokes-Helmert method, topographical effects are calculated by adding together the three parts: Bouguer shell, terrain, and anomalous density [Wichiencharoen, 1982; Martinec, 1993; Martinec et al., 1996]. Gravitational potential of the spherical Bouguer shell is computed by

considering mean topographical density  $\rho$  for the shell thickness equal to the orthometric height of each point ( $H^o(\Omega)$ ) while calculating the gravitational potential of the spherical roughness term (terrain correction) needs digital terrain model (DTM) of the area. To compute the effect of anomalous density on the gravitational potential, the digital density model (DDM) and DTM are required (cf., [Martinec, 1993; Huang, 2002; Foroughi et al., 2015b]).

The term  $\varepsilon_{gg}(r_t, \Omega)$  is the geoid-to-quasigeoid correction applied to gravity anomalies for the compensation of using orthometric height rather the normal heights (Eq. (1.10)) in the boundary condition formulated in the Helmert space [Vaníček and Martinec, 1994]. This correction can be computed using the approximate formula of the geoid-to-quasigeoid separation [Heiskanen and Moritz, 1967, Ch. 4].

Finally, the term  $\varepsilon_g(r_t, \Omega)$  stands for the ellipsoidal corrections needed in the formulation of the boundary value problem in the spherical coordinate system (cf., [Wong, 2002; Vaníček and Martinec, 1994]).

- ***Downward continuation (DWC):***

The Helmert gravity anomaly multiplied by the geocentric radius ( $r_t$ ) is harmonic outside the geoid and therefore can be transferred down from the Earth surface [Vaníček and Martinec, 1994]. The results of this step are the Helmert gravity anomalies on the co-geoid ( $\overline{\Delta g^H}(r_g, \Omega)$ ). The co-geoid is the equipotential surface in the Helmert space which corresponds to the geoid in the real space [Vaníček et al., 1996; Huang et al., 2003; Kingdon and Vaníček, 2010; Goli et al., 2011]. Helmert's gravity anomalies on the co-

geoid are evaluated using a Fredholm integral of the 1<sup>st</sup> kind called Poisson's integral [Heiskanen and Moritz, 1967, Ch. 6]. The Poisson integral reads [Kellogg, 1929]:

$$\Delta g^H(r_t, \Omega) = \frac{R}{4\pi r_t(\Omega)} \iint_{\Omega' \in \Omega_0} K(r_t(\Omega), \psi(\Omega, \Omega'), R) \Delta g^H(R, \Omega) d\Omega', \quad (1.15)$$

where  $\psi(\Omega, \Omega')$  is the spherical angular distance between positions  $\Omega$  and  $\Omega'$ ,  $R$  is the radius of the mean sphere locally approximating the unknown geoid,  $\Omega_0$  represents an integration domain usually chosen as a spherical cap of radius  $\psi_0$  to which the full spatial angle is limited reflecting the limited geographic availability of ground gravity data and  $K(r_t(\Omega), \psi(\Omega, \Omega'), R)$  is the spherical Poisson integration kernel given analytically as [Heiskanen and Moritz, 1967, Ch. 6]:

$$K(r_t(\Omega), \psi(\Omega, \Omega'), R) = R \frac{r_t^2(\Omega) - R^2}{l^3(r_t(\Omega), \psi, R)}, \quad (1.16)$$

where  $l(r_t, \psi, R)$  is the Euclidian distance between positions  $(r_t, \Omega)$  and  $(R, \Omega')$ .

Ground gravity anomalies are available at discrete points, so the Poisson integral equation must be discretized. The discrete form is:

$$\Delta \mathbf{g}_t^H = \mathbf{B} \Delta \mathbf{g}_g^H. \quad (1.17)$$

Where  $\Delta \mathbf{g}_t^H$  is a vector of Helmert gravity anomalies at the surface,  $\Delta \mathbf{g}_g^H$  is a vector of Helmert gravity anomalies on the geoid at their appropriate locations, and  $\mathbf{B}$  is the coefficient matrix containing values of the discretized Poisson integral [Vaníček et al., 1996]:

$$B_{ij} = \frac{R^2(r_i^2 - R^2)}{4\pi r_i} \frac{1}{l^3(r_i, \varphi_i, \lambda_i; R, \varphi_j, \lambda_j)} \cos\varphi_j \Delta\varphi \Delta\lambda. \quad (1.18)$$

The inverse operator of Eq. (1.17) provides the values of gravity on the geoid given those on the surface, i.e.:

$$\Delta\mathbf{g}_g^H = \mathbf{B}^{-1}\Delta\mathbf{g}_t^H. \quad (1.19)$$

Following the definition of Hadamard [1923], DWC is a physically well-posed problem as there exist a unique and finite solution. According to Tikhonov [1963,1964], the fact that the “inverse being bounded” is equivalent to “the inverse being continuous”. Therefore, *the inverse mapping from  $\Delta\mathbf{g}_t^H$  to  $\Delta\mathbf{g}_g^H$  through the linear Fredholm integral equation of the 1<sup>st</sup> kind is continuous* [Wong, 2001]. However, depending on the discretization step size and height of the observed gravity anomaly, the inverse Poisson integral equation, as any Fredholm equation of 1<sup>st</sup> kind, can have a numerically unstable solution. Martinec [1996] investigated the ill-conditioning of the DWC process using different grid resolution and showed that DWC of anomalies on a grid smaller than 1' is an unstable process. Vaníček et al. [1996] also showed that DWC of Helmert anomalies on a regular 5' × 5' grid is a stable problem and can be solved without any kind of regularization. Investigation of numerical instability of DWC process has been studied by many authors before (e.g., Vaníček et al. [1996]; Huang [2002]; Fedi and Florio [2002]; Huang et al. [2003]; Tenzer and Novák [2008]; Kingdon and Vaníček [2010]; Goli et al. [2011]; Zhang et al. [2013]; Foroughi et al. [2016]; Vaníček et al. [2017]; Goli et al. [2018]). With the accessibility of the high-resolution gravity data, a geoid model with finer resolution, e.g., 1' × 1', was desired after the investigation by Vaníček et al. [1996].

To overcome the problem of instability, Kingdon and Vaníček [2010] suggested using the Jacobi iterative technique to solve the system of linear equations. According to their formulation, the gravity anomalies on the geoid reads [Kingdon and Vaníček, 2010]:

$$\Delta\mathbf{g}_g^K = \Delta\mathbf{g}_t + (I - B)\Delta\mathbf{g}_g^{K-1}, \quad (1.20)$$

where  $\Delta\mathbf{g}_g^K$  is the  $K$ -th estimation of  $\Delta\mathbf{g}_g$ . Surface gravity values are usually chosen as the first estimate (initial value) of the gravity values on the geoid. For the purpose of DWC only, Kingdon and Vaníček [2010] suggested to stop the iteration based on a relaxed threshold. A relaxed threshold is defined according to (a rough estimation of) the condition number of the  $B$  matrix as well as the uncertainty of the input data. In their formulation, the threshold was compared with the largest absolute residual value of the surface gravity anomalies between two iterations. Stopping the iterations before their actual convergence (i.e., the stage when a predefined threshold is related to the noise of the observed data and is not relaxed) is called semi-convergence and used to prevent the high-frequency observation noise from creeping into the DWC solution. Goli et al. [2018] investigated different iterative approaches for DWC of surface gravity anomalies and also tried different stopping criteria. They used a simulated data set, synthesized from the Earth gravitational models (EGMs) at the level of the Earth surface and geoid, and evaluated the DWC methods to estimate the geoid gravity anomalies. Their findings confirm the results of Kingdon and Vaníček [2010] and they also suggested using other iterative approaches to better estimate of geoid gravity anomalies in the mountainous areas.

### 1.2.2 Evaluation of the Stokes integral

The disturbing potential in the Helmert space ( $T^H(r, \Omega)$ ) is defined as the difference between actual ( $W^H$ ) and normal ( $U(R, \Omega)$ ) gravity potential on the geoid in that space:

$$\forall r: \quad T^H(r, \Omega) = W^H(r, \Omega) - U(r, \Omega) \quad (1.21)$$

The geoidal heights in the Helmert space (*co-geoidal heights*) can be computed using the Bruns formula when  $r = R$  [Heiskanen and Moritz, 1967, Ch.2]:

$$N^H(\Omega) = \frac{T^H(R, \Omega)}{\gamma_0(\Omega)} \quad (1.22)$$

Since the disturbing potential cannot be measured directly, the boundary value problem (BVP) of the third kind (also called geodetic BVP) [Heiskanen and Moritz, 1967, Ch.1] has to be formulated and solved:

$$\Delta g^H(R, \Omega) = - \left. \frac{\partial T^H(r, \Omega)}{\partial n} \right|_{r=R} + \frac{1}{\gamma_0(\Omega)} \frac{\partial \gamma}{\partial n} T^H(R, \Omega), \quad (1.23)$$

where  $n$  is the normal to the ellipsoidal surface. In this formulation, gravity anomalies at the geoid level serve as boundary values. A highly accurate solution is found by applying the appropriate Green's function for a sphere, resulting in Stokes's integral [Stokes, 1849]. Stokes's integral for determining the geoidal heights in Helmert space from the gravity anomalies on a spherical boundary [Heiskanen and Moritz, 1967, Ch.2]:

$$N^H(\Omega) = \frac{R}{4\pi\gamma_0(\phi)} \iint_{\Omega' \in \Omega_0} S(\psi(\Omega, \Omega')) \Delta g^H(\Omega') d\Omega' , \quad (1.24)$$

where the Stokes kernel is [ibid, 1967]:

$$S(\psi(\Omega, \Omega')) = \frac{1}{\sin(\psi/2)} - 6\sin\frac{\psi}{2} + 1 - 5\cos\psi - 3\cos\psi\ln\left(\sin\frac{\psi}{2} + \sin^2\frac{\psi}{2}\right). \quad (1.25)$$

Evaluating the Stokes integral requires integration over the whole globe. Terrestrial gravity measurements are not available globally with sufficient accuracy (or at all) and satellite gravity data only cover the low to medium frequency components of the gravity field spectrum. To reduce the contribution of the distant gravity anomalies in the practical evaluation of Eq. (1.24), the Stokes kernel is replaced with its modified kernel ( $S^*$ ) [Wong and Gore, 1969; Vaníček and Kleusberg, 1987]. The integration domain of the Stokes integral formula can be divided into the near-zone and far-zone integration sub-domains. The integration over the near-zone is done by the modified Stokes's function. Modification is done to minimize the effect of far-zone in the least-squares sense [Vaníček and Kleusberg, 1987]. Modified Stokes kernel integrates over a small cap around the computation point ( $\psi_0$ ) which is called the “near-zone” contribution (NZ). The effect of the rest of the globe on the co-geoidal heights can be computed spectrally using EGMs and is called the “far-zone” contribution (FZ) or truncation error [Vaníček and Sjöberg, 1991; Vaníček and Martinec, 1994].

With the growing accuracy and degree of EGMs, Vaníček and Kleusberg [1987] introduced the idea of splitting the disturbing gravity field of the Earth into reference (low-frequency) and residual (high-frequency) parts [Featherstone and Sproule, 2006]. Using this formulation, the low-frequency component of the Helmert gravity anomalies, called the reference field, is computed using only the satellite determined part of the EGMs and

subtracted from the Helmert gravity values. The reference field in Helmert space is computed as follows:

$$\Delta g_L^H(\Omega) = -\frac{GM}{r^2} \sum_{l=2}^L \left(\frac{R}{r}\right)^l (l-1) \sum_{m=-l}^l T_{l,m}^h Y_{l,m}(\Omega),$$

$$T_{l,m}^h = \begin{cases} C_{lm}^h & m \geq 0 \\ S_{lm}^h & m < 0 \end{cases} \quad (1.26)$$

$$Y_{l,m} = \begin{cases} P_{lm}(\cos\phi) \cos m\lambda & m \geq 0 \\ P_{lm}(\cos\phi) \sin|m|\lambda & m < 0 \end{cases}$$

where  $T_{l,m}^h$  are the spherical harmonic coefficients of EGMs converted to the Helmert space [Vaníček et al., 1995; Najafi-Alamdari, 1996; Huang et al., 2000] and evaluated at the radius  $r$ ;  $GM$  is the standard gravitational parameter of Earth.  $P_{lm}$  is the fully normalized associated Legendre polynomial function of the degree  $l$  and order  $m$ . The residual Helmert gravity anomalies are:

$$\delta\Delta g^H(R, \Omega) = \Delta g^H(R, \Omega) - \Delta g_L^H(R, \Omega). \quad (1.27)$$

The Stokes kernel can be further modified to omits spherical harmonic bands (up to degree/order  $L$ ) is called “spheroidal” kernel. The spheroidal modified Stokes ( $S_{n>L}^*$ ) kernel is used to evaluate the residual co-geoidal heights using residual Helmert gravity anomalies, i.e., NZ contribution reads:

$$N_{l>L, \Omega'_0}^H(\Omega) = \frac{R}{4\pi\gamma_0(\phi)} \iint_{\Omega' \in \Omega_{\psi_0}} \delta\Delta g^H(R, \Omega') S_{n>L}^*(\psi_0, \psi(\Omega, \Omega')) d\Omega' \quad (1.28)$$



In Eq. (1.28) the subscript  $l > L, \Omega'_{\psi_0}$  indicates that the integration is performed over residual Helmert's gravity anomalies with frequencies higher than  $\delta\Delta g^H$  and limited to a cap size of  $\Omega'_{\psi_0}$ ,  $S_{n>L}^*$  is the modified spheroidal Stokes kernel with modification degree  $L$ . The FZ contribution ( $N_{l>L, \Omega'_0 - \Omega'_{\psi_0}}^h$ ) to residual co-geoidal heights is:

$$\begin{aligned} & N_{l>L, \Omega'_0 - \Omega'_{\psi_0}}^H(\Omega) \\ &= \frac{R}{4\pi\gamma_0(\phi)} \iint_{\Omega' \in \Omega'_0 - \Omega'_{\psi_0}} \delta\Delta g^H(R, \Omega') S_{n>L}(\psi_0, \psi(\Omega, \Omega')) d\Omega'. \end{aligned} \quad (1.29)$$

The residual co-geoidal heights ( $\delta N_{l>L}^H(\Omega)$ ) are then computed by adding the FZ to NZ contribution:

$$\delta N_{l>L}^H(\Omega) = N_{l>L, \Omega'_0}^H(\Omega) + N_{l>L, \Omega'_0 - \Omega'_{\psi_0}}^H(\Omega). \quad (1.30)$$

The reference spheroid of the same degree and order as the reference field ( $L$ ) is then added to residual co-geoidal heights to obtain geoidal heights in the Helmert space:

$$N^H(\Omega) = \delta\delta N_{l>L}^H(\Omega) + N_L^H(\Omega). \quad (1.31)$$

$N_L^H(\Omega)$  is the low frequency part of co-geoidal heights which is evaluated using spherical harmonic synthesis based on EGMs [Heiskanen and Moritz, 1967, Ch.2]:

$$N_L^H(\Omega) = \frac{GM}{r\gamma_0} \sum_{l=2}^L \left(\frac{R}{r}\right)^l \sum_{m=-l}^l T_{l,m}^h Y_{l,m}(\lambda, \phi). \quad (1.32)$$

Finally, the co-geoidal heights read:

$$N^H(\Omega) = \delta N^H(\Omega) + N_L^H(\Omega). \quad (1.33)$$

Based on this formulation, the contribution of the local terrestrial data is defined by the size of the integration cap ( $\psi_0$ ) and the contribution of the global data or EGMs is defined by the degree of the reference field/spheroid. For easier computation, the degree of the modification is usually chosen to be the same as the degree of reference field [Vaníček and Sjöberg, 1991]. To prevent the correlation between local terrestrial gravity data and gravity from EGMs, it is recommended to use satellite only EGMs to compute the reference field and FZ contribution [Foroughi et al., 2017a].

If the EGMs were able to represent the Earth's gravity field accurately enough ( $L$  going to infinity), there would not be any need for evaluating the NZ contribution, i.e. no terrestrial gravity measurements would be needed and therefore  $\psi_0$  would go to  $0^\circ$ . On the other hand, if there were not any EGMs available or they were not being reliable enough to be used in geoid determination, we would have to use the full integration cap ( $\psi_0 = 180^\circ$ ) using only terrestrial gravity data in evaluating the Stokes integral.

The reliability of EGMs (in comparison with terrestrial data) have been investigated by many studies for example Ellmann and Jürgenson [2008] evaluated the EIGEN-GL04c satellite-combined EGM [Förste et al., 2006] over the Baltic countries and reported that there are decimeter level discrepancies between the EGM derived geoidal heights and local models. Hirt et al. [2011] used terrestrial gravity data over Switzerland and Australia and astrogeodetic vertical deflections over Europe and Australia as ground-truth data sets and the full spectrum of EGM2008 [Pavlis et al., 2012] for GOCE model evaluation. Their comparison showed a few tens of mGal differences in terms of gravity data and a few

seconds difference in terms of the deflection of the vertical in some areas of their investigation. Huang and Véronneau [2009] evaluated the GRACE-based EGMs and Ince et al. [2012] investigated the accuracy of the GOCE-based EGMs over Canada. They both reported that the geoidal heights derived from EGMs have decimetre level differences from the Canadian gravimetric geoid model [Huang and Véronneau, 2013]. Bomfim et al. [2013] evaluated the GOCE gravity models with the terrestrial gravity data of Brazil and reported that EGMs should only be used where terrestrial gravity data are scarce. Karpik et al. [2016] compared the EGMs with the terrestrial gravity data in West Siberia and Kazakhstan and reported 70% of the EGM derived anomalies do not match the terrestrial data within a predefined limit. Foroughi et al. [2017c] compared terrestrial and marine gravity data with the gravity anomalies derived from the most recent EGMs over the territory of Iran. They showed that differences might go up to hundreds of mGal. Odera and Fukuda [2017] evaluated the GOCE-based EGMs with the free-air anomalies and geoidal heights of Japan and reported tens of mGal differences between the terrestrial data and EGM derived gravity anomalies. All these studies confirm that if terrestrial gravity data are available, they should not be replaced with EGMs for local geoid modelling.

The application of EGMs in geoid determination is only for filling the gaps in gravity data and to predict the gravity anomalies on grid points [Foroughi et al., 2015a] for removing the low frequency components of the Earth's gravity field [Vaniček et al., 1995], and for computing the FZ contribution to the modified Stokes integral [Vaniček and Kleusberg, 1987]. Speaking of the combination of terrestrial gravity data and EGMs, the optimal solution of the geoid is achieved if EGMs are used only up to the degree which is compatible with terrestrial data, i.e. the optimum degree of the EGMs should be found

when combining with terrestrial data. One way of assessing the compatibility is by checking the continuity between EGM derived gravity anomalies and terrestrial data when they are used to predict the grid anomalies. The other way is by comparing the gravimetric geoidal heights derived using different combinations of terrestrial and EGM data, with the geoidal heights derived from GNSS/Leveling points. The methodology of the latter is explained in Ch. 2.

### 1.2.3 Transferring back to real space

Condensing the topographical and atmospheric masses from the Earth's gravity field in transferring the data from the real space to the Helmert space, affects the shape and size of the geoid [Vaniček and Martinec, 1994; Vaniček et al., 1999]. The differences between gravity anomalies in real and Helmert space are computed by of DTE, DAE, SITE, (and DDE) where the corresponding differences in terms of geoidal heights can be computed by calculating the primary indirect topographical ( $\delta N^t$ ) and atmospheric ( $\delta N^a$ ) effects (PITE and PIAE) [Martinec 1993]:

$$\begin{aligned}\delta N^t(\Omega) &= \frac{V^{ct}(R, \Omega) - V^t(R, \Omega)}{\gamma_0(\Omega)} \\ \delta N^a(\Omega) &= \frac{V^{ca}(R, \Omega) - V^a(R, \Omega)}{\gamma_0(\Omega)}.\end{aligned}\tag{1.34}$$

Computation of the PITE and PIAE, like the DTE and SITE, requires the DTM of the computation area. If the anomalous density information is available, the primary indirect density effect (PIDE) should also be computed and applied for a more accurate transformation of the co-geoidal to geoidal heights [Novák, 2000; Tenzer et al., 2003].

The resulting geoidal height in real space is computed as:

$$N(\Omega) = N^H(\Omega) + \delta N^t(\Omega) + \delta N^a(\Omega) . \quad (1.35)$$

### 1.3 Rigorous Orthometric heights

As mentioned above, heights in the classical height system are called orthometric heights. The orthometric height of a point at the surface is defined as the distance between the geoid and the point measured along the plumb line (see Eq. (1.6) and (1.7)). Computing mean gravity through the integral in Eq. (1.7) requires measuring the actual gravity along the plumbline which is not economical. Helmert [1890] suggested approximating the mean gravity along the plumbline based on the Poincaré-Pray gradient which results in Helmert's orthometric height. According to the Poincaré-Pray theory, the mean value is derived by approximating the topography by the Bouguer plate and free-air gravity gradient at the point of interest, assuming the mass density of the plate to be constant and equal to mean topographic density [cf., Heiskanen and Moritz, 1967; Strang van Hees, 1992]. It was shown by Strang [1982] that mean gravity based on Helmert's approximation is very close to the actual mean gravity (from borehole gravimetry) and in most areas is accurate to better than 3cm. The Helmert orthometric height ( $H^{HO}(\Omega)$ ) is defined as [Heiskanen and Moritz, 1967, Ch. 4]:

$$H^{HO}(\Omega) = \frac{C(r_t, \Omega)}{g(r_t, \Omega) + (0.0424)H^o(\Omega)} . \quad (1.36)$$

The terrain geometry and density heterogeneity within the topography as well as the effect of masses below the geoid was disregarded in Helmert's definition of orthometric heights. Hayford and Bowie [1912], Niethammer [1932, 1939], and Mader [1954] were the first ones who took the terrain geometry into consideration by incorporating the mean planar terrain gravity correction. Niethammer calculated the terrain effects on gravity by averaging the gravity values at discrete points along the plumbline. Mader used only the average of the effects at the two end points of the plumbline, i.e. geoid and the Earth surface. The two methods give similar results but Niethammer was superior [Dennis and Featherstone, 2003]. Wirth [1990] modified the Niethammer method by means of computing the terrain potential difference (between the Earth surface and geoid) instead of the mean terrain gravity correction. Santos et al. [2006] developed Wirth's method by using an Earth gravity field decomposition to compute the effect of terrain on the conversion from the Helmert's to the rigorous orthometric heights. They reported that the terrain effect can go reach to a few decimeters in rough topography areas.

As mentioned above, Helmert's definition of orthometric heights disregards also the topographic density variations Strang [1982] showed that the errors of orthometric heights due to incorrectly modelling the topographic density might be as large as a decimetre for elevations higher than  $3000m$  and recommended applying a density correction to orthometric heights. There are studies discussing the effect of density variation on orthometric heights [Martinec, 1993; Vaniček et al., 1995; Allister and Featherstone, 2001; Huang et al., 2001; Tenzer and Vaniček, 2003; Dennis and Featherstone, 2003; Kingdon et al., 2005; Tenzer et al., 2005; Santos et al., 2006]. Some studies suggest using three-dimensional DDMs for computing the effect of density variations on the orthometric

heights, e.g., [Hwang and Hsiao,2003, Tenzer et al., 2005], but Kingdon et al. [2011] showed that the whole three-dimensional variation of topographical density is expected to have only a few centimetres effect on the orthometric heights which mainly is sensitive to laterally varying density rather vertical variations.

Apart from topographical effects on the orthometric heights, the effect of the remaining unmodelled, or non-topographical effects, can also be modeled using the NT geoid generated gravity disturbances [Vaníček et al., 2004]. The effect of non-topographical masses can improve the orthometric heights on the order of a few decimeters [Tenzer et al, 2005; Santos et al., 2006].

Tenzer et al. [2005] and Santos et al. [2006] have put all the above-mentioned effects together and formed a more complete definition of the orthometric heights called the rigorous orthometric heights. In their definition, the Earth gravity field is decomposed as follows:

$$g(r, \Omega) = \gamma(r, \Omega) + \delta g^{NT}(r, \Omega) + g^t(r, \Omega) + g^a(r, \Omega), \quad (1.37)$$

where  $\delta g^{NT}(r, \Omega)$  is the gravity disturbances generated by the masses below the geoid (No-Topography gravity disturbances); and  $g^t(r, \Omega)$  and  $g^a(r, \Omega)$  are the gravitational attraction of the topographical and atmospheric masses respectively. They further decomposed the topographical gravitational attraction into Bouguer and terrain (roughness) effects:

$$g^t(r, \Omega) = g^B(r, \Omega) + g^R(r, \Omega), \quad (1.38)$$

where  $g^B(r, \Omega)$  is the gravitational attraction of the Bouguer shell and  $g^R(r, \Omega)$  is the gravitational attraction of the terrain which is divided into the effect of mean density ( $g_\rho^R(r, \Omega)$ ) and of anomalous density ( $g_{\delta\rho}^R(r, \Omega)$ ):

$$g^R(r, \Omega) = g_\rho^R(r, \Omega) + g_{\delta\rho}^R(r, \Omega). \quad (1.39)$$

Other than the aforementioned effects, the more rigorous definition of the orthometric heights may account for the second order compensation of the normal gravity and Bouguer shell. These improve the orthometric heights only on the order of a few centimetres for the highest mountains [Santos et al., 2006].

#### 1.4 Congruency of the height system

The regional geoid, which is normally calculated using the gravimetric and topographic data is often called a gravimetric geoid. In this dissertation, the Stokes-Helmert method is used to determine the regional geoid. On the other hand, geoidal heights can be derived by subtracting the orthometric heights from geodetic heights at GNSS/Leveling points. At GNSS/Leveling points orthometric heights are available from spirit leveling observations and applying gravimetric corrections (see Sec.1.3) and geodetic heights that are available from GNSS observations. The GNSS/Leveling derived geoidal heights are used mostly to test the quality of the gravimetric geoidal heights against GNSS/Leveling points and are called “*test points*” in geoid determination approaches. Measuring the quality of a classical height system is intended in this dissertation. One way of measuring the quality of a classical height system (i.e. quality of the local geoid model and the orthometric heights) is assessing the self-consistency of the



system which can be done by measuring the *congruency*. Measuring the congruency means comparing the gravimetric geoidal heights to the GNSS/Leveling derived geoidal heights considered to be independent. If the congruency of the Molodensky height system is being assessed, i.e., assessing the accuracy of a quasigeoid model and normal heights, a similar procedure is used, except that normal heights of the GNSS/Leveling points are used instead of orthometric height.

The discrepancies ( $V$ ) of gravimetric geoidal heights and test geoidal heights read:

$$\forall i : V_i = N_i^{test} - N_i , \quad (1.40)$$

where  $N$  are the gravimetric geoidal heights and  $N_i^{test}$  are the GNSS/Leveling derived geoidal heights:

$$\forall i : N_i^{test} = h_i - H_i^O . \quad (1.41)$$

The congruency of the height system can be measured by  $L_2$  of the discrepancies  $V$  in Eq. (1.40) which reads:

$$\hat{\sigma}_V^2 = \frac{V^T P V}{n} , \quad (1.42)$$

where  $n$  is the number of test points, and  $P$  is the weight matrix defined as:

$$P = \sigma_V^2 (C_N + C_{N^{test}})^{-1} , \quad (1.43)$$

where  $C_N$  and  $C_{N^{test}}$  are the covariance matrices of the gravimetric (predicted at the test points) and GNSS/Leveling derived geoidal heights, and  $\sigma_V^2$  is the *a priori* variance factor computed as follows:

$$\sigma_V^2 = \sigma_N^2 + \sigma_{N^{test}}^2, \quad (1.44)$$

where  $\sigma_N$  and  $\sigma_{N^{test}}$  are the estimated mean standard deviations (uncertainties) of the gravimetric geoid and GNSS/Leveling derived geoidal heights at test points. Using Eq. (1.41), the *a priori* mean STD of the test geoidal heights,  $\sigma_{N^{test}}$ , reads:

$$\sigma_{N^{test}}^2 = \sigma_h^2 + \sigma_{H^o}^2, \quad (1.45)$$

where  $\sigma_h$  and  $\sigma_{H^o}$  are the estimated STD of the geodetic and orthometric heights, estimated from spirit leveling on the GNSS/Leveling points. These values (or at least a rough estimation of them) are usually given by the providers with the test data-set [Duquenne, 2007].

Estimation of the *a priori* mean STD of the gravimetric geoidal heights at test points, i.e.,  $\sigma_N$  in Eq. (1.44), is a more complicated task. Determination of the geoidal heights using the Stokes-Helmert method needs a combination of both the gravimetric and topographic data. This means the uncertainties of each data set must be propagated into the steps of the Stokes-Helmert approach (cf., Ch. 5) to get an estimate of the uncertainties of the final geoidal heights.

Estimation of the accuracy of the quasigeoidal heights, i.e., height anomalies, using gravimetric and topographic data has been extensively investigated by many articles

[Filmer et al., 2014; Godah et al., 2014; Trojanowicz, 2015; Flury and Rummel, 2009; Ha Minh Hoa, 2017; Farahani et al., 2017; Featherstone et al., 2018]. Estimation of the accuracy of the geoidal heights has been less thoroughly studied, e.g., the uncertainties of the geoidal heights, derived by the Stokes-Helmert, were first estimated by Najafi-Alamdari et al. [1999]. At the time of their investigation, the DWC step was not utilized in their computation. The accuracy of the gravimetric geoidal heights in Canada was estimated by Huang and Véronneau [2013] by considering the noises in the ground gravity data and EGMs as the sources of error in evaluation of the Stokes integral. The propagation of uncertainties in the DWC step, i.e., estimation of the uncertainties of the gravity anomalies on the geoid, was neglected in their study too.

If the uncertainties of the components of Eq. (1.40), i.e. gravimetric and test geoidal heights, are not available, the weight matrix ( $P$  in Eq. (1.42)) can be equal to the identity matrix. In this case Eq. (1.42) may be written in a more simplified and well-known form:

$$\sigma_V^2 = \|\mathbf{V}\|_2 = \|\mathbf{N}^{test} - \mathbf{N}\|_2, \quad (1.46)$$

Equation (1.46) is a well-known formula for measuring the congruency of the height system and is usually considered as the Root Mean Square Error (RMSE) of the fit of the geoid model and is used to demonstrate the accuracy of the determined gravimetric geoid.

To best measure the congruency of the classical height system, all the corrections for computing the gravimetric geoidal height and GNSS/Leveling derived geoidal heights must be applied correctly. Although, some of these corrections might only make small change to the value of congruency, they must be applied as they provide the most accurate

solution possible [Foroughi et al., 2017b]. Sjöberg [2018] used the so call term “*topographic bias*” to show that topographic density variation have the same effect, but with opposite sign, on the gravimetric geoidal heights and orthometric heights computed at the GNSS/Leveling points, therefore a better congruency cannot be achieved by applying these types of corrections. However, the topographic density variation is differently taken into in the Stokes-Helmert method than what is investigated in Sjöberg [2018]. First DDM is computed when transferring the gravity anomalies to the Helmert’s space and they are downward continued to the geoid level. After performing the Stokes integral, the PIDE effect is added when transferring back to the real space. The effect of Poisson downward continuation was disregarded in the study done by Sjöberg [2018] and therefore their conclusion is not applicable in this dissertation.

## **1.5 Test data set**

The test data set used throughout this dissertation refers to a location in the centre of France. This data-set was introduced by the Institut Géographique National (IGN) and was meant to be used to evaluate various geoid and quasigeoid determination techniques (see, Figure 1.4) [Duquenne, 2007]. Topographically and geologically, this area is complex; it contains about 60 remarkably fresh volcanoes of so-called “Chaîne des Puys” which covers a significant portion of the large upland area in the southern half of central France [Nowell, 2008]. There are also high mountains (Alps) on the eastern part, which reach up to above 4000m and almost flat areas in the middle and western parts (see Figure 1.5 ).

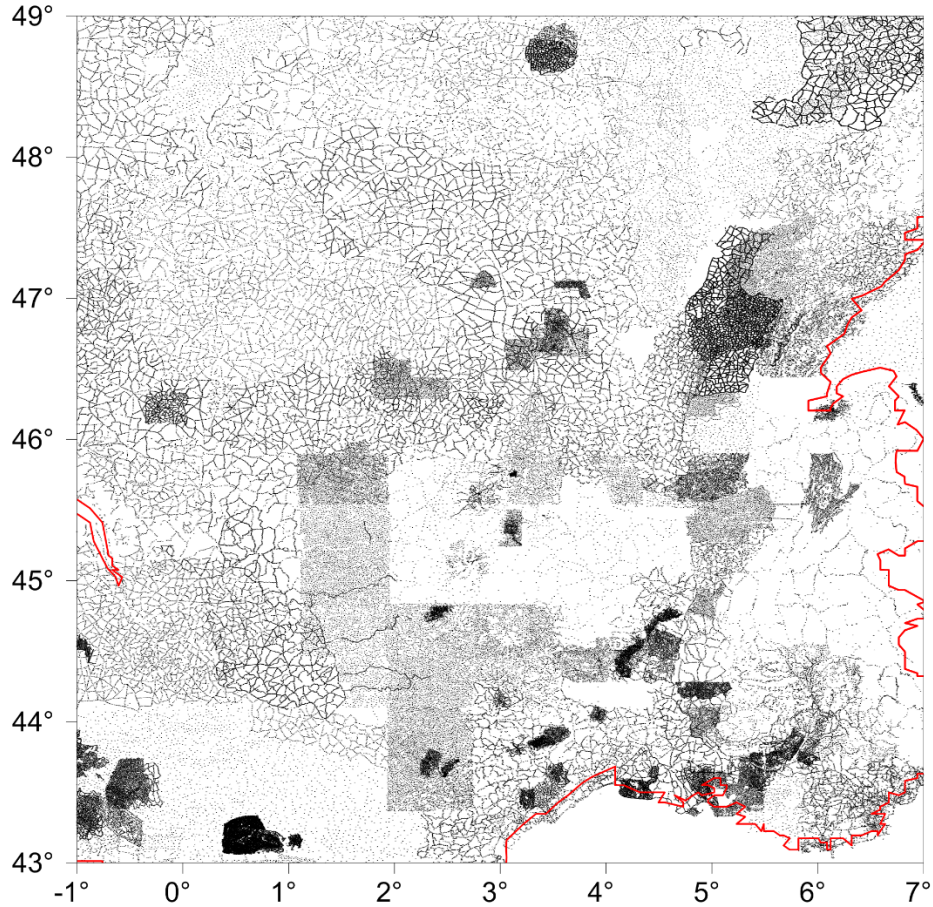


Figure 1.4: Distribution of the terrestrial gravity data in Auvergne

Gravity data coverage is limited to an area between  $-1^\circ < \lambda < 7^\circ$ ,  $43^\circ < \varphi < 49^\circ$  and contains 240000 terrestrial gravity observations extracted from the database of the Bureau Gravimétrique International, supplied by the Bureau de Recherches Géologiques et Minières for the French territory. Distribution of the terrestrial gravity data is shown in Figure 1.4. The stated standard deviation of the gravity values is between  $0.25 - 0.75 mGal$  [Duquenne, 2007]. There are 75 GNSS/Leveling points regularly distributed in the central area ( $1.5^\circ < \lambda < 4.5^\circ$ ,  $45^\circ < \varphi < 47^\circ$ ) given in the RGF93 reference frame. The STD of the geodetic heights at GNSS/Leveling points is between  $2 - 3 cm$ . Another set of 558 GNSS/Leveling points were provided again by IGN within the area of  $1.5^\circ <$

$\lambda < 4.5^\circ$ ,  $44.5^\circ < \varphi < 47.5^\circ$  which were not included in the original data-set. Most of these points are located in the middle and west parts which are flat areas (cf., Ch. 4).

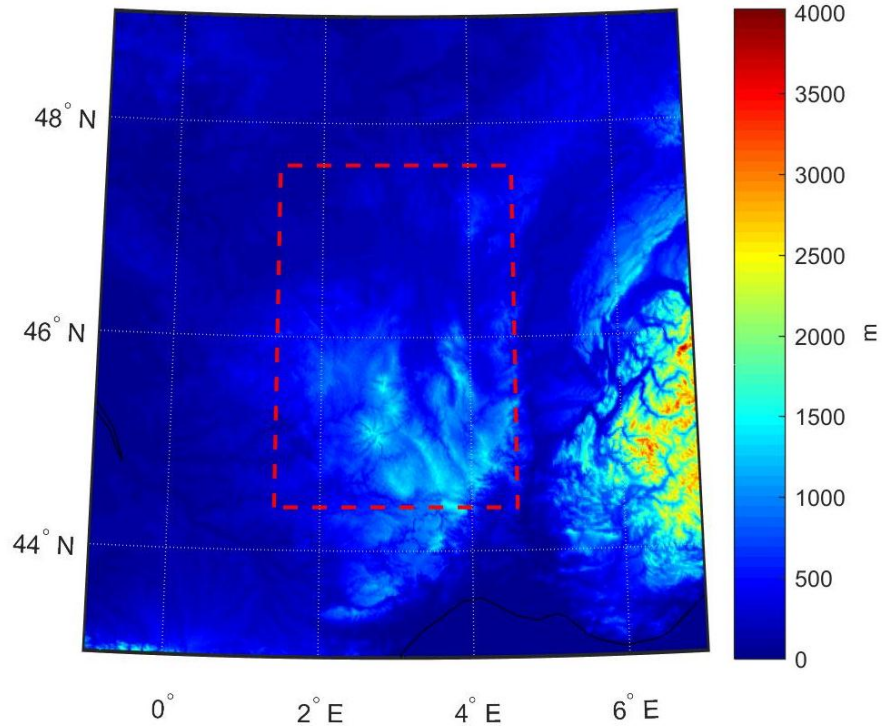


Figure 1.5: Topography of Auvergne, dashed-lines show the geoid computation area

The primary quasigeoid result for Auvergne was computed by Duquenne [2007] using the GRAVSOFTE package [Tscherning et al., 1992] and was compared against the height anomalies derived at 75 GNSS/Leveling points. Later Ågren et al. [2009] computed different quasigeoid models using: least-squares modification of Stokes (LSMS) method [Sjöberg, 2003], least-square collocation (LSC) method [Tscherning et al., 1992], fast collocation approach [Bottoni and Barzaghi, 1993], and spherical fast Fourier transform (FFT) method [Forsberg and Sideris, 1993]. The first geoid model of the area was

computed by Janák et al. [2017] using the Stokes-Helmert approach. Statistics of the comparison between gravimetric quasigeoid and geoid model with height anomalies and geoidal heights at GNSS/Leveling points are summarized in Table 1.1.

Table 1.1: Statistics of comparison of the primary geoid and quasigeoid results with GNSS/Leveling points

<b>METHOD</b>	<b>MODEL</b>	<b>MAX [M]</b>	<b>MIN [M]</b>	<b>MEAN [M]</b>	<b>STD [M]</b>
<b>LSMS</b>	Quasigeoid	0.09	-0.08	0.00	0.03
<b>LSC</b>	Quasigeoid	0.19	-0.25	0.00	0.08
<b>1D FFT</b>	Quasigeoid	0.01	-0.06	0.00	0.04
<b>DUQUENNE [2007]</b>	Quasigeoid	0.07	-0.11	0.00	0.04
<b>STOKES-HELMERT</b>	Geoid	0.22	0.02	0.13	0.03

The mean value of the residuals of all quasigeoid models in Table 1.1 is zero as the one-parameter fitting surface is usually applied to all gravimetric quasigeoid models and therefore the mean value is removed. However, this value is available from the computed geoid model by Janak et al. [2017] and it may be considered as the effect of sea surface topography (SST) on the GNSS/Leveling points [Rülke, et al. 2012].

## 1.6 Importance of articles included

Assessing the quality of the classical height system through its accuracy is the focus of this dissertation. This assessment may be done by measuring the congruency or self-consistency of the height system. The classical height system consists of an equipotential surface, i.e. geoid, and defines the height above this surface as the distance from geoid to points on the Earth surface along the plumbline, i.e. orthometric heights. Measuring the congruency means measuring the self-consistency between geoid and orthometric heights

above it. The components involved in this comparison are: gravimetric geoidal heights predicted at the location of test points, geodetic heights derived from GNSS observations, and orthometric heights provided by spirit leveling along with gravimetric corrections. GNSS/Leveling points are mostly considered as the benchmarks of national vertical networks and therefore the heights on these points need to be provided to a high accuracy (e.g., *mm* level) because the accuracy of other points is related to the accuracy of these benchmarks. To best measure the congruency, its components must be computed as accurately as possible, along with the covariance matrices indicating their uncertainties. There are four articles included in this dissertation, two of which are related to the determination of the geoid model in a conventional way, one which discusses the computation of orthometric heights, and one which estimates the uncertainties of the gravimetric geoidal heights.

### **1.6.1 Articles related to geoid model**

With the advent of satellite gravity missions and accessibility of more terrestrial gravity data across the world, higher orders of EGMs are available and may be used in determining the local geoid. The local geoid model is computed using both global (EGM) and local (gravity observations) data. Maximum degree and order of the EGMs specify the contribution of satellite gravity data and the Stokes integration cap size is used to specify the contribution of the local data. Generally, there are two types of EGMs available: satellite-only and satellite-combined. The satellite-only EGMs are computed using only the satellite data whereas the data used in computing harmonic coefficients of satellite-combined models are both satellite and terrestrial gravity data. To prevent the use of the same data twice, satellite only models are suggested for the computation of regional



geoids. Theoretically, if EGMs were able to represent the Earth gravity field up to infinite degree and order, there would not be any need for evaluating the Stokes integral (i.e. using local terrestrial data) and the geoid model could be computed using harmonic coefficients of the EGMs. If, on the other hand, EGMs were of poor quality, we would have to disregard them and use terrestrial gravity data from the whole world. Both EGMs and local gravity data are burdened with position-dependent noise, the way of optimally combining EGMs and local data may vary from place to place. The article “Optimal combination of satellite and terrestrial gravity data for regional geoid determination using Stokes-Helmert’s method, the Auvergne test case” [Foroughi et al., 2017a], comprising chapter 2 of this dissertation, proposes a numerical method for finding the optimal combination of EGMs with local gravity data. The optimal solution is found by comparing the geoid models, computed using different combinations, with test geoidal heights. The proposed methodology was tested for Auvergne data. This article was presented at the International Association of Geodesy (IAG) meeting: “1<sup>st</sup> joint commission 2 and IGFS meeting on Gravity, Geoid, and height systems” in Thessaloniki, Greece. The full text of this article is published in the Proceedings of the conference.

Chapter 3, “Computation of precise geoid model of Auvergne using current UNB Stokes-Helmert’s approach” [Janak et al., 2017], an article published in “*Contributions to Geophysics and Geodesy*” investigates more thoroughly the method proposed in [Foroughi et al., 2017a] and presents all the numerical values obtained. The geoid model of Auvergne, for the first time, was computed in this article and all the computation steps were described in detail. The effect of laterally varying anomalous density on gravity anomalies, derived from a superficial geological model of Auvergne [Bodelle et al., 1980],

was also computed on gravity anomalies when transferring to the Helmert space and also for geoidal heights when transferring back from the Helmert space to the real space.

### **1.6.2 The article dealing with orthometric height**

Chapter 3, “In defense of the classical height system” [Foroughi et al., 2017b] is an article published in the “*Geophysical Journal International*”, it discusses the computation of the rigorous orthometric heights on the GNSS/Leveling control points of Auvergne. Besides the 75 GNSS/leveling points introduced by Duquenne [2007], another set of 558 points were provided by IGN which do not coincide with the previous 75 points. Rigorous orthometric heights were computed at these points using the methodology proposed by Santos et al. [2006]. A comparison between the Molodensky and classical height system was also performed for this article. The congruency of each system was measured using the quasigeoid/geoidal heights, normal/rigorous orthometric heights, and geodetic heights available at the test points. The Molodensky claim [Molodensky et al., 1960] that the classical height system cannot be used due to the lack of topographical density knowledge, it was shown that even using low-resolution density varying data (derived from superficial geological maps), the classical height system is as congruent as Molodensky system. The advantages of the use of rigorous orthometric heights instead of Helmert orthometric heights were also discussed in this article.

### **1.6.3 The article related to the quality of the classical height system**

Downward continuation of anomalies in a harmonic space in the Stokes-Helmert method is done using a physically rigorous approach; i.e., using Poisson’s integral equation, which is a Fredholm integral equation of the 1<sup>st</sup> kind [Vaníček et al., 1996]. The

Poisson DWC is a physically well-posed problem but depending on the discretization step size and roughness of topography in the area, it can have a numerically unstable solution. Iterative approaches were suggested for DWC of gravity anomalies with grid resolution finer than 2' [Kingdon and Vaníček, 2010]. It was shown by Vaníček et al. [2017] that, if DWC is being sought iteratively, seeking the exact solution requires many iterations, and it makes no sense to seek such a solution which is marred with high-frequency noise which reflects observation noise as well as irregular distribution of surface gravity data rather than the behavior of the gravity field. In fact, DWC magnifies the existing noise of the surface gravity data into estimated gravity anomalies on the geoid [Vaníček et al., 2017]. They suggested seeking the most probable solution rather the exact solution which can be achieved by using a least squares (LS) technique. This method is called LS DWC and introduced in the article “Sub-Centimetre geoid” [Foroughi et al., 2018] published in the *Journal of Geodesy* and represented here in Chapter 4 of this dissertation. As a result of LS DWC, the covariance matrix of the gravity anomalies on the geoid can be computed and used for estimating the uncertainties of the gravimetric geoidal heights. The sources of uncertainty in geoidal height are uncertainties in EGMs, in gravity observations, in topographic heights, and in topographic mass density. The estimated covariance matrix of the Helmert gravity anomalies on the geoid, resulting from the LS DWC process, reflects the existing random errors in the input gravity data, e.g., the effect of the reference field (removed from gravity at the surface), topographic heights and mass density variations (needed for conversion to Helmert’s space; and back to the real space, i.e., for evaluation of DTE, SITE and PITE), and observation errors. The findings of Foroughi et al. [2018] show that the estimated final accuracy of the gravity anomalies on the geoid depends

mostly on the spatial distribution and elevation of gravity observations rather than on the a priori observation errors; using different a priori values for observation errors would not change the estimated covariance matrix of geoid gravity anomalies too much. It was mentioned in Sec.1.4 that to measure the congruency of the classical height system the best, the uncertainties of each component must be known, i.e., the uncertainties of the gravimetric geoidal, orthometric, and geodetic heights. Using the LS DWC, the estimated uncertainties of the gravity anomalies on the geoid can be used to propagate the observation errors through the Stokes integral. Having the uncertainties of the geoidal heights can help to evaluate the congruency of the classical height system in Eq. (1.42) however, uncertainties of geodetic and orthometric heights are also required and can usually be estimated using the observation errors available from the data providers. The estimation of uncertainty of the geoidal heights using the LS DWC method is discussed in detail in chapter 5.

## 1.7 References

- Ågren, J., & Sjöberg, L. (2014). Investigation of Gravity Data Requirements for a 5 mm-Quasigeoid Model over Sweden. *Gravity, Geoid and Height Systems. International Association of Geodesy Symposia.*
- Ågren, J., Barzaghi, R., Carrion, D., Denker, H., Grigoriadis, V., Kiamehr, R., Sona, G., Tscherning, C.C., Tziavos, I. N., Tziavos, I. (2009). Different geoid computation methods applied on a test dataset: results and considerations. *VII Hotine-Marussi Symposium on Mathematical Geodesy.* Rome, Italy.

- Allister, N., & Featherstone, W. (2001). Estimation of Helmert orthometric heights using digital barcode levelling, observed gravity and topographic mass-density data over part of Darling Scarp, Western Australia. *Geomatic Research Australia*, 75, 25-52.
- Amos, M., & Featherstone, W. (2009). Unification of New zeland local vertical datums, iterative gravimetric quasigeoid computations. *Journal of Geodesy*, 83(1), 57-68.
- Bajracharya, S. (2003). *Terrain effect in geoid determination*. Calgary: University of Calgary.
- Bamford, G. (1980). *Geodesy*. Oxford University Press.
- Bayoud, F., & Sideris, M. (2003). Two different methodologies for geoid determination from ground and airborne gravity data. *Geophysical Journal International*, 155(3), 914-922.
- Bodelle, A., & et al. (1980). Carte g´eologique de la France et de la marge continentale, 1:1500 000, 1978-1979.
- Bomfim, E., Braitenberg, C., & Molina, E. (2013). Mutual evaluation of global gravity models (EGM2008 and GOCE) and terrestrial data in Amazon Basin, Brazil. *Geophysical Journal International*, 195(2), 870-882.
- Bottoni, G., & Barzagli, R. (1993). Fast collocation. *Bulletin Geodesque*, 67(2), 119-126.
- Dennis, M., & Featherstone, W. (2003). Evaluation of orthometric and related height systems using a simulated mountain gravity field. *Tziavos IN (ed) 3rd meeting of*

*the International Gravity and Geoid 2002 Dept of Surv and Geodesy. Aristotle University of Thessaloniki*, (pp. 389-394). Thessaloniki.

Duquenne, H. (2007). A data set to test geoid computation methods. Istanbul: First international Symposium of the international gravity field services(IGFS).

Ellmann, A., & Jürgenson, H. (2008). Evaluation of a GRACE-based combined geopotential model over the Baltic countries. *Geodezija ir Kartografija*, 34(2), 35-44.

Ellmann, A., & Vaniček, P. (2007). UNB application of Stokes-Helmert's approach to geoid computation. *Journal of Geodynamics*, 43, 200-213.

Farahani, H., Klees, R., & Slobbe, C. (2017). Data requirements for a 5-mm quasi-geoid in the Netherlands. *Studia Geophysica et Geodetica*, 61(4), 675-702.

Featherstone, W., & Kuhn, M. (2006). Height systems and vertical datums: A review in the Australian context. *Journal of Spatial Sciences*(1), 21-41.

Featherstone, W., & Sproule, D. (2006). Fitting AusGeoid98 to the Australian height datum using GPS-leveling and least squares collocation: application of a cross-validation technique. *Survey Review*, 38(301), 573-582.

Featherstone, W., McCubbine, J., Brown, N., Claessens, S., Filmer, M., & Kirby, J. (2018). The first Australian gravimetric quasigeoid model with location-specific uncertainty estimates. *Journal of Geodesy*, 92(2), 149-168.

Fedi, M., & Florio, G. (2002). A stable downward continuation by using the ISVD method. *Geophysical Journal International*, 151(1), 146-156.

- Ferreira, V., & de Freitas, S. (2012). An attempt to link the Brazilian Height System to a World Height System. *Boletim de Ciências Geodésicas*, 18, 363-377.
- Filmer, M., Featherstone, W., & Claessens, S. (2014). Variance component estimation uncertainty for unbalanced data: application to a continent-wide vertical datum. *Journal of Geodesy*, 88(11), 1081-1093.
- Filmer, M., Featherstone, W., & Kuhn, M. (2010). The effect of EGM2008-based normal, normal-orthometric and Helmert orthometric height systems on the Australian levelling network. *Journal of Geodesy*, 84(8), 501-513.
- Flury, J., & Rummel, R. (2009). On the geoid-quasigeoid separation in mountain areas. *Journal of Geodesy*, 83, 829-847.
- Foroughi, I., Afrasteh, Y., Ramouz, S., & Safari, A. (2017c). Local Evaluation of Earth Gravitational Models, case study: Iran. *Geodesy and Cartography*, 43(1), 1-13.
- Foroughi, I., Janak, J., William Kingdon, R., Sheng, M., C. Santos, M., & Vaníček, P. (2015). Illustration of How Satellite Global Field Should be Treated in Regional Precise Geoid Modelling (Padding of Terrestrial Gravity Data to Improve Stokes-Helmert Geoid Computation). *The EGU General Assembly*. Vienna.
- Foroughi, I., Sheng, M., Kingdon, R., Huang, J., Martinec, Z., Vaníček, P., & Santos, M. (2015). The effect of lateral topographical density variations on the geoid in Auvergne. *26th IUGG General Assembly*. Prague, Czech Republic.

- Foroughi, I., Vaníček, P., Kingdon, R., Novak, P., Sheng, M., & Santos, M. (2016). Poisson downward continuation of scattered Helmert's gravity anomalies to mean values on a raster on the geoid using least squares. *EGU*. Vienna, Austria.
- Foroughi, I., Vaníček, P., Novák, P., Kingdon, R., Sheng, M., & Santos, M. (2017a). Optimal combination of satellite and terrestrial gravity data for regional geoid determination using Stokes-Helmert's method. *International Association of Geodesy Symposia*. Berlin: Heidelberg. doi:10.1007/1345\_2017\_22.
- Foroughi, I., Vaníček, P., Sheng, M., Kingdon, R. W., Santos, M.C. (2017b) In defense of the classical height system, *Geophysical Journal International*, Volume 211, Issue 2, 1 November 2017, Pages 1154–1161, <https://doi.org/10.1093/gji/ggx366>.
- Forsberg, R., & Sideris, M. (1993). Co-geoid computations by the multiband spherical FFT approach. *Manuscripta Geodaetica*, 18, 82-90.
- Förste, C., Flechtner, F., Schmidt, R., König, R., Meyer, U., Stubenvoll, R., Rothacher, M., Barthelmes, F., Neumayer, H., Biancalse, R., Bruinsma, S., Lemoine, J. (2006). A mean global gravity field model from the combination of satellite mission and altimetry/gravimetry surface data - EIGEN-GL04C. *EGU-A-03462*. Vienna, Austria.
- Godah, W., Szelachowska, M., & Krynski, J. (2014). Accuracy assessment of GOCE-based geopotential models and their use for modelling the gravimetric quasigeoid - A case study for Poland. *Geodesy and cartography*, 63(1), 3-24.



- Goli, M., & Najafi-Alamdari, M. (2011). Planar, spherical and ellipsoidal approximations of Poisson's integral in near zone. *Journal of Geodetic Science*, 1(1), 17-24.
- Goli, M., Foroughi, I., & Novák, P. (2018). On a parameter choice for stopping iteration solutions of gravity downward continuation. *Canadian Journal of Earth Sciences*. doi:10.1139/cjes-2017-0208
- Goli, M., Najafi-Alamdari, M., & Vaníček, P. (2011). Numerical behaviour of the downward continuation of gravity anomalies. *Studia Geophysica et Geodaetica*, 55, 191-202.
- Ha Minh Hoa. (2017). Improvement of the accuracy of the quasigeoid model VIGAC2017. *Vietnam Journal of Earth Sciences*, 40(1), 39-46.
- Hadamard, J. (1923). *Lectures on the Cauchy Problem in Linear Partial Differential Equations*. New Haven: Yale University Press.
- Hayford, J., & Bowie, W. (1912). *The effect of topography and isostatic compensation upon the intensity of gravity*. Washington, U.S.A: United States Coast and Geodetic Survey, Government printing office.
- Heck, B. (1995). *Rechenverfahren und Auswertemodelle der Landesvermessung*. Heidelberg: Herbert Wichmann Verlag.
- Heiskanen, W., & Moritz, H. (1967). *Physical Geodesy*. San Francisco: W.H. Freeman and Co.
- Helmert, F. (1884). *Die mathematischen und physikalischen Theorien der höheren*. Technical report, leipzig.

- Hirt, C., Gruber, T., & Featherstone, W. (2011). Evaluation of the first GOCE static gravity field models using terrestrial gravity, vertical deflections and EGM2008 quasigeoid heights. *Journal of Geodesy*, 85(10), 723-740.
- Huang, J. (2002). *Computational Methods for the Discrete Downward Continuation of the Earth Gravity and Effects of Lateral Topographical Mass Density Variation on gravity and The Geoid*. Fredericton: University of New Brunswick.
- Huang, J., & Véronneau, M. (2005). Application of downward continuation in gravimetric geoid modelling: case studies in Western Canada. *Journal of Geodesy*, 79, 135-145.
- Huang, J., & Véronneau, M. (2009). Evaluation of the GRACE-based global gravity models in Canada. *Newton's Bulletin*, 4, 66-72.
- Huang, J., & Véronneau, M. (2013). Canadian gravimetric geoid model 2010. *Journal of Geodesy*, 87(8), 771-790.
- Huang, J., Sideris, M., Vaníček, P., & Tziavos, I. (2003). Numerical investigation of Downward Continuation Techniques for Gravity Anomalies. *Bollettino Di Geodesia E Scienze Affini*, LXII(1), 33-48.
- Huang, J., Sideris, M., Vaníček, P., & Tziavos, I. (2003). Numerical investigation of downward continuation techniques for gravity anomalies. *Bollettino di Geodesia e Scienze Affini*, LXII,, 1, 33-48.

- Huang, J., Vaníček, P., & Novak, P. (2000). An alternative algorithm to FFT for the numerical evaluation of Stokes's integral. *Studia Geophysica et Geodetica*, 44, 374-380.
- Huang, J., Vaníček, P., Pagiatakis, S., & Brink, W. (2001). Effect of topographical mass density variation on gravity and the geoid in the Canadian Rocky mountains. *Journal of Geodesy*, 74(11-12), 805-815.
- Hwang, C., & Hsiao, Y. (2003). Orthometric height corrections from leveling, gravity, density and elevation data: a case study in Taiwan. *Journal of Geodesy*, 77(5-6), 292-302.
- Ince, E., Sideris, M., Hunag, J., & Véronneau, M. (2012). Assessment of the GOCE-Based Global Gravity Models in Canada. *Geomatica*, 66(2), 125-140.
- Janák, J., & Vaníček, P. (2005). Mean Free-Air gravity anomalies in the mountains. *Studia Geophysica et Geodetica*, 49(1), 31-42.
- Janák, J., Vaníček, P., Foroughi, I., Kingdon, R., Sheng, M., & Santos, M. (2017). Computation of precise geoid model using UNB Stokes-Helmert's approach: Case study in Auvergne region. *Contribution to geodesy and geophysics*, 47(3), 201-229.
- Karpik, A., Kanushin, V., Ganagina, I., Goldobin, D., Kosarev, N., & Kosareva, M. (2016). valuation of recent Earth's global gravity field models with terrestrial gravity data. *Contributions to Geophysics and Geodesy*, 46(1), 1-11.

- Kassim, F. (1980). *An evaluation of three techniques for the prediction of gravity anomalies in Canada*. Fredericton: University of New Brunswick.
- Kellogg, O. (1929). *Foundation of potential theory*. Berlin Heidelberg New York: Springer.
- Kingdon, R., & Vaníček, P. (2010). Poisson Downward Continuation Solution by the Jacobi Method. *Journal of Geodetic Science*, 1, 74-81.
- Kingdon, R., Vaníček, P., & Santos, M. (2011). Effects of hypothetical complex mass-density distributions on geoidal heights. *Geodesy for planet Earth*. 139. International Association of Geodesy symposia series.
- Kingdon, R., Vaníček, P., Santos, M., Ellmann, A., & Tenzer, R. (2005). Toward improved orthometric height system for Canada. *Geomatica*, 59, 241-249.
- Klees, R., Tenzer, R., Prutkin, I., & Wittwer, T. (2008). A data-driven approach to local gravity field modelling using spherical radial basis functions. *Journal of Geodesy*, 82(8), 457-471.
- Krikstaponis, B., Parseliunas, E., Petroskevicius, P., Putrimas, R., Urbanas, S., & Zakarevicius, A. (2007). Realization of the Vertical Datum and Height System of Lithuania. *Harita Dergisi*, 142-147.
- Kühtreiber, N. (1998). Precise geoid determination using a density variation model. *Physics and Chemistry of the Earth*, 23(1), 59-63.
- Li, J., Shen, W., & Zhou, X. (2015). Direct regional quasi-geoid determination using EGM2008 and DEM: A case study for Mainland China and its vicinity areas. *Geodesy and Geodynamics*, 6(6), 437-443.

- Lysaker, D., Petterson, B., & Mathisen, O. (2006). The Norwegian Height System NN1954 Revisited. *Nordic Journal of Surveying and Real Estate Research*, 3(1), 7-19.
- MacMillan, W. (1930). *The theory of potential*. New York: Dover Publication .
- Mader, K. (1954). *Die orthometrische Schwerekorrektion des Präzisions-Nivellements*. Vienna: Österreichische Zeitschrift für Vermessungswesen,.
- Martinec, Z. (1993). *Effect of lateral density variations of topographical masses in improving geoid model accuracy over Canada*. Ottawa: Research Report for Geodetic Survey of Canada.
- Martinec, Z. (1996). Stability investigation of a discrete downward continuation problem for geoid determination in the Candian Rocky Mountains. *Journal of geodesy*, 70, 805-828.
- Martinec, Z., Vaníček, P., Mainville, A., & Véronneau, M. (1996). Evaluation of topographical effects in precise geoid computation from density sampled heights. *Journal of Geodesy*, 20, 193-203.
- Molodenskiĭ, M., Yeremeev, V., & Yurkina, M. (1960). *Methods for Study of the External Gravitational Field and Figure of the Earth*. Moscow.: TRUDY TsNIIGAiK, 131, Geodezizdat.
- Moritz, H. (1980). *Advanced Physical Geodesy*. Michigan: Wichmann.
- Moritz, H. (2000). Geodetic Reference System 1980. *Journal of Geodesy*, 74(1), 128-162.

- Najafi-Alamdari, M. (1996). *Contributions towards the computation of a precise regional geoid*. Fredericton: University of New Brunswick.
- Najafi-Alamdari, M., Vaníček, P., Ong, P., & Craymer, M. (1999). Accuracy of a regional geoid. *Geomatica*, 53(3), 297-305.
- Niethammer, T. (1932). *Nivellement und Schwere als Mittel zur Berechnung wahrer*. Berne: Schweizerische Geodätische Kommission.
- Niethammer, T. (1939). Das astronomische Nivellement im Meridian des St Gotthard, Part II, Die berechneten Geoiderhebungen und der Verlauf des Geoidschnittes. *Astronomisch-Geodätische Arbeiten in der Schweiz*, 20, Swiss Geodetic Commission.
- Novák, P. (2000). *Evaluation of gravity data for the Stokes-Helmert solution to the geodetic boundary-value problem*,. University of New Brunswick, Geodesy and Geomatics Engineering. Fredericton: Technical Report No. 207.
- Novák, P. (2000). *Evaluation of gravity data fro Stokes-Helmert solution to the geodetic boundary-value problem*. Fredericton, Canada: University of New Brunswick.
- Nowell, D. (2008). The Chaîne des Puys volcanoes of the Auvergne, France. *Geology Today*, 24(6), 231-238.
- Odera, P., & Fukuda, Y. (2017). Evaluation of GOCE-based global gravity field models over Japan after the full mission using free-air gravity anomalies and geoid undulations. *Earth, Planets and Space*, 69:135.

- Parks, W., & Milbert, D. (1995). A Geoid Height Model for San Diego County, California, to Test the Effect of Densifying Gravity Measurements on Accuracy of GPS Derived Orthometric Heights. *Surveying and Land Information Systems*, 55(1), 21-38.
- Pavlis, N., Holmes, S., Kenyon, S., & Factor, J. (2012). The development and evaluation of the Earth Gravitational Model 2008 (EGM2008). *Journal of Geophysical research*, 117(B4), 1-38. doi:10.1029/2011JB008916
- Rapp, R. (1961). *The orthometric height*. Columbus, U.S.A: Department of GEodetic Science, Ohio State Univeristy .
- Rülke, A., Liebsch, G., Sacher, M., Schäfer, U., Schirmer, U., & Ihde, J. (2012). Unification of European height system realizations. *Journal of Geodetic Science*, 2, 343-354.
- Saadat, A., Safari, A., & Needell, D. (2017). IRG206: RBF-based regional geoid model of Iran. *Studia Geophysica et Geodetica*. doi:10.1007/s11200-016-0679-x
- Santos, M., Vaníček, P., Featherstone, W., Kingdon, R., Ellmann, A., Martin, B.-A., . . . Tenzer, R. (2006). The relation between rigorous and helmert's definition of orthometric heights. *Journal of Geodesy*, 80(12), 691–704.
- Sjöberg, L. (2003). general model for modifying Stokes' formula and its least-square solution. *Journal of Geodesy*, 77(7), 459:464.
- Sjoberg, L. (2010). A strict formula for geoid-to-quasigeoid separation. *Journal of Geodesy*, 84, 699-702.

- Steinberg, G., & Papo, H. (1998). Ellipsoidal heights: the future of vertical geodetic control. *GPS world*, 9(2), 41-43.
- Stokes, G. (1849). *On the variation of gravity at the surface of the Earth*. Cambridge University Press.
- Strang van Hees, G. (1992). Practical formulas for the computation of the orthometric, dynamic and normal heights. *Zeitschrift für Vermessungswesen*, 117(11), 727-734.
- Strange, W. (1982). Evaluation of orthometric height accuracy using bore hole gravimetry. *Bulletin Geodesique*, 56(4), 300-311.
- Sunkel, H. (1986). Digital height and density model and its use for the orthometric height and gravity field determination for Austria. *Proceedings of international symposium on the definition of the geoid*, (pp. 599-604). Florence.
- Tikhonov, A. H. (1963). Regularization of incorrectly posed problems. *Soviet mathematics-doklady*, 4, 1624-1627.
- Tikhonov, A. H. (1964). Solution of nonlinear integral equations of the first kind. *Soviet mathematics-doklady*, 5, 835-838.
- Tenzer, R., & Novák, P. (2008). Conditionality of Inverse Solution to Discretized Integral Equations in Geoid Modelling from Local Gravity Data. *Studia geophysica Geodetica*, 52, 53-70.
- Tenzer, R., & Vaníček, P. (2003). Correction to Helmert's orthometric height due to actual lateral variation of topographical density. *Brazilian Journal of Cartography-Revista Brasileira de Cartografia*, 55(02), 44-47.



- Tenzer, R., Hirt, C., Claessnes, S., & Novak, P. (2015). Spatial and spectral representations of the geoid-to-quasigeoid correction. *Survey in Geophysics*, 36, 627.
- Tenzer, R., Novák, P., Janák, J., Huang, J., Najafi-Alamdari, M., Vajda, P., & Santos, M. (2003). *A review of the UNB Stokes-Helmert approach for precise geoid determination in Honoring the Academic life of Petr Vaníček.*
- Tenzer, R., Vaníček, P., & Novák, P. (2003). Far-Zone contributions to topographical effects in the Stokes-Helmert method of geoid determination. *Studia Geophysica et Geodetica*, 47(3), 467-480.
- Tenzer, R., Vaníček, P., Santos, M., Featherstone, W., & Kuhn, M. (2005). The rigorous determination of the orthometric heights. *Journal of Geodesy*, 79(1), 82-92.
- Trojanowicz, M. (2015). Assessment of the accuracy of local quasigeoid modelling using the GGI method: case study for the area of Poland. *Studia Geophysica et Geodetica*, 59(4), 505-523.
- Tscherning, C., Forsberg, R., & Knudsen, P. (1992). The GRAVSOFTE Package for Geoid Determination. *The first continental workshop on the Geoid in Europe* (pp. 327-334). Prague: Holota, P., & Vermmer, M.
- Vaníček, P. (1998). The height of reason (a letter to the editor). *GPS works*.
- Vaníček, P., & Kleusberg, A. (1987). The Canadian geoid-Stoksonian approach. Compilation of a precise regional geoid. *Manuscripta Geodetica*, 12, 86-98.
- Vaníček, P., & Krakiwsky, E. (1986). *Geodesy, The concepts*. Amsterdam, North Holland.

- Vaníček, P., & Martinec, Z. (1994). Stokes-Helmert scheme for the evaluation of a precise. *Manuscripta Geodaetica*, *19*, 119-128.
- Vaníček, P., & Sjöberg, L. (1991). Reformulation of Stokes's theory for higher than second-degree reference field and modification of integration kernels. *Journal of Geophysical Research: solid Earth*, *96*(B4), 6529-6539.
- Vaníček, P., Huang, J., Novák, P., Pagiatakis, S., Véronneau, M., Martinec, Z., & Featherstone, W. (1999). Determination of the boundary values for Stokes-Helmert problem. *Journal of Geodesy*, *73*, 160-192.
- Vaníček, P., Kingdon, R., & Santos, M. (2012). Geoid versus quasigeoid: a case of physics versus geometry. *Contribution to Geophysics and Geodesy*, *42*(1), 101-118.
- Vaníček, P., Najafi, M., Martinec, Z., Harrie, L., & Sjöberg, L. (1995). Higher-degree reference field in the generalised Stokes-Helmert scheme for geoid computation. *Journal of Geodesy*, *70*, 176-182.
- Vaníček, P., Novák, P., Sheng, M., Kingdon, R., Janák, J., Foroughi, I., . . . Santos, M. (2017). Does Poisson's downward continuation give physically meaningful results? *Studia Geophysica et Geodaetica*. doi: 10.1007/s11200-016-1167-z
- Vaníček, P., Sun, W., Ong, P., Martinec, Z., Najafi-Alamdari, M., Vajda, P., & Ter Host, B. (1996). Downward continuation of Helmert's gravity. *Journal of geodesy*, *71*, 21-34.

- Vaniček, P., Tenzer, R., Sjöberg, L., Martinec, Z., & Featherstone, W. (2004). New views of the spherical Bouguer gravity anomaly. *Geophysical Journal International*, 159(2), 460-472.
- Wichiencharoen, C. (1982). *The indirect effects on the computation of geoid undulations*. Columbus: Department of Geodetic Sciences Ohio State University.
- Wirth, B. (1990). Höhensysteme, Schwerepotentiale und Niveauflächen. *Geodätisch-Geophysikalische Arbeiten in der Schweiz*, 42, Swiss Geodetic Commission.
- Wong, J. (2002). *On Picard criterion and the well-posed nature of harmonic downward continuation*. Fredericton, Canada: University of New Brunswick.
- Wong, L., & Gore, R. (1969). Accuracy of Geoid heights from modified Stokes kernel. *Geophysical Journal International*, 18(1), 81-91.
- Yilmiz, N. (2008). Comparison of Different Height Systems. *Geo-spatial Information Science*, 11(3), 209-214.
- Zhang, H., Ravat, D., & Hu, X. (2013). An improved and stable downward continuation of potential field data: The truncated Taylor series iterative downward continuation method. *Geophysics*, 78(5), 75-86.
- Ziebart, M., Illife, J., Forsberg, R., & Strykowski, G. (2008). Convergence of the UKOSGM05GRACE-based geoid and the UK fundamental benchmark network. *Journal of geophysical research letters*, 113, 12401.
- Zilkoski, D. (1993). *NGS/Caltrans San Diego GPS-Derived Orthometric Heights Cooperative Project, NGS Project Report*. East-West Highway, Silver Spring.

Found

at:

<http://www.ngs.noaa.gov/initiatives/HeightMod/Articles/caltran266c2.pdf>.

## **2 Chapter 2: Optimal combination of satellite and terrestrial gravity data for regional geoid determination using Stokes-Helmert's method, the Auvergne test case**

This article was presented at the 1<sup>st</sup> joint meeting of commission 2 of the international association of Geodesy (IAG) and international gravity field services (IGFS) entitled “Gravity, Geoid, and Height Systems (GGHS)” and held on September 19-23, 2016 in Thessaloniki, Greece. The full-text of this presentation was later published in the proceedings of the meeting in IAG symposia series. The methodology, numerical evaluation, and writing of the article were done by me and my co-authors provided some suggestions when developing the methodology and also revised the manuscript before its submission. The full citation for this article is:

Foroughi I., Vaníček P., Novák P., Kingdon R.W., Sheng M., Santos M.C. (2017) Optimal Combination of Satellite and Terrestrial Gravity Data for Regional Geoid Determination Using Stokes-Helmert's Method, the Auvergne Test Case. International Association of Geodesy Symposia. Springer, Berlin, Heidelberg. DOI: [doi.org/10.1007/1345\\_2017\\_22](https://doi.org/10.1007/1345_2017_22).

The methodology presented in this article may be used for any region as the numerical results of this paper are only valid for the Auvergne dataset and might be different in other regions. The article presented below is almost the same shape as the published article rather some changes in the figure/table/equation numbers and format.

## 2.1 Abstract

The precise regional geoid modeling requires combination of terrestrial gravity data with satellite-only Earth Gravitational Models (EGMs). In determining the geoid using the Stokes-Helmert approach, the relative contribution of terrestrial and satellite data to the computed geoid can be specified by the Stokes integration cap size defined by the spherical distance  $\psi_0$  and the maximum degree  $l_0$  of the EGM-based reference spheroid. Larger values of  $l_0$  decrease the role of terrestrial gravity data and increase the contribution of satellite data and vice versa for larger values of  $\psi_0$ . The determination of the optimal combination of the parameters  $l_0$  and  $\psi_0$  is numerically investigated in this paper. A numerical procedure is proposed to find the best geoid solution by comparing derived gravimetric geoidal heights with those at GNSS/Leveling points. The proposed method is tested over the Auvergne geoid computation area. The results show that despite the availability of recent satellite-only EGMs with the maximum degree/order 300, the combination of  $l_0 = 160$  and  $\psi_0 = 45$  arc-min yields the best fitting geoid in terms of the standard deviation and the range of the differences between the estimated gravimetric and GNSS/Leveling geoidal heights. Depending on the accuracy of available ground gravity data and reference geoidal heights at GNSS/Leveling points, the optimal combination of these two parameters may be different in other regions.

## 2.2 Introduction

Stokes's boundary-value problem requires gravity values to be known on the geoid. Moreover, gravity anomalies used as input data must be solid [Vaníček et al., 2004] in order to be continuable from ground down to the geoid. Helmert's gravity anomalies are solid above the geoid; thus, they can be downward continued. To derive Helmert's gravity

anomalies on the Earth surface, the direct topographical effect (DTE) as well as the direct atmospheric effect on gravity must be applied to free-air (FA) gravity anomalies. The latter effect is small and well known and will not be discussed. This gravity reduction, we call it ‘‘Helmertization’’ (see Figure 2.1), is the first step in the geoid determination using Stokes-Helmert’s method.

The geoidal heights in Helmert’s space ( $N^h$ ) can be evaluated by applying the Stokes integral to Helmert’s gravity anomalies ( $\Delta g^h$ ) on the geoid which should be available globally [Stokes, 1849]. Vaníček and Kleusberg [1987] introduced the idea of splitting the geoidal heights as well as Helmert’s gravity anomalies to reference and residual parts:

$$\begin{aligned} N^h(\Omega) &= N_{ref}^h(\Omega) + N_{res}^h(\Omega) \quad , \quad \Delta g^h(\Omega) \\ &= \Delta g_{ref}^h(\Omega) + \Delta g_{res}^h(\Omega), \end{aligned} \quad (2.1)$$

where  $\Delta g_{res}^h$  is the residual Helmert gravity anomaly and  $N_{res}^h$  is the residual geoidal height in Helmert’s space.  $\Delta g_{ref}^h$  and  $N_{ref}^h$  represent the reference Helmert anomaly and the reference spheroid, respectively; they both can be synthesized from Helmertized EGM as [Najafi-Alamdari, 1996]:

$$\begin{aligned} T_{ref}^h(R, \Omega) &= \frac{GM}{r} \sum_{l=2}^{l_0} \left(\frac{R}{r}\right)^l \sum_{m=-l}^l T_{l,m}^h Y_{l,m}(\lambda, \phi) \\ T_{l,m}^h &= \begin{cases} C_{lm}^h & m \geq 0 \\ S_{lm}^h & m < 0 \end{cases} \\ Y_{l,m} &= \begin{cases} P_{lm}(\cos\phi) \cos m\lambda & m \geq 0 \\ P_{lm}(\cos\phi) \sin |m|\lambda & m < 0 \end{cases} \end{aligned} \quad (2.2)$$

where  $R$  is the mean Earth's radius,  $r$  is the radius for which helmertized spherical harmonic coefficients  $(C_{lm}^h, S_{lm}^h)$  are evaluated;  $GM$  is the product of the Newtonian gravitational constant  $G$  and the Earth's mass  $M$ . The symbol  $\Omega = (\phi, \lambda)$  represents the geocentric direction of the computation point and  $\lambda$  and  $\phi$  are the geocentric spherical coordinates. The  $P_{lm}$  is the fully normalized associated Legendre function of the degree  $l$  and order  $m$ . The parameter  $l_0$  is the maximum degree of the spherical harmonic expansion that defines the maximum contribution of satellite-only EGMs in a spectral way to the Helmert disturbing potential  $T_{ref}^h$ . This potential is defined as follows:

$$\begin{aligned} T_{ref}^h(R, \Omega) &= W_{ref}^h(R, \Omega) - U_0(\phi) , \\ W_{ref}^h(r, \Omega) &= W_{ref}(r, \Omega) - \delta V_{ref}^t(r, \Omega) , \end{aligned} \quad (2.3)$$

where  $U_0$  is the latitude-dependent normal gravity potential and  $W_{ref}$  is the actual gravity potential.  $\delta V_{ref}^t(r, \Omega)$  is the reference residual gravitational potential of the topographic masses [Novák, 2000]. By using Eq. (2.2) the Helmert reference gravity anomaly  $\Delta g_{ref}^h$  and the reference spheroid  $N_{ref}^h(\Omega)$  can be computed using the fundamental equation of physical geodesy and spherical Bruns's formula, respectively [Heiskanen and Moritz, 1967, Eqs. 2-148 and 2-144].

To evaluate the residual geoidal heights in Helmert's space, i.e.,  $N_{res}^h$  in Eq. (2.1), the Stokes integration is employed. Its integration domain  $\Omega_0$  can be split into the near zone  $\Omega_{\psi_0}$  and the far zone  $\Omega_0 - \Omega_{\psi_0}$  [Vaníček & Kleusberg, 1987]. The size of the near zone dictates the contribution of terrestrial gravity data which reads:



$$N_{l>l_0, \Omega'_0}^h(\Omega) = \frac{R}{4\pi\gamma_0(\phi)} \iint_{\Omega' \in \Omega_{\psi_0}} \Delta g_{res}^h(R, \Omega') S_{n>l_0}(\psi_0, \psi(\Omega, \Omega')) d\Omega' , \quad (2.4)$$

where  $N_{l>l_0, \Omega'_0}^h$  is the residual geoid height in Helmert's space computed from the near-zone gravity data. The subscript  $l > l_0, \Omega'_0$  indicates that the integration is performed over residual Helmert's gravity anomalies with frequencies higher than  $l_0$  and limited to the cap size  $\Omega'_0$ . The far-zone contribution ( $N_{l>l_0, \Omega'_0 - \Omega'_0}^h$ ) reads:

$$N_{l>l_0, \Omega'_0 - \Omega'_0}^h(\Omega) = \frac{R}{4\pi\gamma_0(\phi)} \iint_{\Omega' \in \Omega'_0 - \Omega'_0} \Delta g_{res}^h(R, \Omega') S_{n>l_0}(\psi_0, \psi(\Omega, \Omega')) d\Omega' , \quad (2.5)$$

where  $\Omega_0$  stands for the geocentric solid angle  $[\phi \in \langle -\frac{\pi}{2}, \frac{\pi}{2} \rangle , \lambda \in \langle 0, 2\pi \rangle]$ ,  $\Omega'$  represents the pair of the integration point coordinates and  $\psi$  is the spherical distance between the integration and computation points. The modified version of the spheroidal Stokes function ( $S_{n>l_0}$ ) is used here; the modification minimizes the far-zone contribution in the least square sense. For more details, please refer to [Vaníček & Kleusberg, 1987].

The contribution of satellite-only EGMs (in the spectral sense) is given by the maximum degree of the spherical harmonic expansion  $l_0$  in Eq.(2.2) while terrestrial gravity data increasingly contributes to the geoidal height with the increasing size of the spherical integration cap  $\psi_0$  in Eqs. (2.4) and (2.5).

The primary indirect topographical effect (PITE) is then added to the co-geoidal heights computed by Eq. (2.5) to convert them back to the real space; we call this step as “*de-Helmertization*”, see Figure 2.1.

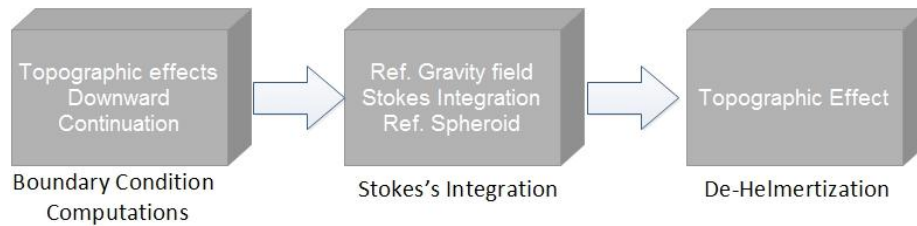


Figure 2.1: Three main computational steps of Stokes-Helmert’s technique

Featherstone and Olliver [1994] analyzed the coefficients of the geopotential model along with the terrestrial gravity data to find the optimal Stokes’s integration cap size and the degree of reference field to compute the geoid in the British Isles. In the end they estimated as the maximum degree 257 and the radius of 1 arc-deg 57 arc-min. They did not use any higher degrees than 257 for computing the reference field because according to their analysis the standard errors of the gravity anomalies computed by then-available geopotential models started to exceed the coefficients themselves.

Vella & Featherstone [1999] set the degree of reference field to 360 and changed the Stokes integration cap size to find the optimal contribution of terrestrial gravity data to compute the geoid model of Tasmania. They compared the resulting geoid models with the geoid height from GPS/Leveling points in their study area and found out that the cap radius of 18 arc-min gives the smallest STD.

These papers date back to the time when global fields did not have any gravity-dedicated satellite mission data included; thus, they were not as accurate in the low- and mid-wavelengths as they are now because of GRACE and GOCE satellite gravity data [Reigber et al., 2005; Pail et al., 2011].

The methodology proposed in the present study investigates all possible options to find the optimal degree of the reference field and the radius of the integration cap. The optimality is defined according to two criteria: minimum values of STD and range of the differences between the computed geoid model and geoidal heights at GNSS/Leveling points described in Sec. 2.3. Numerical results of the proposed method summarized in Secs. 2.4 and 2.5 conclude the paper.

### **2.3 Proposed method**

Theoretically if EGMs represent the Earth's gravity field accurately (for  $l_0$  going to infinity), the near-zone Stokes integration is not needed, i.e., the radius  $\psi_0$  can be put equal to 0. If, on the other hand, EGMs were not good, we would have to disregard them and use terrestrial gravity data from the whole world, i.e.,  $\psi_0 = 180^\circ$ . As both EGMs and terrestrial gravity data are burdened with position-dependent noise, the optimal combination of  $l_0$  and  $\psi_0$  varies from place to place. The pair  $l_0 = 90$  and  $\psi_0 = 2^\circ$  has commonly been used in our previous geoid determinations [Ellmann and Vaniček, 2007]. To find the optimal pair for currently available EGMs in every region, the following algorithm is suggested:

1. Vary the degree of the reference field and spheroid and correspondingly the modification degree of Stokes's kernel function:  $l_0 = 90:300$ . Here we shall go

only up to  $l_0 = 300$  as this degree represents the maximum degree of current satellite-only EGMs.

2. Remove the Helmertized reference field of the degree  $l_0$  from Helmert's gravity anomaly on the geoid.
3. Vary the near-zone contribution by changing the integration radius  $\psi_0 = 30': 2^\circ$ .
4. Compute the residual co-geoid by Stokes's integration as the sum of contributions from both near and far zones.
5. Add the reference spheroid of the degree  $l_0$  to the residual co-geoid.
6. Compute the geoid in the real space by adding PITE to the co-geoid.
7. Evaluate geoidal heights at available GNSS/Leveling points in the computation area.
8. Find the optimal geoid for the chosen  $l_0$  in Step 1, the optimal choice can be based on the minimum norm of differences between the computed geoid and GNSS/Leveling geoidal heights. The two most reasonable choices among all norms are  $\| \cdot \|_2$  ( $L_2$  norm), called also the standard deviation (STD) of the differences, and  $\| \cdot \|_\infty$  ( $L$  infinity norm) equal to the maximum absolute value of the differences. The latter is loosely connected to the range of the discrepancies.
9. Repeat Steps 1 to 8 for all degrees up to  $l_0 < 300$ .
10. Find the "global" optimal pair among the "local" ones which is then the optimal pair  $(l_0, \psi_0)$  for the computation area.

Depending on the step between degree/order of reference field and integration cap size, the computation of the proposed algorithm can be time demanding. The diagram in Figure 2.2: describes how this algorithm works graphically:

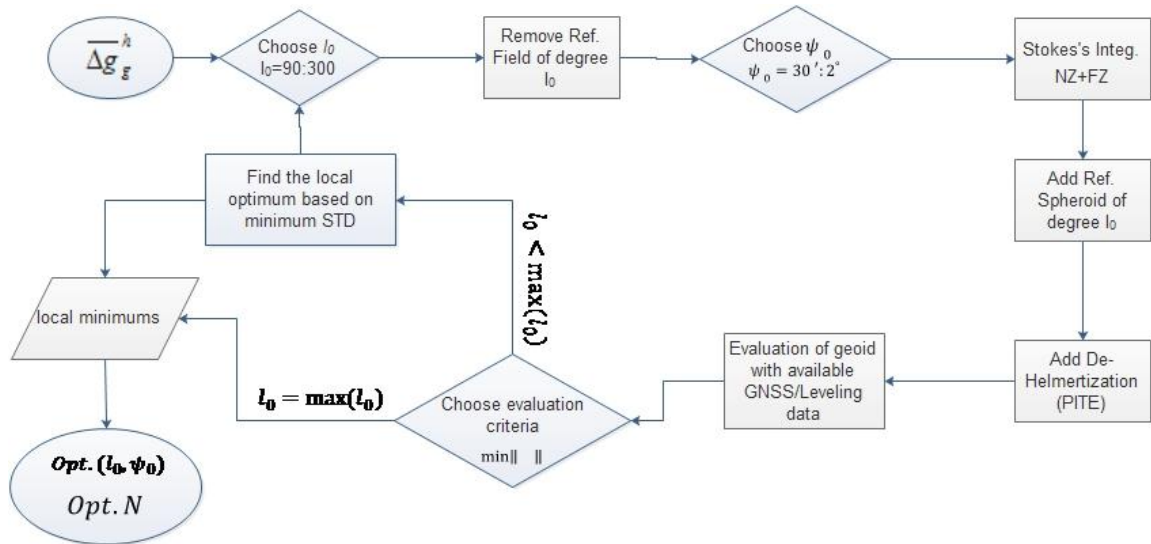


Figure 2.2: Proposed method to estimate the optimal contributions of near-zone (NZ) and far-zone (FZ) in Stokes's integration.

## 2.4 Numerical results

The proposed method was tested in Auvergne, the central area of France, which is limited by  $(-1^\circ < \lambda < 7^\circ, 43^\circ < \phi < 49^\circ)$  [Duquenne, 2006]. The topography of this area is shown in Figure 2.3(a). This area contains about 240 000 scattered free-air gravity points that have been extracted from the database of the Bureau Gravimétrique International (Figure 2.3 (b)). 75 GNSS/Leveling points are also available within the central square of the area of interest for the geoid computation  $(1.5^\circ < \lambda < 4.5^\circ, 45^\circ < \phi < 47^\circ)$ . The data coverage area is larger than the geoid computation area to be able to test the different integration cap radii. Mean gravity anomalies of 1' resolution were computed from scattered observed gravity using complete spherical Bouguer anomalies, also known as NT anomalies, (they are known to be the smoothest) by means of inverse cubic distance interpolation. It was shown by Kassim [1980] that inverse cubic distance

interpolation is superior for predicting gravity anomalies to other interpolation techniques tested in their study, however, there might be other prediction methods with the same accuracy which were not just used in their investigation. Mean Helmert's gravity anomalies on the Earth's surface were obtained by adding the DTE. The secondary indirect topographical effect (SITE), see Vaniček et al. [1999], was added to the predicted anomaly values to prepare them for the downward continuation.

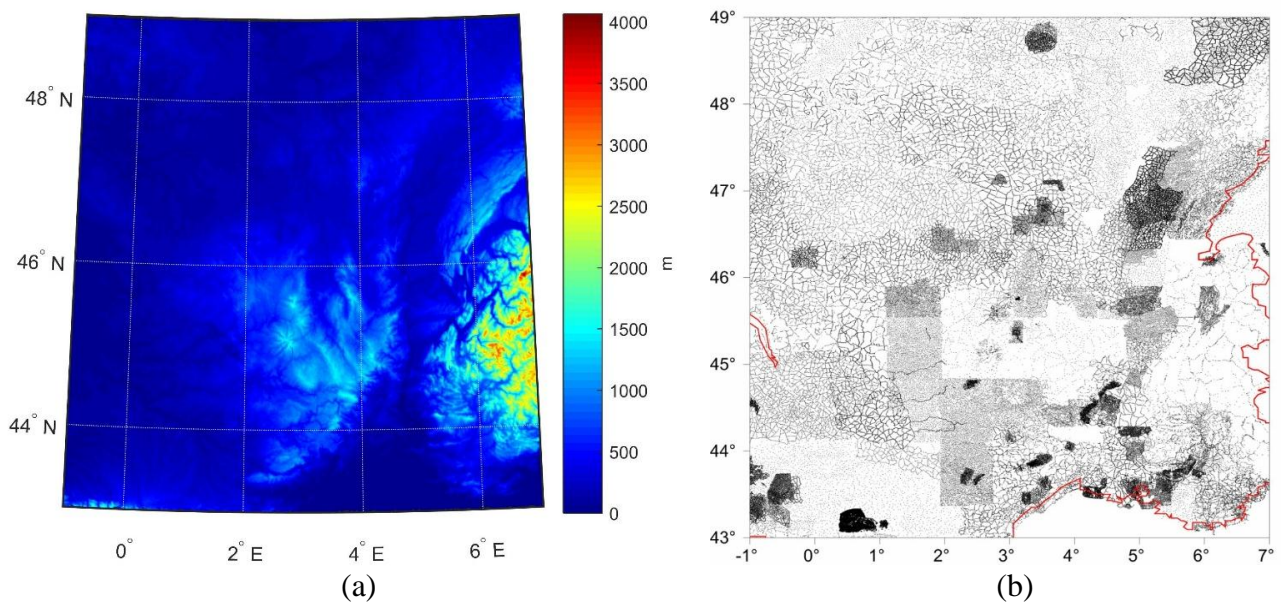


Figure 2.3: Topography of the study area (a); distribution of terrestrial gravity data (b).

For computing the DTE at each gravity point, topographical heights over the entire Earth are needed. The integration is done separately in the inner, near and far zones. SITE was also computed for inner, near and far zones separately, but this effect for Helmert's space is much smaller than DTE. Values of DTE and SITE over the Auvergne area are shown in Figure 2.4.

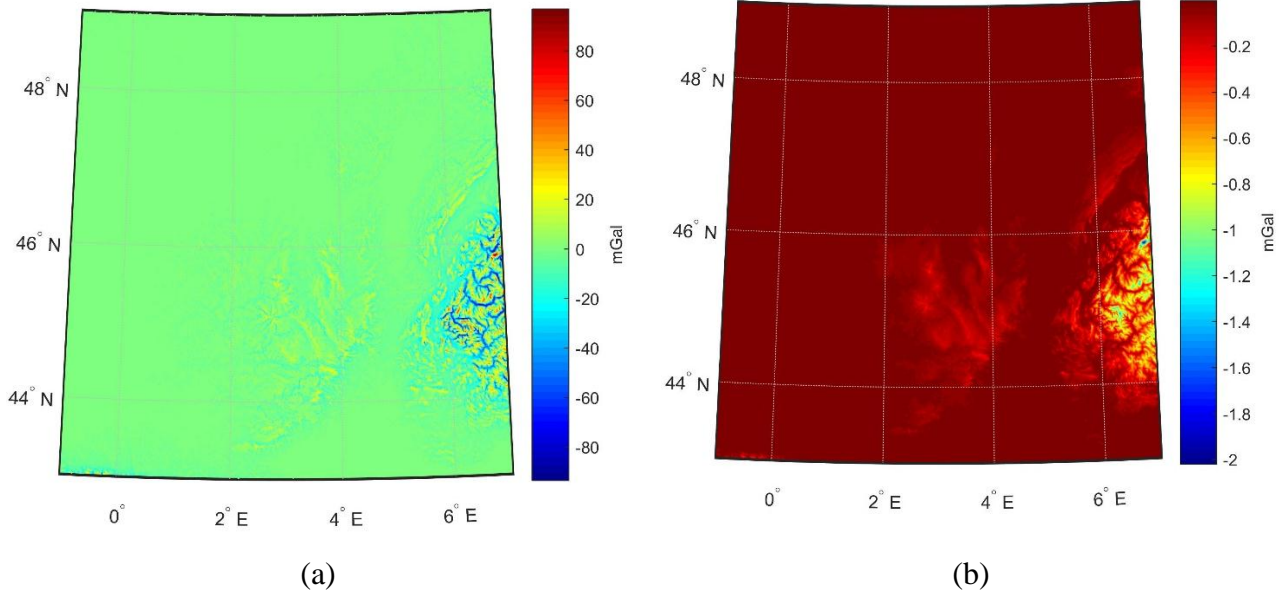


Figure 2.4: Direct topographical effect (a); secondary indirect topographical effect on gravity anomalies (b).

Applying DTE and SITE converts the free-air gravity anomalies to Helmert's gravity anomalies. Figure 2.5 shows the free-air and mean Helmert's gravity anomalies in the Auvergne area.

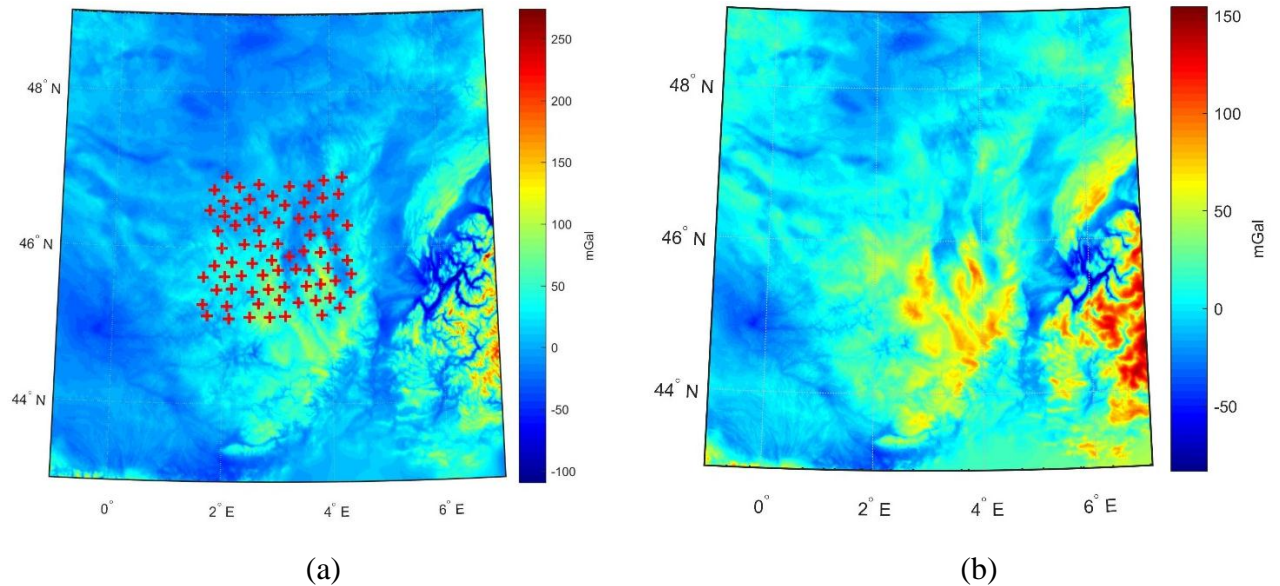


Figure 2.5: Free-air gravity anomaly with red-cross signs showing GNSS/Leveling points (a) and Helmert's gravity anomalies (b).

Mean Helmert's anomalies on the Earth's surface were then downward continued to mean Helmert's anomalies on the geoid. This was done using the Poisson integral equation solved by the iterative Jacobi process [Kingdon and Vaníček, 2010]. The downward continuation was done over 1 arc-deg squared cells augmented by a border strip 30 arc-min wide on all sides. Results from the individual cells were then fused together. On average, seven iterations were needed for the downward continuation in the individual squares. For the purpose of the fusion, an assessment of continuity of Helmert's gravity anomalies along the borders of two adjacent arc-degree cells on the geoid was done by the technique described by Foroughi et al. [2015b]. This assessment showed that discontinuities between the downward continued Helmert anomalies are random within the limits of  $\pm 3\sigma$  ( $\sigma$  is the standard deviation of observed anomalies) which was assumed acceptable.

The next step is the evaluation of Stokes's integral which starts with removing long wavelengths from gravity anomalies using the reference field. In our case, the satellite-only DIR\_R5 EGM (GOCE, GRACE and Lageos) was used for computation of the reference gravity field and the spheroid [Bruinsma et al., 2013]. PITE was then computed for the locations of the 1 arc-min grid on the geoid, again separately for the inner, near and far zones (Figure 2.6). This resulted in the geoid (in real space) for the pre-selected  $(l_0, \psi_0)$ . This geoid was then compared against the results from GNSS/Leveling.



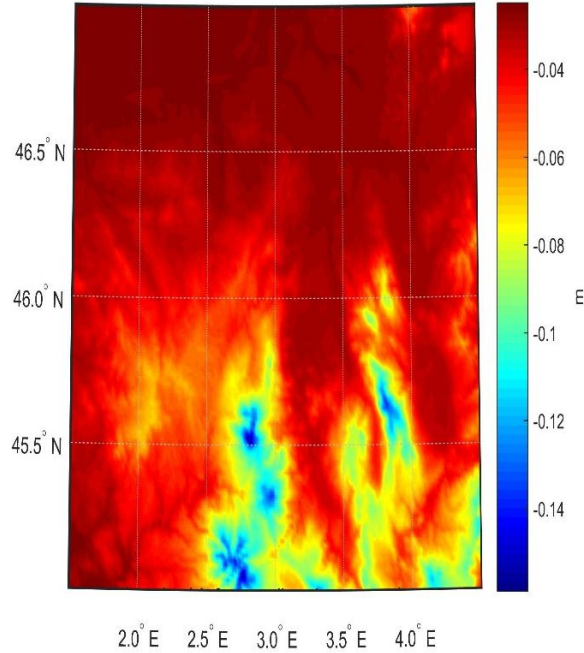


Figure 2.6: Primary indirect topographical effect on geoidal heights in the Auvergne geoid test area.

To find the optimal combination of the degree of the reference field  $l_0$  and the radius of Stokes's integration  $\psi_0$  the above proposed algorithm was repeatedly used. The first computation started with  $l_0 = 90$  and  $0^\circ < \psi_0 < 2^\circ$ ; the maximum integration cap size was chosen 2 arc-deg as commonly used by us with Stokes-Helmert's technique. This choice meant that we actually needed an extra 2 arc-deg data coverage in latitude direction and around 3 arc-deg in longitude direction outside the geoid computation area which was not covered by the original data. Foroughi et al. [2015a] solved this problem by padding the original data coverage by 3 arc-deg from each side, by using free-air gravity anomalies synthesized from EGM2008 up to the degree/order 2160. They showed this method was accurate enough for the purpose of covering a smaller gap in data coverage. This approach was used here wherever there were coverage gaps.

The proposed method tests all the possible choices of the parameter pair  $(l_0, \psi_0)$ . The optimal geoid is chosen based on the agreement between the resulting gravimetric geoid and geoidal heights derived from GNSS/Leveling. STD and ranges of the differences are chosen as tools for finding the optimal combination. Figure 2.7 shows 2D plots of the range and STD of the differences as functions of  $\psi_0$  and  $l_0$ .

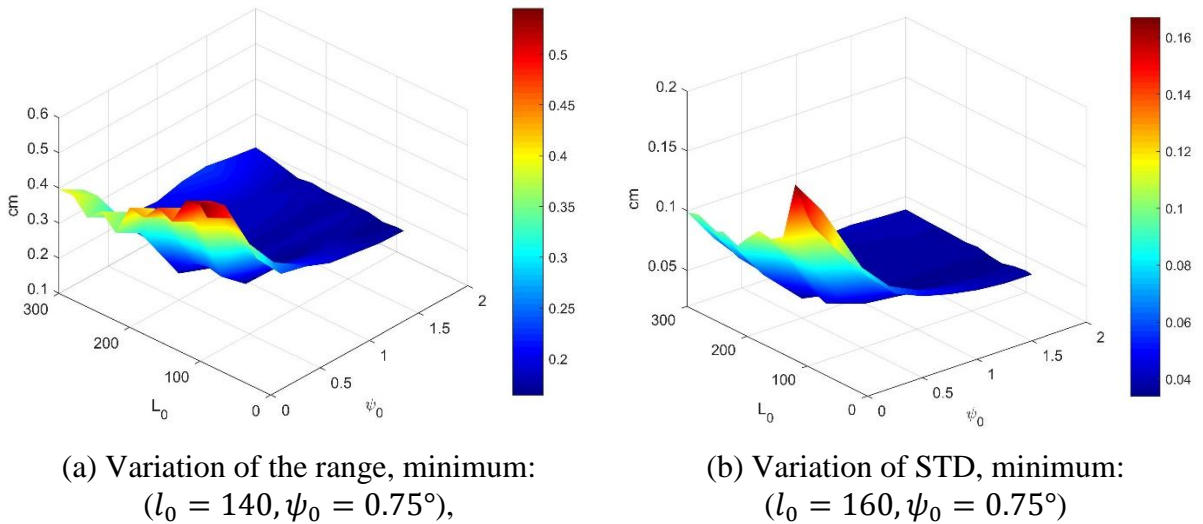


Figure 2.7: Variation of STD and range of differences between resulting geoid and GNSS/Leveling.

Figure 2.7 shows that for all considered degrees  $l_0 = 140$  is the highest one should go to keep the range as small as possible. In combination with  $\psi_0 = 0.75^\circ$  it gives the smallest range of the differences, 16.3 cm in fact. We note that taking the larger integration cap does not improve the range, but larger  $\psi_0$  will not make the range significantly larger either. Looking at STD values, it appears that a similar cut-off value should be used for  $l_0$ , i.e., about 160, while the choice of  $\psi_0$  seems to be even less critical

than for the range minimization criterion. The smallest  $STD = 3.3$  cm is obtained for combination  $l_0 = 160$  and  $\psi_0 = 0.75^\circ$ . Generally, it appears that taking  $l_0$  larger than 160 and  $\psi_0$  smaller than  $0.75^\circ$  should be avoided. The plots seem to indicate, however, that the deterioration of accuracy is much faster with the increasing degree of EGM than with the increasing radius of the integration cap.

## 2.5 Concluding remarks

A numerical method was proposed to optimally combine terrestrial and satellite gravity data for computing the regional geoid using Stokes-Helmert's approach. The optimality of the results was measured by the differences between the derived gravimetric and GNSS/Leveling geoidal heights in terms of their range and STD. This method was tested over the area of Auvergne and the optimal geoid was derived when the maximum contribution of the DIR-R5 EGM was set to  $l_0 = 160$  and the near-zone Stokes integration cap size was set to  $\psi_0 = 0.75^\circ$ . The resulting optimal geoid of this study showed the 0.3 cm improvement in terms of STD and 2.4 cm improvement in the range with respect to the geoid computed by the standard choice of  $l_0 = 90$  and  $\psi_0 = 2^\circ$ . Comparing the optimal geoid with the geoid computed using the maximum contribution from EGM, i.e.,  $l_0 = 300$  and  $\psi_0 = 0.25^\circ$ , showed the improvement of 4 cm in terms of STD and 19 cm in the range. The methodology proposed in this study would have to be tested in other regions as the present results were obtained in the Auvergne study area and might be different for other regions. The choice of the optimal integration cap size depends on the quality and spatial distribution of terrestrial gravity data. However, the estimated optimal degree of reference field ( $l_0=160$ ) could also be valid for other regions as Abdalla et al. (2012) found more or less the same number over the Khartoum state. They investigated

the validation of all GOCE/GRACE geopotential models and concluded that the models do not show better results beyond degree 150. Due to inherent errors of satellite-only EGM higher-degree coefficients, they are not recommended to be used when reasonably good terrestrial gravity data are available.

## **2.6 Acknowledgments**

We wish to acknowledge that the leading author, Prof. Vaníček and Mr. Shang were supported by an NSERC “Discovery grant”.

## **2.7 References**

Abdalla A, H. Fashir, A. Ali, D. Fairhead. (2012). Validation of recent GOCE/GRACE geopotential models over Khartoum state – Sudan. *Journal of Geodetic Science*. 2(2): 88-97.

Bruinsma S, Foerste C, Abrikosov O, Marty J-C, Rio M-H, Mulet S, Bonvalot S (2013). The new ESA satellite-only gravity field model via the direct approach. *Geophysical Research letters*, 3607-3612.

Ellmann A, Vaníček P (2007) UNB application of Stokes-Helmert's approach to geoid computation. *Journal of Geodynamics* 43: 200-213.

Duquenne, H., (2006). A data set to test geoid computation methods. *Proceedings of the 1st International Symposium of the International Gravity Field Service, Istanbul, Turkey, Harita Dergisi*, pp. 61-65.

Featherstone WE, Olliver JG (1994) A new gravimetric determination of the geoid of the British Isles. *Survey Review* 32, 254.

- Foroughi I, Janák J, Kingdon R, Sheng M, Santos M, Vaníček P (2015a). Illustration of How Satellite Global Field Should be Treated in Regional Precise Geoid Modelling (Padding of Terrestrial Gravity Data to Improve Stokes-Helmert Geoid Computation). The EGU General Assembly. Vienna.
- Foroughi, I, Vaníček P, Kingdon R, Sheng M, Santos M (2015b). Assessment of Discontinuity of Helmert's Gravity Anomalies on the Geoid. AGU-GAC-MAC-CGU Joint Assembly. Montreal, Canada.
- Heiskanen W, Moritz H (1967) Physical Geodesy. San Francisco: W.H. Freeman and Co.
- Kassim F (1980) An evaluation of three techniques for the prediction of gravity anomalies in Canada. Technical report of the University of New Brunswick.
- Kingdon R, Vaníček P (2010). Poisson Downward Continuation Solution by the Jacobi Method. *Journal of Geodetic Science* 1: 74-81.
- Najafi-Alamadari, M. (1996) Contributions towards the computation of a precise regional geoid. Doctoral thesis, University of New Brunswick, Fredericton, Canada.
- Novák P (2000) Evaluation of gravity data for Stokes-Helmert solution to the geodetic boundary-value problem. Fredericton, Canada: University of New Brunswick.
- Reigber C, Schmidt R, Flechtner F, König R, Meyer U, Neumayer KH, Schwintzer P, Zhu SY (2005). An Earth gravity field model complete to degree and order 150 from GRACE: EIGEN-GRACE02S, *Journal of Geodynamics*, Vol 39, Issue 1, pp. 1-10.
- Stokes G (1849) On the variation of gravity at the surface of the Earth. Cambridge University Press.
- Pail R, Bruinsma S, Migliaccio F, Förste C, Goiginger H, Schuh W-D, Höck E, Reguzzoni M, Brockmann JM, Abrikosov O, Veicherts M, Fecher T, Mayrhofer R, Krasbutter

- I, Sansò F, Tscherning CC (2011). First GOCE gravity field models derived by three different approaches, *Journal of Geodesy*, Vol 85, Issue 11, pp. 819-843.
- Vaniček P, Huang J, Novák P, Véronneau M, Pagiatakis S, Martinec Z, Featherstone WE (1999). Determination of boundary values for the Stokes-Helmert problem. *Journal of Geodesy* 73: 180-192.
- Vaniček P, Kleusberg A (1987) The Canadian geoid-Stoksonian approach. *Compilation of a precise regional geoid. Manuscripta Geodetica* 12: 86-98.
- Vaniček P, Tenzer, R., Sjöberg LE, Martinec Z, Featherstone WE (2004) New views of the spherical Bouguer gravity anomaly. *Journal of Geophysics International* 159(2): 460-472.
- Vella JP, Featherstone WE (1999) A gravimetric geoid model of Tasmania, computed using the one-dimensional fast Fourier transform and a deterministically modified kernel. *Geomatics Research Australia* 70: 53-76.

### **3 Chapter 3: Computation of precise geoid model of Auvergne using current UNB Stokes-Helmert's approach**

This article is published in the journal of Contributions to Geophysics and Geodesy. The first author of this article, Dr. Juraj Janák, was invited to the department of geodesy and geomatics (GGE) of the University of New Brunswick (UNB) for three summers between 2014-2016. The main purpose of his visits was doing research in the field of geoid computation, specifically in the Auvergne area. During his visits, he prepared the Auvergne input gravity data sets to be used in the determination of the geoid using the Stokes-Helmert method, for instance, by detecting the outliers, reference conversion, interpolation and etc. In appreciation of his research visits, it was suggested by the GGE gravity group to offer him the first authorship of this article, however, all the Stokes-Helmert computation steps and analysis of the results were done by me. The writing of the sections 3-5 of this article was also done by me and I was the corresponding author for the submission of the article to the journal.

The full citation of this article is:

Janák, J., Vaňiček, P., Foroughi, I., Kingdon, R., Sheng, M. B., & Santos, M. C. (2017). Computation of precise geoid model of Auvergne using current UNB Stokes-Helmert's approach, *Contributions to Geophysics and Geodesy*, 47(3), 201-229.

In this article, first, geoid model of Auvergne was computed using the conventional Stokes-Helmert approach and was later improved using the proposed methodology in

Ch.2, i.e., the optimal combination of EGMs with the local data and the results were presented in this article.

The lateral density model used in this article to compute the effect of DDE and PIDE was extracted from a low-resolution publicly available geological map provided by Bodelle et al. [1980]. A higher resolution density map, however, was used later (see, Ch. 5) to compute the DDE and PIDE more precisely. Therefore, the PIDE plots in the Auvergne area are different in this chapter and chapter 5.

### **3.1 Abstract**

The aim of this paper is to show a present state-of-the-art precise gravimetric geoid determination using the UNB Stokes-Helmert's technique in a simple schematic way. A detailed description of a practical application of this technique in the Auvergne test area is also provided. In this paper, we discuss the most problematic parts of the solution: correct application of topographic and atmospheric effects including the lateral topographical density variations, downward continuation of gravity anomalies from the Earth surface to the geoid, and the optimal incorporation of the global gravity field into the final geoid model. The final model is tested on 75 GNSS/Leveling points supplied with normal Molodensky heights, which for this investigation are transformed to rigorous orthometric heights. The standard deviation of the computed geoid model is 3.3 cm without applying any artificial improvement which is the same as that of the most accurate quasigeoid.



## 3.2 Introduction

In 1849 G.G. Stokes [1849] introduced his method of geoid determination from gravity measurements, and his analytical solution for a spherical boundary has become known as Stokes's integral. Stokes made the assumptions that we'd have measured gravity on the geoid and that there are no masses above the geoid. Neither assumption is satisfied in practice and we have to deal with them in one way or another. One reasonable idea to overcome the problem stemming from the later assumption came from F.R. Helmert [Helmert, 1884] who suggested to condense all topographic masses into a 2D layer located on or below the geoid, to mathematically avoid the topographic mass issue. Helmert's approach applied to the geoid (known as the second Helmert's condensation technique) combined with the original Stokes's idea has become known in literature as the Stokes-Helmert (SH) method. During recent decades, the SH method has been developed and coded by the University of New Brunswick (UNB) Geodesy Group and is documented in many publications [Vaniček and Martinec, 1994; Ellmann and Vaniček, 2006].

Similarly, the transformation of gravity observed on and above the Earth surface down to the geoid, known as downward continuation, has been studied by the UNB group. They have opted for using the physically rigorous approach formulated by Poisson [MacMillan, 1930] and the results of their studies of Poisson's method for the downward continuation of harmonic functions are documented in several publications [Vaniček et al., 1996; Sun and Vaniček, 1998; Kingdon and Vaniček, 2010]. As a by-product of their investigation they discovered that in order to downward continue a gravity anomaly, the anomaly must be of a "solid" type [Vaniček et al., 2004], which rules out the use of free-air as well as planar Bouguer gravity anomalies.

To reach a one-centimeter accuracy geoid model at a regional scale is a very challenging task, especially in a mountainous region. Ever since Duquenne [2007] produced a good standard database to test the methods of geoid or quasigeoid computation, several authors, see, (e.g., Ågren et al. [2009] and Yildiz et al. [2012]) have computed regional quasigeoid models in the Auvergne region. The quasigeoid models, presented in Ågren et al. [2009], were tested at 75 GNSS/Leveling points and the standard deviation of residuals (after one-parameter fitting) were all in the vicinity of 3.7cm. It was reported in the same study that the Least Square Modification of Stokes method (LSMS or KTH approach [Sjöberg, 2003]) provides the best quasigeoid model among other methods (STD of 3.3cm). In fact, this method produces geoid model, which is converted to a quasigeoid. Herein, we present a regional geoid model computed using the UNB SH method, providing a detailed description, graphical presentation of intermediate computations, testing of the final model (without any fitting), comparison with other selected models and discussion of theoretical and practical problems and advantages of the SH method.

The first section is dedicated to the theory behind the SH method, mentioning the basic ideas in a schematic way with relevant references for readers who wish to learn the detailed theoretical arguments. Section 3.4 introduces the Auvergne region for which our geoid model has been computed and tested; it also gives some statistical information about the input data. Section 3.5 is focused on the compilation of spherical Bouguer gravity anomalies, also known as NT (No-Topography) anomalies, and on Helmert's gravity anomalies on the topography. In the next section, the downward continuation of Helmert's anomalies is presented together with the rest of the intermediate results of the geoid

solution. Section 3.7 describes the assessment of our geoid model vis-à-vis the 75 GNSS/Leveling points supplied by IGN. The last section is devoted to a brief discussion and conclusions.

### 3.3 Stokes-Helmert method, present state and references

The theory behind the UNB SH method has been described in many publications. Therefore, instead of repeating the mathematical formulae, which can be found in [e.g., Vaníček and Sjöberg, 1991; Vaníček and Martinec, 1994; Tenzer et al., 2003; Ellmann and Vaníček, 2006; Vaníček et al., 2013], we have chosen to show the flow of the computation in elementary steps supplemented by brief descriptions.

$$\Delta g[r_t(\Omega). \Omega] \rightarrow \Delta g^H[r_t(\Omega). \Omega]. \quad (3.1)$$

In the first step, the observed free-air gravity anomalies are converted to Helmert gravity anomalies, one of the couple of anomalies known to be “solid” and thus capable of being continued downwards to the geoid [Vaníček et al., 2004]. This conversion consists of adding the direct topographical and atmospheric effects (DTE) and (DAE), the secondary indirect topographical and atmospheric effects (SITE) and (SIAE) and, if the topographical density model is available, also the direct topographical density effect (DDE). All these effects, except DDE, are evaluated as sums of the near zone and far zone contributions and are computed at the locations of the observed points on the surface of the Earth. Beside these standard corrections if the available topographical heights are of the orthometric kind, a small correction to normal gravity, called the geoid-quasigeoid correction, is also applied. In Eq.(3.1) and throughout this paper,  $\Omega$  stands for geocentric direction, i.e.,  $(\varphi, \lambda)$ , the geocentric latitude and longitude; the subscripts  $t$  and  $g$  denote a

radius-vector ending either at the topography or at the geoid; subscripts beside residual quantities show the degree and order of the reference field and the angular radius of the integration cap; and the meaning of the superscript  $H$  is that the superscripted quantity belongs to Helmert's space.

We refer to this step also as the transformation from the “Real space” to “Helmert's space”. More details about this step can be found, e.g., in [Martinec and Vaníček, 1994a; Martinec, 1998; Vaníček et al., 1999; Novák, 2000]. Concerning lateral topographical density effect studies, see [Martinec, 1993; Martinec et al., 1995; Huang et al., 2001].

$$\Delta g^H[r_t(\Omega). \Omega] \rightarrow \Delta g^H[r_g(\Omega). \Omega]. \quad (3.2)$$

The second step consists only of the downward continuation of Helmert's gravity anomaly from the Earth's surface to the geoid. The UNB Geodesy Group had decided to use the most rigorous approach to downward continuation, i.e., that due to Poisson. This approach requires the gravity anomaly on the Earth surface to be “solid“ and harmonic within the topography, which is indeed the case with Helmert's anomaly. This step is often considered to be somewhat problematic due to the numerical instability of the inverse Poisson integral. After a thorough theoretical and numerical investigation [e.g., Vaníček et al., 1996; Sun and Vaníček, 1998; Huang, 2002; Kingdon and Vaníček, 2010], it was decided to use the Jacobi iterative algorithm for the solution of the inverse Poisson integral.

$$\Delta g^H[r_g(\Omega). \Omega] \rightarrow \delta \Delta g^H[r_g(\Omega). \Omega]. \quad (3.3)$$

This step consists of subtraction of the reference gravity field, (in terms of reference Helmert’s gravity anomalies) of selected degree and order  $L$  resulting in residual Helmert’s gravity anomalies on the geoid. Residual gravity anomalies refer to the reference spheroid of degree and order  $L$ . Before this operation is performed, the earth gravity model (satellite only EGM) used for the generation of reference gravity anomalies has to be “Helmertized”, i.e., transformed to the Helmert space. For the reference, see, [e.g., Vaniček and Sjöberg, 1991; Vaniček et al., 1995; Martinec and Vaniček, 1996]. This transformation requires the knowledge of a global digital elevation model (DEM) in terms of spherical harmonic coefficients. Technically, a part of this step is also the application of ellipsoidal corrections correcting the effect of spherical approximation of the boundary condition. It consists of two terms corresponding to the terms of the boundary condition, which are called the ellipsoidal correction to the gravity disturbance, and the ellipsoidal correction for the spherical approximation [Vaniček et al., 1999].

$$\delta\Delta g^H[r_g(\Omega), \Omega] \rightarrow \delta N_{L,\psi_0}^H(\Omega). \quad (3.4)$$

In this step, we compute the residual Helmert cogeoid on a selected regular grid using Stokes’s integration over the spherical cap of radius  $\psi_0$ , and integration kernel modified to degree  $L$  according to the idea by Molodensky [Molodensky et al., 1960]. We note that the spatial Stokes convolution of  $\delta\Delta g^H[r_g(\Omega), \Omega]$  with the modified Stokes kernel is done using a UNB technique that is faster than Fast Fourier Transform methods [Huang et al., 2000]. The modification is selected so as to minimize the contribution from the far-zone, and by doing this to minimize the contribution from the EGM which is known to approximate the reality only in an asymptotic way. The result of this step can be called

the near-zone (NZ) residual Helmert cogeoid. For details, see Vaníček and Featherstone [1998] and Novák et al. [2001].

$$\delta N_{L,\psi_0}^H(\Omega) \rightarrow \delta N^H(\Omega) . \quad (3.5)$$

Here, the far-zone (FZ) contribution  $\delta N_L^H(\Omega)$  to the residual Helmert cogeoid, also called the “truncation error” by Molodensky, is evaluated in a spectral way using the EGM in the Helmert space, to the appropriate degree higher than that of the reference field ( $L$ ), for the chosen radius  $\psi_0$ , and added to the NZ (spherical cap of radius  $\psi_0$ ) contribution  $\delta N_{L,\psi_0}^H(\Omega)$ . Due to the modification of the Stokes kernel, see the previous step, the truncation error term is relatively small. The result of this step is the total residual Helmert cogeoid. More details are found in [Molodensky et al., 1960; Vaníček and Featherstone, 1998].

$$\delta N^H(\Omega) \rightarrow N^H(\Omega). \quad (3.6)$$

The last step conducted in the Helmert space is the transformation of the total residual cogeoid to the complete Helmert cogeoid. This is done simply by adding to the residual cogeoid the “Helmertized” reference spheroid of degree  $L$ .

$$N^H(\Omega) \rightarrow N(\Omega). \quad (3.7)$$

The final step of the computation is the transformation of the Helmert cogeoid from Helmert space back to the real space. This is done by adding to the Helmert cogeoid  $N^H(\Omega)$  the primary indirect topographical and atmospheric effects (PITE) and (PIAE)

and, if the variations of topographical density are known, the primary indirect topographical density effect (PIDE). For details see Martinec and Vaníček [1994b] and Martinec et al. [1996]. As a part of this step, to preserve the physical correctness of the solution, a small correction due to the shift of the centre of mass of the Earth during the Helmert condensation needs to be applied. This correction is referred to as the Hörmander correction and it reaches up to a few centimetres. For details see Hörmander [1976], Martinec [1998], and Vaníček et al. [2013].

### **3.4 Input data sets**

The overall quality of the geoid model depends directly on the quality of the input data. The geoid model is also affected by other errors coming from various approximations, inconsistencies when merging several data sources, numerical errors due to discretization, interpolation and integration or errors caused by unsatisfied assumptions. The aim of this section is to list the input data used in our geoid computation and provide the original reference and the accuracy, if available.

The main input to our geoid model is the free-air gravity anomaly data set based on the Bureau Gravimétrique International (BGI) gravity database originally supplied by the Bureau de Recherches Géologiques et Minières and provided to us by the Institut Géographique National (IGN) [Duquenne, 2007].

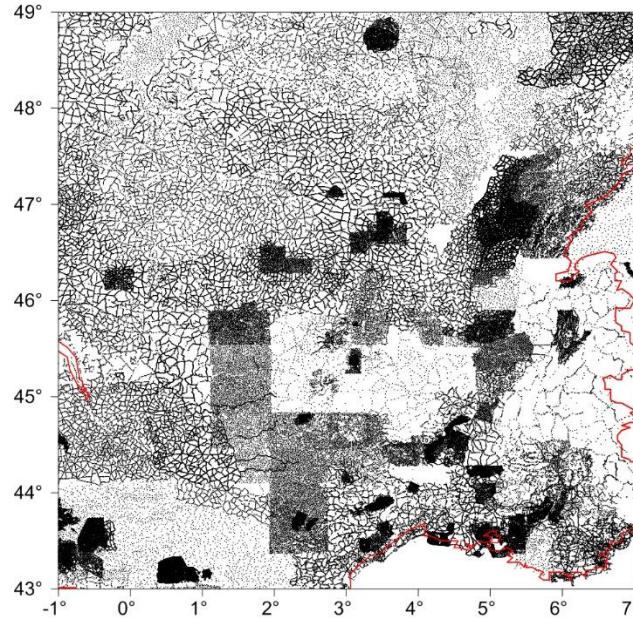


Figure 3.1: Distribution of the free-air gravity anomalies

It contains 244,009 values of the free-air gravity anomalies in the IGSN71 gravity reference system, with horizontal positions (ellipsoidal latitude and longitude) compatible with the ETRS89 terrestrial reference system and the heights of the normal variety [Duquenne, 2007]. It covers the area  $43^\circ \leq \varphi \leq 49^\circ$ ,  $-1^\circ \leq \lambda \leq 7^\circ$ , see Figure 3.1, and the standard deviation of these data, according to Duquenne [2007] ranges from 0.25 to 0.75 mGal. This error can increase to 1 to 2 mGal after computation of gravity anomalies, mainly due to inaccuracy in a horizontal position of the gravity points. Most of the gravity values were measured before 1971 and transformed to IGSN71 from older gravity systems. The density of the gravity data coverage varies significantly in the south-eastern part of the area, see Figure 3.1. In some areas, even in the central part, the coverage is not sufficient for interpolation to a dense grid. The map of the free-air gravity anomalies is shown in Figure 3.2, and the corresponding basic statistical values are listed in Table 3.1.



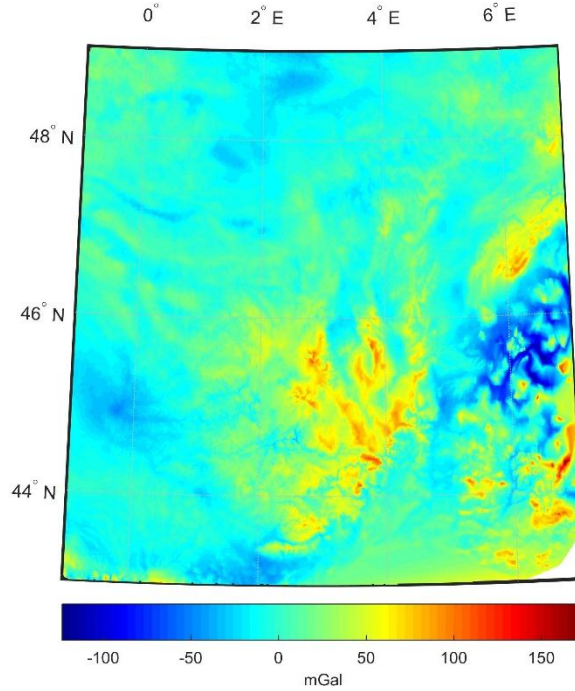


Figure 3.2: Free-air gravity anomalies directly gridded from the original scattered data based on [Duquenne, 2007] database.

We decided to check this gravity database for outliers and duplicate points. 118 couples of duplicate points and 2 outliers were detected and eliminated.

Table 3.1: Statistical values of the observed (scattered) free-air gravity anomalies and normal heights at the 244009 measured points of the data set [Duquenne, 2007].

Quantity	Min	Max	Mean	STD
$\Delta g$ (mGal)	-127.47	177.82	3.06	20.70
$H_n$ (m)	0	2677.27	288.24	234.14

Another type of data set are DEMs. For our computation, we used three DEMs: the SRTM3 version 4 [Werner, 2001; Rodriguez et al., 2005; Reuter et al., 2007], the ACE2 which is based on a combination of the SRTM and Satellite Radar Altimetry data [Berry

et al., 2010] and a global DEM in the form of spherical harmonic coefficients of the JGP95 model [Lemoine et al., 1998]. The SRTM3 model was used for representing a detailed topography on a grid of 3"×3" spacing. It was used mainly for interpolation of the free-air gravity anomalies to get free-air anomalies on a regular grid with 1'×1' resolution and for the computation of the direct topographical effect, as explained in section 3.5. This is a nearly global high-resolution DEM with an absolute vertical error (a linear error with respect to true elevation at 90% probability) of less than 16 m [Hensley et al., 2000; Farr et al., 2007]. Several studies show that this error is actually smaller—about 9 meters [Denker, 2004; Rodriguez et al., 2005]. Some known problems such as the data void due to shadowing and smooth surfaces, or weak penetration of the vegetation canopies were addressed to some extent in version 4 [Reuter et al., 2007].

The ACE2 model is applied in those computations where the mean elevations on a grid of 30"×30", 5'×5' or 1°×1° resolution are needed, see sections 3.5 and 3.6. For accuracy assessment of ACE2 model, see [Berry et al., 2010]. Finally, the JGP95 model is needed in the “Helmerization” of the reference field, see section 3.6. A comparison with the GLOBE global DEM and accuracy assessment of this model can be found in, e.g., Berry [1999]. The topography on a grid of 30"×30" based on the ACE2 DEM over the area covered by terrestrial gravity data is depicted in Figure 3.3.

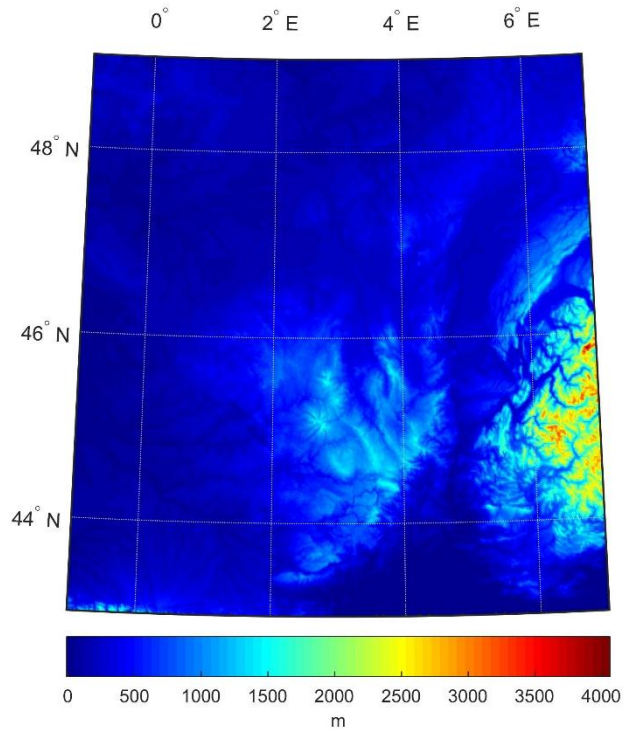


Figure 3.3: Topography of the area covered by terrestrial gravity data with the resolution of  $30'' \times 30''$  based on the ACE2 digital elevation model.

The next input needed in our computational scheme is an Earth gravity model (EGM). The satellite-only EGM GO\_CONS\_GCF\_2\_DIR\_R5 is used for our reference field computation, see section 3.6. Figures of the reference gravity anomalies and the associated reference spheroid are presented in section 3.6.

The last input used in the UNB SH-scheme is a digital topographical density model (DDM). The largest contribution comes from lateral inhomogeneity and this was the one we concentrated on here. We prepared our own lateral DDM based on an analogous geological map of France by Bodelle et al. [1980], as was also investigated by Foroughi et al. [2015b], that despite the low resolution of the map improves the accuracy of the gravimetric geoid in Auvergne. The DDM affects the direct topographic effect, and the primary and secondary indirect topographic effects. However, the influence on the

secondary indirect topographic effect is usually negligible and was therefore not evaluated. The two remaining effects, called the direct density effect (DDE) and primary indirect density effect (PIDE) are shown in subsection 3.6.2. Details about the preparation and testing of the DDE for the Auvergne and surrounding area can be found in Foroughi et al. [2015b].

### **3.5 Interpolation of free-air gravity anomalies on topography**

The observed free-air gravity anomalies are scattered irregularly on the Earth surface. Most geoid computation algorithms, including ours, require an input of free-air gravity anomalies on a regular grid. Therefore, an interpolation of free-air gravity anomalies, which is not a trivial task, has to be performed. A procedure published by Janák and Vaníček [2005] was adopted. The scattered free-air gravity anomalies were transformed first into refined spherical Bouguer gravity anomalies, which are locally smooth enough to make interpolation easier. Interpolation of these anomalies into a regular geographical  $1' \times 1'$  grid, see Figure 3.4, was performed by the Kriging method with a linear variogram assuming an anisotropy factor due to the convergence of meridians. The basic statistical values of both scattered and interpolated refined spherical Bouguer gravity anomalies are shown in Table 3.2.

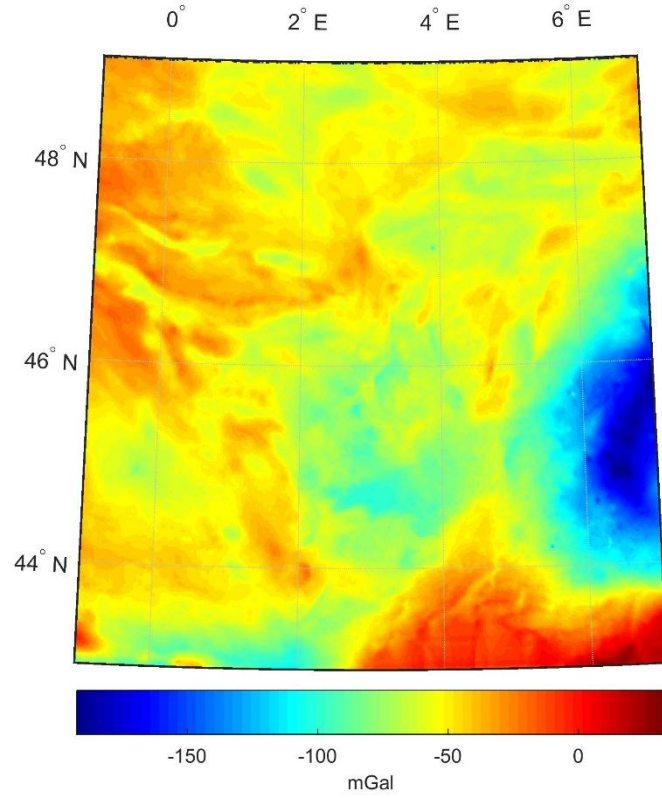


Figure 3.4: Refined spherical Bouguer gravity anomalies on the Earth surface interpolated to 1'×1' geographical grid.

Table 3.2: Statistics of the 243889 scattered and 1'×1' interpolated refined spherical Bouguer gravity anomalies and free-air gravity anomalies.

Quantity	Min	Max	Mean	STD
$\Delta g_{scatt}$ (mGal)	-127.47	177.82	3.06	20.70
$\Delta g_{RB\_scatt}$ (mGal)	-193.66	28.44	-56.74	19.95
$\Delta g_{RB\_grid}$ (mGal)	-192.87	28.50	-59.98	28.50
$\Delta g_{grid}$ (mGal)	-111.36	292.33	8.82	29.03

Free-air gravity anomalies on the same geographical grid of  $1' \times 1'$  (see Figure 3.5), were obtained by adding back the topographical mass effect with the elevation of the grid nodes and the shape of the surrounding terrain were taken from the SRTM3 DEM. Basic statistics are shown in the last row of Table 3.2.

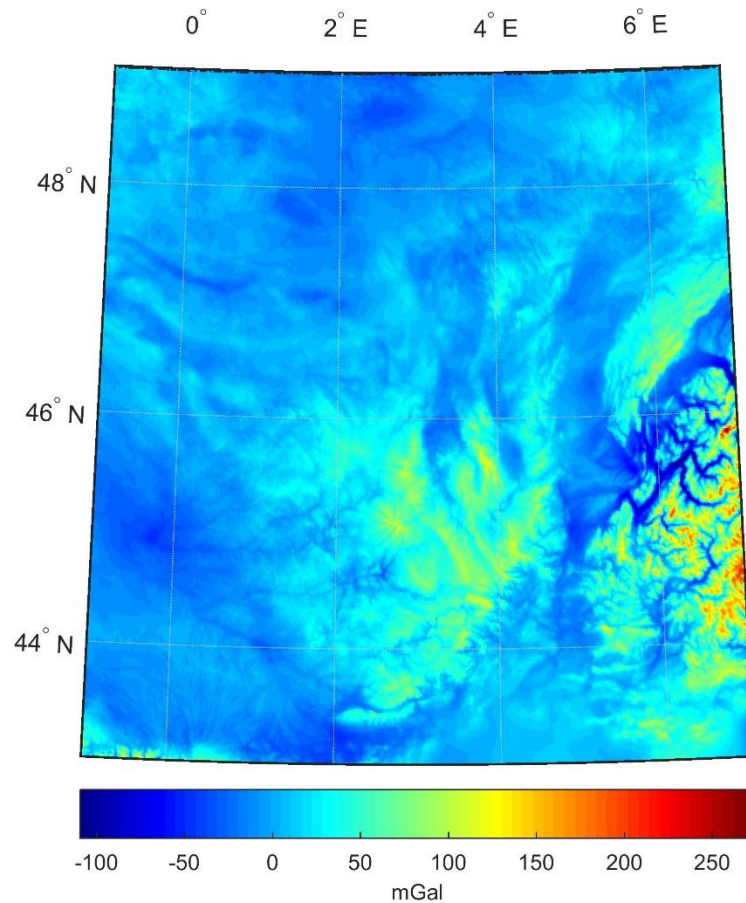


Figure 3.5: Free-air gravity anomalies on a regular  $1' \times 1'$  geographical grid obtained from interpolated refined spherical Bouguer gravity anomalies.

### 3.6 Computation of geoid model

In this section, we present the intermediate and final results of the SH geoid computation process following the computational steps outlined in Section 3.3. Foroughi

et al. [2017a] suggested a numerical technique to arrive at the optimal degree/order of reference field (this equals also the modification of Stokes's integral) and Stokes's integration radius to compute cogeoid heights. They suggested to vary the degree of reference field and Stokes's integration cap size and evaluate the final geoid with GNSS/Leveling points. In case gravity data in surrounding areas are needed when using larger integration cap sizes, they can be filled with EGM-generated grid points [Foroughi et al., 2015a]. According to their investigation, the degree/order of 160 for the reference field and integration radius of 45' gives the best results in the sense of fitting the geoidal heights with GNSS/Leveling points in the area of Auvergne. We adopted these parameters for our study, but it should be stated that these parameters can differ for different areas.

### **3.6.1 Geoid model under the assumption of standard topographic density**

In order to transfer the free-air gravity anomalies to Helmert space, and thus to obtain the Helmert gravity anomalies, the effects DTE and SITE and DAE (see step 1 in Section 3.3) have to be applied to free-air gravity anomalies. The secondary indirect atmospheric effect, the SIAE, can safely be neglected, as its magnitude is exceedingly small. The other effects are shown in Figure 3.6 and Figure 3.7 and their statistical values are presented in Table 3.3.

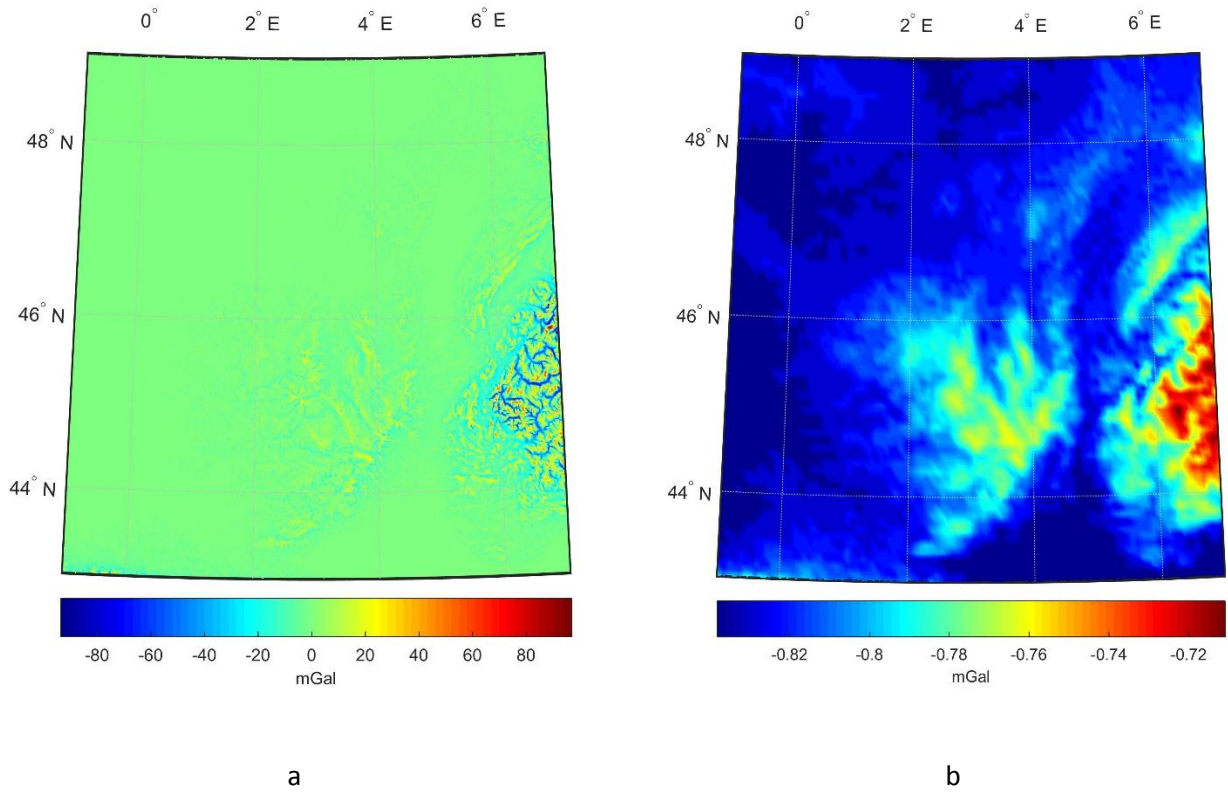


Figure 3.6: Direct topographical effect (a) and direct atmospheric effect (b) used for transformation of the free-air gravity anomalies to the Helmert space.

Table 3.3: Statistics of Helmertization terms (mGal).

Quantity	Min	Max	Mean	STD
DTE	-103.61	110.41	-1.01	7.57
SITE	-2.23	0.00	-0.03	0.10
DAE	-0.84	-0.71	-0.82	0.02



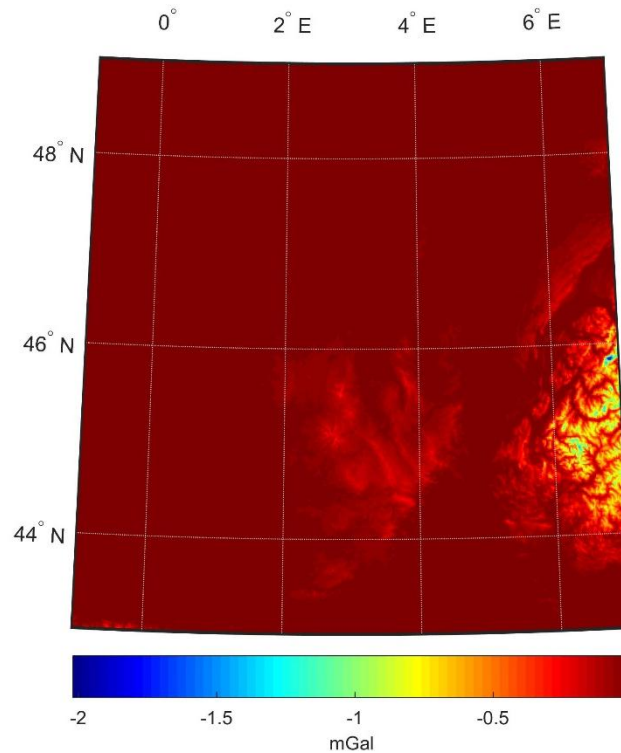


Figure 3.7: Secondary indirect topographic effect used for the transformation of the free-air gravity anomalies to the Helmert space.

Helmert's gravity anomalies multiplied by geocentric radius  $r$  can be continued down from the Earth surface to the geoid as they are a harmonic function. For this downward continuation, we used the Jacobi iterative procedure complemented by the determination of the maximum necessary number of iterations, as discussed by Kingdon and Vaniček [2010] and described in step #2 of section 3.3 above. Figure 3.8a displays the Helmert gravity anomalies on the Earth surface and Figure 3.8b shows the Helmert gravity anomalies on the geoid after applying the downward continuation.

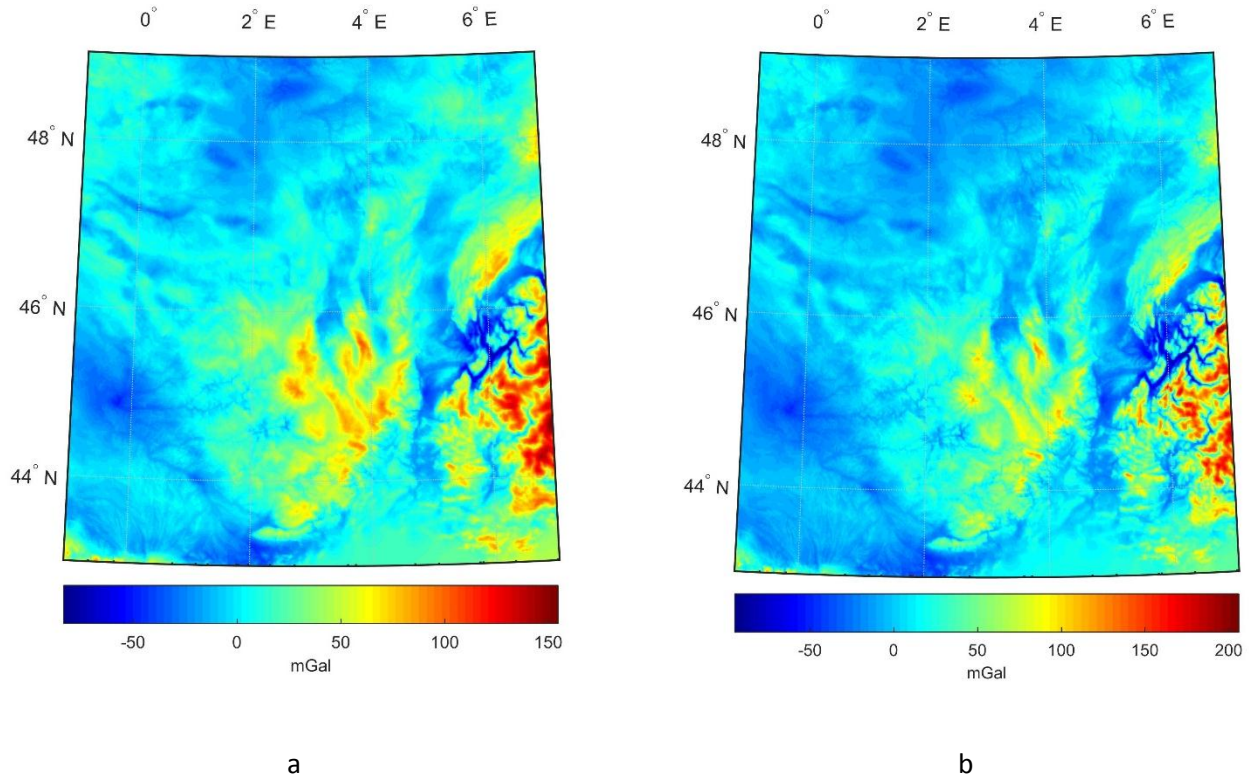


Figure 3.8: Helmert's gravity anomalies on the Earth surface (a) and on the geoid (b).

Table 3.4: Statistics of Helmert's gravity anomalies on the earth surface and on the geoid (mGal).

Quantity	Min	Max	Mean	STD
Helmert gravity anomalies on surface	-86.82	155.08	9.84	27.36
Helmert gravity anomalies on geoid	-97.92	208.50	10.52	30.17

The reference gravity anomalies in Helmert's space were computed by means of the DIR\_R5 up to degree/order 160 and the global digital terrain model JGP95 using the linear and quadratic coefficients, see Figure 3.9a. Subtracting the reference Helmert gravity anomalies from the Helmert gravity anomalies on the geoid, as obtained from terrestrial gravity measurements, we get the residual Helmert gravity anomalies, as demanded by

step #3 in section 3.3 above, see Figure 3.9b. These anomalies are further corrected by adding two ellipsoidal corrections due to spherical approximation of the boundary condition, see Figure 3.10a and Figure 3.10b.

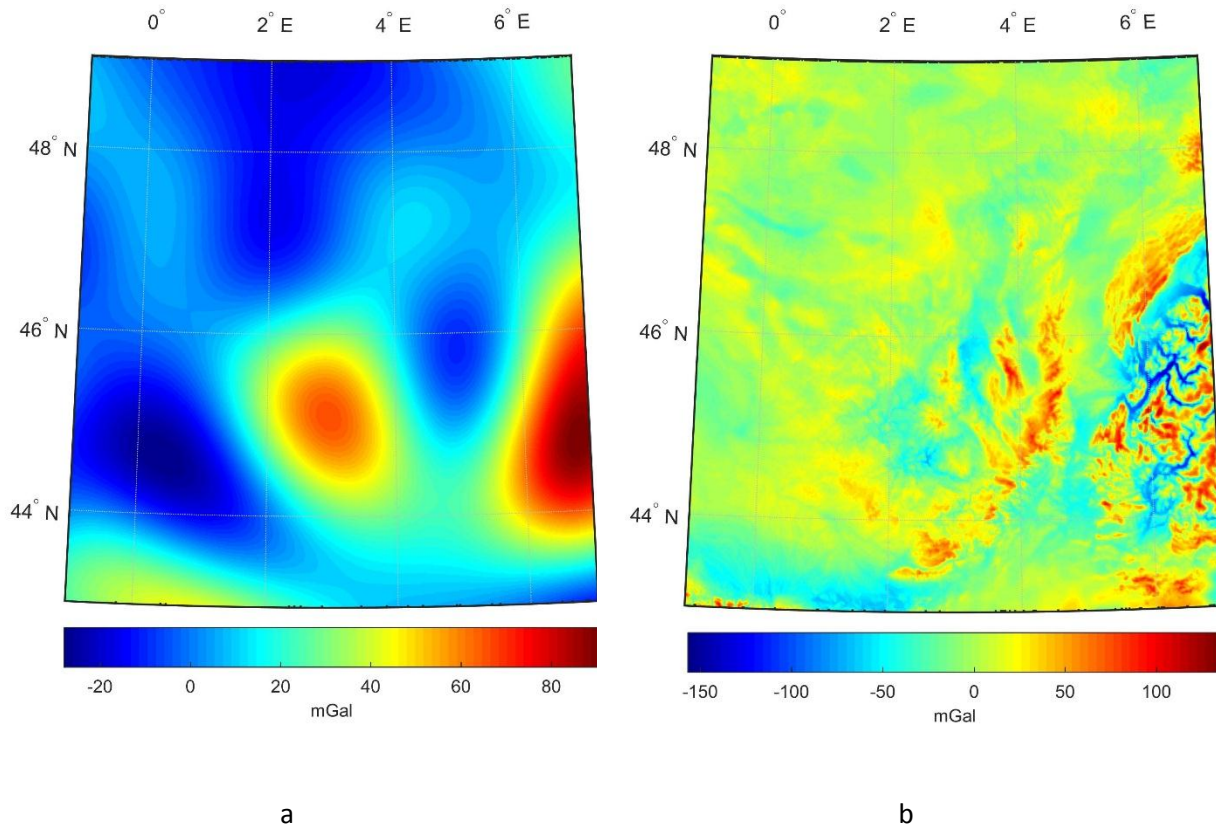


Figure 3.9: Reference Helmert's gravity anomalies computed using DIR-R5 up to degree/order 160 (a) and residual Helmert's gravity anomalies (b).

Table 3.5: Statistics of reference Helmert's gravity anomalies and residual Helmert's gravity anomalies (mGal).

Quantity	Min	Max	Mean	STD
Reference Helmert gravity anomaly	-28.04	90.63	11.31	22.35
Residual Helmert gravity anomaly	-161.69	138.47	-0.75	23.71

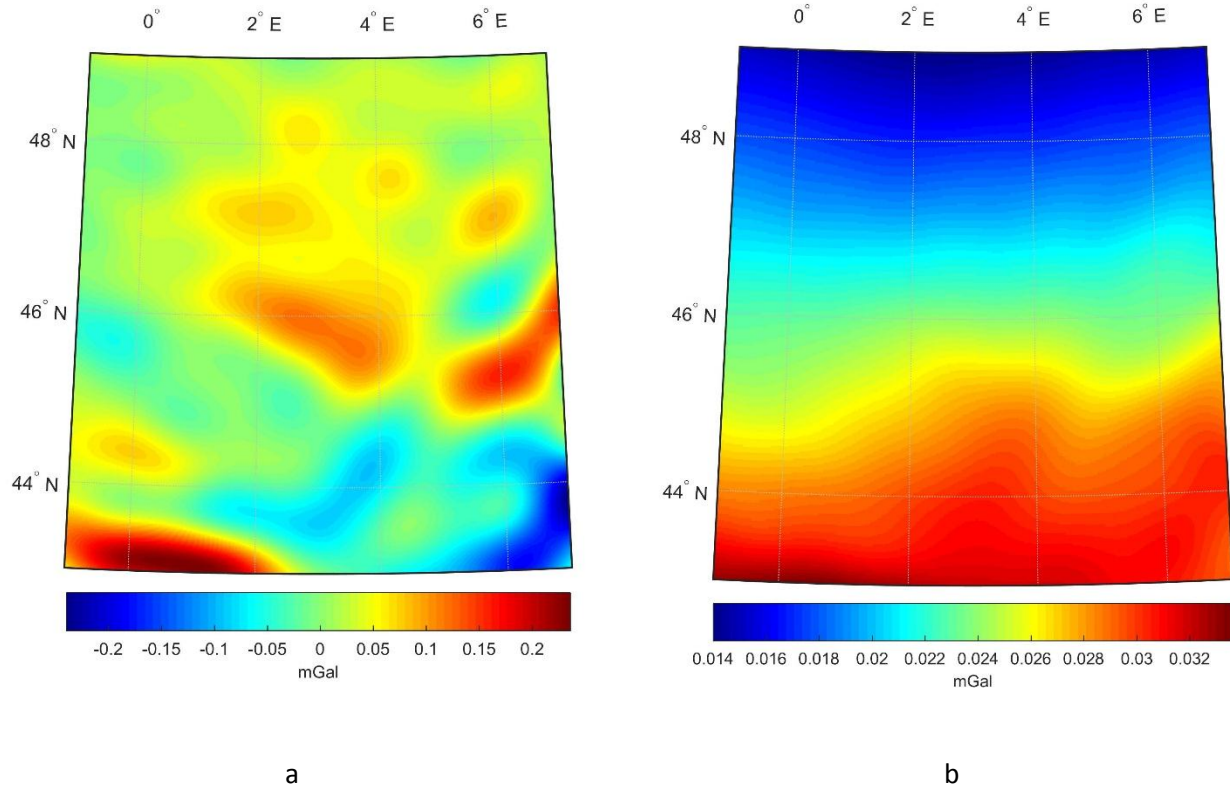


Figure 3.10: Ellipsoidal corrections: correction to gravity disturbance (a) and correction for spherical approximation (b).

Table 3.6: Statistics of ellipsoidal corrections (mGal).

Quantity	Min	Max	Mean	STD
Ellipsoidal correction to gravity disturbance	-0.239	0.235	0.019	0.059
Ellipsoidal correction to spherical approximation	0.014	0.034	0.023	0.005

Applying the Stokes integration to the residual Helmert gravity anomalies, the residual NZ co-geoid was computed at the nodal points of 1'x1' grid using modified Stokes's convolution integral (integration cap  $\psi=45'$ , modification degree of 160) in

$2^\circ \times 3^\circ$  central area,  $45^\circ < \varphi < 47^\circ$ ,  $1.5^\circ < \lambda < 4.5^\circ$ , in which all the GNSS/Leveling points are located. For this integration, the UNB “Faster than the FFT” technique was employed as already mentioned in step #4 in section 3.3 above.

The FZ contribution, a.k.a., the truncation correction (or truncation error with the opposite sign), was then evaluated from DIR\_R5 using spherical harmonic coefficients (transformed into the Helmert space) of degree/order 161 up to full degree/order (300).

This contribution is shown in Figure 3.12a.

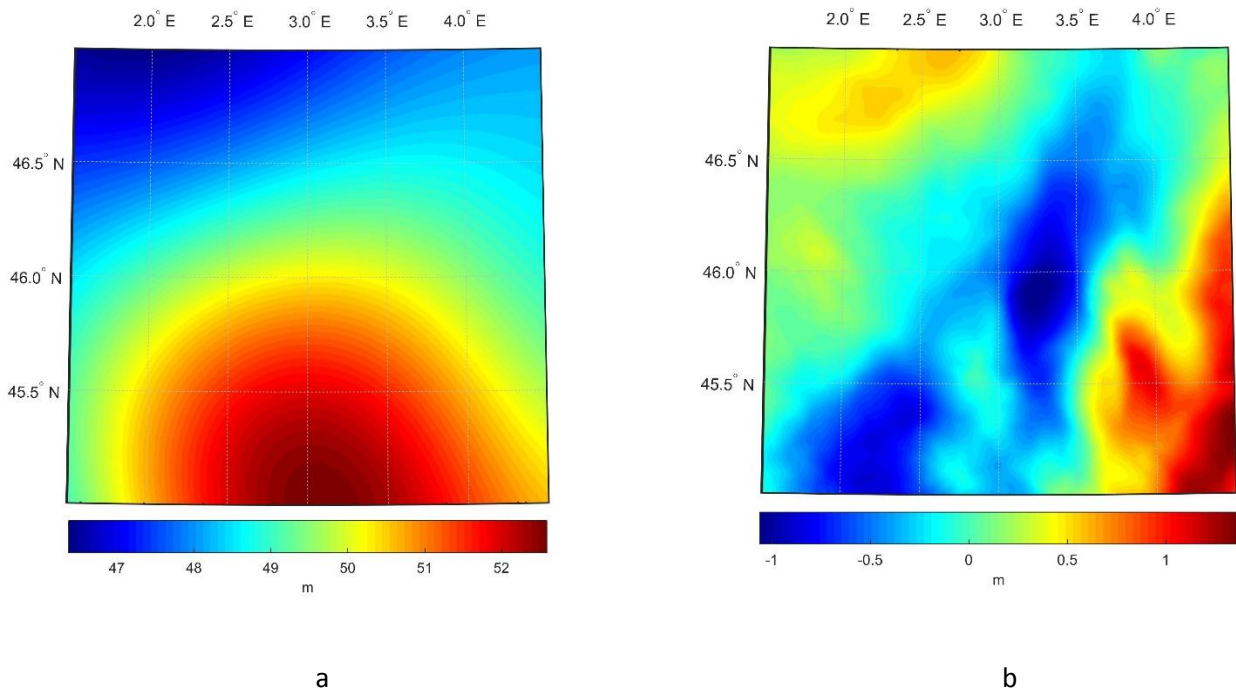


Figure 3.11: Reference Spheroid computed using DIR-R5 model and up to degree/order 160 in Helmert’s space (a) and residual co-geoid (b).

The low frequency part of the co-geoid, the reference spheroid, as well as the truncation correction must be added to residual co-geoid values to get the co-geoid (cf., step #6 in section 3.3 above), i.e., the geoid in Helmert’s space, which contains all harmonic frequencies. The reference spheroid was computed using the DIR-R5 and JGP95

models up to the same degree/order 160 as for the reference Helmert gravity anomaly. Figure 3.11a shows the undulation of the reference spheroid and Figure 3.11b the residual co-geoid in the central area of the Auvergne region. The statistics are presented in Table 3.7.

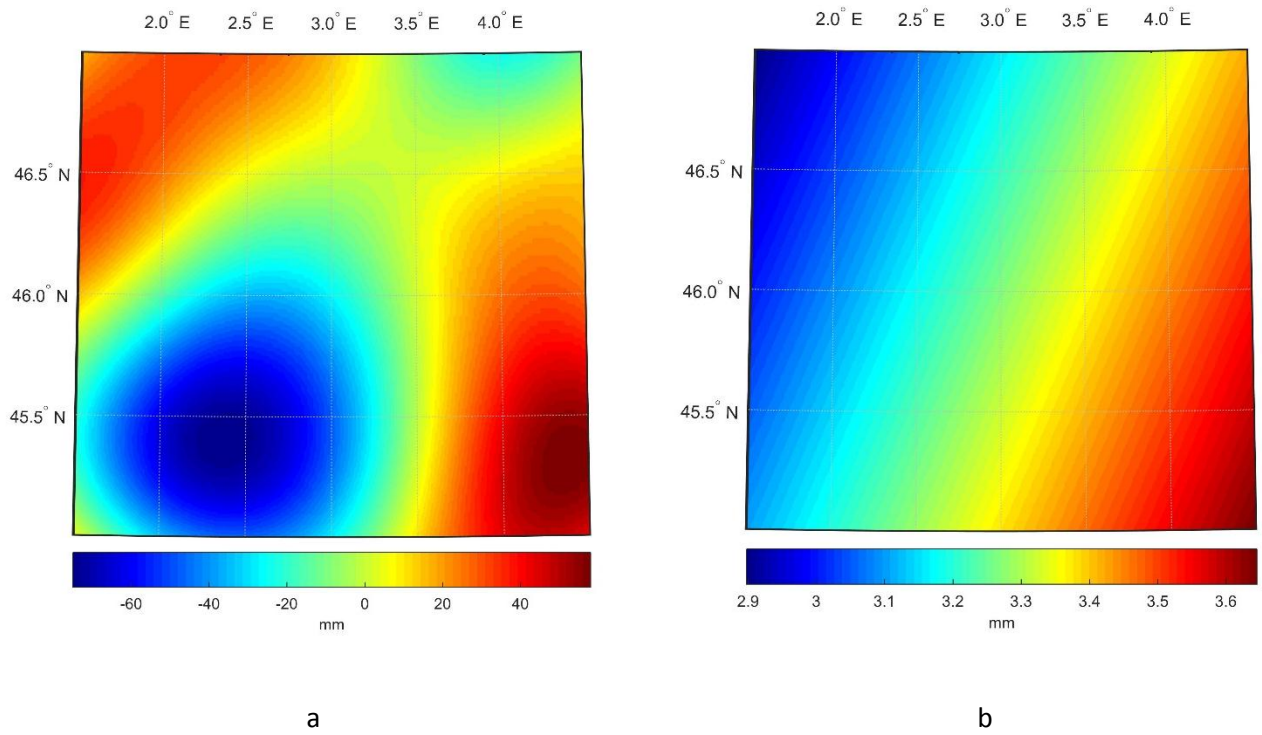


Figure 3.12: Far-zone contribution to residual NZ co-geoid, a.k.a., truncation correction (a) and Hörmander correction (b).

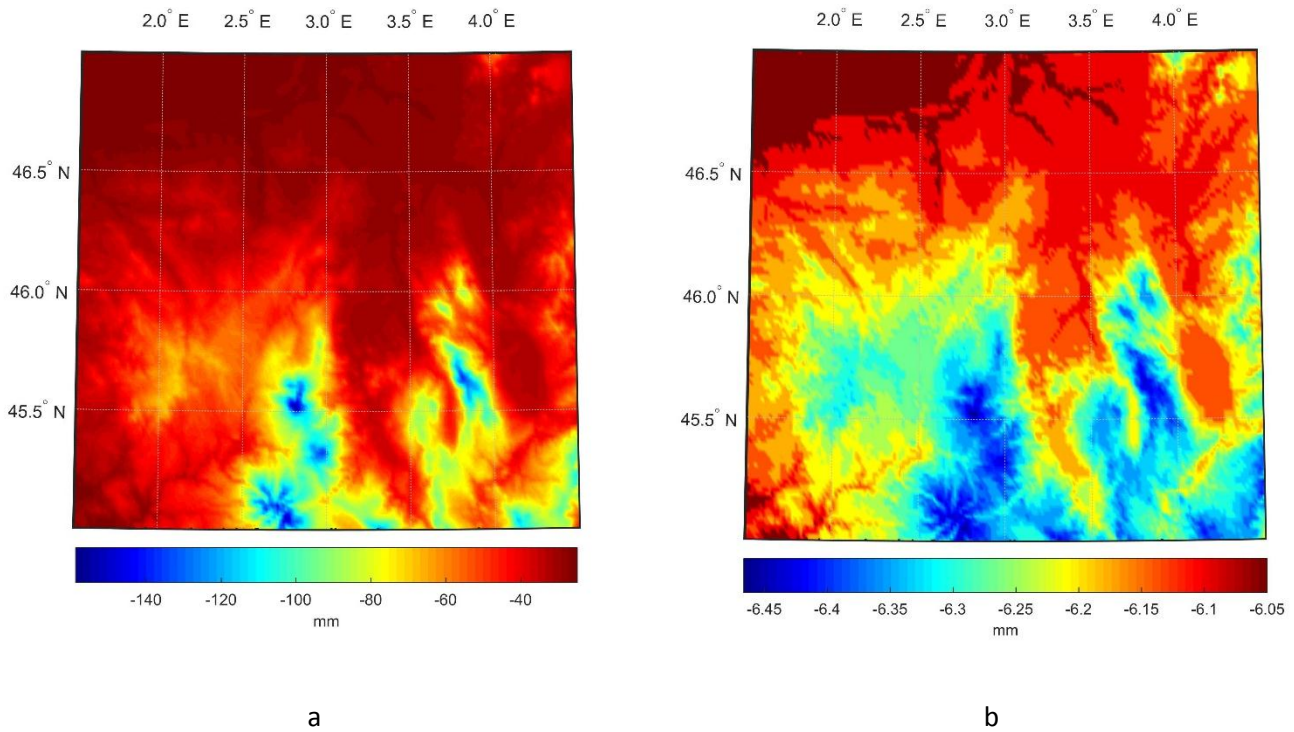


Figure 3.13: Primary indirect topographical effect (a) and primary indirect atmospheric effect (b).

Transformation of the co-geoid in a Helmert space to the geoid in a real space needs to be done by applying the primary indirect topographical and atmospheric effects, the PITE and PIAE (step #7 in section 3.3 above), see Figure 3.13. These effects were computed using the ACE2 digital terrain model. At the end of the computation process a Hörmander correction which corrects for the small shift of the centre of the Earth mass during the Helmert condensation needs to be computed (step #7 in section 3.3 above), see Figure 3.12b and Table 3.7. The residual co-geoid, reference spheroid, truncation correction and all other correction terms were computed at the nodal points of 1'×1' regular geographical grid.

Final geoid model was obtained by the summation of the co-geoid, the two primary indirect effects PITE and PIAE and the Hörmander correction. The geoid height in this

area varies between 46.62 m and 52.53 m, see Table 3.7. Figure 3.14 shows the geoid height variation in the computation area.

Table 3.7: Statistics of final geoid computation components (m).

Quantity	Min	Max	Mean	STD
Reference Spheroid	46.371	52.587	49.560	1.570
Residual Co-geoid	-1.063	1.366	0.00	0.479
Truncation correction	-0.075	0.058	-0.004	0.032
PITE	-0.159	-0.025	-0.044	0.020
PIAE	-0.007	-0.006	-0.006	0.000
Hörmander correction	0.003	0.004	0.003	0.000
Geoid	46.595	52.480	49.512	1.487

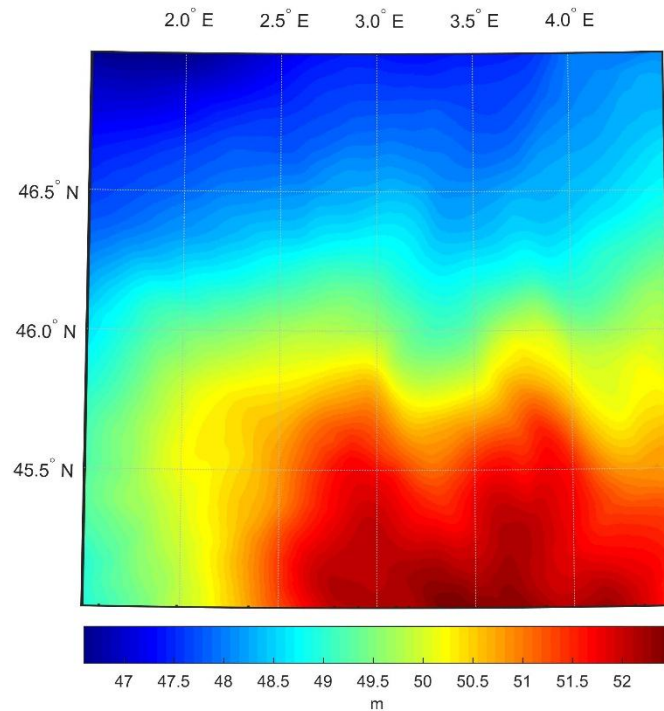


Figure 3.14: Geoid model in the Auvergne area assuming the standard density of topographic masses  $2670 \text{ kg.m}^{-3}$ .



### **3.6.2 The effect of lateral topographical density variations on the geoid**

Lateral topographical density variations in this area were estimated from surface geology on a 5'×5' grid from publicly available geological map introduced in section 3.4. The effect of these approximate density variations on the geoid were computed in two terms of direct density effect DDE (cf., step #1 in section 3.3 above) and primary indirect density effect PIDE (cf., step #7 in section 3.3 above). The total effect of lateral topographical density varies between -5.8 and 2.4 cm. These corrections were applied to the final geoid model in Auvergne area; for more details see Foroughi et al. [2015b]. Figure 3.15 shows the effects of lateral density variation on the geoid in the Auvergne area. Due to the lack of accurate density information the lateral topographical density model was created on a relatively coarse grid and thus the contribution to the geoid has been evaluated only approximately. The statistics of both components and the geoid model assuming the density variation is shown in Table 3.8.

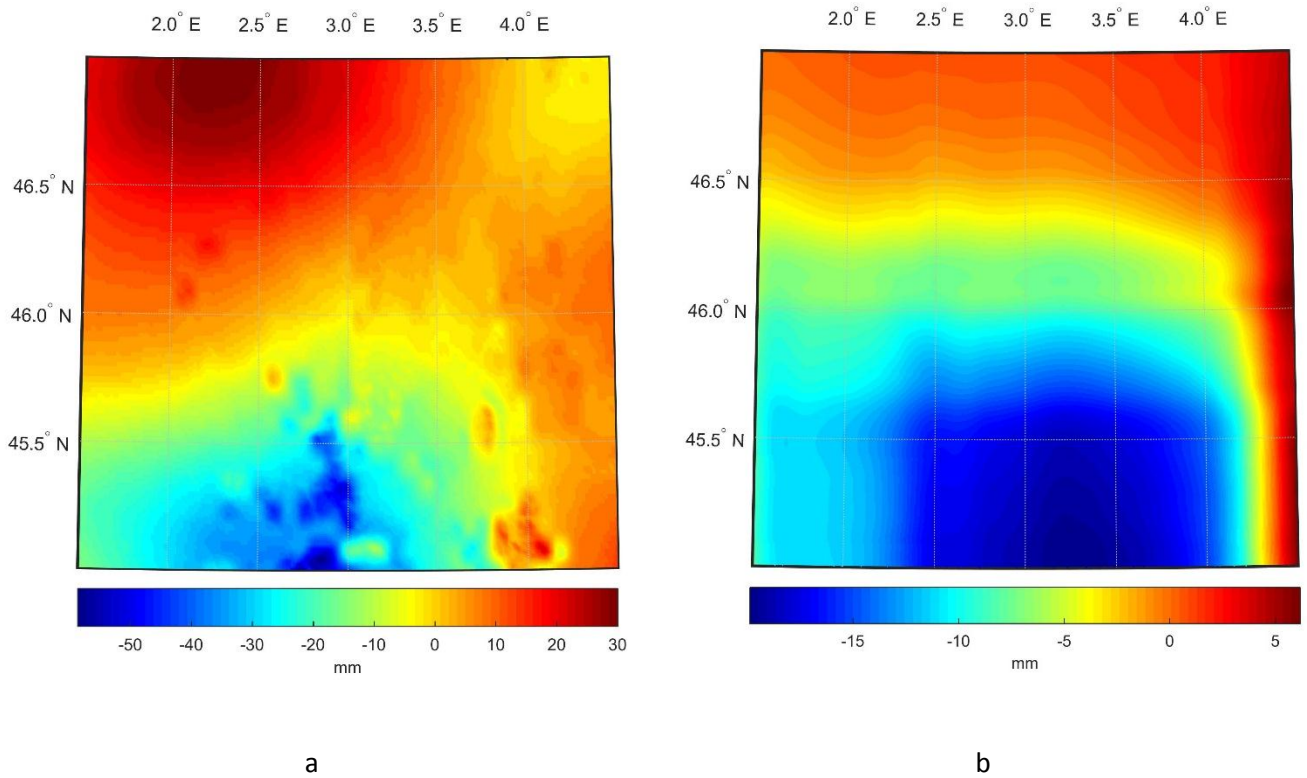


Figure 3.15: Effects of lateral topographical density variations in Auvergne area: direct topographical density effect (a) and primary indirect topographical density effect (b).

Table 3.8: Statistics of the direct and primary indirect density effects on the geoid and statistics of the geoid model assuming the lateral topographical density variation (m).

Quantity	Min	Max	Mean	STD
DDE	-0.059	0.030	0.000	0.016
PIDE	-0.020	0.006	-0.007	0.007
Geoid	46.620	52.492	49.528	1.491

### 3.7 Testing and comparison

The 75 points on which both the GNSS-determined geodetic heights and levelled heights, expressed as “normal heights“, are located in the area of Auvergne [Duquenne, 2007]. These points have been used for the assessment of our geoid model. First, the

rigorous orthometric heights were calculated from the normal Molodensky heights based on the theory published by Santos et al. [2006]. The implementation of this transformation is described by Foroughi et al. [2017b]. The locations of these control points over the test area are shown in Figure 3.16. The statistics of the differences between the two heights, rigorous orthometric minus normal, is shown in Table 3.9.

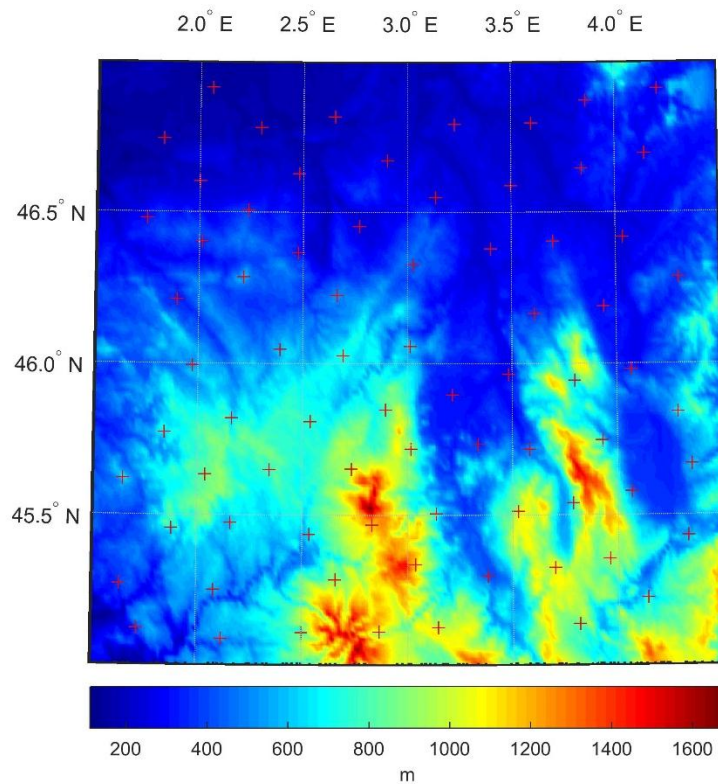


Figure 3.16: Topography over the Auvergne area and locations of control GNSS/Leveling points.

Table 3.9: Statistics of differences between the rigorous orthometric and normal heights (mm).

Quantity	Min	Max	Mean	STD	Range
$H^o - H^n$	1.6	70.4	22.3	14.7	68.8

After obtaining the set of the rigorous orthometric heights, the geoid heights were evaluated at the location of the 75 control points, and the differences between the gravimetric geoid heights and the differences of geodetic and rigorous orthometric heights at these points were computed. These differences are characterized by the standard deviation of 3.4 cm and the mean difference of 12.4 cm, see Table 3.10. After the effects of lateral topographical density variation were added to the final geoid model, the comparison showed 1.4 mm improvement in the standard deviation and 7.3 mm change in the mean difference, see Table 3.10. Figure 3.17 shows the differences between the final geoid model and the GNSS/Leveling control points.

The same evaluation was done in Ågren et al. [2009] for their quasigeoid solution using five different methods and normal heights of the same 75 control points [cf., Ågren, et al. 2009]. According to their results the KTH method Sjöberg [2003] gives the smallest standard deviation (3.3 cm) when one-parameter corrector plane is applied. This confirms our results presented here as the KTH method is basically a simplified geoid determination (using Stokes's technique) which is then converted to quasigeoid for comparison with normal heights. However, the comparison of mean of differences is not possible since the quasigeoid results are always presented after applying a corrector surface.

Table 3.10: Statistics of differences between the gravimetric geoid heights and GNSS/Leveling geoidal heights computed at 75 control points (m).

Quantity	Min	Max	Mean	STD	Range
Geoid	0.028	0.207	0.124	0.034	0.178
Geoid (density effect included)	0.024	0.222	0.133	0.033	0.197

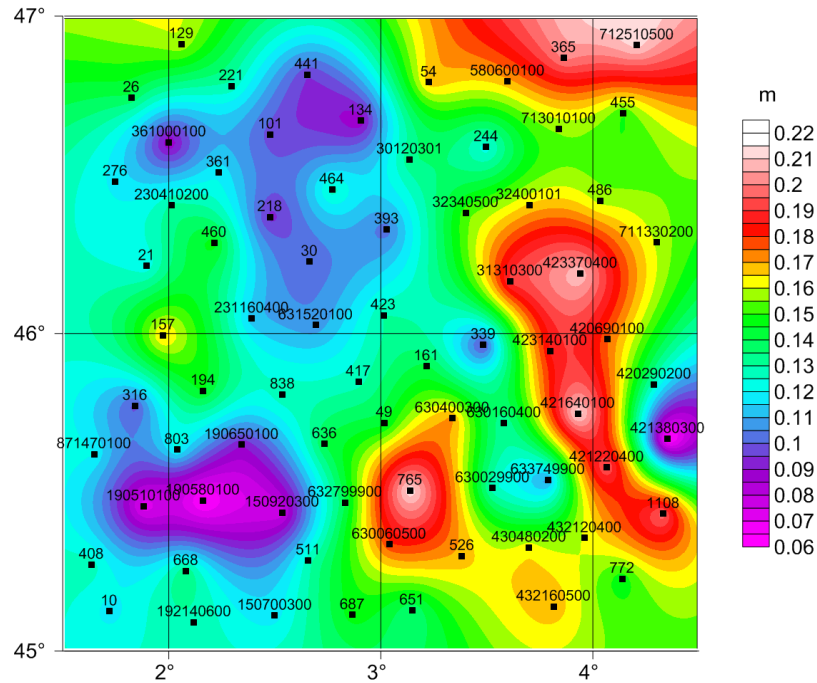


Figure 3.17: Map of differences between the gravimetric geoid model that includes the lateral topographical density effect and GNSS/Leveling geoid heights at control points.

More detailed statistical information about the differences can be seen from the histograms plotted in Figure 3.18.

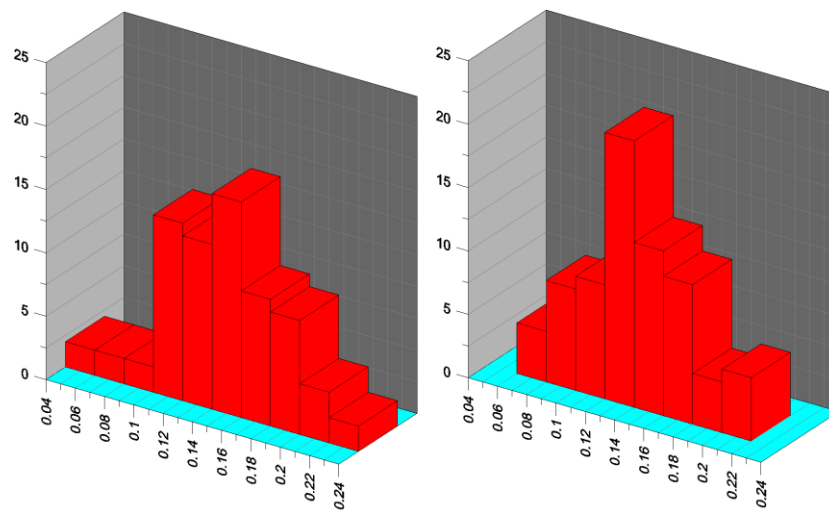


Figure 3.18: Histograms of differences between the gravimetric geoid heights (standard density – left; lateral topographical density variation included – right) and GNSS/Leveling geoid heights at 75 control points.

From the histograms shown in Figure 3.18 it can be seen that there has been an improvement in the distribution of the differences in spite of very poor resolution of the digital density model that was used for the computation. The histogram on the right appears to be more normally distributed around the mean value.

### **3.8 Discussion and conclusions**

As stated in the abstract, the intention of this paper is to show how the current version of the Stokes-Helmert geoid determination technique works with real data at least as well as the quasigeoid determination techniques do. The S-H's technique, as a result of several decades of investigation and refinements performed mainly at the University of New Brunswick was already tested on an Australian synthetic gravity field constructed at the Curtin University [Baran et al., 2006]. The test was not very successful because the synthetic field lacked the required accuracy and self-consistency. However, it confirmed the hypothesis that the S-H theory is accurate to about 2.5 cm (standard deviation) and to a range of 20 cm when used with errorless data [Vaníček et al., 2013] Assuming that the errors in the SH theory (and in the code) are independent of the errors in input data, we would deduce that the effect of the data errors (observed gravity, topographical heights, topographical density, levelled heights and GNSS determined geodetic heights) combined is about 2.6 cm which is less than one should expect.

Our study in the Auvergne test region revealed, without employing any beautification technique such as corrector surfaces, and with a very inaccurate evaluation of the topographical density contribution, that the gravimetric geoid can certainly be

determined to the same accuracy as, if not a better accuracy than, quasigeoid models in the same area, (see, e.g., Yildiz et al. [2012]). This also demonstrates the successful application of Helmert's second condensation technique (see, e.g., Martinec [1998]), which generates very small indirect topographical effects. Moreover, it substantially reduces the requirement of knowing the topographic mass-density distribution, as the error in density committed in the topographical effect is to a large extent compensated by the error produced in the condensed topographical effect. Therefore, reasonable results can be obtained even when a standard density assumption or a coarse density model is used. However, we believe, that the presented geoid model can be further improved with finer digital density model, if it becomes available.

The mean value of our geoid solution is 13.3 cm above the average of GNSS/Leveling values. This corresponds very well with the estimated constant height system offset for France which is -13.2 cm according to Rülke et al. [2012, Table 3]. This result is also an important topic for further discussion as we believe that the mean value of computed gravimetric geoid model compared to the GNSS/Leveling geoidal heights can be a useful information on the used height system.

Last but not least, we would like to emphasize the importance of the physical rigor in the choice of the computation techniques. This is especially true of the most problematic step of the geoid computation procedure, the downward continuation. This task is in the background of the motivation for using the Helmert space, where we construct gravity functionals which are harmonic above the geoid (to the extent to which the assumed topographical density is known) and can therefore be continued downward rigorously

using the Poisson technique. The numerical evaluation of this step is widely discussed, mainly due to its numerical instability, but the results obtained in our experiment show that it is possible to evaluate this step with a reasonable accuracy even for data on 1'×1' mesh.

### **3.9 Acknowledgement**

The research and the numerical experiment presented in this paper was made possible by the Canadian NSERC “Individual Discovery” grant to P. Vaníček and by the Slovak national project VEGA 1/0954/15 to J. Janák. The gravity and GNSS/Leveling data were given to us by Institut Géographique National.

### **3.10 References**

- Ågren J, Barzagi R, Carrion D, Denker H, Grigoriados VN, Klamehr R, Sona G, Tscherning CC, Tziavos IN (2009) Different geoid computation methods applied on a test data set: results and considerations. Poster presented at Hotine-Marrussi Symp., Rome, 6-12 July, 2009.
- Baran I, Kuhn M, Claessens SJ, Featherstone WF, Holmes SA, Vaníček P (2006) A synthetic Earth gravity model designed specifically for testing regional gravimetric geoid determination algorithms. *J Geodesy* 80: 1-16. doi: 10.1007/s00190-005-0002-z.
- Bodolle et al. (1980) Carte géologique de la France et de la marge continentale, 1:1500 000, 1978-1979.



- Berry PAM (1999) Global digital elevation models - fact or fiction? *Astron Geophys* 40: 3.10 – 3.13. doi: 10.1093/astrog/40.3.3.10.
- Berry PAM, Smith RG, Benveniste J (2010) ACE2: The new global digital elevation model. In: *Gravity, Geoid and Earth Observation. IAG Symposia 135*, Mertikas SP (ed), Springer, Berlin: 231-237. doi: 10.1007/978-3-642-10634-7\_30.
- Denker S (2004) Evaluation of SRTM3 and GTOPO30 terrain data in Germany. In: *Gravity, Geoid and Space Misions. IAG Symposia 129*, Jekeli C et al. (eds), Springer, Berlin: 218-223.
- Duquenne H (2007) A data set to test geoid computation methods. *Proceedings of the 1<sup>st</sup> Internatiaonal Symposium of the International Gravity Field Service (IGFS)*, Istambul, Turkey. *Harita Dergisi, Special Issue 18*: 61-65.
- Ellmann A, Vaníček P (2006) UNB application of Stokes-Helmert's approach to geoid computation. *J Geodyn* 43: 200-213.
- Farr TG et al (2007) The Shuttle Radar Topography Mission. *Rev Geophys* 45, RG2004. doi: 10.1029/2005RG000183.
- Foroughi I, Janák J, Kingdon RW, Sheng MB, Santos MC, Vaníček P (2015a) Illustration of how satellite global field should be treated in regional precise geoid modelling. (Padding of terrestrial gravity data to improve Stokes-Helmert geoid computation). *Geophysical Research Abstracts 17*, EGU2015-6655-1, European Geoscience Union General Assembly, Vienna, Austria.

- Foroughi I, Sheng MB, Kingdon RW, Huang J, Martinec Z, Vaníček P, Santos MC (2015b) The effect of lateral topographical density variations on the geoid in Auvergne. 26<sup>th</sup> IUGG General Assembly, Prague, Czech Republic.
- Foroughi I, Vaníček P, Novák P, Kingdon RW, Sheng MB, Santos MC (2017a) Optimal combination of satellite and terrestrial gravity data for regional geoid determination using Stokes-Helmert's method. Submitted to IAG proceeding of Gravity, Geoid, and Height System 2016 meeting in Thessolinki, Greece.
- Foroughi I, Vaníček P, Sheng MB, Kingdon RW, Santos MC (2017b) In defence of the classical heihgt system.(Geophysical Journal International, <https://doi.org/10.1093/gji/ggx366>).
- Helmert FR (1884) Die matematischen und physikalischen Theorien der höheren Geodäsie. Vol. 2, B.G. Treubner, Leipzig.
- Hensley S, Rosen P, Gurrola E (2000) The SRTM topographic mapping processor. In: Geoscience and Remote Sensing Symposium IGRASS 2000. IEEE 2000 Int., 3: 1168-1170.
- Hörmander L (1976) The boundary problems of physical geodesy. Arch Ration Mech Anal 62: 1-52. doi: 10.1007/BF00251855.
- Huang J (2002) Computational Methods for the Discrete Downward Continuation of the Earth Gravity and Effedts of Lateral Topographical Mass Density Variation on gravity and The Geoid. University of New Brunswick, Fredericton, Canada.

- Huang J., Sideris M.G., Vaníček P. and Tziavos I.N., 2003. Numerical investigation of downward continuation techniques for gravity anomalies. *Bollettino di Geodesia e Scienze Affini*, LXII, 33–48.
- Huang J, Vaníček P, Novák P (2000) An alternative algorithm to FFT for the numerical evaluation of Stokes's integral. *Stud Geophys Geod* 44: 374-380.
- Huang J, Vaníček P, Pagiatakis S, Brink W (2001) Effect of topographical mass density variation on gravity and the geoid in the Canadian Rocky mountains. *J Geodesy* 74: 805-815.
- Janák J, Vaníček P (2005) Mean free-air gravity anomalies in the mountains. *Stud Geophys Geod* 49: 31-42.
- Kingdon R, Vaníček P (2010) Poisson downward continuation solution by the Jacobi method. *Journal of Geodetic Science* 1: 74-81. doi: 10.2478/v10156-010-0009-0.
- Lemoine FG et al (1998) The Development of the Joint NASA GSFC and the National Imagery and Mapping Agency (NIMA) Geopotential Model EGM96. NASA/TP-1998-206861.
- MacMillan W (1930) *The Theory of Potential*. Dover Publications, New York.
- Martinec Z (1993) Effect of lateral density variations of topographical masses in view of improving geoid model accuracy over Canada. Final report of contract DSS No. 23244-2-4356, Geodetic Survey of Canada, Ottawa.
- Martinec Z, Vaníček P (1994a) Direct topographical effect of Helmert's condensation for a spherical approximation of the geoid. *Manuscr Geodaet* 19: 257-268.

- Martinec Z, Vaníček P (1994b) The indirect effect of topography in the Stokes-Helmert technique for a spherical approximation of the geoid. *Manuscr Geodaet* 19: 213-219.
- Martinec Z, Vaníček P, Mainville A, Véronneau M (1995) The effect of lake water on geoidal heights. *Manuscr Geodaet* 20: 193-203.
- Martinec Z, Vaníček P (1996) Formulation of the boundary-value problem for geoid determination with a higher degree reference field. *Geophys J Int* 126: 219-228.
- Martinec Z, Vaníček P, Mainville A, Véronneau M (1996) Evaluation of topographical effects in precise geoid computation from densely sampled heights. *J Geodesy* 70: 746-754.
- Martinec Z (1998) Boundary-value problems for gravimetric determination of a precise geoid. *Lecture Notes in Earth Sciences* 73, Springer, Berlin.
- Molodensky MS, Eremeev VF, Yurkina MI (1960) Methods for study of the external gravitational field and figure of the Earth. Transl. from Russian by the Israel Program for Scientific Translations. Office of technical Services, Department of Commerce, Washington, D.C., 1962.
- Novák P (2000) Evaluation of gravity data for the Stokes-Helmert solution to the geodetic boundary-value problem. Technical Report No. 207, University of New Brunswick, Fredericton.

- Novák P, Vaníček P, Véronneau M, Featherstone WE, Holmes SA (2001) On the accuracy of modified Stokes's integration in high-frequency gravimetric geoid determination. *J Geodesy* 74: 644-654.
- Reuter HI, Nelson A, Jarvis A (2007) An evaluation of void filling interpolation methods for SRTM data. *Int J Geogr Inf Sci* 21: 983-1008.
- Rodriguez E, Morris CS, Belz JE, Chapin EC, Martin JM, Daffer W, Hansley S (2005) An assessment of the SRTM topographic products. Technical Report JPL D-31639, Jet Propulsion Laboratory, Pasadena, California.
- Rülke A, Liebsch G, Sacher M, Schäfer U, Schirmer U, Ihde J (2012) Unification of European height system realizations. *Journal of Geodetic Science* 2: 343-354.
- Santos MC, Vaníček P, Featherstone WE, Kingdon R, Ellmann A, Martin BA, Kuhn M, Tenzer R (2006) The relation between rigorous and Helemert's definitions of orthometric heights. *J Geodesy* 80: 691-704. doi: 10.1007/s00190-006-0086-0.
- Sjöberg LE (2003) A computational scheme to model the geoid by the modified Stokes' formula without gravity reductions. *J Geod* 77: 423-432.
- Stokes GG (1849) On the variation of gravity at the surface of the earth. *Trans. Cambridge Philos. Soc., Vol. VIII: 672-695.*
- Sun W, Vaníček P (1998) On some problems of the downward continuation of 5' x 5' mean Helmert's gravity disturbance. *J Geodesy* 72: 411- 420.
- Tenzer R, Novák P, Janák J, Huang J, Najafi M, Vajda P, Santos M (2003) A review of the UNB approach for precise geoid determination based on the Stokes-Helmert

method. Honoring the academic life of Petr Vaníček. Technical Report No. 218, University of New Brunswick, Fredericton, pp.132-176.

Vaníček P, Sjöberg LE (1991) Reformulation of Stokes's theory for higher than second-degree reference field and modification of integration kernels. *J Geophys Res* 96, B4: 6529-6539.

Vaníček P, Martinec Z (1994) The Stokes-Helmert scheme for the evaluation of a precise geoid. *Manuscr Geodaet* 19: 119-128.

Vaníček P, Najafi M, Martinec Z, Harrie L, Sjöberg LE (1995) Higher-degree reference field in the generalized Stokes-Helmert scheme for geoid computation. *J. Geodesy* 70: 176-182.

Vaníček P, Sun W, Ong P, Martinec Z, Najafi M, Vajda P, Horst B (1996) Downward continuation of Helmert's gravity. *J. Geodesy* 71: 21-34.

Vaníček P, Featherstone WE (1998) Performance of three types of Stokes's kernel in the combined solution for the geoid. *J. Geodesy* 72: 684-697.

Vaníček P, Huang J, Novák P, Pagiatakis S, Véronneau M, Martinec Z, Featherstone WE (1999) Determination of the boundary values for the Stokes-Helmert problem. *J. Geodesy* 73: 180-192

Vaníček P, Tenzer R, Sjöberg LE, Martinec Z, Featherstone WE (2004) New views of spherical Bouguer gravity anomaly. *Geophys J Int* 159: 460-472. doi: 10.1007/s00190-006-0086-0.

- Vaniček P, Kingdon R, Kuhn M, Ellmann A, Featherstone WE, Santos MC, Martinec Z, Hirt Ch, Avalos-Naranjo D (2013) Testing Stokes-Helmert geoid model computation on a synthetic gravity field: experiences and shortcomings. *Stud Geophys Geod* 57: 369-400.
- Werner M (2001) Shuttle Radar Topography Mission (SRTM), Mission overview. *J Telecom (Frequenz)* 55: 75-79.
- Yildiz H, Forsberg R, Ågren J, Tscherning CC, Sjöberg LE (2012) Comparison of remove-compute-restore and least squares modification of Stokes' formula techniques to quasi-geoid determination over the Auvergne test area. *Journal of Geodetic Science* 2: 53-64. doi: 10.2478/v10156-011-0024-9.

## 4 Chapter 4: In defense of the classical height system

This article has been published in *Geophysical Journal International*. The idea of this article started when a new data set of 558 GNSS/Leveling points in the Auvergne area were given to the gravity research group at UNB by IGN and it was thought that it could help to better evaluate the gravimetric geoid model of this area. Besides, the lateral density variation model of the Auvergne area was extracted from a better resolution lithological model and it was shown that it could improve the gravimetric geoid model. The UNB rigorous orthometric height software was modified by me and the corrections to convert the normal heights to rigorous orthometric height were computed at these GNSS/Leveling points and used to compute the test geoidal heights.

The full citation for this article is:

Foroughi, I., Vaníček, P., Sheng, M., Kingdon, R. W., Santos, M.C; In defense of the classical height system, *Geophysical Journal International*, Volume 211, Issue 2, Pages 1154–1161.

The Molodensky's claim that classical height system cannot be computed as accurate as normal height system was argued in this article by measuring the congruency of both systems for Auvergne data set. According to Ågren et al. [2009], the LSMS method is the best performing method for computing the quasigeoid of the area. This model was evaluated against the height anomalies available at GNSS/Leveling points. The same comparison was done using geoid model computed by Janák et al. [2017] (cf., Ch. 3) and was compared against geoidal heights derived at the same points. The results show the same STD for both classical and normal height system besides the mean value of the discrepancies in classical height system was in a good agreement with the reported shift



in the French height system due to sea surface topography. It is mentioned in this article that the LSMS method provides the geoid model first and then is converted to quasigeoid using the classical formula. This was taken from our email corresponding with Dr. Ågren, which later he did let us know that this was not the case for Auvergne and actually the LSMS method was modified to compute the quasigeoid directly in the Auvergne area.

It is also mentioned in this article that the original 75 GNSS/Leveling points introduced by Duquenne [2007] are included in the 588 set of points however this is not the case and the new 588 points do not coincide with the 75 points.

It

#### **4.1 Abstract**

In many European countries, normal heights referred to the quasi-geoid as introduced by Molodensky in the mid-twentieth century are preferred to the classical height system that consists of orthometric heights and the geoid as a reference surface for these heights. The rationale for this choice is supposed to be that in the classical height system, neither the geoid, nor the orthometric height can be ever known with centimeter level accuracy because one would need to know the topographical mass density to a level that, can never be achieved. The aim of this paper is to question the validity of this rationale.

The common way of assessing the congruency of a local geoid model and the orthometric heights is to compare the geoid heights with the difference between orthometric heights provided by levelling and geodetic heights provided by GNSS. On the other hand, testing the congruency of a quasi-geoidal model with normal height a similar

procedure is used, except that instead of orthometric heights, normal heights are employed. For the area of Auvergne, France, which is now a more or less standard choice for precise geoid or quasi-geoid testing, only the normal heights are supplied by the Institute Geographic National (IGN), the provider of the data. This is clearly the consequence of the European preference for the Molodensky system. The quality of the height system is to be judged by the congruency of the difference of the geoid/quasi-geoid heights subtracted from the geodetic heights and orthometric/normal heights.

To assess the congruency of the classical height system, the Helmert approximation of orthometric heights is typically used as the transformation between normal and Helmert's heights is easily done. However, the evaluation of the differences between Helmert's and the rigorous orthometric heights is somewhat more involved as will be seen from the review in this paper. For the area of interest, the differences between normal and Helmert's heights at the control leveling-points range between  $-9.5\text{ cm}$  and  $0\text{ cm}$ , differences between Helmert's and the rigorous orthometric heights vary between  $-3.6\text{ cm}$  and  $1.1\text{ cm}$ . The local gravimetric geoid model of Auvergne, computed by the Stokes-Helmert (S-H) technique, is used here to illustrate the accuracy of the classical height system. Results show a very reasonable standard deviation (STD) of  $3.2\text{ cm}$  of the differences between geoid values, derived from control levelling-points, and gravimetric geoid heights when Helmert's heights are employed and even a smaller STD of  $2.9\text{ cm}$  when rigorous orthometric heights are used. A corresponding comparison of a quasi-geoid model, computed by Least-Square Modification of Stokes (LSMS) method, with normal heights show a STD of  $3.4\text{ cm}$ .

## 4.2 Introduction

The computed gravimetric geoidal height ( $N$ ), or quasi-geoidal height, a.k.a. the height anomalies ( $\xi$ ), can be compared against differences between heights ( $H$ ) “above the geoid” and geodetic heights ( $h$ ) above the reference ellipsoid obtained from GPS or GNSS observations. The fit of the geoid/quasi-geoid heights and GNSS minus orthometric/normal height is the best measure of the congruency of the height system in question. The geoidal/quasi-geoidal heights are computed using gravimetric information and orthometric/normal heights are computed independently from spirit leveling. If the congruency of the classical height system is tested the geoidal heights are required and the heights above the geoid should be of the orthometric kind ( $H^o$ ). If the congruency of Molodensky’s system [Molodensky et al., 1960] is investigated, the quasi-geoidal heights and normal heights ( $H^N$ ) are used. i.e.:

$$\begin{aligned} N &= h - H^o \\ \xi &= h - H^N . \end{aligned} \tag{4.1}$$

Normal heights are defined by the mean (between the quasi-geoid and the Earth surface) normal gravity along the normal plumbline and are simple to compute; for Auvergne, they are provided for all the 558 control leveling-points by the Institute Geographic National (IGN). Computing orthometric heights requires information about mass-density distribution along the plumbline inside topography and to avoid this necessity was the reason why Molodensky formulated his theory. To assess the quality of the gravimetric geoid by means of independent test data as accurately as possible, rigorous orthometric heights of the control points must be used.

There are various errors associated with the test data such as the effect of sea surface topography, systematic errors in levelling, adjustment errors, etc. Geodetic heights have their own errors in point height determination, network adjustment, etc. These types of errors are outside our interest in this paper as we focus only on converting normal heights to rigorous orthometric heights in a theoretically correct manner.

The difference between normal and orthometric height can be written as:

$$H^o - H^N = \xi - N, \quad (4.2)$$

which is clearly identical to the geoid-to-quasi-geoid separation. It is important to point out here that Eq. (4.1) and Eq. (4.2) are only approximately valid as they neglect the differences between the normal plumbline for measuring the normal height and the plumbline for orthometric heights. But this is only a second, or rather third order effect and can be certainly neglected when we are dealing with accuracies of the order of one centimeter. According to the definitions of the geoid and quasi-geoid the formula for their difference, Eq. (4.2), can be obtained from the conversion of normal to orthometric heights as [Santos et al., 2006]:

$$H^o - H^N = H^N \frac{\mu(g') - \mu(\gamma')}{\mu(g')}, \quad (4.3)$$

where  $\gamma'$  is the normal gravity along the normal plumbline,  $g'$  is the real gravity along the real plumbline, and  $\mu$  is the integral mean operator applied between the geoid and the Earth surface [Heiskanen and Moritz, 1967, Sec. 4.6]. If Helmert's orthometric

heights ( $H^H$ ) are to be computed then  $g'$  in Eq.(4.3) is replaced by the Helmert's gravity model along the plumbline,  $g^H$ .

The differences between normal heights and Helmert's orthometric heights have been computed in many countries and we shall not discuss them here. Clearly, normal height computation does not require information about topographical mass density. However, as Molodensky reminded us, to compute the rigorous orthometric heights the distribution of topographical mass density between the surface and the geoid ought to be known. Due to the lack of precise knowledge of density inside topography, a simplified topographic model of the Earth can be considered by assuming constant density within a Bouguer shell at each point. Approximating the mean value of gravity in this simplified topographic model by the average of the values at the Earth surface and at the geoid, is the basis of Helmert's orthometric height [Heiskanen and Moritz, 1967, Ch 4].

The real topography does not resemble a shell; topographical roughness with respect to the shell, a.k.a., the terrain, gives a better approximation of mean gravity. The gravitational attraction of the terrain can be approximated by various functions of depth as suggested by Mader [1954] or Niethammer [1982]. Sünkel [1986], Vaníček et al. [1995], Allister and Featherstone [2001], Tenzer and Vaníček [2003], Dennis and Featherstone [2003], Kingdon et al. [2005], and Tenzer et al. [2005] considered the gravitational attraction correction due to density variations inside topography in different ways. Here we shall follow the modelling suggested by Martinec [1993] and illustrated by Huang et al. [2001], as their modelling is based on lateral variations of topographical density as indicated by superficial geological maps of as large a scale as available.

Foroughi et al. [2015b] suggested to use the publicly available geological maps of the study area and digitise them using the information on density values. This procedure for the area of Auvergne was tried and it was reported in the same study that even using a low resolution density map, the effect on geoidal heights improves the fit of the gravimetric geoidal height to the control leveling-points to a certain degree. It stands to reason to expect that the dependence observed in the case of geoidal heights would apply to the orthometric height as well. If high resolution density maps are available, the effect of topographical density variations on both geoidal and orthometric heights will be probably larger. The “rigorous” orthometric heights have been formulated by Tenzer, et al. [2005] and the corrections to Helmert’s orthometric heights (to obtain the “rigorous” orthometric heights) derived by Santos, et al. [2006]; they will be recapitulated here in the next section for completeness.

### 4.3 Review of the height system theory

From the geometrical point of view, orthometric heights are defined as the distance between a point of interest and the point on the geoid located at the bottom of the plumbline that goes through the point of interest. If the mean gravity along the plumbline,  $\mu(g)$ , is known, orthometric heights can be computed as follows [Heiskanen and Moritz, 1967, Eq 4-21]:

$$\forall \Omega \in \Omega_0 : H^o(\Omega) = \frac{c(r_t, \Omega)}{\mu[g^o(\Omega)]}, \quad (4.4)$$

where  $\Omega$  represents the geocentric spherical coordinates ( $\lambda$ : *longitude*,  $\varphi$ : *latitude*) of the point of interest,  $\Omega_0$  is the full solid angle,  $r_t \approx R + H^o$  is the radius of the point at

the Earth surface,  $R$  is the mean radius of the Earth and  $C$  is the geopotential number at  $(r_t, \Omega)$  defined as the difference between the gravity potential at the geoid and that at the topographical surface;  $\mu(g')$  is the integral-mean gravity along the plumbline and  $H^o(\Omega)$  is the orthometric height of the point  $(r_t, \Omega)$ .

As the actual gravity along the plumbline cannot be measured at each point, it is not possible to compute the exact mean gravity between the geoid and the Earth's surface. Yet, the differences between height systems are governed by this quantity. The mean gravity can be approximated by mean normal gravity which results in normal height; when the Poincaré-Pray model is used Helmert's orthometric height are obtained. According to the Poincaré-Pray theory, the mean value is caused by the Bouguer plate and free-air gravity gradient at the point of interest, assuming the mass density of the plate to be constant and equal to  $\rho_0 = 2670 \frac{kg}{m^3}$ , [Heiskanen and Moritz, 1967, Eq. 4-24]:

$$\forall \Omega \in \Omega_0 : \mu[g^H(\Omega)] = g(r_t, \Omega) - \left( \frac{1}{2} \frac{\partial \gamma}{\partial h} + 2\pi G \rho_0 \right) H^o(\Omega), \quad (4.5)$$

where  $\partial \gamma / \partial h$  is the vertical gradient of normal gravity at the surface of the Earth, and  $G$  is the Newtonian gravitational constant. The vertical gradient in the first term within the brackets can be approximated by its linear value above the geoid ( $-0.3086 \text{ mGal/m}$ ) and the second term under the assumption of constant density equals to  $-0.1119 \text{ mGal/m}$  and the general form can be written as:

$$\forall \Omega \in \Omega_0 : \mu[g^H(\Omega)] = g(r_t, \Omega) + (0.0424) H^o(\Omega), \quad (4.6)$$

where  $g$  and  $H$  are in  $mGal$  and metres respectively and the term in brackets is in  $mGal/m$ . Eq. (4.6) approximates the gravity gradient by a constant value and the plumbline by a straight line. This approximation only reduces the surface gravity value half way down the plumbline using the Poincaré-Pray gradient while completely neglecting the effect of the terrain and the variations of density inside topography.

The correction to normal height to get Helmert's orthometric height ( $\varepsilon_H^H$ ) is given by Eq. (4.3). To get the rigorous orthometric height from Helmert's orthometric height, corrections mentioned in the Introduction, i.e., the terrain correction, varying topographical density correction, and non-topographic correction must be applied [Santos et al., 2006]. In addition, the consideration of a more rigorous definition of the normal gravity along the normal plumbline ( $\varepsilon_H^Y$ ) and that of the Bouguer shell effect ( $\varepsilon_H^B$ ) leads to two additional corrections. These corrections are:

$$\varepsilon_H^Y(\Omega) = -\frac{\gamma H^{\circ 3}(\Omega)}{g^H(\Omega)a^2}, \quad (4.7)$$

where  $a$  is the major semi-axis of the reference ellipsoid, and  $\varepsilon_H^Y$  is the correction to compute the mean normal gravity along the plumbline. The correction to compute mean Bouguer shell effect reads:

$$\varepsilon_H^B(\Omega) = -\frac{4}{3}\pi G\rho_0 \frac{H^{\circ 3}(\Omega)}{g^H(\Omega)(R+H^{\circ}(\Omega))} \left(2 - \frac{H^{\circ}(\Omega)}{R+H^{\circ}(\Omega)}\right). \quad (4.8)$$

These corrections can be considered generally to be of second order and they are directly correlated with the heights of the points. For the highest point on Earth, Mount



Everest, the  $\varepsilon_H^Y$  will be about 1.5 cm and  $\varepsilon_H^B$  will be  $-1.6$  cm respectively and can thus be omitted in practice for other parts of the world [Santos et al., 2006].

The correction to Helmert orthometric height due to neglected terrain effect in the Poincaré-Pray model reads [ibid, 2006, Eq. (50) & Eq. (52)]:

$$\begin{aligned} \varepsilon_H^R(\Omega) = & \\ \frac{G\rho_0}{g^H(\Omega)} \left( H^o(\Omega) \iint_{\Omega' \in \Omega_0} \int_{r'=R+H^o(\Omega)}^{r'=R+H^o(\Omega')} \frac{\partial l^{-1}(r, \Omega; r', \Omega')}{\partial r} \Big|_{r=R+H^o(\Omega)} r'^2 dr' d\Omega' - \right. & \\ \left. \iint_{\Omega' \in \Omega_0} \int_{r'=R+H^o(\Omega)}^{r'=R+H^o(\Omega')} (l^{-1}[R, \Omega, r', \Omega'] - l^{-1}[R + \right. & \\ \left. H^o(\Omega), \Omega, r', \Omega']) r'^2 dr' d\Omega' \right), & \end{aligned} \quad (4.9)$$

where all the symbols have been already defined. The correction to Helmert's orthometric height by employing the laterally varying density information ( $\delta\rho(\Omega)$ ) of the topographical masses, i.e., masses above the geoid, is evaluated as [ibid, 2006, Eq. (54) & Eq. (56)]:

$$\begin{aligned} \varepsilon_H^{\delta\rho}(\Omega) = & \\ \frac{G}{g^H(\Omega)} \left( H^o(\Omega) \iint_{\Omega' \in \Omega_0} \int_{r'=R+H^o(\Omega)}^{r'=R+H^o(\Omega')} \delta\rho(r', \Omega') \frac{\partial l^{-1}(r, \Omega; r', \Omega')}{\partial r} \Big|_{r=R+H^o(\Omega)} r'^2 dr' d\Omega' - \right. & \\ \left. \iint_{\Omega' \in \Omega_0} \int_{r'=R+H^o(\Omega)}^{r'=R+H^o(\Omega')} \delta\rho(r', \Omega') (l^{-1}[R, \Omega, r', \Omega'] - l^{-1}[R + \right. & \\ \left. H^o(\Omega), \Omega, r', \Omega']) r'^2 dr' d\Omega' \right), & \end{aligned} \quad (4.10)$$

where,  $\delta\rho(\Omega)$  is the anomalous topographical density with respect to mean density  $\rho_0$ . The correction to Helmert's orthometric heights due to the masses contained inside the geoid, (the non-topographic correction) is calculated as [ibid, 2006, Eq. (37)]:

$$\varepsilon_H^{NT}(\Omega) = \frac{1}{g^H(\Omega)} \left( H^o(\Omega) \delta g^{NT}(r_t, \Omega) - \frac{R}{4\pi} \iint_{\Omega' \in \Omega_0} \int_{r=R}^{R+H^o} \frac{1}{r} K[r, \psi(\Omega, \Omega'), R] dr \delta g^{NT}(R, \Omega') d\Omega' \right), \quad (4.11)$$

where  $K$  is the Poisson kernel of upward continuation [Kellogg, 1929] and  $\psi(\Omega, \Omega')$  represents the spherical distance between computation and integration points, and  $\delta g^{NT}(r_t, \Omega)$  is the No-Topography (NT) gravity disturbance at the surface of the Earth also known as spherical complete Bouguer anomaly, cf., [Vaníček et al., 2004]. Thus, the correction to Helmert's orthometric height reads:

$$\forall \Omega \in \Omega_0: \varepsilon_H(\Omega) = \varepsilon_H^R(\Omega) + \varepsilon_H^{\delta\rho}(\Omega) + \varepsilon_H^{NT}(\Omega). \quad (4.12)$$

Kingdon et al. [2005] computed the differences between Helmert's and rigorous orthometric heights on a regular mesh of points in Canada and reported that differences reach up to the decimeter level. Santos et al. [2006] computed the corrections over a profile at  $50^\circ N$  across Canadian Rocky Mountains with maximum heights reaching 2500 *m*. Their results show that the total correction reaches a maximum of 13 *cm* and a minimum of  $-5$  *cm*. In their study, the effect of laterally varying topo-density was not very pronounced as the topographical density in their area of study is quite smooth. Odera and Fukuda [2015] computed the correction to Helmert's orthometric height over Japan's levelling-points. Although the effect of laterally varying density was ignored in their

computation, they claim that the total rigorous orthometric correction to Helmert's heights is between  $-30\text{ cm}$  and  $0$ .

Although, the 3D density model of topography is needed in order to compute the effect of density variation most accurately, Kingdon et al. [2011] investigated the effect of 3D varying density on geoidal heights and concluded that the vertically varying density effect is significantly smaller than that due to the lateral variations. So the laterally varying density effect is only considered in this paper.

#### **4.4 Numerical results**

The data set of the Auvergne geoid computation test area was prepared by Duquenne [2007]. The area is delimited by  $-1^\circ < \lambda < 7^\circ$  and  $43^\circ < \varphi < 49^\circ$  and contains 244000 terrestrial gravity observations, with STD ranging from  $0.25$  to  $0.75\text{mGal}$ , and 558 levelling-points, with STD of  $2 - 3\text{cm}$ , in the middle of the area ( $1.5^\circ < \lambda < 4.5^\circ$ ) and ( $43.5^\circ < \varphi < 47.5^\circ$ ) which is where the geoid is computed. The orthometric heights of the points were interpolated from the  $3''$  by  $3''$  DEM information from the Shuttle Radar Topography Mission (SRTM) version 4.1 [Jarvis et al., 2008]. The topographical heights in the study area vary between  $0\text{m}$  and  $1300\text{m}$  but go up to  $4000\text{m}$  in the near-zone area. Most of the control points are located in the western part where the topography is smooth. Figure 4.1 shows the topography and the locations of control points are denoted with red crosses.

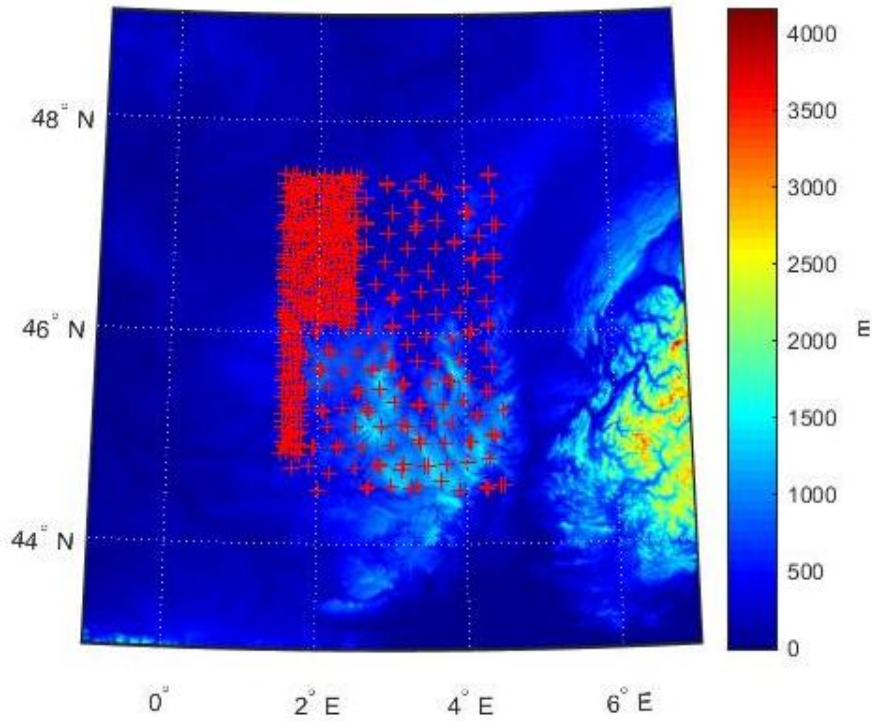


Figure 4.1: Variation of topography in Auvergne with red crosses showing the positions of levelling-points.

The control point data set contains, apart from the horizontal location information, the geodetic height derived from GNSS observations, normal height derived from spirit levelling, and the differences between geodetic and normal heights, which are the quasi-geoidal heights, a.k.a., height anomalies.

The topographical density model (DDM) of the Auvergne region is needed to compute the effect of lateral density variation on Helmert's orthometric heights as explained above. The digital lateral density model of this area is derived by the digitization of an analog geological map of France [Bodelle et al., 1980]. The digitization was done according to density values associated with the color bar of the map and the digital density

model was computed for a 5' by 5' grid in the data coverage area. The evaluation of this density model was done by Foroughi, et al. [2015b] and according to their investigation, the lateral density model improved the accuracy of the gravimetric geoid (computed by S-H method) by 2 mm in the STD of residuals of comparison of the geoid model with orthometric heights of levelling-points. The 2mm improvement is relatively small because the DDM used was obtained from publicly available geological map that does not have high enough accuracy and because the control points in the study area are located in rather low elevation regions.

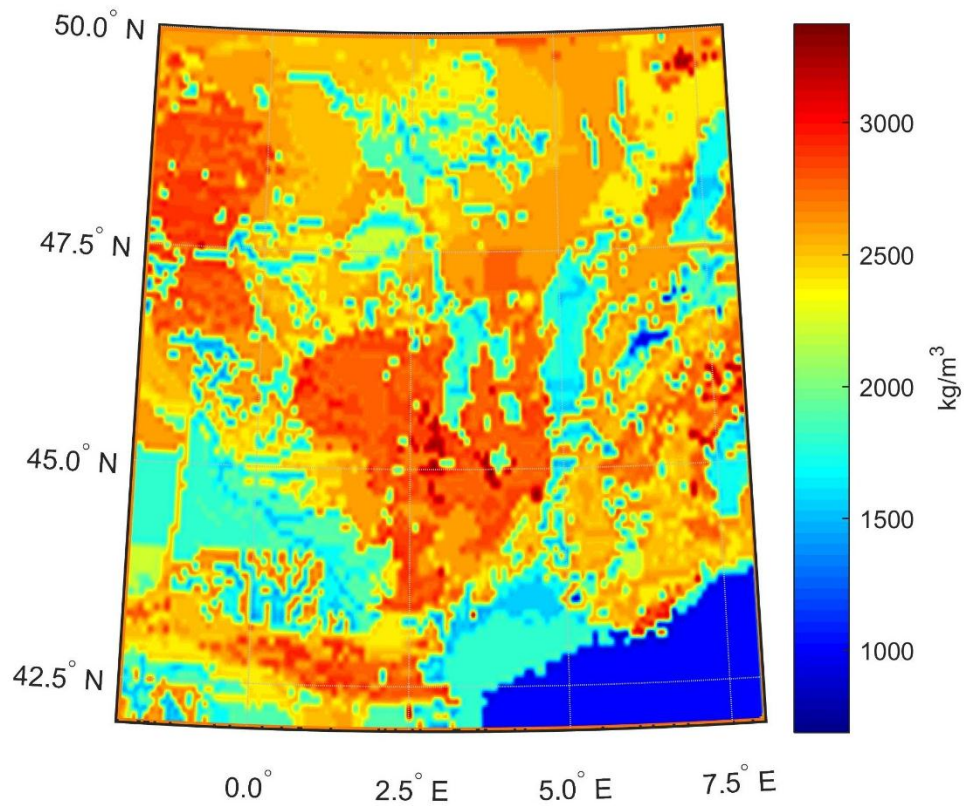


Figure 4.2: Digitized map of lateral topographical density variation in Auvergne ( $kg/m^3$ ).

By inserting Eq. (4.6) into Eq. (4.3), Helmert's approximation of orthometric heights is obtained. The differences between normal and Helmert's orthometric heights are shown in Figure 4.3. These differences are at the decimeter level, clearly large enough to be taken seriously. Looking at the central part of Figure 4.1 (where the levelling-points are located) and Figure 4.3, one can see that the differences are, to some degree, correlated with the topography of the area.

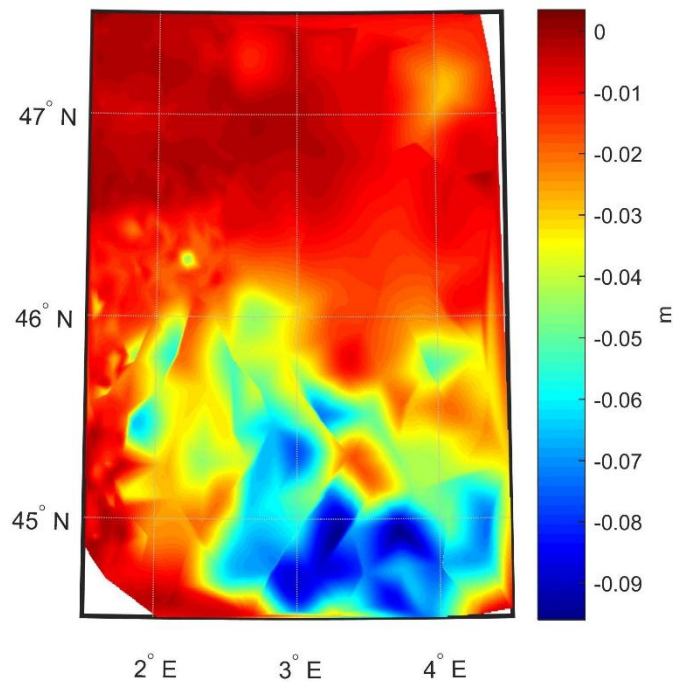


Figure 4.3: Differences between normal and Helmert's orthometric heights.

We shall evaluate the corrections to be applied to Helmert's orthometric heights at control points in the reversed order, i.e., in the order of increasing importance. To begin with, the second order corrections, i.e., the normal gravity correction ( $\varepsilon_H^Y$ ) from Eq. (4.7) and spherical Bouguer gravity correction ( $\varepsilon_H^B$ ) from Eq. (4.8), attain the maximum values of  $0.04mGal$  and  $0.25mGal$  in our area, where the highest elevation is  $1300m$ . These

values translate to less than a 1 *mm* contribution to heights and are thus negligible for the desired accuracy in in Auvergne.

Computing the non-topographic correction to Helmert's orthometric heights from Eq. (4.11), we need to know NT gravity disturbances, as opposed to anomalies, at the geoid level ( $\delta g^{NT}(R, \Omega)$ ). These can be evaluated from the following expression [Heiskanen and Moritz, 1967, Eq. 2-151]:

$$\forall \Omega \in \Omega_0 : \delta g^{NT}(R, \Omega) = \Delta g^{NT}(R, \Omega) + \frac{2}{R} T^{NT}(R, \Omega) , \quad (4.13)$$

where  $\Delta g^{NT}(R, \Omega)$  is the NT-gravity anomaly and  $T^{NT}(R, \Omega)$  is the disturbing potential in the NT space [Vaniček et al., 2004] both on the geoid, approximated to the order of flattening by the mean sphere of radius  $R$ . In order to compute  $T^{NT}$ , all the topographic (and atmospheric) masses above geoid must be removed and we get:

$$\forall \Omega \in \Omega_0 : T^{NT}(R, \Omega) = T(R, \Omega) - V^T(R, \Omega) - V^A(R, \Omega) , \quad (4.14)$$

where,  $T(R, \Omega)$  is the disturbing potential in the real space and can be obtained from a regional geoid model using Bruns's formula. The  $V^T(R, \Omega)$  and  $V^A(R, \Omega)$  are the gravitational potentials of topographical and atmospheric masses respectively [cf., Novák, 2000].

To evaluate the first term on the right-hand side of Eq. (4.13), the NT-gravity anomalies on the geoid are needed; these are obtained by downward continuing the surface NT anomalies. The scattered (observed) free-air anomalies of Auvergne are thus first transferred to NT-space, and then the mean NT anomalies on a grid are computed by

means of inverse-cubic distance interpolation on 1' by 1' grid points. The NT anomalies are harmonic above the geoid, so Poisson's downward continuation is applied to reduce the surface values down to geoid. The Poisson integral equation is solved by the iterative Jacobi process used for this application the first time by Kingdon & Vaníček [2010]. The integration is then done over one arc-degree squared cells augmented by a border strip of 30 arc-minutes on all 4 sides. The results from the individual cells (after discarding the 30 arc-minutes border strip, of course) are fused together. On average, eight iterations were needed for the downward continuation in the individual squares.

For the purpose of the cell fusion on the geoid, an assessment of continuity along the borders (of the one arc-degree squared cells) was done by Foroughi, et al. [2015a]. This study showed that discontinuities between anomalies on the geoid are randomly distributed and are within the limit of  $\langle -3\sigma, +3\sigma \rangle$  where  $\sigma$  is the STD of observed anomalies which is, according to Duquenne [2007], 0.5 mGal. This was considered to be a very acceptable threshold for the fusion of individual cells. Figure 4.4 (a) shows the NT-gravity anomalies on the topographical surface and Figure 4.4 (b) shows the differences between surface and geoid NT-gravity anomalies. A cursory inspection would convince us that there is no sign of the cell border artifacts in Figure 4.4b, i.e., that the fusion results in a smooth field.



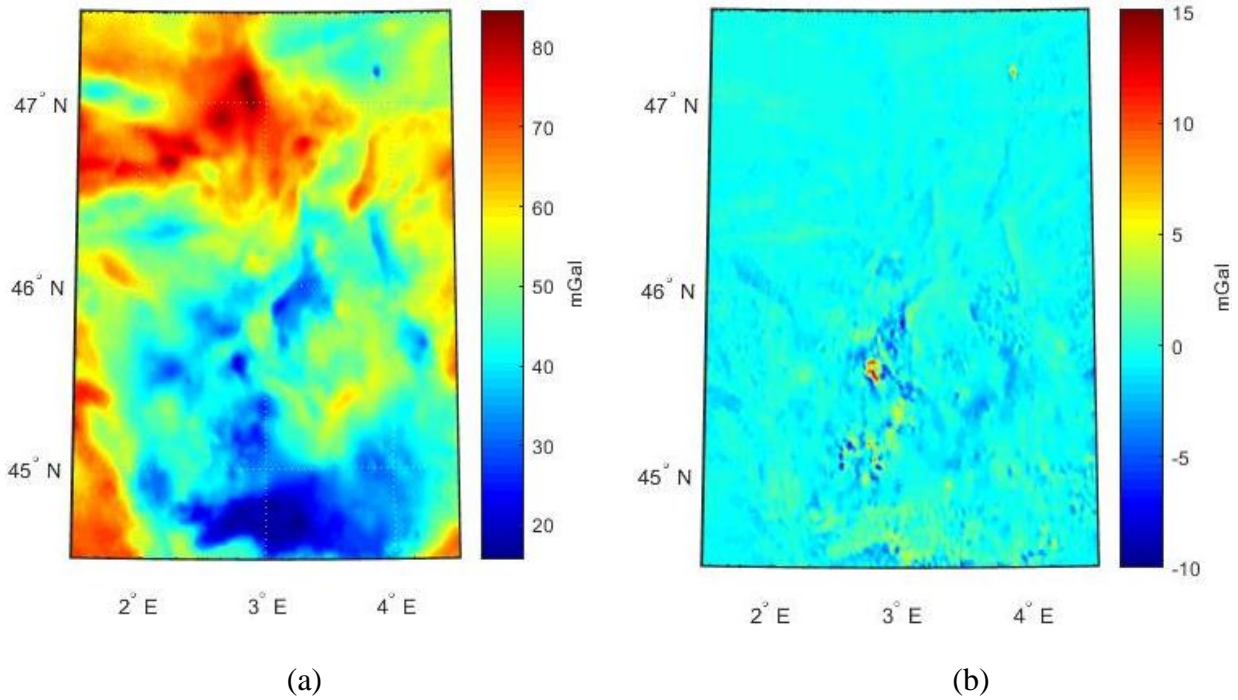


Figure 4.4: NT-gravity anomalies (a) at the Earth surface, (b) differences between NT-gravity anomalies on the Earth surface and the geoid.

To compute the second term on the right-hand side of Eq. (4.13), the regional geoid model obtained by Janák et al. [2017] was chosen. To derive the  $T(R, \Omega)$  and finally to calculate the  $V^T$  of each point on the geoid, topographical information of the Earth was broken down to three zones: inner-zone, near-zone and, far-zone. The inner-zone area covers a spherical cap of 25 arc-minutes around each point and includes orthometric heights of topography on a 30'' by 30'' grid. The near-zone comprises a 5 arc-degree spherical cap and contains 5' by 5' heights and finally the far-zone which covers the rest of the world with a 30' by 30' global DEM. The DEM information for the integration zones was obtained from the SRTM-V4 data sets [Jarvis et al., 2008]. The effect of  $V^A$  is negligible and is not shown here. The non-topographic correction to Helmert's orthometric heights is shown in Figure 4.5 (a) and its statistics are given in Table 4.1.

To evaluate the terrain generated correction (Eq. (4.9)), integration was done for each control point in the geoid computation area in four zones: innermost, inner, near, and far zones. The innermost-zone comprises a 9 arc-minute spherical cap which contains 3'' by 3'' height information. The inner-zone covers a 25 arc-minute spherical cap with a 30'' by 30'' DEM. The near-zone covers a 3 arc-degree spherical cap consisting of 5' by 5' elevation data and, finally, the rest of the world is covered by 30' by 30' height information as a far-zone integration area. The terrain generated correction to Helmert's orthometric heights in Auvergne is shown in Figure 4.5 (b) and its statistics are given in Table 4.1.

When computing the effect of laterally varying topographical density (Eq. (4.10)), the integration was done over a 1 arc-degree spherical cap containing 30'' by 30'' density anomalies (interpolated from the 5' by 5' DDM) around each point. The correction to Helmert's orthometric heights at control points due to laterally varying density of topographic masses is shown in Figure 4.5 (c) and the statistics are given in Table 4.1.

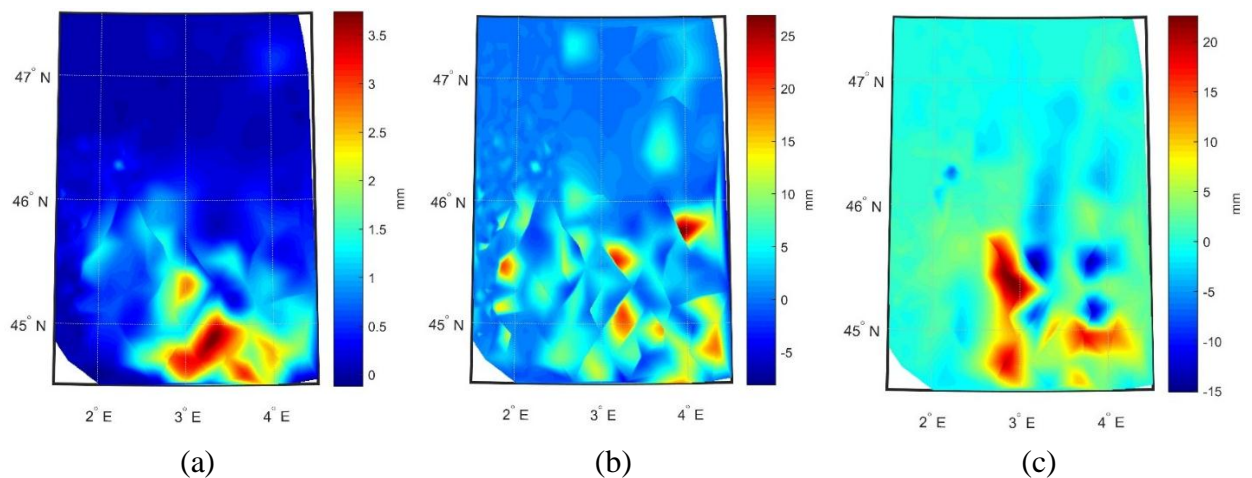


Figure 4.5: The correction terms to Helmert's orthometric height to get rigorous orthometric height: (a) non-topographic  $\varepsilon_H^{NT}$ , (b) terrain generated  $\varepsilon_H^R$ , (c) lateral topographical density anomaly generated  $\varepsilon_H^{\delta\rho}$ , (c).

Table 4.1: The statistics of corrections to Helmert's orthometric height (in mm)

Correction	Min	Max	Mean	STD
$\varepsilon_H^{NT}$	0.0	3.6	0.3	0.5
$\varepsilon_H^R$	-3.1	26.8	1.3	3.2
$\varepsilon_H^{\delta\rho}$	-15.8	21.2	0.6	3.2

The cumulative corrections to Helmert's orthometric height are shown in Figure 4.6, and their statistics are provided in Table 4.2.

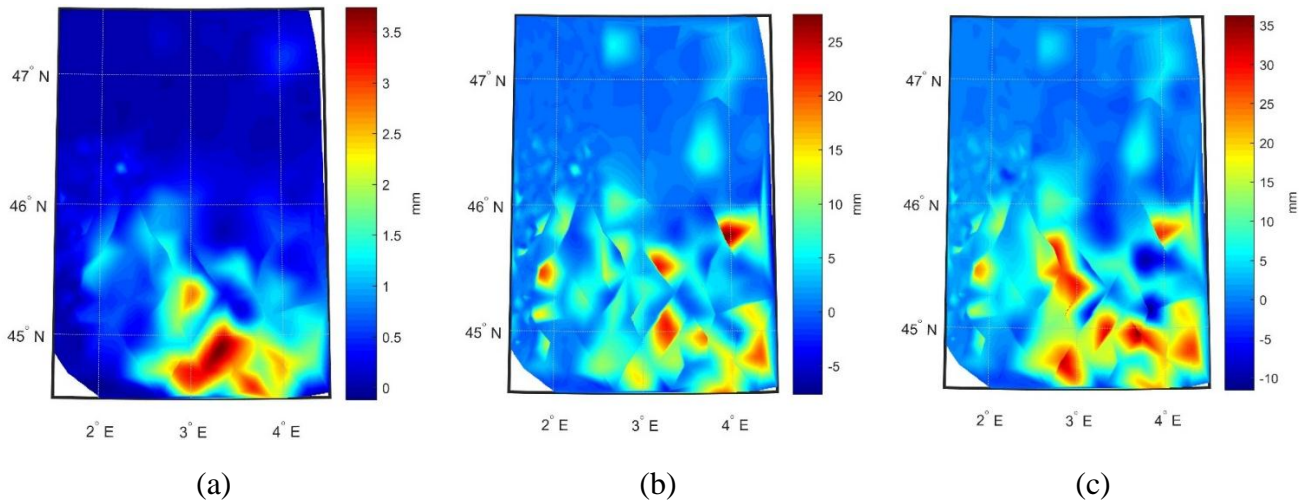


Figure 4.6: The cumulative corrections to Helmert's orthometric height: (a) non-topographic  $\varepsilon_H^{NT}$ , (b) non-topographic and terrain generated  $\varepsilon_H^{NT} + \varepsilon_H^R$ , (c) non-topographic, terrain generated, and lateral topographical density anomaly generated  $\varepsilon_H^{NT} + \varepsilon_H^R + \varepsilon_H^{\delta\rho}$ .

Table 4.2: Statistics of cumulative corrections to Helmert's orthometric height (in mm).

Accumulated corrections terms	Min	Max	Mean	STD
$\varepsilon_H^{NT}$	0	3.6	0.3	0.5
$\varepsilon_H^{NT} + \varepsilon_H^R$	-2.4	27.5	1.6	3.5
$\varepsilon_H^{NT} + \varepsilon_H^R + \varepsilon_H^{\delta\rho}$	-11.3	36.4	2.2	5.5

As expected, the higher the elevation, the larger the total correction values. According to Figure 4.5 and Table 4.1, the largest correction to Helmert orthometric heights are from lateral density variation (range of  $3.6\text{cm}$ ) and the second largest corrections is that due to the terrain (range of  $3.0\text{cm}$ ). The non-topographic corrections to Helmert orthometric heights have direct correlation with heights and are all positive and less than half a centimeter. The relation of terrain generated and lateral density variation corrections with heights of the points are somewhat more complicated.

Rigorous orthometric heights were computed by applying the total corrections (the third line of Table 4.2) to Helmert orthometric heights. The statistics of the rigorous orthometric heights are summarized in Table 4.3. Just to be completely clear, let us repeat: since the range of differences between Helmert orthometric heights and the rigorous orthometric heights is  $4.7\text{ cm}$  (cf., Table 4.2) we have to conclude that the use of rigorous orthometric heights instead of Helmert's heights is mandatory if high accuracy heights are required. This is true especially for higher elevation area.

#### **4.5 Discussion and conclusions**

The self-consistency of the classical height system in Auvergne was assessed by using the regional geoid and the rigorous orthometric heights computed for a set of control levelling-points. The regional geoid model of this area was computed using the S-H technique with modifications suggested by Foroughi et al. [2016] and implemented by Janák et al. [2017]. Foroughi et al. [2016] suggested modifying the regional geoid using the optimum reference field and integration cap size for evaluating the Stokes integral and Janák et al. [2017] later computed the Auvergne geoid model using S-H technique

enriched by these modifications. This latest geoid model is showed for completeness in Figure 4.7.

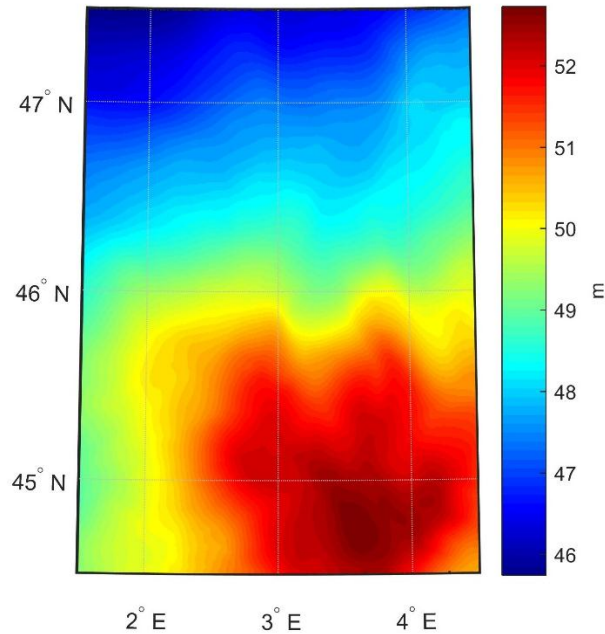


Figure 4.7: Geoid model of Auvergne computed by Stokes-Helmert's method [Foroughi et al., 2016].

Table 4.3: Statistics of Rigorous orthometric height of levelling-points.

	Min [m]	Max [m]	Mean [m]	STD [m]
Rigorous Orthometric height	84.906	1324.408	373.310	263.844

For the assessment of the congruency of the height system, the geoidal heights are subtracted from the geodetic heights obtained for the 558 control points by GNSS (and supplied to us by IGN). These alternatively obtained orthometric heights have to match the rigorous orthometric heights (computed the way described in this paper). The differences, that may be perhaps called residuals, between rigorous orthometric heights

and those obtained from the geoid model and geodetic heights give us the means to measure the congruency we want to assess. In an ideal world, these residuals would be all equal to 0; in the real world, they are different from 0, but their magnitudes can be measured in statistical sense. The smaller the statistical measure of the residuals (STD or range) the better the congruency.

These differences give us also a tool for measuring just how much the congruency improves when different corrective steps are taken. Table 4.4 shows the trend of improvement in congruency when the individual corrections are applied; the  $\varepsilon_H^Y$  and  $\varepsilon_H^B$  corrections are not considered because their effect is negligible for Auvergne.

Table 4.4: Statistics of the fit of various (partially corrected) orthometric heights with the S-H regional geoid model and GNSS- generated orthometric heights.

	Min [cm]	Max [cm]	Mean [cm]	STD [cm]
Helmert's Orthometric heights	7.5	26.4	18.5	3.01
Applying $\varepsilon_H^{NT}$	7.6	26.4	18.5	2.99
Applying $\varepsilon_H^R$	7.4	26.5	18.6	2.97
Applying $\varepsilon_H^{\delta\rho}$	7.3	26.2	18.6	2.94

Looking at the STDs of the residuals in Table 4.4, we can conclude that even though the individual corrections are rather small and have therefore a limited impact on the corrected height, they all go in the right direction: i.e., the STD gets smaller, with respect to the application of each correction. This points out to the fact that the corrections are formulated in a physically correct manner.

The same assessment can be done for the Molodensky height system: the differences to work with are between quasi-geoid heights (height anomalies) subtracted from geodetic heights and normal heights of corresponding points. The quasi-geoid model used in the

assessment treated in this paper was computed using the LSMS method, a.k.a., the KTH method [Ågren et al., 2009a,b]. The normal heights used in this assessment are those determined by IGN.

The statistics of the comparison between the classical and Molodensky’s systems are given in Table 4.5.

Table 4.5: Statistics of the residuals between computed rigorous orthometric heights and those estimated from local geoid S-H model and the GNSS-determined heights; also, residuals between computed normal heights and those estimated from local quasi-geoid KTH model.

Model	Min [cm]	Max [cm]	Mean [cm]	STD [cm]
Rigorous orthometric height and geoid	7.3	26.6	18.7	2.9
Normal height and quasi-geoid	2.1	21.3	12.5	3.4

It should be pointed out that the LSMS quasi-geoid computation technique, the results of which are used here, is really a simplified geoid computation technique augmented by a transformation from geoid to quasi-geoid. Results obtained by Ågren [2009b] without adding any “corrector surface” show that the congruency of Molodensky’s system looks worse when other techniques for quasi-geoid determination are used. Another thing must be mentioned here: Ågren’s results (in Ågren [2009b]) were generated only for the 75 original GNSS control points, while our results referred to the classical system refer to the full set of 558 points mentioned above. Thus, to be able to make a direct comparison of the congruency of the classical and Molodensky systems we had to re-compute our results for the original 75 control points. For those original points, the STD equals  $3.3\text{cm}$  and the mean equals to  $13.3\text{cm}$  for the classical system.

The mean value of the residuals for the classical system in Table 4.5 is 18.7 *cm* above the average of levelling-point values using all the 558 control points. The same value drops to 13.3*cm* when only the original 75 control points are used. The estimated constant height system offset (presumably the effect of Sea Surface Topography, cf., [Vaníček and Krakiwsky, 1986] for France is 13.2 *cm* according to Rülke et al. [2012]. A similar observation of the Molodensky height system can be made when a quasi-geoid model without any “correction surface” is used, and the constant term is equal to 12.5*cm* [Ågren; 2009b].

Hence, according to Table 4.5, it has to be concluded that the classical height system has better congruency/self-consistency than the Molodensky height system. Taking a look at the levelling heights and the GNSS-determined geodetic heights, can we really believe that their combined STD, as a measure of the congruency can be much better than 3cm? A STD of 2.9 cm corresponds to a combination of two statistically independent STDs of 2 cm; hence if one believes in a 2 cm STD of leveled heights combined with a 2 cm STD of GNSS geodetic heights, it does not leave much room for an error caused by the uncertainty in topographical density, does it?

So where has the problem that Molodensky perceived in the 1940’s: “The classical height system, neither the geoid, nor the orthometric height can be ever known with sufficient accuracy because one would need to know the topographical mass density to a level that, can never be achieved” disappeared? We have to conclude, at least in the Auvergne area, that the effect of topographical mass density variations is not as damaging as Molodensky had thought it would be. This discovery cannot be extended to be globally



valid, of course, but with Auvergne being a fairly representative area – this was the reason why it became popular for geoid or quasi-geoid testing ground - the conclusion should be valid for large parts of the world. This is the crux of our argument presented above.

There are two more additional arguments that speak in favor of the classical height system. First and foremost, its reference surface, i.e., the geoid, is a smooth, physically meaningful surface, convex everywhere and describable by a simple mathematical expression while the Molodensky reference surface, the quasi-geoid, has no physical meaning and contains folds, making it quite difficult to describe mathematically. As the quasi-geoid is not definable by a function in the normal mathematical sense, it does not make sense to even ask about its behavior in an asymptotic sense. Second, the statistics of the classical system are physically meaningful. For instance, the constant difference between the computed geoid and the geoid obtained from differences between the geodetic and orthometric heights can be clearly associated with the offset of the levelled height datum and the geoid, i.e., by the constant part of the Sea Surface Topography (SST).

#### **4.6 Acknowledgement**

Authors would like to thank to Dr. Ågren for proving the quasi-geoid model of Auvergne without the corrector surface. The research and the numerical experiment presented in this paper was made possible by the Canadian NSERC “Individual Discovery” grant to P. Vaniček. The Institute Geographic National (IGN) of France is acknowledged to provide the normal and geodetic heights of the additional 483 control levelling-points.

## 4.7 References

- Allister, N., & Featherstone, W. (2001). Estimation of Helmert orthometric heights using digital barcode levelling, observed gravity and topographic mass-density data over part of Darling Scarp, Western Australia. *Geomatic Research Australia*, 75, 25-52.
- Ågren J. Sjoberg, L. E., Kiamehr, R., 2009a The new gravimetric quasigeoid model KTH08 over sweden. *Journal of applied Geodesy* 3 143-153.
- Ågren J., Barzaghi R., Carrion D., Denker H., Grigoriadis V.N., Kiamehr R., Sona G., Tscherning C.C., Tziavos I.N., 2009b, Different geoid computation methods applied on a test dataset: results and considerations, Poster presented at Hotine-Marussi Symp., Rome, 6–12 July, 2009.
- Dennis, M., & Featherstone, W. (2003). Evaluation of orthometric and related height systems using a simulated mountain gravity field. Tziavos IN (ed) 3rd meeting of the International Gravity and Geoid 2002 Dept of Surv and Geodesy. Aristotle University of Thessaloniki, (pp. 389-394). Thessaloniki.
- Duquenne, H. (2007). A data set to test geoid computation methods. Istanbul: First international Symposium of the International Gravity Field Services (IGFS).
- Foroughi, I., Sheng, M., Kingdon, R., Huang, J., Martinec, Z., Vaniček, P., and Santos, M. (2015). The effect of lateral topographical density variations on the geoid in Auvergne. 26th IUGG General Assembly. Prague, Czech Republic.
- Foroughi, I., Vaniček, P., Kingdon, R., Sheng, M., and Santos, M. (2015). Assessment of Discontinuity of Helmert's Gravity Anomalies on the Geoid. AGU-GAC-MAC-CGU Joint Assembly. Montreal, Canada.

- Foroughi, I., Vaníček, P., Novák, P., Kingdon, R., Sheng, M., and Santos, M. (2016). Optimal combination of satellite and terrestrial gravity data for regional geoid determination using Stokes-Helmert's method. IAG proceeding. Thessaloniki.
- Heiskanen, W., and Moritz, H. (1967). *Physical Geodesy*. San Francisco: W.H. Freeman and Co.
- Huang, J., Vaníček, P., Pagiatakis, S., and Brink, W. (2001). Effect of topographical mass density variation on gravity and the geoid in the Canadian Rocky Mountains. *Journal of Geodesy*, 74(11-12), 805-815.
- Hwang, C., and Hsiao, Y. (2003). Orthometric height corrections from leveling, gravity, density and elevation data: a case study in Taiwan. *Journal of Geodesy*, 77(5-6), 292-302.
- Janák, J., Vaníček, P., Foroughi, I., Kingdon, R., Sheng, M., Santos, M., and Novák, P. (2017). Computation of precise geoid model using UNB Stokes-Helmert's approach: Case study in Auvergne region. Submitted to *Journal of Geophysical Research (Solid Earth)*.
- Jarvis, A., Reuter, H., Nelson, A., and Guevara, E. (2008). Hole-filled SRTM for the globe Version 4, available from the CGIAR-CSI SRTM 90m Database. Retrieved from <http://srtm.csi.cgiar.org>.
- Kellogg, O. (1929). *Foundation of potential theory*. Berlin Heidelberg New York: Springer.

- Kingdon, R., Vaníček, P., and Santos, M. (2011). Effects of Hypothetical Complex Mass-Density Distributions on Geoidal Height. *International Association of Geodesy Symposia (IAG SYMPOSIA)*, 136, pp. 427-433. Buenos Aires.
- Kingdon, R., and Vaníček, P. (2010). Poisson Downward Continuation Solution by the Jacobi Method. *Journal of Geodetic Science*, 1, 74-81.
- Kingdon, R., Vaníček, P., Santos, M., Ellmann, A., and Tenzer, R. (2005). Toward improved orthometric height system for Canada. *Geomatica*, 59, 241-249.
- Mader, K. (1954). Die orthometrische Schwerekorrektion des Präzisions-Nivellements. Vienna: Österreichische Zeitschrift für Vermessungswesen.
- Martinec, Z. (1993). Effect of lateral density variations of topographical masses in improving geoid model accuracy over Canada. Ottawa: Research Report for Geodetic Survey of Canada.
- Martinec, Z. (1998). Boundary value problems for gravimetric determination of a precise geoid, lecture note in Earth sciences. Berlin, Heidelberg New York: Springer.
- Molodensky, M., Yeremeev, V., and Yurkina, M. (1960). Methods for Study of the External Gravitational Field and Figure of the Earth. Moscow.: TRUDY TsNIIGAiK, 131, Geodezizdat.
- Niethammer, T. (1982). Nivellement und Schwere als Mittel zur Berechnung wahrer. Berne: Schweizerische Geodätische Kommission.
- Novák, P. (2000). Evaluation of gravity data for Stokes-Helmert solution to the geodetic boundary-value problem. Fredericton, Canada: University of New Brunswick.

- Odera, P., & Fukuda, Y. (2015). Comparison of Helmert and rigorous orthometric heights over Japan. *Earth, Planets and Space*, 67(27). doi:10.1186/s40623-015-0194-2.
- Rülke A, Liebsch G, Sacher M, Schäfer U, Schirmer U, Ihde J (2012) Unification of European height system realizations. *Journal of Geodetic Science* 2: 343-354.
- Santos, M., Vaníček, P., Featherstone, W., Kingdon, R., Ellmann, A., Martin, B.-A., . . . Tenzer, R. (2006). The relation between rigorous and helmert's definition of orthometric heights. *Journal of Geodesy*, 80(12), 691–704.
- Sünkel, H. (1986). Digital height and density model and its use for the orthometric height and gravity field determination for Austria. *Proceedings of international symposium on the definition of the geoid*, (pp. 599-604). Florance.
- Tenzer, R., and Vaníček, P. (2003). Correction to Helmert's orthometric height due to actual lateral variation of topographical density. *Brazilian Journal of Cartography-Revista Brasileira de Cartografia*, 55(02), 44-47.
- Tenzer, R., Vaníček, P., Santos, M., Featherstone, W., and Kuhn, M. (2005). The rigorous determination of the orthometric heights. *Journal of Geodesy*, 79(1), 82-92.
- Vaníček & Krakiwsky, 1986 *Geodesy the concept*, North Holland.
- Vaníček, P., Kleusberg, A., Martinec, Z., Sun, W., Ong, P., Najafi, M., Horst, B. (1995). *Compilation of a precise regional geoid model*. Fredericton: Final report on research done for the Geodetic Survey Division.

Vaníček, P., Tenzer, R., Sjöberg, L., Martinec, Z., and Featherstone, W. (2004). New views of the spherical Bouguer gravity anomaly. *Geophysical Journal International*, 159(2), 460-472.

## 5 Chapter 5: Sub-Centimetre geoid

This article has been published in the Journal of Geodesy. The idea of this article was to compute the most probable solution of the gravity anomalies on the geoid using LS DWC process. In the previous studies, mean gravity anomalies on grid points at the Earth surface were used to estimate the mean anomalies on the same points at the geoid where as in this study, all available (scattered and gridded) gravity anomalies at the Earth surface are used in solving the Poisson probabilistic downward continuation. The program for LS DWC was written by me to compute the mean gravity anomalies on grid points at the geoid using the LS technique. The program was later modified to compute the covariance matrix of gravity anomalies on the geoid using a priori variance matrix of surface gravity data. Having the covariance matrix of the gravity anomalies on the geoid allowed us to estimate the uncertainties of the geoidal heights contributed from NZ. Beside NZ contribution, the effect of other contributions to the geoidal heights, e.g., FZ, reference spheroid, PITE, and PIDE effect were also computed and for the first time, the total uncertainty of the geoidal heights determined by Stokes-Helmert method was estimated in this article. All the computation parts of this article and preparing the first draft of the article was done by me and revised by co-authors.

The full citation for this article:

Foroughi, I., Vaníček, P., Kingdon, R. W., Goli, M., Sheng, M., Afrasteh, Y., Novák, P., Santos, M.C, Journal of Geodesy (DOI: <https://doi.org/10.1007/s00190-018-1208-1>).

## 5.1 Abstract

This paper represents a milestone in the UNB effort to formulate an accurate and self-consistent theory for regional geoid determination. To get the geoid to a sub-centimetre accuracy we had to formulate the theory in a spherical rather than linear approximation, advance the modelling of the effect of topographic mass density, formulate the solid spherical Bouguer anomaly, develop the probabilistic downward continuation approach, incorporate improved satellite determined global gravitational models and introduce a whole host of smaller improvements. Having adopted Auvergne, an area in France as our testing ground, where the mean standard deviation of observed gravity values is 0.5 mGal, according to the Institute Geographique Nationale [Duquenne, 2007], we obtained the standard deviation of the gravity anomalies continued downward to the geoid, as estimated by minimizing the  $L_2$  norm of their residuals, to be in average 3-times larger than those on the surface with large spikes underneath the highest topographic points. The standard deviations of resulting geoidal heights range from a few millimetres to just over 6 cm for the highest topographic points in the Alpine region (just short of 2000 m). The mean standard deviations of the geoidal heights for the whole region is only 0.6 cm, which should be considered quite reasonable even if one acknowledges that the area of Auvergne is mostly flat. As one should expect, the main contributing factors to these uncertainties are the Poisson probabilistic downward continuation process, with the maximum standard deviation just short of 6 cm (the average value of 2.5 mm) and the topographical density uncertainties, with the maximum value of 5.6 cm (the average value of 3.0 mm).



The comparison of our geoidal heights with the testing geoidal heights, obtained for a set of 75 control points (regularly spaced throughout the region) show the mean shift of 13 cm which is believed to reflect the displacement of the French vertical datum from the geoid due to sea surface topography. The mean root square error of the misfit is 3.3 cm. This misfit, when we consider the estimated accuracy of our geoid, indicate that the mean standard deviation of the “*test geoid*” is about 3 cm, which makes it about 5 times less accurate than the Stokes-Helmert computed geoid.

Table 5.1: Abbreviations used throughout this article

<b>UNB</b>	University of New Brunswick
<b>DWC</b>	downward continuation
<b>UPC</b>	upward continuation
<b>LS</b>	least-squares
<b>EGM</b>	Earth gravitational model
<b>PITE</b>	primary indirect topographic effect
<b>PIAE</b>	primary indirect atmospheric effect
<b>PIDE</b>	primary indirect density effect
<b>LS DWC</b>	least-squares downward continuation
<b>GNSS</b>	Global Navigation Satellite System
<b>DTE</b>	direct topographic effect
<b>DDE</b>	direct density effect
<b>DAE</b>	direct atmospheric effect
<b>SITE</b>	secondary indirect topographic effect
<b>NT</b>	no-topography anomaly (spherical complete Bouguer gravity anomaly)
<b>STD</b>	standard deviation
<b>NZ</b>	near-zone (contribution of close gravity data to geoidal heights)
<b>FZ</b>	far-zone (contribution of distant gravity data to geoidal heights)
<b>RMS</b>	root mean square error
<b>DTM</b>	digital terrain model

## 5.2 Introduction

When a generation ago Martinec and Vaníček revived and improved the classical Stokes-Helmert technique for computing the geoid and stated that it would be possible to compute the geoid with an “error of the order of one centimetre”, the statement was not universally accepted basically for two reasons: the effect of the topographic mass density on observed gravity could not be evaluated to a high enough accuracy and “the downward continuation of gravity anomalies” was considered to be a very questionable procedure. Now, 25 years later, we can show on the example of the Auvergne area, France, where there is an excellent gravity coverage, both accurate and dense, as well as all supporting data, that the geoid can be indeed evaluated to a sub-centimetre accuracy. Clearly, that does not mean that the geoid can be provided to this accuracy everywhere in the world though. The accuracy of the geoid deteriorates in areas of higher topographical heights and if gravity data coverage and accuracy are worse than those of Auvergne.

Stokes-Helmert’s method for determining geoidal heights from terrestrial gravity, developed at the University of New Brunswick (UNB) during the past three decades, has been applied in different studies [Bajracharya, 2003; Huang and Véronneau, 2005; Ellmann and Vaníček, 2007; Afrasteh et al., 2017; Foroughi et al., 2017a; Janák et al., 2017]. To evaluate the Stokes integral, gravity anomalies must be known on the geoid. Moreover, there should not be any masses above the geoid. Whereas gravity observations are usually available at or above the topography, they must be continued down to the geoid. To continue the gravity anomalies down to the geoid, the anomalies must be of the solid kind [Vaníček et al. 2004]. Helmert’s gravity anomalies are one type of the solid gravity anomalies that can be continued down and up [ibid]. To get the Helmert anomalies,

the free-air gravity anomalies must be transformed from the real space to the Helmert space which is done by applying topographic and atmospheric effects on gravity to the free-air gravity anomalies (cf. Novák [2000]).

The process of continuing the Helmert gravity anomalies down to the geoid is called the downward continuation (DWC) of the Helmert anomalies which is perhaps the most challenging task in the geoid determination process. DWC is done in the Helmert space using a physically rigorous approach, i.e., through solving the Poisson integral equation [Kellogg, 1929]. The Poisson integral can be used for the upward continuation (UPC) of the gravity anomalies from the geoid to any point external to the geoid in the Helmert space where the Helmert gravity anomaly multiplied by its distance from the geocentre is a harmonic function. While UPC attenuates the values of gravity anomalies with growing degree and order of their spherical harmonic expansion, DWC amplifies the values for higher spatial frequencies.

Gravity values are observed at randomly distributed discrete points, but the Poisson integral equation is conveniently solved numerically using gravity data given on a regular coordinate grid. Thus, the integration domain of the Poisson integral is usually discretized to the regular grid for convenient numerical evaluation. According to Hadamard [1923], DWC is a physically well-posed problem but depending on the discretization step size and roughness of topography in the computation area, the Poisson integral equation, as any Fredholm equation of the 1<sup>st</sup> kind, can have a numerically unstable solution. Martinec [1996] showed that DWC of the ground gravity anomaly given on the grid with the angular resolution smaller than 1' is a numerically unstable problem. Sun and Vaníček [1998]

concluded that DWC of the 5' gravity anomalies has a numerically stable solution for the entire range of topographic heights on Earth. To deal with the instability of DWC in case of higher-resolution gravity anomalies, an iterative solution of the discretized Poisson integral equation was applied by Kingdon and Vaniček [2010]. Finding the solution of DWC by iterations, attaining convergence (i.e., the stage when the norm of differences between solutions of two successive iteration steps is smaller than a predefined threshold related to the noise of the observed data) results in a solution which is unique but may be marred by a high-frequency noise [Vaniček et al., 2017].

A condition number of the matrix of coefficients representing values of the Poisson integral kernel can be used to measure the level of the numerical instability of the Poisson DWC. Kingdon and Vaniček [2010] suggested to stop the iterative process when a preset value, which depends on the condition number as well as on the largest topographic height in the area, is reached. Stopping the iterative DWC based on physical characteristics of the desired solution, and not on actual convergence, is called semi-convergence which is often used when the system of linear equations is numerically unstable [Favati et al., 2014]. Stopping the iterative DWC at the semi-convergence point may be considered as regularization as it prevents the high-frequency observation noise from creeping into the DWC solution. For details on the stopping criteria and on the iterative DWC, please refer to Kingdon and Vaniček [2010] and Goli et al. [2018].

Kingdon and Vaniček [2010] and later again Vaniček et al. [2017] showed numerically that DWC of ground gravity anomalies is a physically well-posed problem with a finite and unique solution as required by Hadamard [1923]. According to their

results, if DWC is being sought iteratively, seeking the exact solution may require thousands of iterations (for high resolution data and for high topography), so it makes no sense to seek the exact solution. Indeed, after semi-convergence is reached, further iterations are marred with the high-frequency noise which reflects high topography, observation errors and an irregular spatial distribution of gravity data. They suggested that the DWC solution should be sought in the statistical sense, i.e., as the most probable rather than exact values of Helmert's gravity anomalies on the geoid. If one assumes that the observation noise is random with the normal distribution, which is indeed quite a standard assumption, then the most probable solution is obtained using the least-squares (LS) technique. Moreover, the LS technique can provide a fully populated covariance matrix for the estimated Helmert gravity anomalies on the geoid. The estimated uncertainties of the gravity anomalies on the geoid result from the physical model used for DWC as well as from random errors in the gravity observations and topographic heights used in the transformation of observed gravity from real to Helmert's space.

Once the gravity anomalies and their covariance matrix are estimated on the geoid, the residual co-geoidal heights (residual geoidal heights in Helmert's space) are evaluated using Stokes's integral. By propagating the random errors through the Stokes integration, the uncertainties coming from local gravity data can be estimated. The contribution of gravity data from the rest of the world to the residual co-geoidal heights is evaluated using an Earth's gravitational model (EGM). Estimating the uncertainties to geoidal heights from EGM is done by summing up the errors of the spherical harmonic coefficients (commission errors). The co-geoidal heights can be then transferred from Helmert's space back to the real space by adding the primary indirect topographic effect (PITE), primary

indirect atmospheric effect (PIAE) and the primary indirect density effect (PIDE). Their uncertainties can be added to the estimated uncertainty of the geoidal heights.

An accuracy of the geoidal heights determined by the Stokes-Helmert method was already investigated by Najafi-Alamdari et al. [1999]. At the time of their investigations, the DWC step was not utilized in error propagation computations, covariances amongst gravity anomalies on the geoid were considered negligible and ignored in estimating the uncertainties of the geoidal heights. Later Huang and Véronneau [2013] estimated the uncertainties of the geoidal heights in Canada using the Stokes-Helmert method. They considered the error in the geoidal height as a combination of the commission error in EGM and of ground gravity errors in evaluating the Stokes integral. The errors originating in DWC of gravity anomalies were also neglected in their computation.

The LS technique used in this study for DWC makes it possible to propagate the uncertainties of the gravity anomalies into the geoidal height errors. The uncertainties result from the irregular spatial distribution of gravity observations, their random errors and from the physical model of DWC. In all previous studies, the initial gravity data in the Stokes-Helmert approach were predicted on a regular coordinate grid on the Earth's surface before performing their DWC. In contrary, in this study the LS technique allows us to use all available gravity data, gridded as well as scattered, at or above the surface of the Earth.

The proposed methodology in the present study was applied to the Auvergne gravity data set [Duquenne, 2007]. The quasigeoid models of the Auvergne area have been computed using different methods, e.g., Agren, et al. [2009]. Some of them were

subsequently converted to the geoid models by adding the geoid-to-quasigeoid approximate correction. The first geoid model of the Auvergne area was computed by Janák et al. [2017] using the Stokes-Helmert approach. The optimal combination of terrestrial and satellite gravity data in this study was determined based on the methodology suggested by Foroughi et al. [2017a]. In all previous studies, the mean gravity anomalies on the regular grid points were predicted from those at scattered points and used as the input data. In the present study, both scattered and grid gravity anomalies at the Earth surface were continued down to mean gravity anomalies at the geoid level using the LS DWC approach; they were then used to evaluate the Stokes integral.

The theory of the Stokes-Helmert approach has been documented in many publications, e.g., [Vaniček and Kleusberg 1987; Vaniček and Martinec, 1994; Ellmann and Vaniček, 2007; Janák et al., 2017]. Thus, we do not herein repeat all the equations and formulas used in the Stokes-Helmert method. Only the mathematical expressions used for the LS DWC and for the error propagation into the geoidal heights will be recapitulated. The theory of the LS DWC and its numerical evaluation are presented in Sec. 5.3. The Stokes theory in the UNB rendition and the estimation of the uncertainties of the geoidal heights are summarized in Sec. 5.4 and numerical results in Sec. 5.5. The assessment of the estimated geoidal heights using available GNSS/Leveling points, called “control points” in the sequel, is done in Sec. 5.6, and the discussion of the results and concluding remarks can be found in Sec. 5.7.

## 5.3 Least Squares Downward Continuation (LS DWC)

### 5.3.1 The theory

The first step of the geoid determination from gravity data by the Stokes-Helmert method consists of transformation of observed gravity from the real space to Helmert's space. Free-air gravity anomalies are converted to Helmert's gravity anomalies by applying the direct topographic effect (DTE), direct density effect (DDE), direct atmospheric effect (DAE) and secondary indirect topographic effect (SITE) [e.g., Martinec and Vaníček, 1994; Martinec, 1998; Vaníček et al., 1999; Novák, 2000].

In order to remove long-wavelength variations from observed gravity data, residual Helmert's gravity anomalies are computed by subtracting the Helmert reference gravity anomalies of the degree/order  $L$  at the surface of the Earth ( $\Delta g_L^t$ ). To compute the Helmert reference gravity field, spherical harmonic coefficients of the gravitational potential available from satellite-only EGMs are transferred to Helmert's coefficients by applying topographic effects on gravity expressed in the spectral form [Vaníček et al., 1995]. The reference gravity field is then upward continued to the surface of the Earth using the Poisson integral. The optimal degree/order of the reference field ( $L$ ) can be estimated by the method explained in Foroughi et al. [2017a]. Residual Helmert's anomalies ( $\delta\Delta g^t$ ) at the surface of the Earth are solid anomalies, c.f., Vaníček et al. [2004]; thus, they can be continued down to the geoid. The residual anomalies are computed as:

$$\delta\Delta g^t(\Omega) = \Delta g^t(\Omega) - \Delta g_L^t(\Omega) . \quad (5.1)$$



The spherical form of the Poisson integral reads [Heiskanen and Moritz, 1967; Sec 1-6]:

$$\delta\Delta g^t(\Omega) = \frac{R}{4\pi r_t} \int_{\Omega_0} \delta\Delta g^g(\Omega') K(r_t, \psi(\Omega, \Omega'), R) d\Omega', \quad (5.2)$$

where  $\Omega$  represents the geocentric angular position (defined by spherical latitude  $-\pi/2 \leq \varphi \leq +\pi/2$  and longitude  $0 \leq \lambda \leq 2\pi$ ) of the residual gravity anomaly  $\delta\Delta g^t$  (computation point) and  $\Omega'$  stands for the geocentric direction of the residual gravity anomaly on the geoid  $\delta\Delta g^g$  (integration point).  $\Omega_0$  represents an integration domain usually chosen as a spherical cap of radius  $\psi_0$  to which the full spatial angle is shrunk reflecting the limited geographic availability of ground gravity data.  $R$  is the radius of the mean sphere approximating locally the unknown geoid,  $r_t$  is the geocentric radius of the computation point at the topography and  $K(r_t, \psi, R)$  is the spherical Poisson integral kernel given analytically as follows [ibid, 1967]:

$$K(r_t, \psi, R) = R \frac{r_t^2 - R^2}{l^3(r_t, \psi, R)} \quad (5.3)$$

where  $l(r_t, \psi, R)$  is the Euclidian distance between the computation and integration points and  $\psi$  is their spherical distance. As ground gravity anomalies are observed only in discrete points, the Poisson integral must be discretized for the numerical evaluation, which leads to the system of linear equations:

$$\delta\Delta \mathbf{g}^t = \mathbf{B} \delta\Delta \mathbf{g}^g, \quad (5.4)$$

where  $\mathbf{B}$  is the coefficient matrix containing values of the discretized Poisson integral [Vaníček, et al., 1996]:

$$B_{ij} = \frac{R^2(r_i^2 - R^2)}{4\pi r_i} \frac{1}{l^3(r_i, \varphi_i, \lambda_i; R, \varphi_j, \lambda_j)} \cos \varphi_j \Delta \varphi \Delta \lambda . \quad (5.5)$$

where  $j$  counts for the number of points used for discrete representation of the residual gravity anomalies on the geoid and  $i$  counts for the number of the gravity observation at or above the surface of the Earth. In our methodology,  $i \geq j$ , i.e., LS DWC provides an overdetermined solution. In general, in the DWC process the number of observations at the surface must be as large as the number of grid points on the geoid, i.e., the design matrix  $B$  is a square matrix [Kingdon and Vaníček, 2010]. We note that DWC is described by the system of Eqs. (5.4), i.e., by the discretized form of the integral Fredholm equation of the first kind. This equation system is nothing else but the system of observation equations known in adjustment calculus [Vaníček and Krakiwsky, 1986, Ch. 10.2]. If the LS technique is employed to estimate the residual Helmert gravity anomalies on the geoid, the observation equations are solved in the standard LS fashion whereby the residual gravity anomalies from the capture area on the surface are used to “estimate” residual anomalies in the target area on the geoid. The LS solution of the observation equations, i.e., LS DWC, reads:

$$\delta \Delta \mathbf{g}_{LS}^g = (\mathbf{B}^T \mathbf{P} \mathbf{B})^{-1} \mathbf{B}^T \mathbf{P} \delta \Delta \mathbf{g}^t , \quad (5.6)$$

where  $\mathbf{P}$  is the weight matrix equal to

$$\mathbf{P} = \text{diag}\left(\frac{\sigma_0^2}{\sigma_i^2}\right) \text{ and } \sigma_0^2 = 1, \quad (5.7)$$

and  $\sigma_0^2$  is the a priori variance factor, which is usually chosen to equal to 1, and  $\sigma_i$  is the standard deviation of the individual observations.

The a posteriori variance factor can be computed as

$$\hat{\sigma}_0^2 = \frac{\mathbf{v}^T \mathbf{P} \mathbf{v}}{\dim(\delta\Delta\mathbf{g}^t) - \dim(\delta\Delta\mathbf{g}^g)} \quad (5.8)$$

where  $\mathbf{v}$  is the vector of residuals, i.e., differences between the estimated ( $\delta\widehat{\Delta\mathbf{g}}^t$ ) and observed surface gravity anomalies ( $\delta\Delta\mathbf{g}^t$ ), which are linked through the observation equations:

$$\begin{aligned} \delta\widehat{\Delta\mathbf{g}}^t &= \mathbf{B}\delta\Delta\mathbf{g}_{LS}^g, \\ \mathbf{v} &= \delta\widehat{\Delta\mathbf{g}}^t - \delta\Delta\mathbf{g}^t. \end{aligned} \quad (5.9)$$

The covariance matrix of residual Helmert's anomalies on the geoid ( $C_{\delta\Delta\mathbf{g}^g}$ ) is given by the following well known expression:

$$\mathbf{C}_{\delta\Delta\mathbf{g}^g} = \hat{\sigma}_0^2 (\mathbf{B}^T \mathbf{P} \mathbf{B})^{-1}. \quad (5.10)$$

### 5.3.2 Numerical evaluation of LS DWC

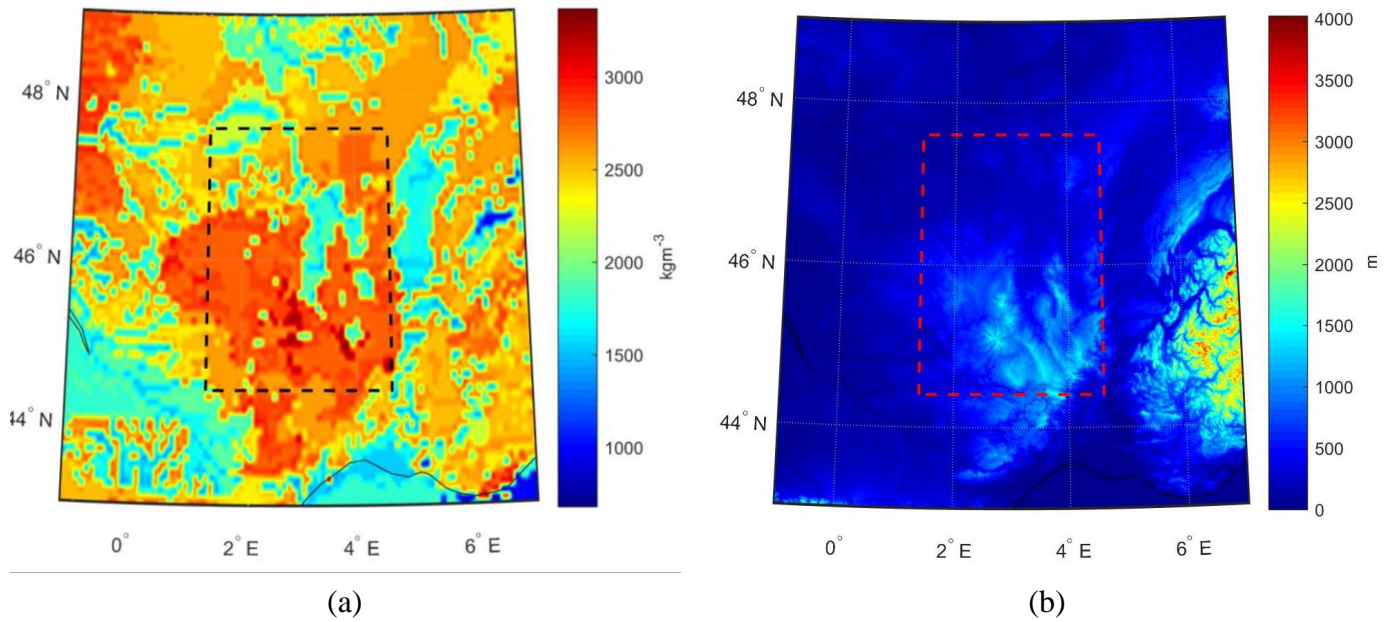
#### 5.3.2.1 Prediction of gravity at grid points

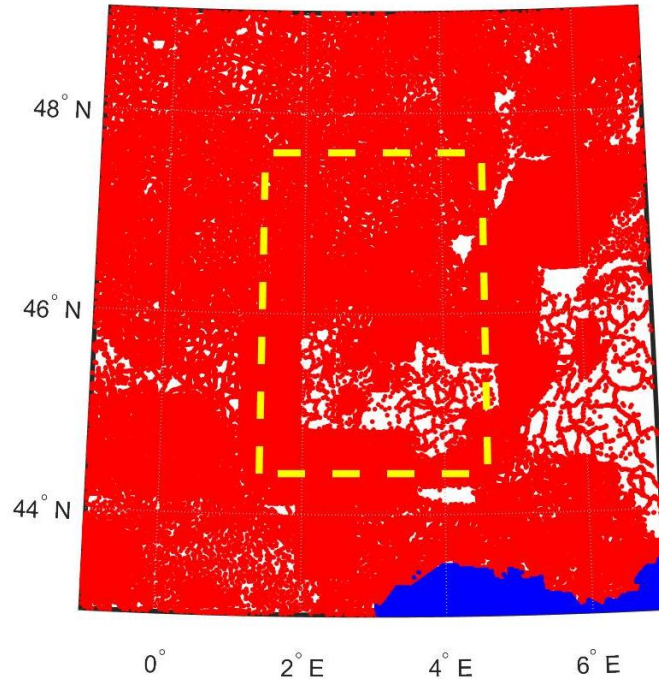
The purpose of this step is to predict the gravity anomalies on the grid points from scattered gravity data at the Earth surface. Any prediction technique works better with a smooth rather than rough function. For that reason, we transform observed rather rough free-air gravity anomalies at the scattered points to smooth spherical complete Bouguer

gravity anomalies also known as no-topography (NT) gravity anomalies. The NT gravity anomalies at the scattered points are computed by removing the complete Bouguer gravity correction, i.e., topographic corrections due to the spherical Bouguer shell and respective terrain. The NT gravity anomalies, known to be the smoothest of all gravity anomalies [Vaniček et al., 2004], are used for prediction of gravity anomalies on an equiangular grid with the resolution of 1' by employing the inverse-distance squared prediction method. This method predicts the gravity anomalies on the grid points by taking a weighted, by the inverse distance squared, mean of the nearest gravity observations surrounding the grid point. This technique was chosen as it had been shown in several cases that it yielded reasonable results while being easily implemented [Kassim, 1980]. After predicting the gravity anomalies on the grid, the values of the NT anomalies are transformed back to the real space and converted into Helmert's anomalies. The observed anomalies are transformed into Helmert's anomalies one by one by applying DTE, DAE, SITE and DDE. The mean value of topographic density ( $2670 \text{ kg/m}^3$ ) is used to compute DTE and SITE [Hinze, 2003], whereas a lateral mass density model of the area is needed to compute DDE [Martinec, 1993]. In Auvergne, the lateral density model was obtained by digitizing a superficial geological map [Bodelle et al., 1980] which is shown in Figure 5.1(a). The lateral topographic density values of this area range from  $\sim 800$  to  $3500 \text{ kg m}^{-3}$  which confirms that the Auvergne area is geologically challenging. Values of DDE on the geoidal heights also range from  $-6$  to  $3 \text{ cm}$ , see Janák et al. [2017].

The Auvergne area limited by  $-1^\circ < \lambda < 7^\circ$ ,  $43^\circ < \varphi < 49^\circ$  [Duquenne, 2007] was chosen as the study area because it was geologically, see Figure 5.1(a), and topographically, see Figure 5.1(b), quite challenging. It also has been well surveyed and

studied by different groups which are in the geoid determination field; there are 248000 scattered terrestrial and marine gravity observations of a fairly good overall accuracy. Marine gravity anomalies were extracted from the global sea surface topography model provided by Sandwell et al. [2014] using radar altimeter measurements from the CryoSat-2 and Jason-1 satellites. The spatial distribution of the scattered observations is not exactly uniform as the observations had been conducted for various reasons in different parts of the region, see Figure 5.1(c).





(c)

Figure 5.1: Topographic mass density variations (a), topographic heights (b), distribution of ground (red) and marine (blue) gravity observations (c). Dashed lines show the geoid computation area.

### 5.3.2.2 Construction of the weight matrix

Once predicted as well as scattered Helmert's gravity anomalies at the Earth's surface become available, they are reduced for the reference Helmert gravity field of the chosen degree and order to remove the long-wavelength content. The optimal degree and order of the reference field are chosen based on the methodology suggested by Foroughi et al. [2017a]. For details on computation of Helmert's effects for the Auvergne data set, please refer to Janák et al. [2017].

According to Duquenne [2007], values of the standard deviation (STD) of scattered gravity values are between 0.25 and 0.75 mGal. Thus, we choose 0.5 mGal as the uniform error for all scattered points. STD values of marine gravity anomalies were extracted from

the global marine gravity model provided by Sandwell et al. [2014]. The mean value of these STDs, i.e., 1.2 mGal, was used as a uniform STD for marine gravity points in the southern part of Auvergne (blue points in Figure 5.1c). Based on these estimates we compute the errors of gridded gravity anomalies. For the prediction of the gridded anomalies, weights inversely proportional to the squares of the distances between the observation and the prediction points ( $\mathbf{D}_i^2$ ) are assigned to gravity observations at the scattered points. The mathematical model is given by [Kearsley, 1977]:

$$\Delta g_P = \frac{\sum_{i=1}^n \Delta g_i^{sct} \mathbf{D}_i^{-2}}{\sum_{i=1}^n \mathbf{D}_i^{-2}} \quad (5.11)$$

where  $n$  is the number of observations ( $\Delta g_i^{sct}$ ) in the radius of  $1^\circ$  around each prediction point.

Kearsley [1977] estimated STDs of the gridded gravity values as contribution of two uncorrelated error sources including (i)  $\sigma_e^2$ , which represents the effect of roughness of the scattered points, and (ii)  $\sigma_g^2$ , which accounts for STD of the scattered observations. These two sources of STDs contribute as follows:

$$\sigma_e^2 = \frac{\sum_{i=1}^n \mathbf{D}_i^{-2} (\Delta g_P - \Delta g_i^{sct})^2}{(n-1) \sum_{i=1}^n \mathbf{D}_i^{-2}} \quad (5.12)$$

$$\sigma_g^2 = \frac{\sum_{i=1}^n \mathbf{D}_i^{-4} \sigma_{\Delta g_i^{sct}}^2}{\sum_{i=1}^n \mathbf{D}_i^{-4}} \quad (5.13)$$

Finally, assuming there are no correlations between the two error sources, STD of the predicted value is estimated as:

$$\sigma_{\Delta g_P} = \sqrt{\sigma_e^2 + \sigma_g^2} \quad (5.14)$$

Figure 5.2 shows the estimated values of STD of the gridded gravity anomalies at the Earth surface and Table 5.2 summarizes their statistics.

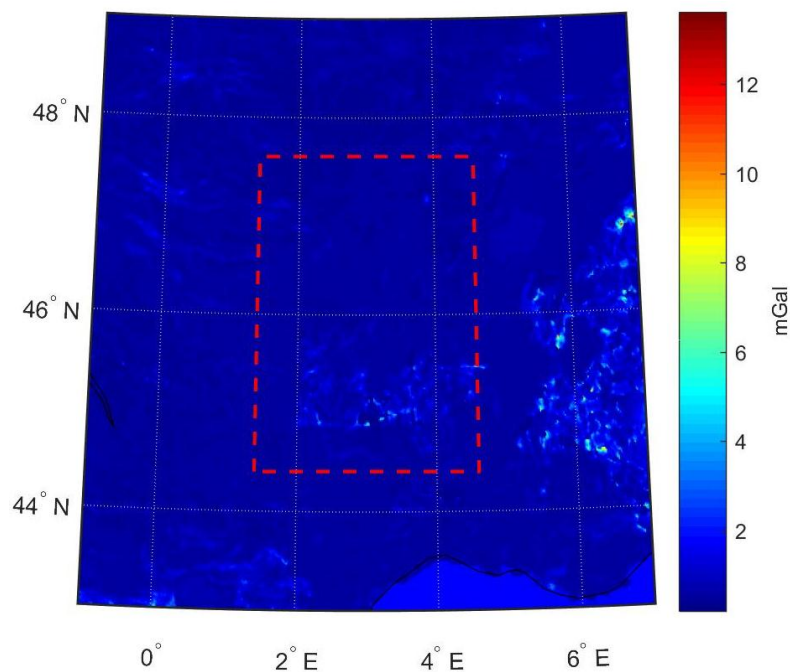


Figure 5.2: STD values of the gridded gravity anomalies on the Earth's surface. Dashed line shows the geoid computation area.

Table 5.2: Estimated STD values of the gridded gravity anomalies on the Earth surface

	Min [mGal]	Max [mGal]	Mean [mGal]
STD of grid points	0.51	13.61	0.61



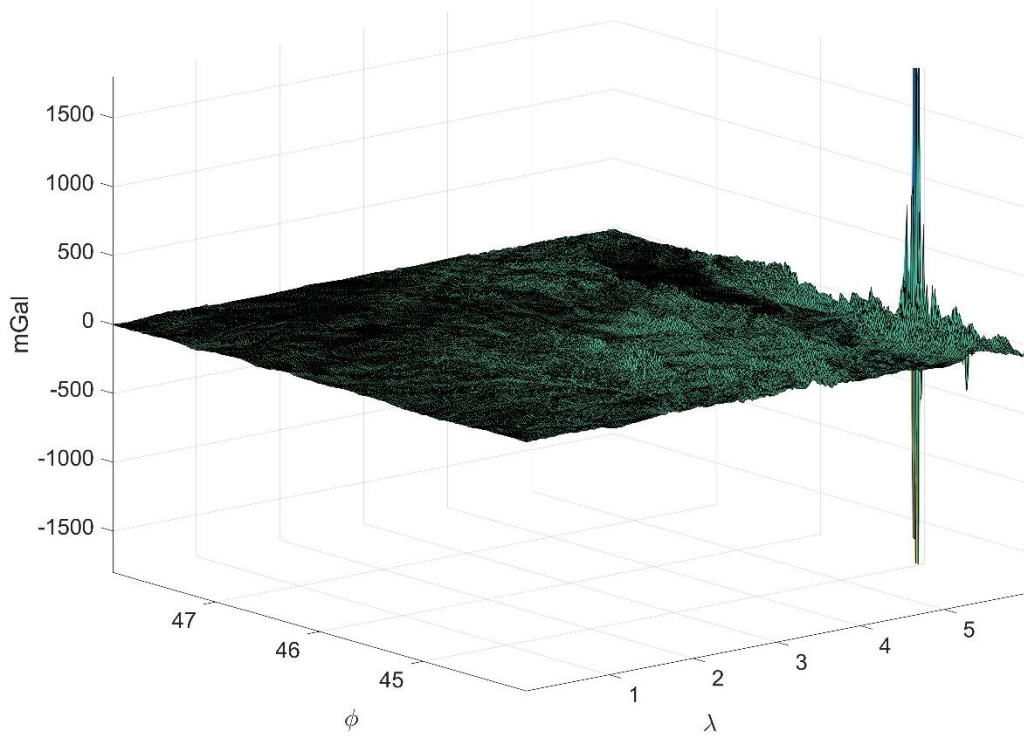
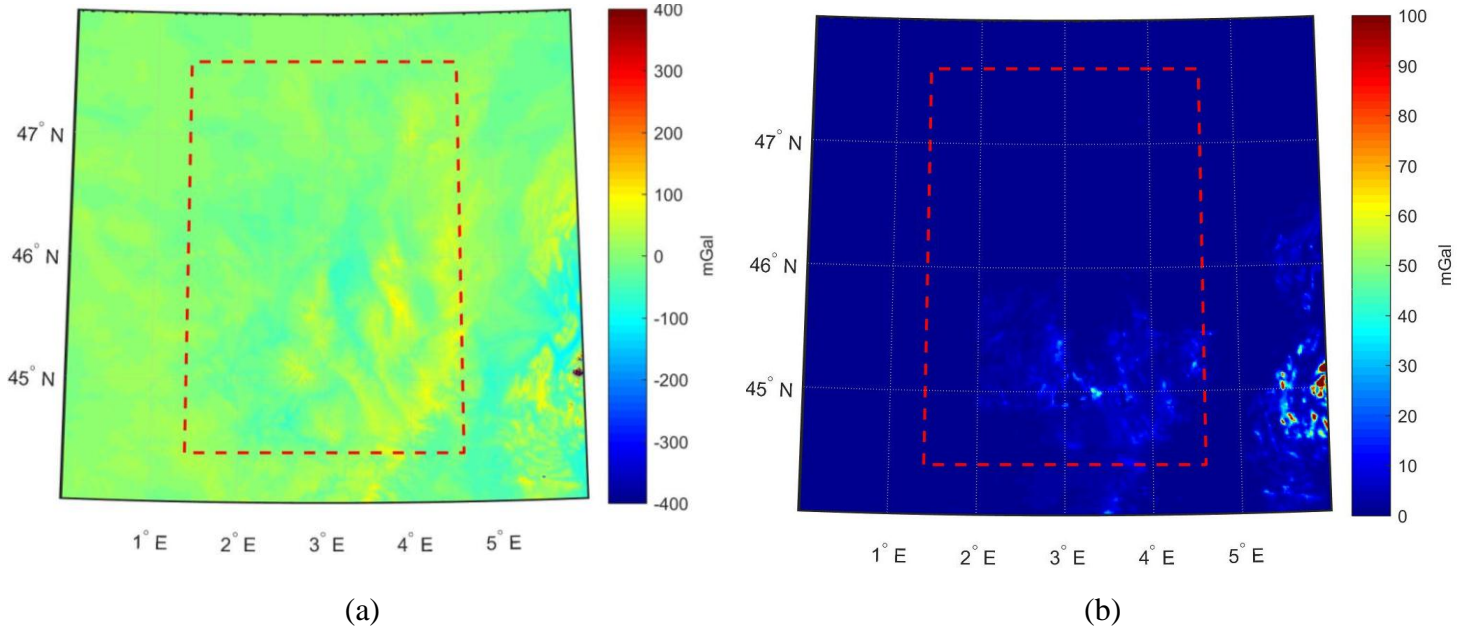
The estimated accuracy of the gridded gravity anomalies is almost as good as the accuracy of observed gravity (mean STD of 0.61 mGal compared to 0.50 mGal). Figure 5.2 shows also a good homogeneity of the estimated STDs over the area except for a few places where gravity observations are scarce.

### 5.3.2.3 Performing the LS DWC

After subtracting the reference gravity field and using the uniform STD of scattered gravity and the estimated STD of gridded gravity, the diagonal  $\mathbf{P}$  matrix in Eq. (5.6) can be constructed and LS DWC performed. Due to the limited computational power, in practice DWC is carried out individually over target cells of a certain size, normally  $1^\circ \times 1^\circ$ , on the geoid. The results of individual cells are then fused together which can reliably be done if there are no significant discontinuities between the downward continued values in the adjacent cells. Discontinuities between the downward continued gravity anomalies were investigated by Foroughi et al. [2015]. They showed that both the capture area and target area must be extended by a border strip of at least 30' width. In the LS technique gridded (predicted) and scattered (observed) gravity values from the capture area can be used together. The a posteriori variance factor  $\hat{\sigma}_0^2$ , computed using Eq. (5.8), corresponds to the extended capture area on topography and also to the target area on the geoid.

Figure 5.3 shows 2-D plots of the LS DWC solution of the residual Helmert gravity anomalies on the geoid and their estimated STDs, these being the square roots of the diagonal values of the covariance matrix of the downward continued gravity anomalies multiplied by the estimated a posteriori variance factor, see Eq. (5.8). Statistics of the

residual Helmert gravity anomalies on the geoid and their STDs are summarized in Table 5.4.



(c)

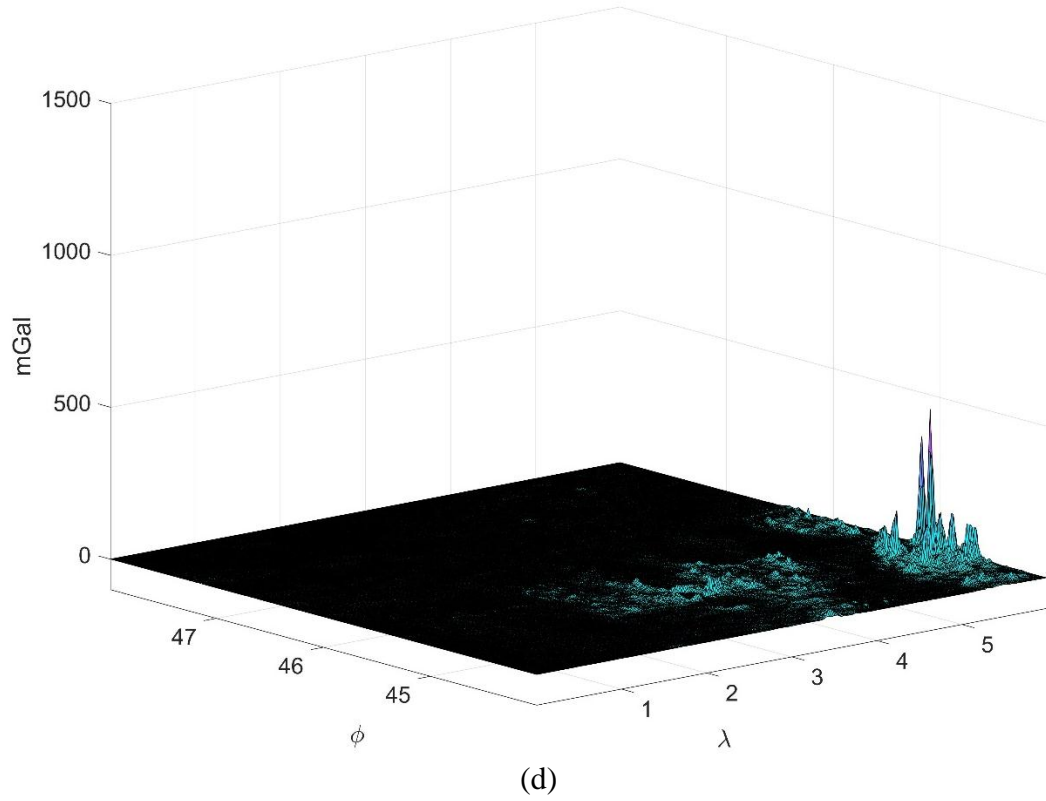


Figure 5.3: LS DWC solution of the gravity anomalies on the geoid: 2-D plot (a) and 3-D plot (c), estimated STDs: 2-D plot (b) and 3-D plot (d). Dashed lines show the geoid computation area.

The a posteriori variance factors ( $\hat{\sigma}_0^2$ ) for each  $1^\circ \times 1^\circ$  cell, see Eq. (5.8), are provided in Table 5.3. The results point out to the fact that the a priori STDs for the low laying areas are too pessimistic while those for the higher areas are too optimistic.

Table 5.3: The a posteriori variance factor values of each extended cell

$$\varphi = 48^\circ, \lambda = 0^\circ$$

$$\varphi = 48^\circ, \lambda = 6^\circ$$

0.40	0.24	0.20	0.33	0.39	0.36
0.54	0.55	0.55	0.58	0.47	0.78
0.56	1.40	1.26	0.9	1.07	1.75
0.39	0.71	1.57	1.94	2.52	1.81

$$\varphi = 44^\circ, \lambda = 0^\circ$$

$$\varphi = 44^\circ, \lambda = 6^\circ$$

Table 5.4: Statistics of the LS DWC solution

	Min [mGal]	Max [mGal]	Mean [mGal]
Residual Helmert's anomalies on the geoid	-1852.1	1821.4	0.6
Estimated STD	0.1	388.1	1.5

The STD of the gravity anomalies on the geoid (last line of Table 5.4) was estimated by evaluating square roots of the diagonal terms of the covariance matrix in the LS DWC process, see Eq. (5.10). The maximum values of the estimated gravity anomalies as well as their STDs on the geoid are quite large. To better illustrate the behavior of the variations of the estimated gravity anomalies, we plot them in 3-D view, see Figure 5.3(c) and Figure 5.3(d). Looking at STDs of the gravity anomalies on the geoid, we see that the largest values are confined to a few peaks over a limited horizontal dimension, indeed the largest estimated STD (388.09 mGal) corresponds to the highest point in the east part of Auvergne. The accuracy of DWC is controlled almost solely by the elevation of observed gravity: high elevations translate directly into large errors. The effect of the assumed a priori observation error is only marginal. The mean STD of the gravity anomalies on the

geoid is magnified almost 3-times from the mean STD value of the gravity anomalies on the surface of the Earth by the process of DWC.

#### 5.3.2.4 Saving the covariance matrix

As mentioned above, to perform DWC, the area of interest was broken down to  $1^\circ \times 1^\circ$  cells and additional 30' border strips were used. This means each 1arc-deg cell has a covariance matrix with the dimension of  $3600 \times 3600$  which is quite demanding on computer memory and makes it difficult to save as a whole for further usage. Fortunately, the covariances practically diminish after 1 to 2 steps away from the main diagonal, i.e., 2' away from the computational point. So, it seems to be sufficient to save only the variances and the covariances within the distance of only 2' from the point of interest (in both longitudinal and latitudinal sense) to be used for the propagation of STDs through the Stokes integral. This means that only 24 covariance values for each point on the geoid grid are saved in this step for later use. Moreover, the sub-matrices of the whole covariance matrix are symmetric which means that only half of the covariance matrix has to be saved.

## 5.4 Estimating the uncertainty in the geoidal heights

### 5.4.1 Sources of uncertainties

There are four sources of uncertainties affecting the accuracy of the geoidal heights determined by the Stokes-Helmert approach: uncertainties in EGMs, gravity observations, topographic heights and in topographic mass density. Some of these sources affect the accuracy of gravity observations (input data) and some affect directly the final geoidal heights in the real space. The uncertainties in EGM affect the gravity observations when

the reference field is subtracted from them in Helmert's space. The EGM errors also affect the geoidal heights in terms of the reference spheroid and evaluation of far-zone contributions to the modified Stokes integral. The uncertainties in topographic heights and topographic mass density will affect the uncertainty of gravity observations via DTE, DDE and SITE, and will affect the geoidal heights in terms of PITE and PIDE.

These errors would also have some effect on transformation of the reference field and reference spheroid from the real to Helmert's space and the inverse transformation. As the reference field is subtracted from gravity anomalies and then added in the form of the reference spheroid to the residual geoidal heights on the geoid, we assume that their errors, small to begin with, would most likely cancel each other to the large extent. Therefore, we neglect these errors completely.

The estimated covariance matrix of the residual Helmert gravity anomalies on the geoid, that resulted from the LS DWC process, reflects the existing random errors in the input gravity data, e.g., the effect of the reference field (removed from gravity at the surface), topographic heights and mass density variations (needed for conversion to Helmert's space and back to the real space, i.e., for evaluation of DTE, SITE and PITE), and observation errors. Values in the covariance matrix depend on elevation and distribution of gravity data, and on the a priori weight matrix of the gravity data, see Eq. (5.7). The results of our experiments using different a priori values for observation errors showed that the estimated final accuracy of the gravity anomalies on the geoid depends mostly on the spatial distribution and elevation of gravity observations rather than on a priori observation errors. Thus, we did not account for the uncertainty in Helmert's gravity

anomalies on the Earth surface due to topographic height and mass density errors hoping that these uncertainties are at least partially accounted for by Duquenne's [2007] estimates. As DTE and PITE uncertainties due to topographic height and mass density errors are likely to have very similar effects on the geoid, except that the effect would probably be of opposite signs, by including PITE and excluding DTE, we are probably erring on the pessimistic side.

The covariance matrix of the gravity anomalies on the geoid is used to estimate the uncertainties in the near-zone (NZ) contribution of the geoidal heights. The other sources of uncertainties in the geoidal heights is reference spheroid, far-zone (FZ) contribution, PITE, and PIDE. We summarize below the formulas to estimate the uncertainties in the final geoidal heights as contributed by these effects.

#### 5.4.2 Uncertainty in the NZ contribution

The Stokes integral used to determine the geoidal heights  $N(\Omega)$  at any geocentric direction  $\Omega$  may be written as:

$$N(\Omega) = N_L(\Omega) + \delta N_L(\Omega) , \quad (5.15)$$

where  $N_L$  is the reference spheroid of degree  $L$  computed using the selected EGM and  $\delta N_L$  is the contribution of local ground gravity data (near-zone contribution):

$$\delta N_L(\Omega) = \frac{R}{4\pi\gamma} \int_{\Omega' \in \Omega_0} S^*(\psi(\Omega, \Omega')) \delta \Delta g(\Omega') d\Omega' , \quad (5.16)$$

where  $S^*$  is the modified Stokes function [Vaníček and Kleusberg, 1987],  $\Omega_0$  is the integration domain on the spherical manifold (approximating the geoid), usually defined as a spherical cap with the radius defined by the spherical angle  $\psi_0$ . In theory, the cap should cover the full spatial angle, i.e.,  $\psi_0 = \pi$ , but in practical computations a limited area called NZ for  $\psi \in \langle 0, \psi_0 \rangle$  is used, while the contribution of the rest of the world is called FZ for  $\psi \in \langle \psi_0, \pi \rangle$ . The NZ and FZ contribution can be written as:

$$\begin{aligned}
\delta N_L(\Omega) &= \delta N^{NZ}(\Omega) + \delta N^{FZ}(\Omega) \\
&= \frac{R}{4\pi\gamma(\Omega)} \int_{\Omega' \in \Omega_{\psi_0}} S^*(\psi_0, \psi(\Omega, \Omega')) \delta\Delta g(\Omega') d\Omega' \\
&+ \frac{R}{4\pi\gamma(\Omega)} \int_{\Omega' \in \Omega_0 - \Omega_{\psi_0}} S^*(\psi_0, \psi(\Omega, \Omega')) \delta\Delta g(\Omega') d\Omega'.
\end{aligned} \tag{5.17}$$

According to Molodensky et al. [1960], and Vaníček and Kleusberg [1987], the Stokes integral is modified in a way that the FZ contribution is minimized in the least-squares sense. The FZ contribution is computed in the spectral way using EGM while the NZ contribution is evaluated by numerical integration using the modified Stokes function.

In the NZ contribution, the modified Stokes integral is weakly singular for the spherical distance  $\psi = 0$ . So, for computing the solution in the spatial form, the Cauchy technique is used which consists of splitting the integral into the differential neighborhood of the singularity point and the rest of the integration area – resulting in the sum of two integrals taken over the whole integration area, one over the Stokes function multiplied by the value of the gravity anomaly at the singularity point, the other of the Stokes function



multiplied by the differences of the anomalies minus the value of the gravity anomaly at the singularity point which reads [Martinec, 1993]:

$$\begin{aligned} \delta N(\Omega)^{NZ} = & \frac{R}{4\pi\gamma(\Omega)} \delta\Delta g(\Omega) \int_{\Omega' \in \Omega_{\psi_0}} S^*(\psi_0, \psi(\Omega, \Omega')) d\Omega' \\ & + \frac{R}{4\pi\gamma(\Omega)} \int_{\Omega' \in \Omega_{\psi_0}} S^*(\psi_0, \psi(\Omega, \Omega')) [\delta\Delta g(\Omega') \\ & - \delta\Delta g(\Omega)] d\Omega'. \end{aligned} \quad (5.18)$$

The first part of the right-hand side of Eq. (5.18) is the contribution of gravity at the computation point called here the “epicenter contribution” (in mathematics it is called the contribution of the differential neighborhood of the point of singularity) and denoted by epc ( $\delta N(\Omega)^{epc}$ ) and the second part is the effect of rest of the cap ( $\delta N(\Omega)^{dNZ}$ ).

The epc contribution can be computed as follows [Novák et al., 2001]:

$$\delta N(\Omega)^{epc} = \frac{R\delta\Delta g(\Omega)}{2\gamma(\Omega)} \int_{\psi=0}^{\psi_0} S^*(\psi_0, \psi(\Omega, \Omega')) \sin(\psi) d\psi \quad (5.19)$$

and the contribution of the rest of the cap:

$$\delta N(\Omega)^{NZ-epc} = \frac{R}{4\pi\gamma(\Omega)} \iint_{\Omega' \in \Omega_{\psi_0}} S^*(\psi_0, \psi(\Omega, \Omega')) [\delta\Delta g(\Omega') - \delta\Delta g(\Omega)] d\Omega'. \quad (5.20)$$

Thus, the singularity is automatically removed from Eq. (5.20) because for  $\psi = 0$  the value of the integrand  $\delta\Delta g(\Omega') - \delta\Delta g(\Omega)$  equals to zero. The integral of the modified Stokes function  $S^*(\psi_0, \psi(\Omega, \Omega'))$  can be computed analytically [Novák et al., 2001]:

$$\begin{aligned}
\delta N(\Omega)^{\text{epc}} &= \frac{R\delta\Delta g(\Omega)}{2\gamma(\Omega)} \int_{\psi=0}^{\psi_0} S^*(\psi_0, \psi(\Omega, \Omega')) \sin(\psi) d\psi \\
&= \frac{R\delta\Delta g(\Omega)}{2\gamma(\Omega)} \tilde{Q}_0^*(\psi_0) \approx c \delta\Delta g(\Omega)
\end{aligned} \tag{5.21}$$

where  $\tilde{Q}_0^*(\psi_0)$  is the integral of the modified Stokes's function computed analytically and  $c$  is a constant equal to  $\frac{R\tilde{Q}_0^*(\psi_0)}{2\gamma(\Omega)}$  for each computation point.

Equation (5.20) has to be evaluated numerically. If the values of gravity anomalies on the geoid represent mean values over the grid cells, the integral may be written in the discretized form as follows:

$$\begin{aligned}
\forall i = 1, 2, \dots, n: \delta N(\Omega_i)^{\text{NZ-epc}} \\
&= \frac{R}{4\pi\gamma(\Omega_i)} \sum_{j=1}^m S^*(\psi_0, \psi(\Omega_i, \Omega_j)) [\delta\Delta g(\Omega_j) \\
&\quad - \delta\Delta g(\Omega_i)] \Delta\Omega_j,
\end{aligned} \tag{5.22}$$

for  $n$  geoidal heights computed using  $m$  gravity anomalies. Equation (5.18) can be written as:

$$\begin{aligned}
\forall i = 1, 2, \dots, n: \delta N(\Omega_i)^{\text{NZ}} &= (N(\Omega_i)^{\text{epc}} + N(\Omega_i)^{\text{NZ-epc}}) = \\
&= \frac{R\delta}{2\gamma(\Omega_i)} \left\{ \tilde{Q}_0^*(\psi_0) \Delta g(\Omega_i) + \right. \\
&\quad \left. \frac{1}{2\pi} \sum_{j=1}^m S^*(\psi_0, \psi(\Omega_i, \Omega_j)) [\delta\Delta g(\Omega_j) - \Delta g(\Omega_i)] \Delta\Omega_j \right\}
\end{aligned} \tag{5.23}$$

The covariance matrix of the LS DWC solution can be used to propagate STDs of the observed data to STDs of the NZ contribution to the residual co-geoidal heights. Propagation of STDs through the Stokes integral, i.e., the NZ contribution, can be written

in the matrix form. Assuming  $m$  gravity anomalies are used to compute the NZ contribution, Eq. (5.21) can be written in the matrix form as:

$$\delta N(\Omega)^{\text{epc}} = c[0,0, \dots, 1, \dots, 0]_{1,m} \begin{bmatrix} \delta\Delta g(\Omega_1) \\ \vdots \\ \delta\Delta g(\Omega_n) \\ \vdots \\ \delta\Delta g(\Omega_m) \end{bmatrix}_{m,1} = c \mathbf{d} \delta\Delta \mathbf{g}. \quad (5.24)$$

According to Eq. (5.22), we can also write  $\delta N(\Omega)^{\text{NZ-epc}}$  in the matrix form as:

$$\delta N(\Omega)^{\text{NZ-epc}} = k[S_1^* S_2^* \dots S_m^*]_{1,m} \begin{bmatrix} \delta\Delta g(\Omega_1) - \delta\Delta g(\Omega_n) \\ \vdots \\ 0 \\ \vdots \\ \delta\Delta g(\Omega_m) - \delta\Delta g(\Omega_n) \end{bmatrix}_{m,1}, \quad (5.25)$$

where  $k = \frac{R}{4\pi\gamma(\Omega_i)}$  and Eq. (5.25) can be written as:

$$\begin{aligned} & \delta N(\Omega)^{\text{NZ-epc}} \\ &= k [S_1^* S_2^* \dots S_m^*]_{1,m} \begin{bmatrix} 1 & \dots & -1 & \dots & 0 \\ \vdots & & \ddots & & \vdots \\ 0 & \dots & -1 & \dots & 1 \end{bmatrix}_{m,m} \begin{bmatrix} \delta\Delta g(\Omega_1) \\ \vdots \\ \delta\Delta g(\Omega_n) \\ \vdots \\ \delta\Delta g(\Omega_m) \end{bmatrix}_{m,1} \\ &= k \mathbf{S}_m^* \mathbf{b} \delta\Delta \mathbf{g}, \end{aligned} \quad (5.26)$$

where  $\mathbf{S}_m^* = [S_1^* S_2^* \dots S_m^*]$ . In this vector the value of  $S^*$  for  $\psi = 0$  is set to zero. The NZ contribution, see Eq. (5.23) in the matrix form can be written as:

$$\delta N(\Omega)^{\text{NZ}} = [C\mathbf{d} + K\mathbf{S}_m^* \mathbf{b}] \delta\Delta \mathbf{g} = \mathbf{q} \delta\Delta \mathbf{g}. \quad (5.27)$$

By applying the covariance law to Eq. (5.27), the uncertainties of the residual geoidal heights can be estimated using the following formula:

$$\sigma_{\delta N(\Omega)NZ}^2 = \mathbf{q}^t \mathbf{C}_{\delta \Delta g} \mathbf{q} \quad (5.28)$$

where  $\mathbf{C}_{\delta \Delta g}$  is the covariance matrix of the residual gravity anomalies on the geoid computed using Eq. (5.10).

Once the residual co-geoidal heights are computed, the reference spheroid of the same degree and order as the reference field is added to the residual co-geoidal heights [Vaníček et al., 1995]. PITE, PIDE, and PIAE are then applied to the co-geoidal heights to transfer them to the real space. For details on transferring the co-geoidal heights to the real space, see Martinec and Vaníček [1994b], and Martinec et al. [1996].

### 5.4.3 Uncertainty in the reference spheroid

The reference spheroid of the degree  $L$ , i.e.,  $N_L(\Omega)$  in the Helmert space, is expressed as a finite series of spherical harmonics. Using the spherical approximation [Vaníček and Krakiwsky, 1986], we get:

$$N_L(\Omega) = \frac{GM}{R\gamma} \sum_{n=2}^L T_n(\Omega), \quad (5.29)$$

where  $R$  is the mean radius of the Earth,  $\gamma$  is normal gravity on the reference ellipsoid and  $T_n(\Omega)$  are the surface harmonics of the disturbing gravity potential given by:

$$T_n(\Omega) = \sum_{m=0}^n [\bar{T}_{nm}^C \bar{Y}_{nm}^C(\Omega) + \bar{T}_{nm}^S \bar{Y}_{nm}^S(\Omega)] \quad (5.30)$$

where

$$\begin{bmatrix} \bar{Y}_{nm}^C \\ \bar{Y}_{nm}^S \end{bmatrix} = \begin{pmatrix} \cos m\lambda \\ \sin m\lambda \end{pmatrix} \bar{P}_{nm}(\sin \varphi), \quad (5.31)$$

are the fully normalized spherical harmonics [Heiskanen and Moritz, 1967], and  $\bar{T}_{nm}^C$  and  $\bar{T}_{nm}^S$  are the fully normalized disturbing potential coefficients transferred to the Helmert space (cf., Vaníček et al. [1995]).

Uncertainties in the disturbing potential coefficients are due to the errors in EGM coefficients. If we denote the error variances of  $\bar{T}_{nm}^C$  and  $\bar{T}_{nm}^S$  by  $(\sigma_{nm}^C)^2$  and  $(\sigma_{nm}^S)^2$ , the variance of the reference spheroid  $\sigma_{N_L}^2$  can be estimated as follows:

$$\sigma_{N_L}^2(\Omega) = \left(\frac{GM}{R\gamma}\right)^2 \sum_{n=2}^L \sum_{m=0}^n [(\sigma_{nm}^C)^2 (\bar{Y}_{nm}^C)^2 + (\sigma_{nm}^S)^2 (\bar{Y}_{nm}^S)^2] \quad (5.32)$$

#### 5.4.4 Uncertainty in the FZ contribution

The FZ contribution of Helmert's anomalies to the residual co-geoidal heights is computed from [Novák, 2000]:

$$\delta N(\Omega)^{FZ} = \frac{R}{2} \sum_{n=L+1}^{n_{max}} Q_n(\psi_0, \psi(\Omega, \Omega')) \sum_{m=0}^n \bar{T}_{nm}^C \bar{Y}_{nm}^C(\Omega) + \bar{T}_{nm}^S \bar{Y}_{nm}^S(\Omega) \quad (5.33)$$

where,  $Q_n$  are the truncation coefficients of the modified Stokes function of the degree  $L$  and integration cap size of  $\psi_0$  (cf., Novák [2000]). Following the same strategy as we applied in Sec.5.4.3, we get:

$$\sigma_{\delta N^{FZ}}^2(\Omega) = \left(\frac{R}{2}\right)^2 \sum_{n=L+1}^{n_{max}} (Q_n(\psi_0, \psi(\Omega, \Omega')))^2 \sum_{m=0}^n (\sigma_{nm}^C)^2 (\bar{Y}_{nm}^C)^2 + (\sigma_{nm}^S)^2 (\bar{Y}_{nm}^S)^2. \quad (5.34)$$

#### 5.4.5 Uncertainty in the transformation of the co-geoid back to the real space

According to Vaníček and Martinec [1994] the Bouguer shell constituent of PITE ( $\delta V^B$ ), which is the dominant component of this effect, reads:

$$\delta V^B(R, \Omega) = -2\pi G \bar{\rho}(\Omega) H^2(\Omega) \left(1 + \frac{2}{3} \frac{H(\Omega)}{R}\right) \quad (5.35)$$

where  $\bar{\rho}$  is the mean topographic density. When a laterally-varying density model is used, taking the first order approximation as a basis for an approximate error propagation, we find the derivatives with respect to height and density to be:

$$\frac{\partial \delta V^B(R, \Omega)}{\partial H} = -4\pi G \bar{\rho}(\Omega) H(\Omega) \left(1 + \frac{H(\Omega)}{R}\right) \approx -4\pi G \bar{\rho}(\Omega) H(\Omega), \quad (5.36)$$

$$\frac{\partial \delta V^B(R, \Omega)}{\partial \bar{\rho}(\Omega)} = -2\pi G H^2(\Omega) \left(1 + \frac{2}{3} \frac{H(\Omega)}{R}\right) \approx -2\pi G H^2(\Omega). \quad (5.37)$$

The uncertainty in PITE and PIDE, coming from random errors in topographic heights ( $\sigma_H$  resulting from random errors in DTM heights) and from random errors in estimated anomalous topographic mass density ( $\sigma_\rho$ ), can be determined by the formulae:

$$\begin{aligned} \sigma_{PITE}^2 &= \gamma^{-2} (4\pi G \bar{\rho}(\Omega) H(\Omega))^2 \sigma_H^2, \\ \sigma_{PIDE}^2 &= \gamma^{-2} (2\pi G H^2(\Omega))^2 \sigma_\rho^2. \end{aligned} \quad (5.38)$$

In Eq. (5.38),  $\sigma_\rho$  is the uncertainty of horizontal density model over the computation area which may be given by the data provider or estimated from the range of density values assigned to a certain rock type (cf., Huang [2002]).

Using Eqs. (5.28), (5.32), (5.34) and (5.38), the total STD of the geoidal height can be computed as follows:

$$\sigma_N^2 = \sigma_{N_L}^2 + \sigma_{\delta_{N}^{NZ}}^2 + \sigma_{\delta_{N}^{FZ}}^2 + \sigma_{PITE}^2 + \sigma_{PIDE}^2. \quad (5.39)$$

## 5.5 Numerical evaluation of the geoidal heights and their uncertainties

The geoid computation area is limited by  $1.5^\circ < \lambda < 4.5^\circ$  and by  $44.5^\circ < \varphi < 47.5^\circ$ . The optimal integration cap size of the Stokes integral was estimated using the method described by Foroughi et al. [2017a]. Based on their suggested method, the optimal integration cap size and the degree of the reference field are chosen based on the best primarily agreement between gravimetric geoidal heights and geoidal heights derived from GNSS/Leveling which yields  $1^\circ$  for the integration cap size and 140 for the degree of the reference field.

The solution of LS DWC described above was used in evaluating the modified Stokes integral ( $\psi_0 = 1^\circ$ ,  $L = 140$ ). The DIR\_R5 model [Bruinsma et al., 2014] was used to compute the FZ contribution up to the degree 300, i.e.,  $n_{max} = 300$  in Eq. (5.33). The same EGM was employed up to the degree 140 to define the reference spheroid. Transformation of the co-geoid in the Helmert space to the geoid in the real space needs to be done by applying PITE, PIDE and PIAE. The ACE2 digital elevation model [Berry et al., 2010] was used here to compute PITE. The values of PIAE were too small so they

were neglected in this study. Figure 5.5 shows the NZ and FZ contributions, reference spheroid, PITE and PIDE to the geoidal heights. Their statistics are summarized in Table 5.5. The average topographic density of  $2670 \text{ kg/m}^3$  was chosen to compute PITE (cf., Hinze, 2003) and the laterally varying topographic density of the Auvergne, shown in Figure 5.1 (a), was used for computation of PIDE. The PIDE contribution to the geoidal heights is at the level of  $\pm 2\text{cm}$  which confirms that this effect must be taken into account when a geoid model with accuracy better than one-centimetre is required.

The STDs of the residual geoidal heights originating from the NZ contribution, see Eq. (5.28), were estimated using the parameters discussed in Sec 5.3.2 ( $\psi_0 = 1^\circ, L = 140$ ). The STDs due to the FZ contribution was also computed using Eq. (5.34). The estimated STD of the reference spheroid was computed using Eq. (5.32). Estimated random errors in the ACE2 model reach values of  $\pm 16 \text{ m}$  [Berry et al., 2010]. They were used for computing the uncertainty of PITE. The range of topographic density values assigned to respective rock types of the superficial geological map of Auvergne was used to compute random errors of the topographic density model (cf., Huang [2002]). These random errors, shown in Figure 5.4, were used for computing the STD value corresponding to PIDE. The NZ and FZ contributions, reference spheroid, PITE and PIDE to estimation of the uncertainties of the geoidal heights are shown in Figure 5.6, their statistics are summarized in Table 5.6.



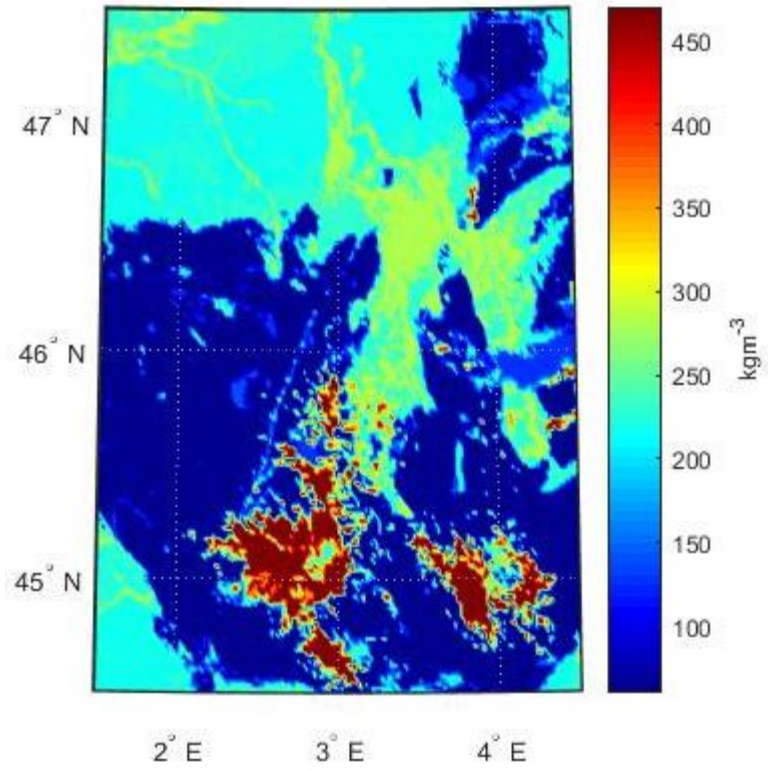
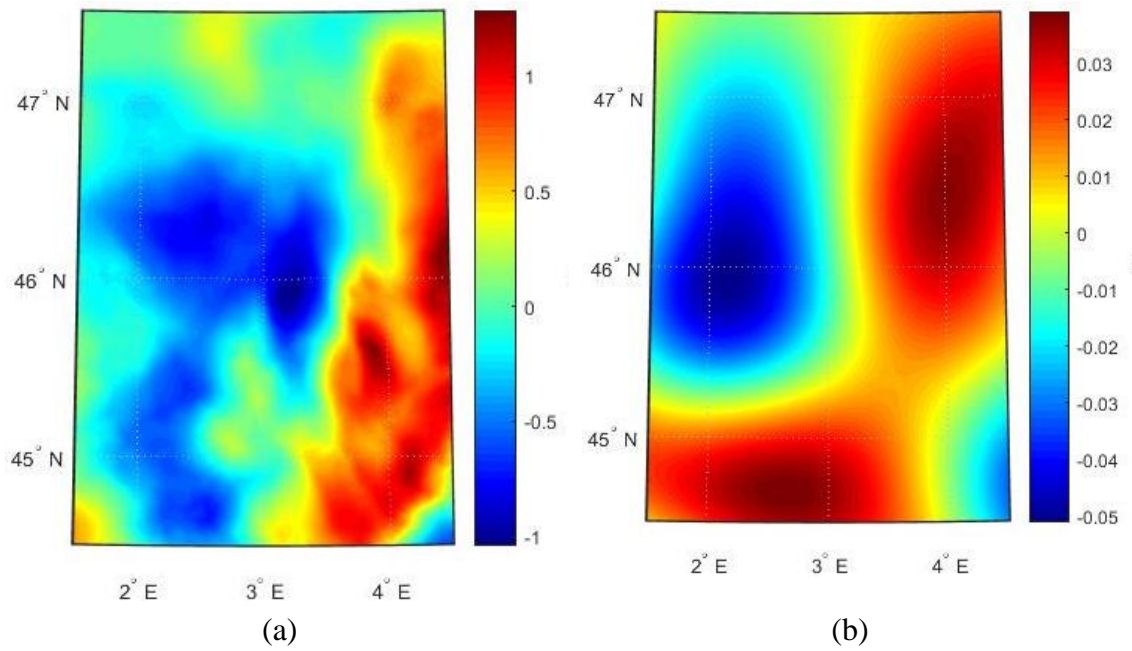


Figure 5.4: STDs of the topographic mass density



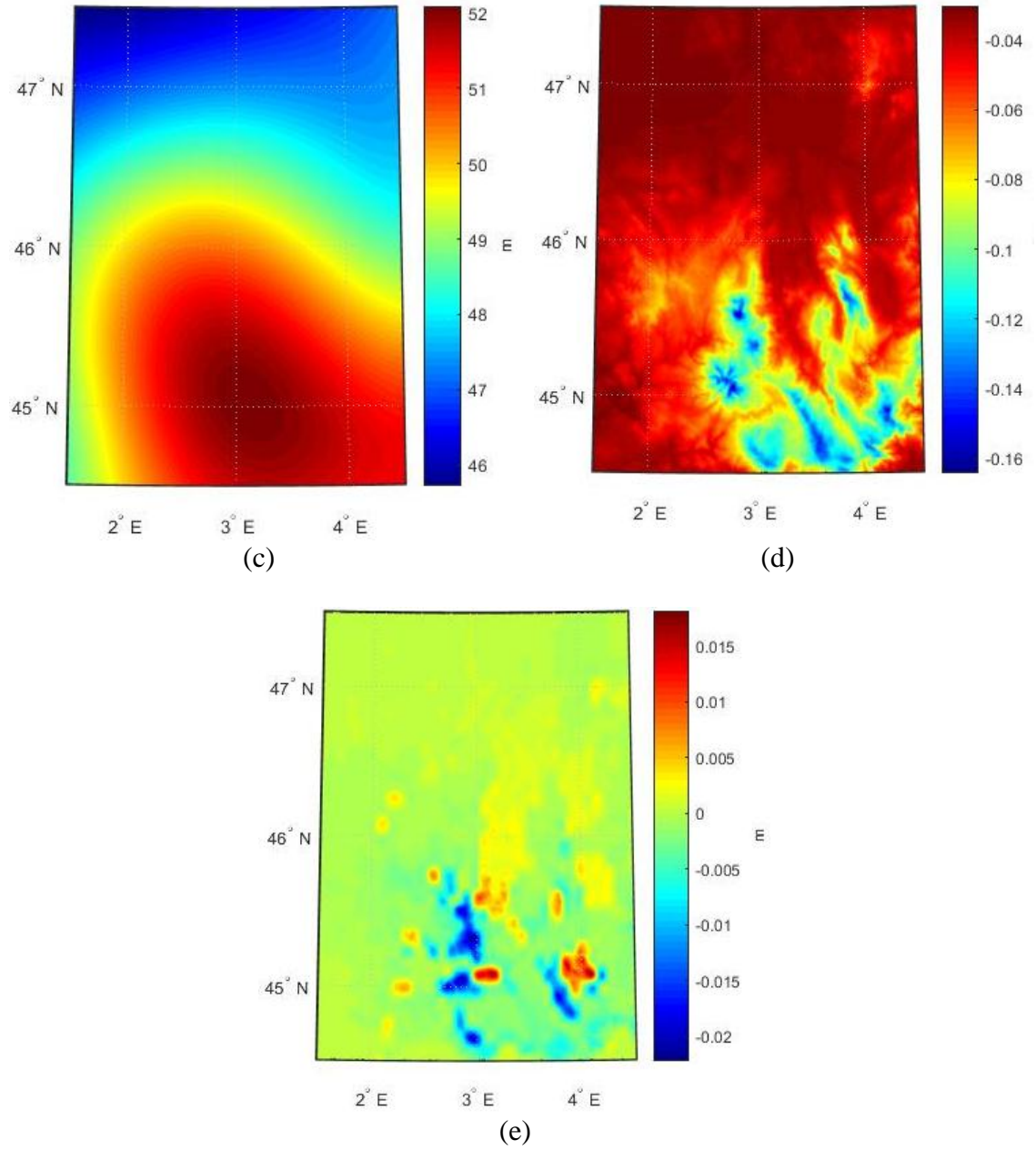
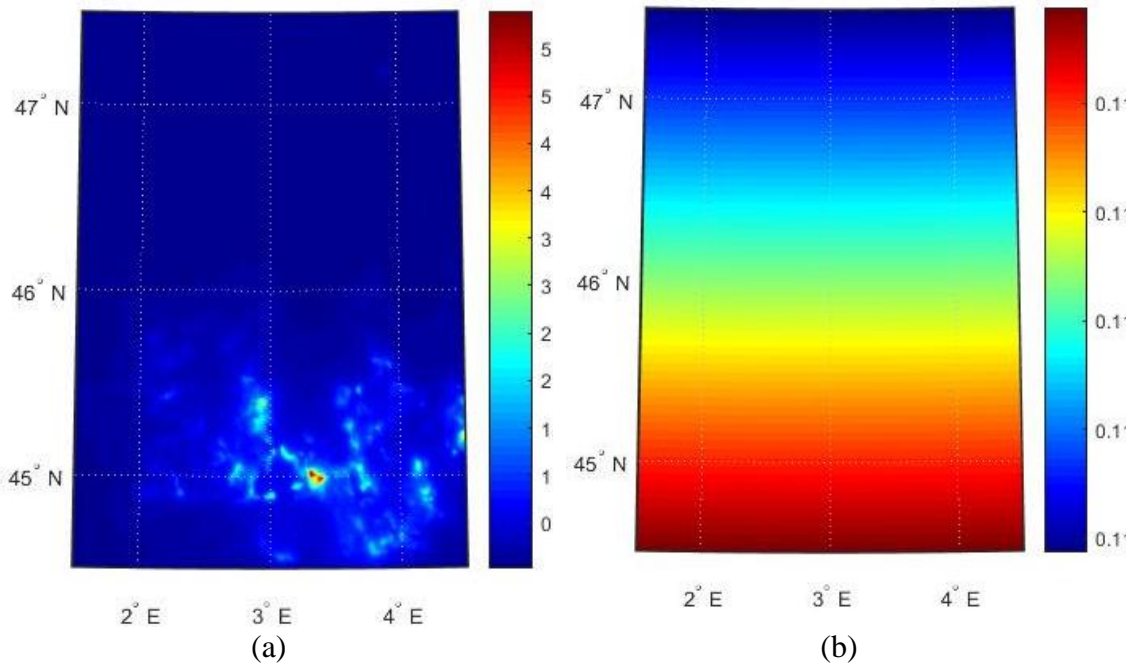


Figure 5.5: NZ (a), FZ (b), reference spheroid (c), PITE (d) and PIDE (e) contributions to the geoidal heights

Table 5.5: Statistics of contributions to the computed geoidal heights

contributions to geoidal heights	Min [m]	Max [m]	Mean [m]	RMS [m]
NZ	-1.05	1.34	0.02	0.50
FZ	-0.05	0.04	0.00	0.02
reference spheroid	45.72	52.09	49.37	1.79
PITE	-0.16	-0.03	-0.05	0.02
PIDE	-0.02	0.02	0.00	0.00



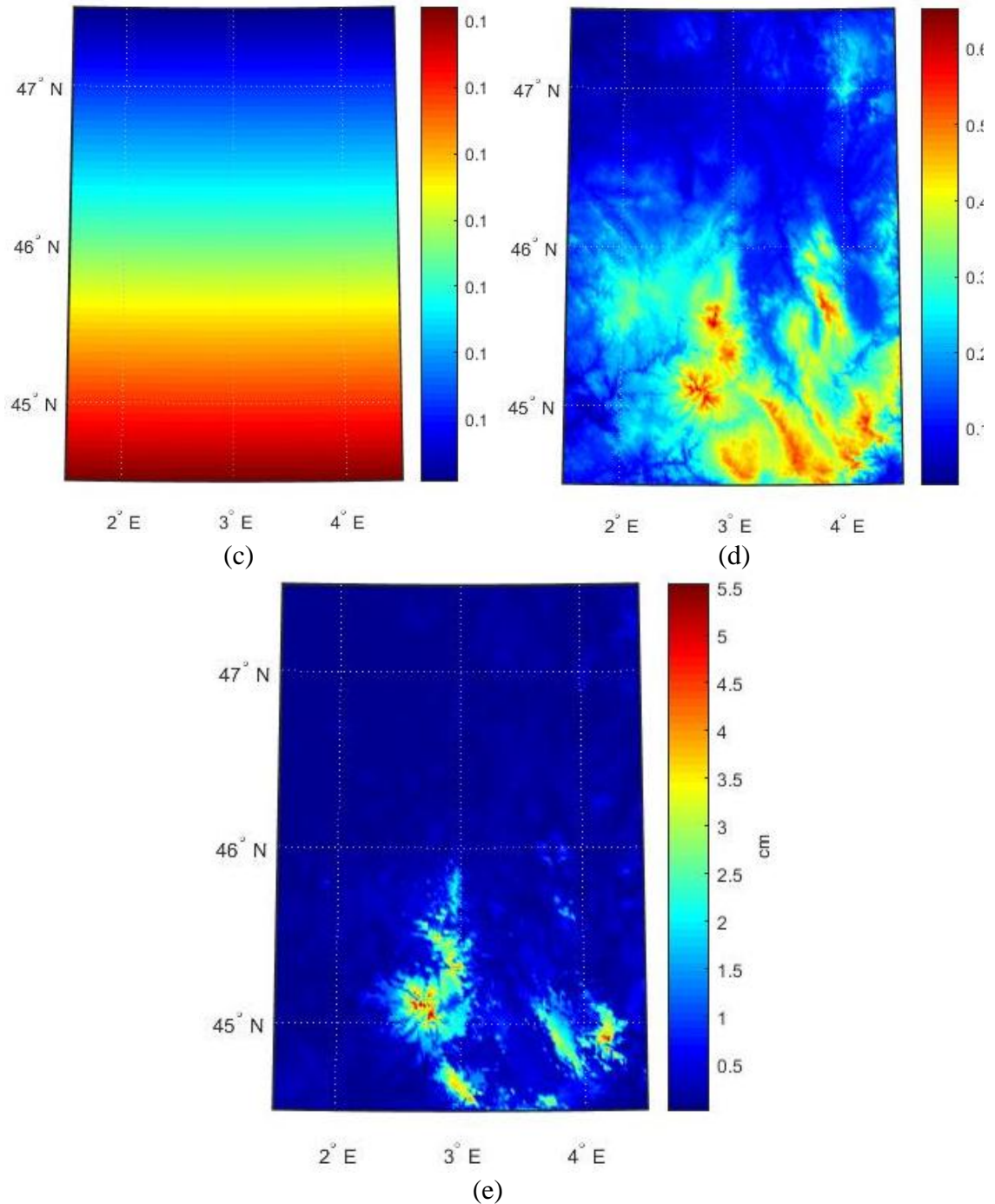


Figure 5.6: STDs of NZ (a), FZ (b), reference spheroid (c), PITE (d), and PIDE (e) [cm]

Table 5.6: Statistics of the estimated uncertainties

Uncertainty	Min[cm]	Max[cm]	Mean[cm]
NZ	0.02	5.96	0.25
FZ	0.11	0.12	0.11
reference spheroid	0.17	0.18	0.17

PITE	0.02	0.65	0.19
PIDE	0.00	5.55	0.26

The estimated uncertainties of the FZ contribution to the geoidal heights, see Figure 5.6(b), look much like the uncertainties in the reference spheroid as they are both functions of STDs of the spherical harmonic coefficients of the DIR\_R5 model scaled only by the truncation coefficients. Depending on the size of the integration cap and on the modification degree of the Stokes kernel, truncation coefficients will change and uncertainties of the FZ contribution must be estimated for each case separately.

According to Table 5.6, even though PITE and PIDE on the geoidal heights are small, the STD of PIDE is the second largest after NZ. This is because uncertainties of the topographic mass density values are large, see Figure 5.4, and scaled by the square of heights, see Eq. (5.38). This confirms that a better geological model of the study area would further reduce the total estimated STD of the geoidal heights.

The FZ contribution, the reference spheroid of the degree 140, PITE and PIDE were added to the residual co-geoid heights computed to obtain the geoidal heights in the real space, see Figure 5.7(a). The estimated STD of the geoidal heights computed from Eq. (5.39) are shown in Figure 5.7(b). Statistics are summarized in Table 5.7.

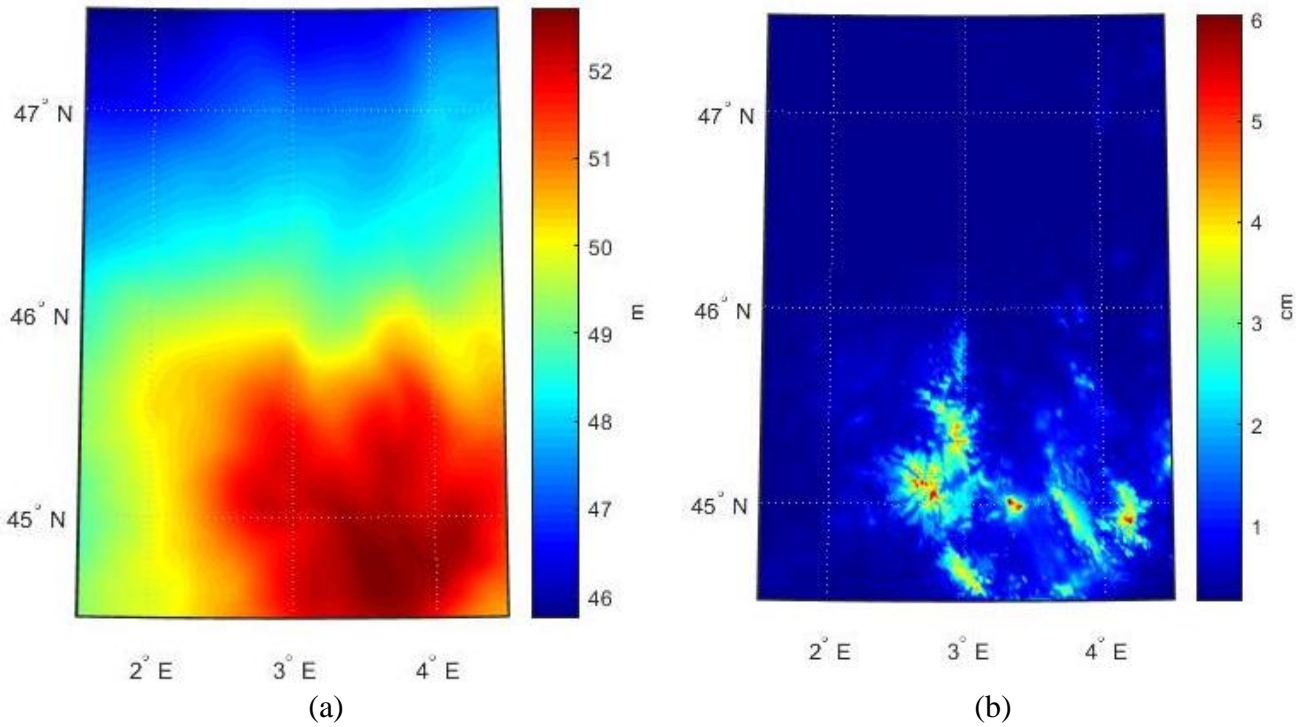


Figure 5.7: Geoidal heights (a), STDs of the geoidal heights (b)

Table 5.7: Statistics of the geoidal heights and their uncertainties

	Min [m]	Max [m]	Mean [m]
geoidal heights	45.75	52.71	49.35
uncertainties of the geoidal heights	0.002	0.063	0.006

The mean value of the geoidal heights in this study area is about 49 m whereas the mean STD of the estimated heights is less than centimeter. This actually shows how good the geoid obtained via the Stokes-Helmert is. This is also because the maximum elevation in the area of the geoid is less than 2000 m and of course larger STDs are expected for the areas with higher topography.

## 5.6 Comparison with the GNSS/Leveling control points

There are 75 GNSS/Leveling control points available in the geoid computation area which are distributed regularly between  $1.5^\circ < \lambda < 4.5^\circ$ ,  $45^\circ < \varphi < 47^\circ$  [Duquenne,

2007]. These points were used to validate our final geoid. The residuals of the comparison between the geoidal heights (from model computed here) and the geoidal heights derived from GNSS/Leveling points (geodetic minus rigorous orthometric heights) are defined as:

$$\forall i : V_i = N_i^{GNSS/lev} - N_i . \quad (5.40)$$

Figure 5.8 shows the discrepancies at the locations of the control points (note that there are some unsubstantiated patterns in this plot created by the used interpolation procedure); the statistics of the discrepancies are summarized in Table 5.8.

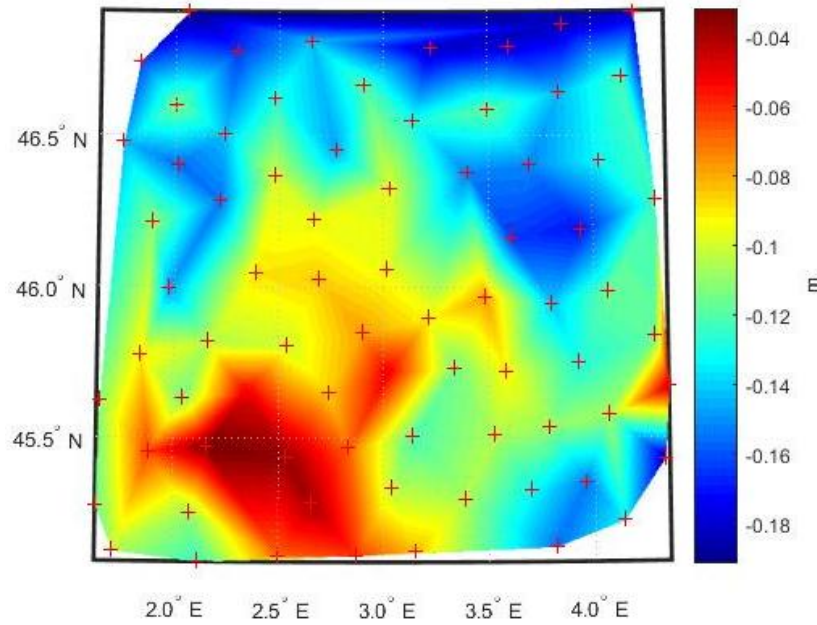


Figure 5.8: Differences between the geoidal heights and GNSS/Leveling at the control points.

As the two sources of the geoidal heights at the control points are not known to be correlated, the mean STD of the discrepancies from Eq. (5.40) must obey the following probabilistic law:

$$\sigma_V^2 = \sigma_N^2 + \sigma_{N^{GNSS/lev}}^2 , \quad (5.41)$$

where the  $\sigma_N$  and  $\sigma_{N^{GNSS/lev}}$  stand for the mean STDs of our solution and of the control geoid. The STDs of the geoidal heights ( $\sigma_N$ ) are now available from the computations described above on the same grid as the geoidal heights are. They can easily be predicted for the locations of the control points (GNSS/Leveling points) using the same inverse distance squared algorithm. The mean STDs for the 75 control points is 0.6 cm but the maximum value reaches up to 3 cm. The value of 0.36 cm<sup>2</sup> for the mean  $\sigma_N^2$  can be then considered to be the a priori variance factor of our geoidal heights at control points. Duquenne [2007] estimated that the STDs of the geodetic heights at the control points in Auvergne are about 2 to 3 cm and STD of the leveling observations is 2 cm or, perhaps, better. As these two kinds of heights are not correlated, the STDs of the test geoidal height at the control points should be somewhere between 2.8 and 3.6 cm. Thus, the mean STD of the GNSS/Leveling implied geoidal heights, i.e.,  $\sigma_{N^{GNSS/lev}}$ , should equal to 3.2 cm and we have taken the square of this value as an a priori variance factor of the test geoidal heights at control points. Thus, the square root of the a priori variance factor of the discrepancies in Eq. (5.41) can be considered to be  $\sigma_V = 3.25$  cm.

We also know that if the random variable we deal with has normally distributed values of STD, then from the adjustment calculus [Vaníček and Kakiwsky, 1986, Par. 13.3] we get:

$$E\left(\frac{\hat{\sigma}_V^2}{\sigma_V^2}\right) = 1, \quad (5.42)$$

where the hat denotes the a posteriori estimate. The a posteriori variance factor of the discrepancies  $V$ , see Eq. (5.40), can be estimated as:



$$\hat{\sigma}_V^2 = \frac{\mathbf{v}^T \mathbf{P} \mathbf{v}}{n}, \quad (5.43)$$

where  $\mathbf{P}$  is their weight matrix defined as:

$$\mathbf{P} = \sigma_v^2 (\mathbf{C}_N + \mathbf{C}_{N^{GNSS/lev}})^{-1}. \quad (5.44)$$

Here, we take  $\mathbf{C}_N$  as being the diagonal covariance matrix of the geoidal heights at the control points computed in this study,  $\mathbf{C}_{N^{GNSS/lev}}$  is the uniform diagonal covariance matrix of the GNSS/Leveling implied geoidal heights, and  $\sigma_v^2$  is the *a priori* variance factor computed from Eq. (5.41). The *a posteriori* variance factor for the 75 control points is  $10.89 \text{ cm}^2$  which implies a STD of 3.3 cm. We can now write an equivalent of Eq. (5.41) for the *a posteriori* counterparts of the *a priori* mean variances:

$$\hat{\sigma}_V^2 = \hat{\sigma}_N^2 + \hat{\sigma}_{N^{GNSS/lev}}^2, \quad (5.45)$$

and using the available values for  $\hat{\sigma}_V^2$  and assuming  $\hat{\sigma}_N^2 = \sigma_N^2$ , the *a posteriori* STD of the geoidal heights at the control points is 3.2 *cm* which confirms the estimate by Duquenne [2007].

Finally, we can construct the histogram of the discrepancies using standardized discrepancies which are computed as:

$$v^*_i = v_i \sigma_{V_i}^{-1} = v_i (\hat{\sigma}_{N_i}^2 + \hat{\sigma}_{N^{GNSS/lev}}^2)^{-\frac{1}{2}}. \quad (5.46)$$

Figure 5.9 shows the histogram of these standardized discrepancies that seems to be somewhat similar to the normal distribution. We note that all 75 discrepancies are

confined between  $-2.5$  STDs and  $+2.5$  STDs of their zero mean. But there is an accumulation of discrepancies around  $-2$  STDs and around  $+2$  STDs. We do not have any explanation for this occurrence, but we should not find it too strange just from looking at the plot of the discrepancies in Figure 5.8 that suggests some systematic effects in the south-east part of the Auvergne area.

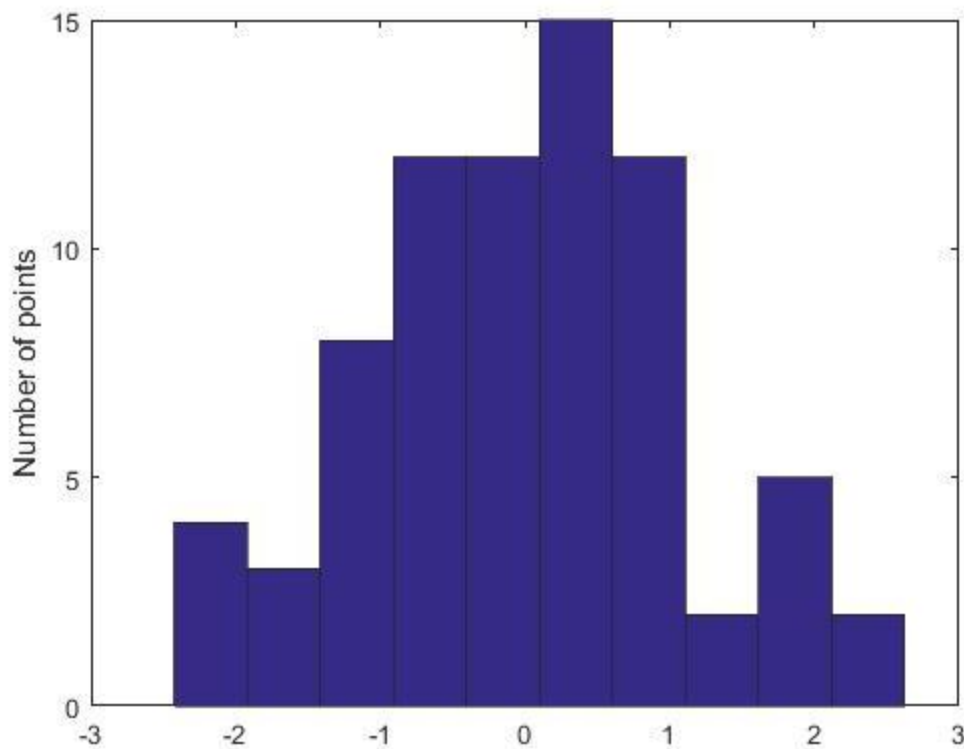


Figure 5.9: Histogram of the standardized residuals between the geoidal heights (computed from the model) and the GNSS/Leveling derived geoidal heights.

Table 5.7 summarizes the statistics of the discrepancies defined by Eq. (5.40). The weighted mean of the discrepancies computed using Eq. (5.40) is  $-13$  cm. This value is close to what is reported as bias of the French height system in [Rülke et al., 2012]. The mean RMS of the fit between our and GNSS/Leveling implied geoidal heights using Eq.

(5.43) is 3.3 cm. This is no worse than the fit of the best quasigeoid model computed for this area, see [Agren et al., 2009].

There is another set of 558 GNSS/Leveling points available in Auvergne reported already by Foroughi et al. [2017b], provided to us by the Institute Geographique Nationale. The mean STD of the fit between our geoidal heights and those at the 558 control points is 3.1 cm. As these 558 points are predominantly located in lowlands, they are not giving an objective picture of the geoid accuracy and we do not use them in our discussions.

Table 5.8: Statistics of comparison of the computed geoidal heights with the geoidal heights at GNSS/Leveling points.

	Min [m]	Max [m]	Weighted Mean [m]	RMS [m]
75 GNSS points	-0.19	-0.03	-0.13	0.033

## 5.7 Discussion and conclusions

The most probable values of the DWC'd Helmert's gravity anomalies were found by solving the discretized overdetermined Poisson integral equation using the LS technique. The uniform STDs of scattered gravity and implied STDs of gridded gravity were used to construct the fully populated (a priori) covariance matrix whose counterpart on the geoid, the a posteriori variance matrix, was then used to extract STDs of the computed geoidal heights.

The downward continued 1' Helmert's anomalies continued down from larger elevations showed as large spikes in gravity on the geoid. On the other hand, these spikes seem to be filtered out, or at least are attenuated, by the Stokes integration so that the

geoidal heights at these higher elevations do not exhibit too disturbing a behavior of the geoid. This means that the spikes in the gravity anomalies do not do affect the geoid too much but their effect is certainly seen in the STDs of the geoidal heights.

Figure 5.10 shows STDs of the residual Helmert anomalies on the geoid. Comparison with Figure 5.6 (a) shows that there is practically a total correlation between STDs of the gravity anomalies on the geoid and STDs of the NZ contribution to the residual co-geoidal heights. This is because of the character of the modified Stokes function for the used high degree and order  $L$  of the reference field. Figure 5.11 shows the shape of the modified Stokes function  $S^*$  of the degree 140 (and integration cap radius of 1 arc-deg) which makes quite clear that  $S^*$  approximates the Dirac distribution quite closely. As the Dirac distribution is the quintessential reproducing kernel, the similarity of STDs of the geoid anomalies and that of the NZ contribution to the residual co-geoid height must be expected.

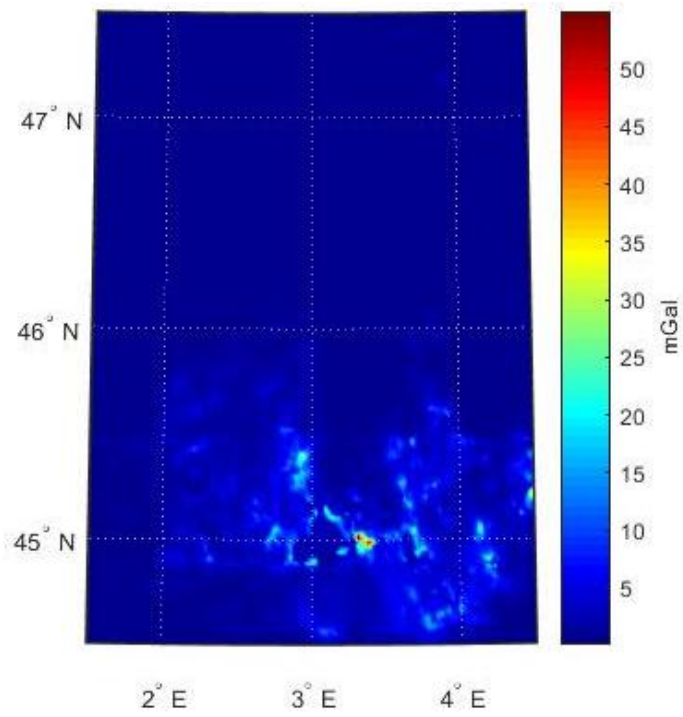


Figure 5.10: STDs of the residual Helmert anomalies over the geoid computation area

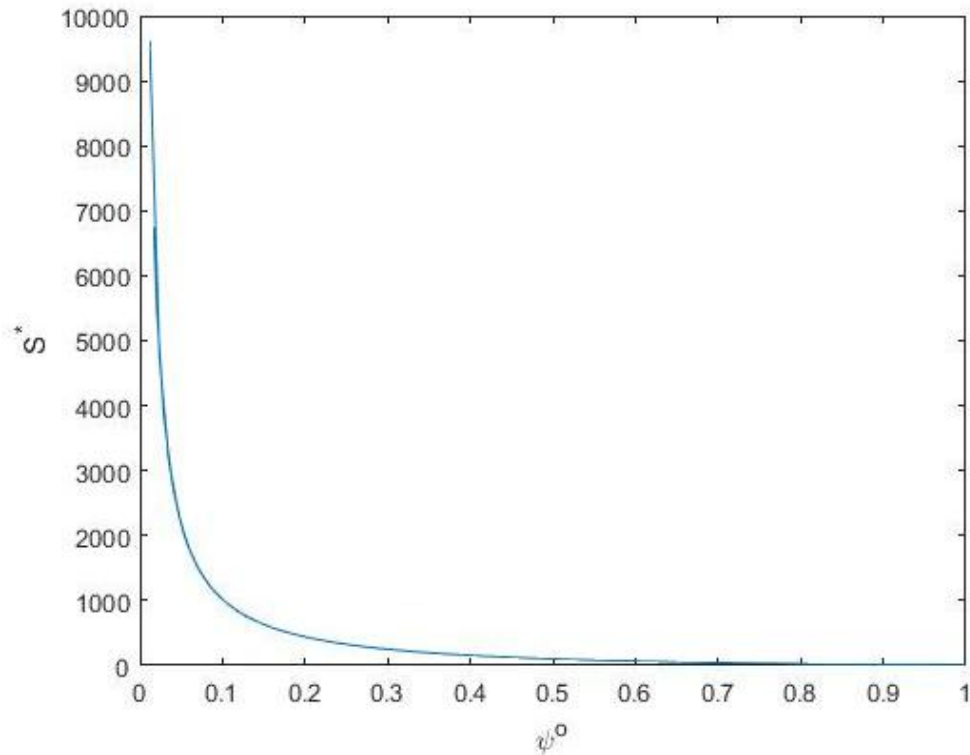


Figure 5.11: Modified Stokes's function of the degree 140 and  $\psi_0 = 1^\circ$

Janák et al. [2017], Foroughi et al. [2017a], and Foroughi et al. [2017b] computed also the geoid model in the Auvergne test area using Stokes-Helmert method and reported 3.3 cm as the smallest STD of the fit at the 75 control points. These studies used Jacobi's iterative method to downward continue the Helmert gravity anomalies and as such the downward continued anomalies should be considered as results of a regularized solution. However, the geoid computed in this study uses the most probable values of the Helmert gravity anomalies on the geoid, clearly not regularized.

Gravity observations at the Earth surface, both scattered and gridded values, were used together to estimate the mean anomalies on the geoid using LS DWC in this study for the first time in our computations. In all previous studies, only grid points were used. Figure 5.12 shows the differences between the geoid computed in this study and that computed by Janák et al. [2017]. The differences range between  $-9$  and  $+13$  cm with the RMS of 2 cm. Comparing these differences with topography and with the distribution of gravity observations, see Figure 5.1( b, c) in this area, one can conclude that the largest differences occur in locations with sparse gravity observations and high topography. The geoid model computed in this study is the most probable solution and is obtained without any regularization (only discretization of the Poisson integral equation is used as the only process originating in personal selection) where the previously computed solutions were regularized to overcome the numerical instability of the DWC process. Interestingly, the differences between the previous and the present solutions seem to be somewhat correlated with the STDs of the present solution, see Figure 5.7(b), but a complete explanation of these differences will have to wait till later.

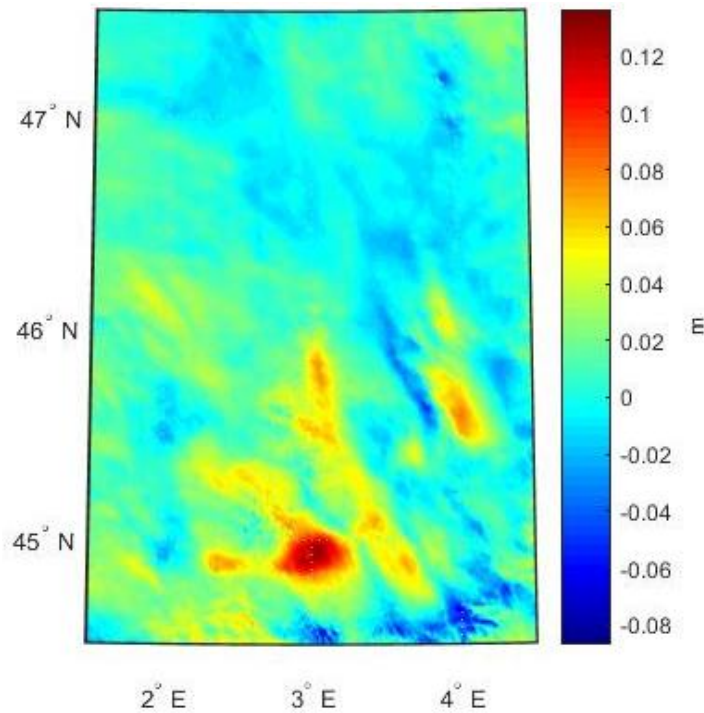


Figure 5.12: Differences between previously computed geoid and the geoid computed in this study

The estimate of the total errors, see Figure 5.7(b), shows STDs of the Stokes-Helmert computed geoidal heights to be well below 1 cm in the flat areas and up to 6 cm in the highest areas where the elevations reach 1600 m. We note that just outside the computation area the heights grow to over 4000 m, cf., Figure 5.1 (a), which confirms the expected accuracy of the Stokes-Helmert method as predicted by Vaniček and Martinec [1994]. Our results also are compatible with the results of previous studies, e.g., for the maximum elevation in Canada (6000 m) the geoid error is reported as being approximately 30 cm by Huang and Véronneau [2013], or the reported STD of about 10 cm by Featherstone et al. [2018] for the maximum elevation of (2200 m) in Australia, suggesting an accuracy deterioration by about 5 cm for each increment of one kilometre in height.



Even though it is not quite clear where the errors of the test geoidal heights at the control points are coming from – as they seem to be of a systematic nature, probably affecting the levelled heights from south-west to north-east, see Figure 5.8 and Figure 5.9 – it is still quite clear that the mean error of the directly computed geoidal heights (the ground truth) is larger than that of the geoidal heights derived by the Stokes-Helmert method, by a factor of 5, if input gravity data of the decent accuracy and spatial distribution are used in the computation.

Thus, this study confirms that the geoidal heights can be determined with better than a centimetre accuracy – at least in the in the low-lying areas – whereas the “ground truth” (GNSS/Leveling implied geoidal heights at the control points), used typically to evaluate the accuracy of computed geoidal heights, are not precise enough to be used for the assessment of the accuracy of the gravimetric geoid model, see also [e.g., Šprlák, 2008; Novák et al., 2009; Godah et al., 2015; Godah et al., 2017]. Thus, one should not pay too much attention to the quality of the fit of the computed geoidal heights to the test geoidal heights as a better fit might be just a fluke. Perhaps, we should rather start thinking about the Stokes-Helmert geoid to be used as a standard for testing and investigating the accuracy of leveling and/or GNSS determined geodetic heights. Needless to repeat here that, of course, not all the world has such a good coverage with gravity observations as Auvergne has but, perhaps, with aerial gravity this problem can be remedied.

## 5.8 Acknowledgments

The authors wish to acknowledge that the final stages of their work were supported by the NSERC Discovery grant to P. Vaníček. P. Novák was supported by the project 18-06943S of the Czech Science Foundation. As the research reported here is based on a hard work of scores of researchers we should mention at least those who contributed the most during the past 25 years. We feel that at least Z. Martinec, J. Huang, M. Najafi, W. Featherstone, S. Wenke, J. Janák and A. Ellmann should be thanked in particular. This research was built on their shoulders.

## 5.9 References

- Afrasteh, Y., Safari, A., Sheng, M., Kingdon, R., & Foroughi, I. (2017). The effect of noise on geoid height in Stokes-Helmert method. *International Association of Geodesy Symposia*. Berlin, Heidelberg: Springer.
- Agren, J., Barzaghi, R., Carrion, D., Denker, H., Grigoriadis, V., Kiamehr, R., Sona, G., Tscherning, C. C., Tziavos, I. (2009). Different geoid computation methods applied on a test dataset: results and considerations. VII Hotine-Marussi Symposium on Mathematical Geodesy. Rome, Italy.
- Bajracharya, S. (2003). *Terrain effect in geoid determination*. Calgary: University of Calgary.
- Berry, P., Smith, R., & Benveniste, J. (2010). ACE2: The New Global Digital Elevation Model. Mertikas S. (eds) *Gravity, Geoid and Earth Observation*. International Association of Geodesy Symposia, 135, Springer-Verlag Berlin, Heidelberg.

- Bodelle, A., Goguel, J., Autran, A. (1980). Carte géologique de la France et de la marge continentale, 1:1500 000, 1978-1979 Bureau de recherches géologiques et minières, Orléans.
- Bruinsma, S., Forste, C., Abrikosov, O., Lemonie, J., Marty, J., Mulet, S., Rio, M. H., Bonvalot, S. (2014). ESA's satellite-only gravity field model via the direct approach based on all GOCE data. *Geophysical Research Letters*, 41(21), 7508-7514.
- Duquenne H., 2007: A data set to test geoid computation methods. Proceedings of the 1st International Symposium of the International Gravity Field Service (IGFS), Istanbul, Turkey. *Harita Dergisi, Special Issue 18*, 61–65.
- Ellmann, A., & Vaníček, P. (2007). UNB application of Stokes-Helmert's approach to geoid computation. *Journal of Geodynamics*, 43, 200-213.
- Favati, P., Lotti, G., Menchi, O., Romani, F. (2014). Generalized Cross-Validation applied to Conjugate Gradient for discrete ill-posed problems . *Appl. Math. Comput.*, 243, 258–268.
- Featherstone, W., McCubbine, J., Brown, N., Claessens, S., Filmer, M., & Kirby, J. (2018). The first Australian gravimetric quasigeoid model with location-specific uncertainty estimates. *Journal of Geodesy*, 92(2), 149-168.

- Foroughi, I., Vaniček, P., Kingdon, R., Sheng, M., & Santos, M. (2015). Assessment of Discontinuity of Helmert's Gravity Anomalies on the Geoid. AGU-GAC-MAC-CGU Joint Assembly. Montreal, Canada.
- Foroughi, I., Vaniček, P., Novák, P., Kingdon, R., Sheng, M., & Santos, M. (2017a). Optimal combination of satellite and terrestrial gravity data for regional geoid determination using Stokes-Helmert's method. International Association of Geodesy Symposia. Springer Verlag Berlin, Heidelberg.
- Foroughi, I., Vaniček, P., Sheng, M., Kingdon, R., & Santos, M. (2017b). In defence of the classical height system. *Geophysical Journal International*, 211, 1176-1183.
- Goli, M., Foroughi, I., & Novák, P. (2018). On a parameter choice for stopping iteration solutions of gravity downward continuation. *Canadian Journal of Earth Sciences*. doi:10.1139/cjes-2017-0208
- Hadamard, J. (1923). *Lectures on the Cauchy Problem in Linear Partial Differential Equations*. New Haven: Yale University Press.
- Heiskanen, W., & Moritz, H. (1967). *Physical Geodesy*. San Francisco: W.H. Freeman and Co.
- Hinze, W. (2003). Bouguer reduction density, why 2.67? *Geophysics*, 68, 1559-1560.
- Huang, J. (2002). Computational methods for the discrete downward continuation of the Earth gravity and effects of lateral topographical mass density variation of gravity and geoid. Technical Report No. 216, Department of Geodesy and Geomatics Engineering, University of New Brunswick, Fredericton, Canada.

- Huang, J., & Véronneau, M. (2005). Application of downward continuation in gravimetric geoid modelling: case studies in Western Canada. *Journal of Geodesy*, 79, 135-145.
- Huang, J., & Véronneau, M. (2013). Canadian gravimetric geoid model 2010. *Journal of Geodesy*, 87(8), 771-790.
- Godah W., Krynski J., Szelachowska M. (2015): On the accuracy assessment of the consecutive releases of GOCE-based GGMs over the area of Poland, Assessment of GOCE Geopotential Models, Special Issue: Newton's Bulletin, 5, 49-62.
- Godah W., Krynski J., Szelachowska M. (2017): The use of absolute gravity data for the validation of Global Geopotential Models and for improving quasigeoid heights determined from satellite-only Global Geopotential Models, *Journal of Applied Geophysics*, 152, 38-47.
- Janák, J., Vaníček, P., Foroughi, I., Kingdon, R., Sheng, M., & Santos, M. (2017). Computation of precise geoid model using UNB Stokes-Helmert's approach: Case study in Auvergne region. *Contribution to geodesy and geophysics*, 47(3), 201-229.
- Kassim, F. (1980). An evaluation of three techniques for the prediction of gravity anomalies in Canada. Technical Report No. 73, Department of Geodesy and Geomatics Engineering, University of New Brunswick, Fredericton, Canada.

- Kearsley, W. (1977). The prediction and mapping of geoidal undulations from GEO-5 altimetry. Columbus, Ohio: Report No. 267, Department of Geodetic Science, Ohio State University.
- Kellogg, O. (1929). Foundation of potential theory. Berlin Heidelberg New York, Springer.
- Kingdon, R., & Vaníček, P. (2010). Poisson downward continuation solution by the Jacobi method. *Journal of Geodetic Science*, 1, 74-81.
- Martinec, Z. (1993). Effect of lateral density variations of topographical masses in improving geoid model accuracy over Canada. Research Report for Geodetic Survey of Canada, Ottawa, Canada.
- Martinec, Z. (1996). Stability investigation of a discrete downward continuation problem for geoid determination in the Candian Rocky Mountains. *Journal of Geodesy*, 70, 805-828.
- Martinec, Z. (1998). Boundary value problems for gravimetric determination of a precise geoid. *Lecture Notes in Earth Sciences*, Springer Verlag Berlin, Heidelberg New York.
- Martinec, Z., & Vaníček, P. (1994a). Direct topographical effect of Helmert's condensation for a spherical geoid. *Manuscripta Geodetica*, 19, 257–268.
- Martinec, Z., & Vaníček, P. (1994b). Indirect effect of topography in the Stokes-Helmert technique for a spherical approximation of the Geoid. *Manuscripta Geodaetica*(19), 213-219.

- Martinec, Z., Vaníček, P., Mainville, A., & Véronneau, M. (1996). Evaluation of topographical effects in precise geoid computation from density sampled heights. *Journal of Geodesy*, 20, 193-203.
- Molodensky, M., Yeremeev, V., & Yurkina, M. (1960). *Methods for Study of the External Gravitational Field and Figure of the Earth*. Moscow: TRUDY TsNIIGAiK, 131, Geodezizdat (in Russian).
- Najafi-Alamdari, M., Vaníček, P., Ong, P., & Craymer, M. (1999). Accuracy of a regional geoid. *Geomatica*, 53(3), 297-305.
- Novák, P. (2000). Evaluation of gravity data for the Stokes-Helmert solution to the geodetic boundary-value problem. Technical Report No. 207, Department of Geodesy and Geomatics Engineering, University of New Brunswick, Fredericton, Canada.
- Novák P, Klokočník J, Kostelecký J, Zeman A. (2009) Testing EGM08 using Czech GPS/leveling data. *Newton's Bulletin* 4: 126-132, ISSN 1810-8555.
- Novák, P., Vaníček, P., Véronneau, M., Holmes, S., & Featherstone, W. (2001). On the accuracy of modified Stokes's integration in high frequency gravimetric geoid determination. *Journal of Geodesy*, 74, 644-654.
- Rülke, A., Liebsch, G., Sacher, M., Schäfer, U., Schirmer, U., & Ihde, J. (2012). Unification of European height system realizations. *Journal of Geodetic Science*, 2, 343-354.

- Sandwell, D., Muller, R., Smith, W., Garcia, E., & Francis, R. (2014). New global marine gravity model from CryoSat-2 and Jason-1 reveals buried tectonic structure. *Science*, 346(6205), 6567.
- Šprlák M (2008) Numerical Testing of Procedures for the Determination of the Quasigeoid. Doctoral Thesis, Department of Theoretical Geodesy, Faculty of Civil Engineering, Slovak University of Technology, Bratislava, Slovakia, (in Slovak).
- Sun, W., & Vaníček, P. (1998). On some problem of downward continuation of the 5'x5' mean Helmert gravity disturbance. *Journal of Geodesy*, 72, 411-420.
- Vaníček, P., & Kleusberg, A. (1987). The Canadian geoid – Stokesian approach. *Compilation of a precise regional geoid. Manuscripta Geodetica*, 12, 86-98.
- Vaníček, P., & Krakiwsky, E. (1986). *Geodesy, The concepts*. Amsterdam, North Holland.
- Vaníček, P., & Martinec, Z. (1994). Stokes-Helmert scheme for the evaluation of a precise. *Manuscripta Geodaetica*, 19, 119-128.
- Vaníček, P., Najafi, M., Martinec, Z., Harrie, L., Sjoberg, L. E. (1995) High-degree reference field in the generalized Stokes-Helmert scheme for geoid computations. *Journal of Geodesy (70)*: 176-182.
- Vaníček, P., Novák, P., Sheng, M., Kingdon, R., Janak, J., Foroughi, I., Martinec, Z., Santos, M. (2017) Does Poisson's downward continuation give physically meaningful results? *Stud Geophysica et Geodaetica* 61: 412-428.



## 6 Chapter 6: Conclusions

The accuracy of the classical height system was investigated in this dissertation. Measuring the accuracy was done by measuring the self-consistency, i.e., comparing the gravimetric geoidal heights against the geoidal heights derived at GNSS/Leveling points; this comparison is also called congruency. The components for measuring the congruency of the classical height system are geoidal heights derived from a gravimetric geoid model, geodetic heights derived from GNSS observations, and orthometric heights computed by applying gravimetric corrections to spirit leveling observation. The geodetic and orthometric heights in this system are usually available at national leveling benchmarks which are also called control points in geoid determination. Four articles were included in this dissertation to address measuring the accuracy of the classical height system precisely. The Auvergne data was used through the whole dissertation [Duquenne, 2007]. This area has fairly good terrestrial gravity data coverage with an average STD of  $0.5 \text{ mGal}$ . On the east side of Auvergne, there are mountains with heights just above  $4000 \text{ m}$  and there are flat areas in the middle and western part. Auvergne is also a geologically challenging area due to existing volcanos and large variations in topographic density values. The first article “*Optimal combination of satellite and terrestrial gravity data for regional geoid determination using Stokes-Helmert’s method, the Auvergne test case*” is published in a book series of *International Association of Geodesy (IAG) symposia*. This article provides

a discussion on a numerical method to find the optimal combination of terrestrial and satellite gravity data to determine the geoid using the Stokes-Helmert method. The degree and order of 140 was suggested as the maximum beneficial contribution of EGMs to geoidal heights through computing the reference field and the rest of the contribution is suggested to be computed from terrestrial data, i.e., NZ. The optimal level of NZ contribution was found to be 45' around each point when evaluating the Stokes integral. Although the methodology of this article needs to be applied separately in each region to find the best level of combination, there is similar studies which suggest almost the same degree and order of EGMs giving the most reliable contribution of global data [Abdalla et al., 2012].

The second article “*Computation of precise geoid model of Auvergne using current UNB Stokes-Helmert’s approach*” is published in the journal of *Contributions to Geophysics and Geodesy*. This article presents the details of the numerical steps of geoid determination using the Stokes-Helmert approach when the methodology outlined in the previous paper is applied. The terrestrial gravity data in Auvergne were predicted on a  $1' \times 1'$  grid points and used throughout the whole process of geoid determination. All the data requirements for transferring the free-air gravity to Helmert gravity anomalies when computing DTE, DAE, DDE, and SITE were presented in this study. The Helmert gravity anomalies on the Earth surface were transferred down to the geoid level using the Poisson integral equation which was solved by the Jacobi iterative technique suggested by Kingdon and Vaníček [2010]. The maximum degree and order of reference field was set to 140 and 45' integration capsize was chosen when evaluating the Stokes integration. The determined co-geoidal heights were transferred back to the real space by computing

the indirect topographical effects on geoid, i.e., PITE and PIDE. The discrepancies between gravimetric geoidal heights and the geoidal heights derived at 75 GNSS/Leveling points showed a STD of 3.3 *cm*. This value was compatible with the smallest STD of the fit between the quasigeoid models of the area to the height anomalies at the same GNSS/Leveling points. The effect of anomalous topographical density was investigated separately in this article. It was shown that the maximum contribution of DDE and PIDE together to geoidal heights can reach up to 7 *cm* in Auvergne region but can only improve the STD of the fit of the gravimetric geoid to the GNSS/Leveling points by 1 *mm*.

The third article “*In defense of the classical height system*” has been published in *Geophysical Journal International*. The claim of Molodensky et al. [1960] of insufficiency of accurate determination of the geoid and orthometric heights due to insufficient topographical density information is discussed in this article. It is shown that even using a low resolution lateral density model, the effects of density variation on the geoidal heights can be computed with sufficient accuracy. The normal heights of the 75 GNSS/Leveling points (provided by IGN) were converted to rigorous orthometric heights by considering the effect of terrain, density variation, and remaining unmodelled masses. It was shown that terrain and density variation have the largest effects on converting the normal heights to rigorous orthometric heights. The geoidal heights at the GNSS/Leveling points were computed by subtracting the geodetic heights from rigorous orthometric heights. Another set of 558 GNSS/Leveling points, also provided by IGN, was introduced in this article, and both sets of control points were used to evaluate the gravimetric geoid model. It was shown that the STD of the fit between gravimetric geoidal heights and geoidal heights derived at GNSS/Leveling points is the best when rigorous orthometric

heights rather than from Helmert orthometric heights. The concept of measuring the congruency as a measure of the accuracy of a height system was introduced in this paper. It was shown, for the Auvergne area, the congruency of the classical height system is at least as good as Molodensky's height system even when a low-resolution model of density variation is used.

The forth article "*Sub-centimetre geoid*" has been published in *Journal of Geodesy*. In this article the most probable solution of a gravimetric geoid model was computed using least-squares downward continuation. Unlike all the previously computed geoid models, the scattered and grid gravity data were both used in the determination of the geoid. The least-squares technique was used to get the most probable solution of downward continuation on the geoid. The uniform STDs of the input terrestrial gravity data were used to construct the a priori covariance matrix and the a posteriori covariance matrix of gravity anomalies on the geoid was computed; this was then used to extract the STDs of the residual geoidal heights estimated from NZ. The STDs of geoidal heights from other sources, e.g., FZ, reference spheroid, PITE, and PIDE contributions were also evaluated by error propagation. The largest uncertainties of the geoidal heights come from the NZ and PIDE contributions. The estimated STD of geoidal heights varies from a few millimeters to 6 *cm* with the mean of 0.6 *cm*. This confirms that geoidal heights can be determined with sub-centimetre accuracy even if one acknowledges the range of STDs is larger. The GNSS/Leveling derived geoidal heights were compared again with the most probable gravimetric geoidal heights and show the mean difference of 13 *cm* which agrees well with the displacement of the vertical datum due to sea surface topography [Rülke, et al., 2012]. The RMS of the misfit of the geoid versus GNSS/Leveling derived geoidal

heights was 3.3 *cm* which is as good as that of the previously published geoid models. The covariance matrix of the gravimetric geoidal heights along with rough estimation of the covariance matrix of the GNSS/Leveling derived geoidal heights was used to construct a weight matrix of discrepancies to measure the weighted congruency. The results were almost the same as those when using the identity weight matrix.

In summary, in this dissertation, it was shown that downward continuation of gravity anomalies from the Earth surface and above it to the geoid level can be done without any regularization and in fact the LS technique provides the most probable result. Two geoid models of Auvergne were determined, one using the conventional Stokes-Helmert approach with some small modifications (specifically in the area of the combination of the global and local data and also density variation effects), and the other using the most probable solution of gravity anomalies on the geoid. The two solutions were different only for a few centimetres. It was also shown that rigorous orthometric heights can nowadays be easily computed using freely available data sets, they should be used if one chooses the geoid as the vertical datum in the height system.

## **6.1 Recommendation for future studies**

The differences between the two geoid models computed in this dissertation need further investigation. Both models are in good agreement with maximum differences of ~10 *cm* but the differences are not correlated with topography. The STDs of the GNSS/Leveling derived geoidal heights were only estimated using approximate values provided by data distributor. A more precise investigation in this area is required to compute a more accurate picture of the congruency of the classical height system. In

constructing the a priori covariance matrix of gravity anomalies to be used in the LS DWC process, a uniform STD of the gravity anomalies was used; a better estimation of each point can be computed by considering the removed topographical effects and cross-validation techniques.

## **6.2 References**

Abdalla, Ahmed, H. H. Fashir, Abobakr Ali, and D Fairhead. 2012. "Validation of recent GOCE/GRACE geopotential models over Khartoum state-Sudan." *Journal of geodetic science* 2 (2): 88-97.

Duquenne, H. 2007. "A data set to test geoid computation methods." Istanbul: First international Symposium of the international gravity field services (IGFS).

Kingdon, Robert, and Petr Vaniček. 2010. "Poisson Downward Continuation Solution by the Jacobi Method." *Journal of Geodetic Science* 1: 74-81.

Rülke, A, G Liebsch, M Sacher, U Schäfer, U Schirmer, and J Ihde. 2012. "Unification of European height system realizations." *Journal of Geodetic Science* 2: 343-354.

## Vita

**Candidate's full name:** Ismael Foroughi

**Place and date of birth:** Tehran, Iran / 24/05/1988

**Address:** 1-180 Westmorland St, Fredericton, NB, Canada.

## Education

**PhD** University of New Brunswick (UNB), Geodesy and Geomatics November 2018

**MS** University of Tehran, Geodesy and Geomatics August 2013

**BS** University of Tehran, Geodesy and Geomatics August 2010

## Publications

### *First author refereed journal articles*

- **Foroughi, I.**, Vaníček, P., Kingdon, R.W., Goli, M., Sheng, M., Afrasteh, Y., Novák, P., Santos, M. (2018) Sub-centimetre geoid. **Journal of Geodesy** (<https://doi.org/10.1007/s00190-018-1208-1>)
- **Foroughi, I.\***, Vaníček, P., Sheng, M., Kingdon, R., Santos, M. (2017) In defense of classical height system. **Geophysical Journal International**, 211 (2), pp:1176-1183.

- **Foroughi, I.\***, Vaníček, P., Novák, P., Kingdon, R., Sheng, M., Santos, M. (2017) Optimal combination of satellite and terrestrial gravity data for regional geoid determination using Stokes-Helmert's method, the Auvergne test case. **IAG Symposia series**, Thessaloniki, Greece.
- **Foroughi, I.**, Tenzer, R. (2017) Comparison of different methods for estimating the geoid-to-quasigeoid separation. **Geophysical Journal International**, 210 (2) pp 1001-1020.
- **Foroughi, I.\***, Afrasteh, Y., Ramuz, S., Safari, A. (2017) Local evaluation of earth gravitational models, case study: Iran. **Geodesy and Cartography** 43(1), pp: 1–13.
- **Foroughi, I.\***, Tenzer, R. (2014) Assessment of the direct inversion scheme for the quasigeoid modeling based on applying the Levenberg–Marquardt algorithm. **Journal of Applied Geomatics**, 6 (3),pp 171-180.

*Second author refereed journal articles*

- Tenzer, R., **Foroughi, I.** (2018) On the applicability of Molodensky's concept of heights in planetary sciences. **Geosciences** 8 (7) pp 239.
- Tenzer, R., **Foroughi, I.**, Sjoberg, L.E., Bagherbandi, M., Hirt, C., Pitonak, M. (2018) Definition of Physical Height Systems for Telluric Planets and Moons. **Survey in Geophysics** 39 (3) pp 313-335.
- Tenzer, R., **Foroughi, I.** (2018) Effect of the mean dynamic topography on the geoid-to-quasigeoid separation offshore. **Marine Geodesy**  
<https://doi.org/10.1080/01490419.2018.1452810>.



- Goli, M., **Foroughi, I.\***, Novák, P. (2018) On estimation of stopping criteria for iterative solutions of gravity downward continuation. **Canadian Journal of Earth Sciences**, 55(4): 397-405.
- Tenzer, R., **Foroughi, I.**, Pitonak, M., Sprlak, M. (2017) Effect of the Earth's inner structure on the gravity in definitions of height systems. **Geophysical Journal International**, 209 (1) pp: 297-316.
- Tenzer, R., **Foroughi, I.**, Novák, P., Hirt, C., Pitonak, M. (2018) How to compute Bouguer gravity anomalies in telluric planets. **Survey in Geophysics** (<https://doi.org/10.1007/s10712-018-9504-0>).
- Goli, M., **Foroughi, I.**, Novák, P. (2018) The effect of the noise, spatial distribution, and interpolation of ground gravity data on uncertainties of estimated geoidal heights. **Studia Geophysica et geodetica** (Accepted and in press for publication).

*Co-author refereed journal articles*

- Janák, J., Vaníček, P., **Foroughi, I.\***, Kingdon, R., Sheng, M., Santos, M. (2017) Computation of precise geoid model of Auvergne using current UNB Stokes-Helmert's approach, **contribution to Geodesy and Geophysics** 47(3): 201-229.
- Afrasteh, Y., Safari, A., Sheng, M., Kingdon, R., **Foroughi, I.** (2017) The effect of noise on geoid height in Stokes-Helmert method. **IAG Symposia series**, Thessaloniki, Greece.
- Ghalenoi, E., Hasanlou, M., Sharifi, M.A., Vignudelli, S., **Foroughi, I.** (2017) Spatiotemporal monitoring of upwelled water motions using optical flow method in the Eastern Coasts of Caspian Sea. **Journal of Applied Remote Sensing** 11 (3), 036016.

- Mahbuby, H., Safari, A., **Foroughi, I.\*** (2017) Local gravity field modelling using spherical radial basis functions and genetic algorithm. **Comptes Rendus Geoscience**, 349 (3) pp 106-113.
- Vaniček, P., Novák, P., Sheng, M., Kingdon, R., Janák, J., **Foroughi, I.**, Martinec, Z., Santos, M. (2017) Does Poisson's downward continuation give physically meaningful results. **Studia Geophysica Geodetica**, 61 (3) pp 412-428.
- Shahbazi, A., Safari, A., **Foroughi, I.**, Tenzer, R. (2016) A numerically efficient technique of regional gravity field modeling using Radial Basis Functions. **Comptes Rendus Geoscience**, Vol. 348 pp. 99-105.
- Safari, A., Sharifi, M. A., Amin, H., **Foroughi, I.\***, Tenzer, R. (2014) Determination of the Gravitational Gradient Tensor Using Satellite-Altometry Observations over the Persian Gulf. **Marine Geodesy**, 37(4), pp: 404:418.
- Safari, A., Sharifi, M. A., Amin, H., **Foroughi, I.** (2014) Gravity acceleration at the sea surface derived from satellite altimetry data using harmonic splines. **Journal of the Earth and Space Physics**, 40 (3), pp 35-46.
- Safari, A., Sharifi, M. A., **Foroughi, I.\***, Amin, H. (2014) An Approach to Height Datum Unification Based on Local Gravity Field Modelling Using Radial Basis Function, Case Study: Height Datum Unification of Leveling Network of Class 1 at Iran. **Journal of Earth and Space Physics**, 40 (1) pp 69-81.
- Safari, A., Sharifi, M. A., **Foroughi, I.\*** (2013) Local Gravity Field Modeling by Radial Basis Functions, Case Study: Coastal Area of Persian Gulf. **Journal of Earth and Space Physics**, 39 (3), pp 33-48.

- Safari, A., Sharifi, M. A., Amin, H., **Foroughi, I.** (2013) A new approach for the determination of the gravitational gradient tensor using the observations from satellite altimetry, case study: Persian Gulf. **Journal of Geomatics Science and Technology**. 3(2), pp 83-100.

### *Selected Conference Papers*

- **Foroughi, I.\***, Santos, M., Afrasteh, Y., Kingdon, R., Vaníček, P. (2018) Rigorous orthometric heights: theoretical overview and advantages of use. EGU 2018, Vienna, Austria.
- **Foroughi, I.**, Kingdon, R., Sheng, M., Vaníček, P., Santos, M. (2017) Local spectral model of geoid-to-quasigeoid separation in North America. Canadian Geophysical Union annual meeting, Vancouver, British Columbia, Canada.
- **Foroughi, I.\***, Vaníček, P., Novák, P., Kingdon, R., Sheng, M., Santos, M. (2016) Optimal combination of satellite and terrestrial gravity data for regional geoid determination using Stokes-Helmert method. Gravity, Geoid and Height Systems symposium, Thessaloniki Greece 2016.
- **Foroughi, I.\***, Vaníček, P., Novák, P., Kingdon, R., Goli, M., Sheng, M., Santos, M. (2016) Harmonic downward continuation of scattered point gravity anomalies to mean anomalies on a mesh on the geoid. Canadian Geophysical Union annual meeting, Fredericton, NB, Canada. (Best student paper award)
- **Foroughi, I.\***, Vaníček, P., Kingdon, R., Novák, P., Sheng, M., Santos, M. (2016) Poisson downward continuation of scattered Helmert's gravity anomalies to mean values on a raster on the geoid using least square. European Geoscience Union (EGU) General Assembly 2016, Vienna, Austria.

- **Foroughi, I.\***, Sheng, M., Kingdon, R., Huang, J., Martinec, Z., Vaníček, P. (2015)  
The effect of lateral topographical density variations on the geoid in Auvergne. 26<sup>th</sup>  
IUGG General Assembly, Prague, Czech Republic.
- **Foroughi, I.\***, Janák, J., Kingdon, R., Sheng, M., Santos, M., Vaníček, P. (2015)  
Illustration of How Satellite Global Field Should be Treated in Regional Precise  
Geoid Modelling (Padding of Terrestrial Gravity Data to Improve Stokes-Helmert  
Geoid Computation). European Geoscience Union (EGU) General Assembly,  
Vienna, Austria.
- **Foroughi, I.\***, Vaníček, P., Kingdon, P., Sheng, M., Santos, M. (2015) Assessment of  
Discontinuity of Helmert's Gravity Anomalies on the Geoid. Canadian Geophysical  
Union annual meeting, Montreal, Canada.
- **Foroughi, I.\***, Tenzer, R., Safari, R. (2013) Application of the Levenberg-Marquardt  
algorithm in local gravity field modeling using radial basis functions, IAG Scientific  
Assembly, Helmholtz Centre Potsdam, GFZ German Research Centre for  
Geosciences.